PALLADIUM AND NICKEL CATALYZED OLEFIN ISOMERIZATION AND POLYMERIZATION

Alexandra H. Farquhar

A dissertation submitted to the faculty at the University of North Carolina at Chapel Hill in partial fulfillment of the requirements for the degree of Doctor of Philosophy in the Department of Chemistry.

Chapel Hill
2019

Approved by:

Alexander J. M. Miller,

Maurice S. Brookhart,

Joseph L. Templeton,

Frank A. Leibfarth,

Cynthia K. Schauer

ABSTRACT

Alexandra H. Farquhar: Palladium and Nickel Catalyzed Olefin Isomerization and Polymerization
(Under the direction of Alexander J. M. Miller)

This work describes the preparation of palladium complexes supported by aminophosphinite pincer ligands and their reactivity in the presence of electrophilic reagents and olefins, respectively. An additional study into the oligomerization and polymerization of 5-ethylidene-2-norbornene (ENB) by cationic allyl Ni and Pd catalysts is also described.

Chapter 2 investigates the challenges particular to palladium in the metalation of aminophosphinite pincer ligands. Three aminophosphinte ligands with a methoxy blocking group installed *ortho* to the phosphinite were prepared of varying amine substitution: a macrocycle-containing 15-aza-crown-5 ether ($^{15c5}N^{MeO}$COP-H), an acyclic bis(methoxy)diethylamine ($^{MeOEt}N^{MeO}$COP-H), and a diethylamine analogue containing no ether donor ligands ($^{Et}N^{MeO}$COP-H). Neutral and cationic complexes of palladium based on these three different ligand scaffolds were prepared. Attempts to access Pd^{IV} complexes based on the macrocycle-containing aminophosphinite scaffold are described, but no Pd^{IV} intermediates were isolated or observed.

Chapter 3 explores the reactivity of cationic macrocycle-containing $[(^{15c5}N^{MeO}COP)Pd]^+$ and dialkylamine-containing $[(^{Et}N^{MeO}COP)Pd]^+$ with alkenes. The olefins 2,3-dimethyl-1-butene and allylbenzene were observed to be dimerized under catalytic conditions with macrocycle-containing $[(^{15c5}N^{MeO}COP)Pd]^+$ and $LiBAr^F{}_4$. Only isomerization of 1-hexene was observed under the same catalytic conditions. A comparative study of the isomerization of 1-hexene by

macrocycle-containing [($^{15c5}N^{MeO}$COP)Pd]$^+$ and dialkylamine-containing [($^{Et}N^{MeO}$COP)Pd]$^+$ is described. This work provided the first comparative reactivity studies of macrocycle-containing aminophosphinite pincer catalysts and a dialkylamine-containing analogue with no hemilabile ether donors.

Chapter 4 diverges from the chemistry of pincer-crown ether palladium complexes to study the oligomerization and polymerization of ENB by cationic allyl Ni and Pd catalysts. The relative activity of these catalysts towards the homopolymerization of ENB is substantially lower than towards unsubstituted norbornene (NB) polymerization. Added tertiary phosphine co-ligands *in situ* increases both Ni and Pd catalysts activity towards ENB homopolymerization. The oligomerization of ENB in the presence of these catalysts and chain transfer agents (CTAs) produces α-olefin terminated oligomers. These reactions proceed under mild conditions to predictably and selectively prepare ENB oligomers ca. 270 Da to high polymer (ca. 100,000 Da) with glass transition temperatures between -18 ^oC and 200 ^oC.

ACKNOWLEDGMENTS

I am forever grateful to my mentors, friends, and family for their incredible support both before my time at Carolina and during this wild adventure.

I would first like to thank my advisor, Alex, for mentoring me these last five years. Thank you for always supporting my academic and career endeavors—from making it possible for me to research in Israel prior matriculating into Carolina, to encouraging me to branch out into polymer chemistry in a collaboration with Eastman, and for cheering me on in my goal to pursue patent law. I will always remember your thoughtfulness, from the delicious challah and macaroons that you would share with me on Rosh Hashana and Passover, to lending an ear for challenging and unexpected hurdles in life. Thank you for always being there and for your mentorship.

Thank you to Brook, for being the best (and only) "consultant" I have ever had the privilege to work with. I am so thankful to you for taking the time to mentor me. Working on the polymer project together is one of my best memories in graduate school. Thank you for always lending a kind ear and thought—I will always be grateful for your mentorship, candor, patience, and encouragement.

Thank you to my Eastman collaborators: Mark, Dawn, and Vikram. Working with you all reinvigorated what I love about chemistry, and pushed me to grow as a professional and as a person. Thank you all for your hard work, support, and laughter.

I am incredibly grateful to my committee members: Joe, Cindy, and Frank. Thank you, Joe, for always taking a genuine interest in my progress, and for sharing your sense of humor—running into you in Kenan and talking with you always brightens my day. Thank you to Cindy, for mentoring me while I was a teaching assistant for inorganic synthesis lab—I am so grateful to you for always welcoming me into your office and helping me when I needed it. Thank you, Frank, for always lending a hand in my polymer project, your insight, and for letting me use your lab's instruments (and more importantly, for hiring an incredible group of people who always assisted me in countless ways).

Thank you to Brandie Ehrmann and Marc ter Horst for all of your guidance throughout the years. We are all so lucky to have you both at UNC, and I am so appreciative of all of the trouble-shooting, training, and mentorship you give to all of us. Carolina Chemistry also would not run without Randy Simmons, Fred Young, Donnyell Batts, Jill Fallin, and Karen Gilliam—thank you all for your hard work and friendship—each one of you never hesitated to lend a hand, and I am so grateful to have known you.

Thank you to all of my lab mates: Brian, Sergio, Scott, Changho, Tianfei, Andrew, Quinton, Bethany, Henry, Eric, Sebastian, and Noah. I am so grateful for your friendship over the years. I am especially grateful for Kristen—thank you for sticking it out with me for three years, and being one of the best humans I know. I am excited to see where your talents, compassion, and courage take you.

I am forever grateful to my mentors in college—Nancy Scott Williams, Anna Wenzel, Bob Grubbs, Keith Keitz, Vanessa Marx, Scott Virgil, and David Milstein—thank you for investing your time in me. You all helped shape who I am today. I would not be here without early mentorship from my high school chemistry and biology teachers, Mr. Johnson and Mr.

Barnes. Teaching at a small public high school in Nevada with few resources isn't always easy, but you both were an inspiration to me.

Finally, thank you to my family. I love you all so much, and could never have made it through without you. Thank you, Mom, for always listening to me, for your love, and patience. Thank you to my Dad, for teaching me the value of hard work, to have confidence in my ability to learn, and to have the humility to keep trying. Thank you to Uncle Raymond, Aunt Diane, and Adam, for giving me a home when I first moved to North Carolina, and for your love and support through the years. Thank you to my Opa for working two manual labor jobs, on the railroads and in the paper mill, to support your family when you moved to the United States—all of your children and grandchildren have opportunities because of your hard work and endless devotion to our family. You taught me the meaning of true love and devotion. Thank you to my incredible in-laws: Will, Michele, Jamie, Char, and Tom. I love you all and feel so incredibly lucky to call you my family. Finally, thank you to my husband, Doug. You were the best surprise waiting for me in North Carolina, and I wouldn't want to continue on this crazy journey without you. I love you.

TABLE OF CONTENTS

LIST OF TABLES

LIST OF SCHEMES

LIST OF FIGURES

LIST OF ABBREVIATIONS AND SYMBOLS

°	degree(s)
α	Greek alpha: first carbon attached to a functional group
β	Greek beta: second carbon attached to a functional group
δ	Greek delta: denotes chemical shift reference scale
η	Greek eta: ligand hapticity
κ	Greek kappa: denotes coordination to metal by x atoms
π	Greek pi: denotes bond
θ	Greek theta: general angle
σ	Greek sigma: denotes coordination to a metal via a single atom
Δ	Greek capital delta: denotes separation between values or applied heat
Å	angstrom(s)
atm	Atmosphere
Ar	general aromatic
BAr^{F}_{4}	tetrakis(3,5-trifluoromethylphenyl)borate
^{13}C	Carbon NMR
C	Celsius
D	Deuterium
d	doublet
DFT	Density Functional Theory
DSC	Differential Scanning Calorimetry
ΔG°	standard Gibbs energy
eq	equation

equiv.	equivalents
Et	ethyl, $-CH_2CH_3$
^{19}F	Fluorine NMR
g	gram
GPC	Gel Permiation Chromatography
h	hour(s)
^{1}H	Proton NMR
Hz	Hertz
PF_6^-	hexafluorophosphate
Ir-H	Iridium-hydrogen bond
Ir-O	Iridium-oxygen bond
^{X}JYZ	magnetic coupluing between atoms Y and Z through a distance of x bonds
K	Kelvin
kcal	kilocalorie
L	general ligand
m	multiplet
M	molar
M	general metal atom
μL	microliter
Me	methyl
mg	milligram
mL	milliliter
mM	millimolar

mmol	millimole
min	minutes
M_n	number-average molecular weight
M_w	weight-average molecular weight
mol	mole
NMR	Nuclear Magnetic Resonance
OAc	Acetate
oligo	oligomer
OTf	Triflate
^{31}P	Phosphorous NMR
Pd	Palladium
Pd-O	oxygen bond to palladium
Pd-X	halide bond to palladium
PDI	Polydispersity Index
Ph	Phenyl
ppm	parts per million
poly	polymer
R	general alkyl group
s	singlet (NMR spectrum)
s	seconds
t	triplet (NMR spectrum)
^{t}Bu	tertiary-butyl
TGA	Thermogravimetric Analysis

THF tetrohydrofuran

TOF Turnover frequency

TON Turnover number

X general halogen atom

CHAPTER 1 - INTRODUCTION

Introduction to Hemilabile Ligands

Hemilabile ligands are chelating ligand scaffolds that contain at least one strongly binding ligand that does not freely dissociate from the metal center, and one or more ligands that can reversibly coordinate to the metal center.[1–4] The concept of hemilability in coordination complexes was first introduced by Jefferey and Rauchfuss in 1979, with their investigation of ruthenium complexes supported by phosphinoanisole chelating ligands.[5] Jefferey and Rauchfuss found that these phosphinoanisole chelating ligands imparted both thermal and oxygen stability to the ruthenium complexes, but that the weak ether donor of the phosphinoanisole backbone was readily displaced by a variety of ligands, including strong donor ligands such as carbon monoxide. While dissociation of strong donor ligands in metal complexes lacking hemilabile ligands is often triggered thermally or photolytically,[6,7] a key feature of many catalysts incorporating hemilabile ligands is that their weak, reversibly coordinated ligands can be readily displaced and allow for the binding of incoming substrate, Figure 1.1.

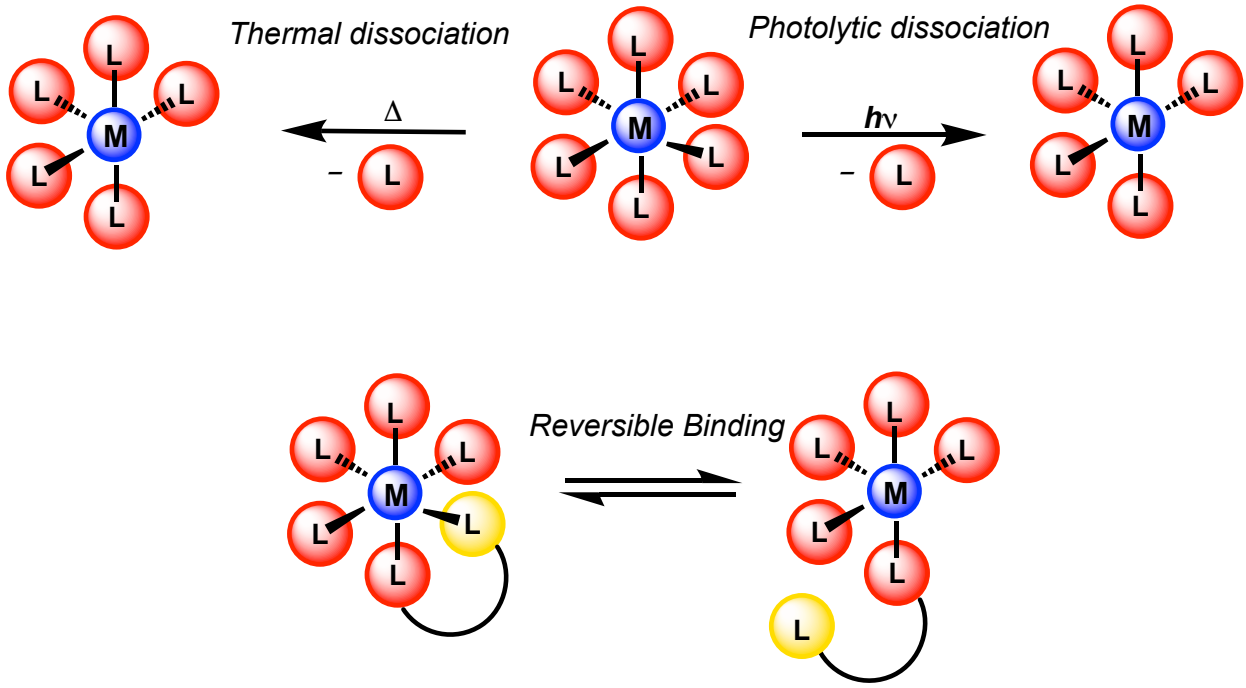

Figure 1.1. Ligand dissociation from metal complexes with and without hemilabile donors.

Hemilabile scaffolds incorporate a host of substitutionally inert and labile ligands, and vary in donor number from bidentate chelates, to multidentate scaffolds of three or more donors.[1,2,8] Geometries of these scaffolds vary widely, from rigid planar structures, to flexible scorpionate morphologies. Substitutionally inert counterparts of these scaffolds can be carbon-based, including alkyl sigma bonds, cyclopentadienyl rings, arenes, and even an alkene in some examples.[9,10] Other common substitutionally inert moieties on hemilabile ligand backbones are nitrogen or phosphorus-containing. Substitutionally labile counterparts within hemilabile scaffolds are often harder ligands with respect to hard-soft acid base theory than their substitutionally inert counterparts, and are usually oxygen, sulfur, or nitrogen containing.[11]

As observed by Rauchfuss and Jefferey,[5] one advantage and often invoked motivation to install hemilabile ligands in catalytic systems is the stability they provide to metal complexes by maintaining saturated coordination geometries. For example, a hemilabile ligand may stabilize a

cationic metal center upon halide abstraction of the neutral species by filling the empty coordination site through coordination of the pendent and substitutionally labile ligand of the scaffold.[12] Reversibly coordinated moieties of hemilabile ligands also protect active sites on metal centers,[13,14] where their reversible coordination to the metal center enables more facile displacement in favor of incoming substrate.[8] One such example is the Grubbs ruthenium metathesis catalyst,[15] which employs an ether chelate that is much more readily displaced than the PR_3 in the parent complex,[16] increasing the rate of olefin metathesis and enabling milder reaction conditions. Many such complexes utilize this aspect of hemilability, shown in Figure 1.2, where substitutionally inert ligands of the depicted hemilabile scaffolds are shown in red, and the substitutionally labile ligands shown in blue.

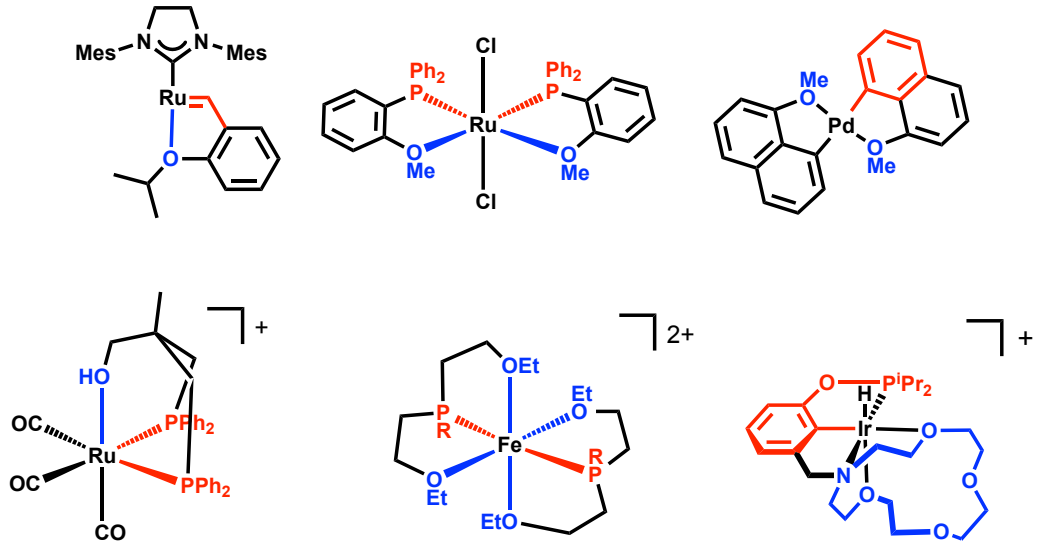

Figure 1.2. Hemilabile ligand scaffolds with substitutionally inert (red) donors and substitutionally labile ether (blue) donors.

While hemilabile ligands are often utilized for protecting active sites on metal centers through chelation of the weak donor ligand, these weak donors of hemilabile ligands are not solely limited to acting as spectators when de-coordinated from the metal center, Figure 1.3.[17]

Substitutionally labile ligands of hemilabile scaffolds are typically Lewis basic sites that can also act cooperatively in catalysis. Some of these functions include stabilizing reactive intermediates,[12,18] promoting bond formation,[19,20] or direct activation of a substrate.[3] For example, substitutionally labile ligands can coordinate to a metal center upon its oxidation,[21] providing electron density and thereby stabililizing a reactive high valent intermediate metal center.[22,23] Conversely, a hemilabile ligand may also de-chelate from electron-poor metal centers, promoting new bond formation via reductive elimination. Finally, pendent Lewis basic donors of hemilabile ligands may participate in chemical steps directly through substrate activation,[24] such as direct deprotonation of a substrate to facilitate proton shuttling in a reaction.[3,25–31]

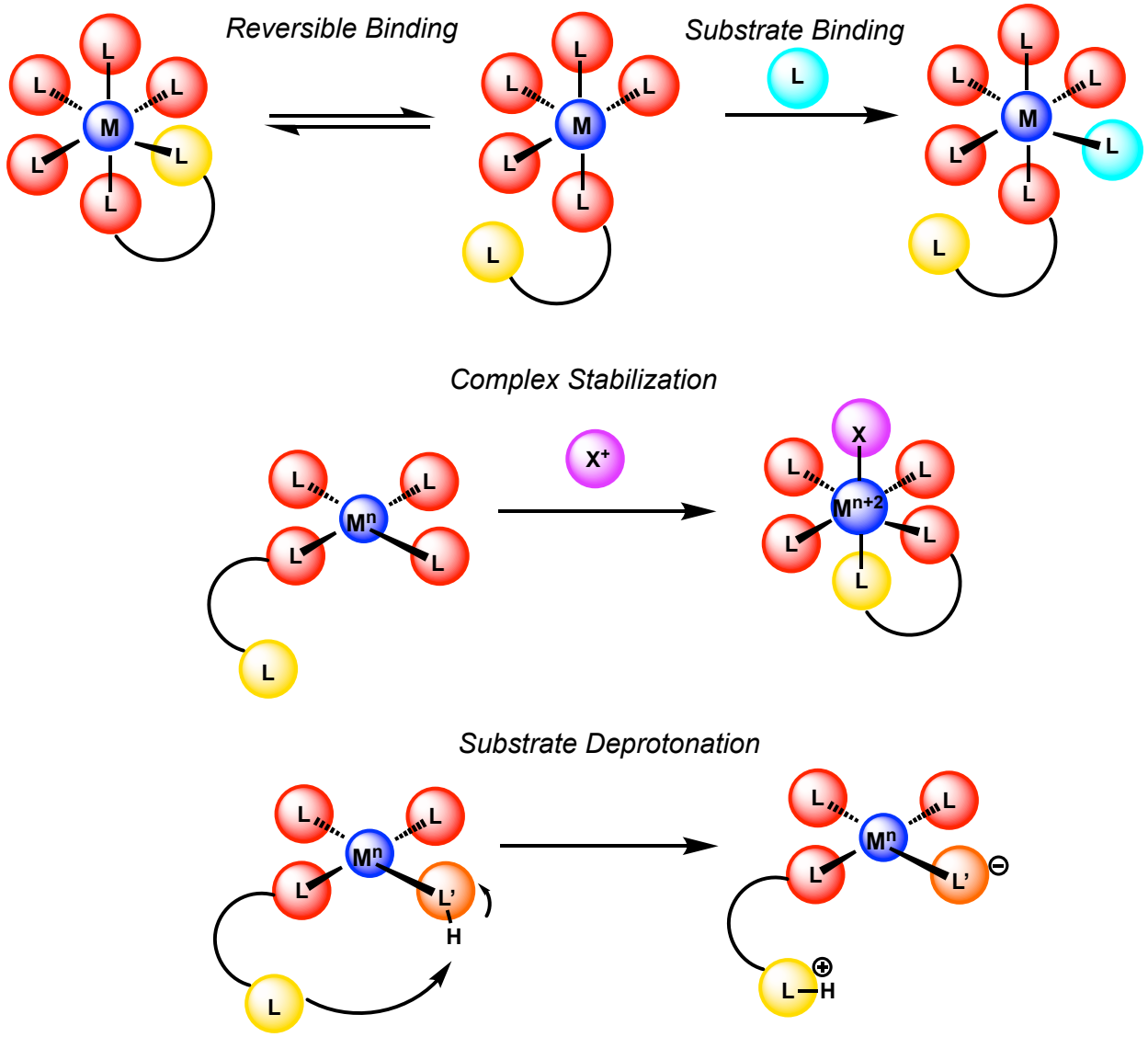

Figure 1.3. Hemilabile ligands as substrate gates and cooperative actors through complex stabilization or substrate activation.

A central goal in this thesis work was to leverage our own hemilabile aminophosphinite pincer scaffold towards stabilizing highly reactive intermediates in catalysis, as well as to activate substrates in chemical steps. The scope of this introduction aims to note previously reported examples demonstrating the specific utility of hemilabile ligands as cooperative actors in catalysis and chemical steps, via substrate activation or reactive intermediate stabilization, as

well as to explore our own ligand scaffold for its potential in this type of cooperative hemilability.

Hemilabile Ligands Stabilizing High-Valent Metal Centers

Besides reversibly coordinating to the metal center to provide open active sites, the substitutionally labile moieties of hemilabile ligands can also participate in chemical transformations by stabilizing reactive intermediates in a catalytic cycle. For example, a pendent reversibly binding ligand may dissociate from the metal center when it is low valent, or bind to the metal center to stabilize high valent species. In this way, preferred geometries of metal complexes can be mediated between oxidation states, allowing one multidentate hemilabile ligand to accommodate changes in the oxidation state of the metal center.

This type of behavior is beautifully displayed in the gold-catalyzed arylation of arenes with aryl halides in an Au^{I}/Au^{III} cycle supported by a P-N chelating ligand, Me-Dalphos (Figure 1.4).[23] In this case, the hemilabile Me-Dalphos ligand plays a seminal role in the stabilization of both the Au^{I} and Au^{III} species, as shown in Figure 1.4. While Au^{I} typically shows a strong preference for linear geometries, Au^{III} species are often unstable unless four-coordinate. In this example, the low valent Au^{I} complex is stabilized in a two-coordinate linear geometry with the substitutionally inert phosphine of the P-N chelate bound to the metal center. Upon oxidative addition of the aryl halide, the resultant Au^{III} species is stabilized by the coordination of the pendent amine of the P-N chelate to achieve a preferred four-coordinate geometry. Direct arylation of aryl halides and arenes in the presence of (Me-Dalphos)AuCl and $AgSbF_6$ is achieved at room temperature and results in high yields of a diverse range of biaryl products, and is facilitated by the cooperative hemilability of this ancillary ligand.

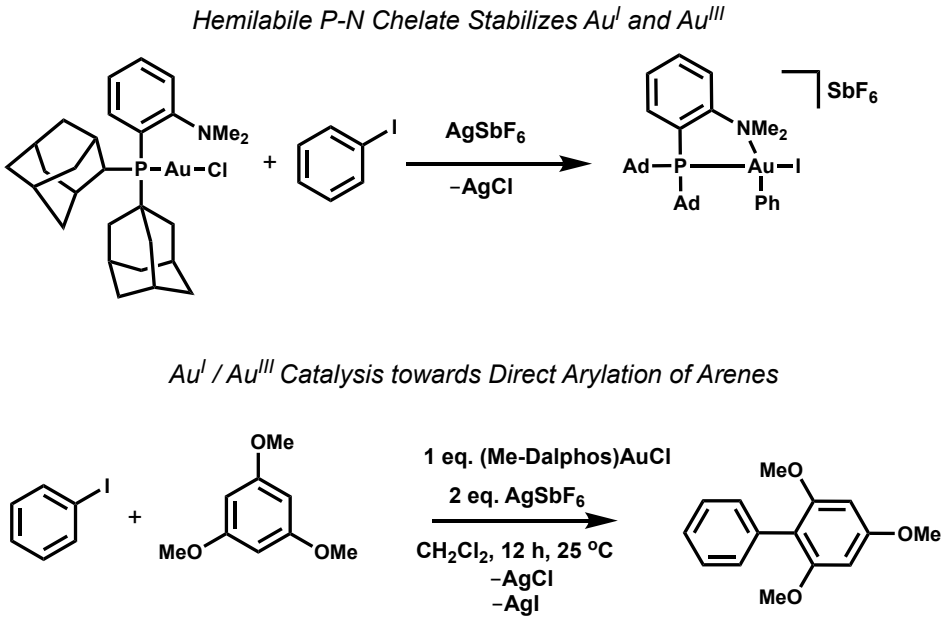

Figure 1.4. Reversible binding of bidentate P—N hemilabile ligands stabilizes Au^{I} and Au^{III} intermediates in catalysis.

Another similar $Au^{I/III}$ example that utilizes hemilabile ligands to toggle between stable two-coordinate Au^{I} and four-coordinate Au^{III} states involves the hydroarylation of styrenes with anilines, Figure 1.5.[22] These transformations are achieved in the presence of a gold catalyst supported by a hemilabile cyclic(alkyl)(amino)carbene with a pendent imine. As with the case with the phosphine Me-Dalphos, the strong carbene donor stabilizes the two-coordinate Au^{I}, whereas coordination of the pendent imine stabilizes Au^{III} intermediates during hydroarylation.

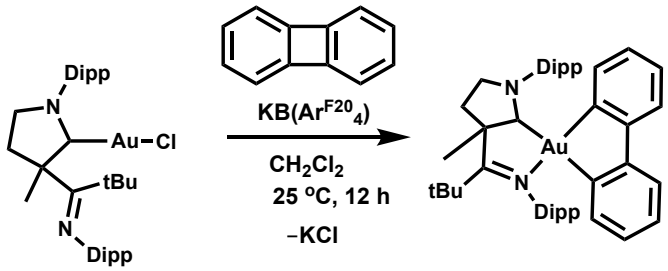

Figure 1.5. A bidentate carbene hemilabile ligands stabilizes Au^{I} and Au^{III} intermediates in catalysis.

Even the phosphinoanisole hemilabile ligand scaffold described by Jefferey and Rauchfuss, which was touted for the thermal and oxidative stability it imparted to their ruthenium complexes, was also reported by Shaw and coworkers to have a direct impact on the rate of oxidative addition of methyl iodide to phosphinoanisole-supported iridium complexes, Figure 1.6.[32]

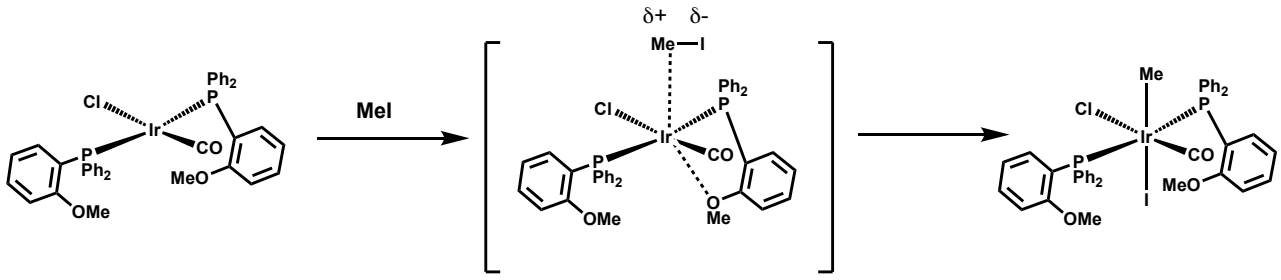

Figure 1.6. Hemilabile ether donation proposed to increase rates of oxidative addition.

They found that methyl iodide oxidatively added to the iridium complexes supported by phosphinoanisole much faster than complexes supported by more basic monodentate tertiary phosphines. If only considering the phosphine donor, one might expect the more basic and electron-rich monodentate phosphines to donate more electron density to the metal center, thereby imparting faster rates of oxidative addition than complexes supported by the more

electron-poor phosphinoanisole. However, it was proposed that the pendent ether on the phosphinoanisole coordinates to Ir prior to oxidative addition, thereby imparting more electron density to the metal center than the more basic monodentate phosphine ligands.

Stabilization of reactive or high valent intermediates is not limited to bidentate scaffolds, however. Several metal complexes featuring tridentate scorpionate ligand scaffolds are also stabilized in a similar fashion, particularly palladium and platinum complexes, with some of the classic platinum examples from the Templeton lab featuring hydridotris(3,5-dimethylpyrazolyl)-borate) ligands (Tp'), Figure 1.7.[33–35] These hemilabile Tp'Pt systems can toggle between κ^2 and κ^3 binding modes, where the κ^3 binding mode stabilizes the high valent Tp'Pt^{IV} species.[35] Thermolysis or the presence of Lewis acidic boranes is proposed to weaken the Pt^{IV}-N bonds, allowing the dissociation of one of the pyrazolyl rings of the Tp' ligand. From this coordinatively unsaturated κ^2 species, aryl migration to the bound olefin is proposed. Re-coordination of the pyrazolyl ring to bring the Tp' ligand back to its κ^3 state then stabilizes the final Tp'Pt^{IV} hydride.

Frauhiger and Templeton also showed that modification of this hemilabile scorpionate ligand motif to include much weaker pyrazolyl ring donation from a "click" triazole allows for even more facile interconversion between κ^2 and κ^3 states at much milder temperatures than the Tp'-supported complexes. The relatively low barrier of interconversion relative to the more strongly donating Tp' ligand allows for the formation of the reactive Pt^{II} intermediate from which the phenyl inserts into the bound olefin to form a stable Pt^{IV} metallacycle at room temperature. [35]

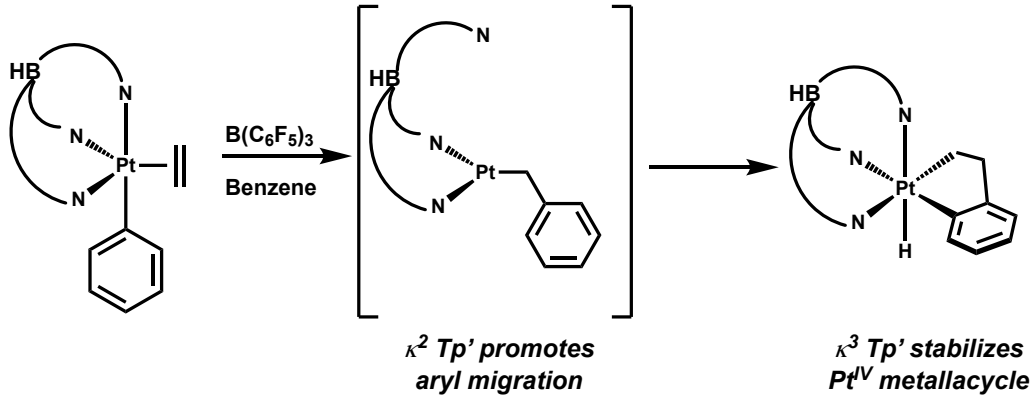

Figure 1.7. Hemilabile κ^2 Tp' promotes aryl migration and κ^3 Tp' stabilizes Pt^{IV}.

Cyclic ethers and thioethers can also provide excellent stability to metal complexes changing oxidation state by interconverting through κ^2 and κ^3 coordination modes. An excellent example of a hemilabile thioether ligand stablilizing high-valent Pd^{IV} comes from a report by Willis et. al. presented in Figure 1.8.[36] Upon the oxidative addition of methyl iodide, this six-coordinate thioether-supported complex was resistant to both reductive coupling of the methyl ligands to form ethane and to iodide coordination.

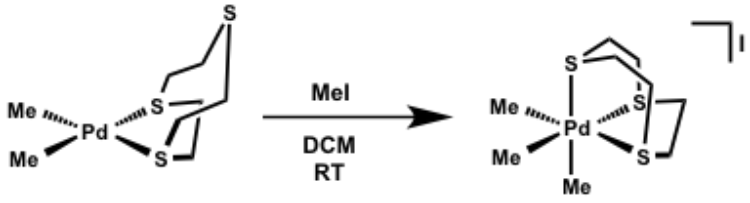

Figure 1.8. A macrocyclic hemilabile cyclic thioether stabilizes Pd^{IV} oxidation state upon the oxidative addition of methyl iodide to the Pd^{II} precursor.

Hemilability and Internal Bases

Hemilabile ligands are not limited to only mediating oxidation states in metal complexes. They can also participate cooperatively in chemical steps by activating substrates, such as serving as an internal base towards substrate deprotonation.

For example, in octahedral iron complexes supported by three chelating and hemilabile bis(diphenylphosphino)amine ligands, the bridging phosphinoamines promote H_2 activation by accepting a proton of hydrogen, while the iron center formally accepts a hydride. Under higher pressures of hydrogen, two molecules of dihydrogen are activated at the iron center, assisted by deprotonation at the pendent amines to form the iron dihydride, resulting in the dissociation of an equivalent of the protonated phosphinoamine and the iron dihydride supported by two chelating and protonated phosphinoamines, Figure 1.9.[31]

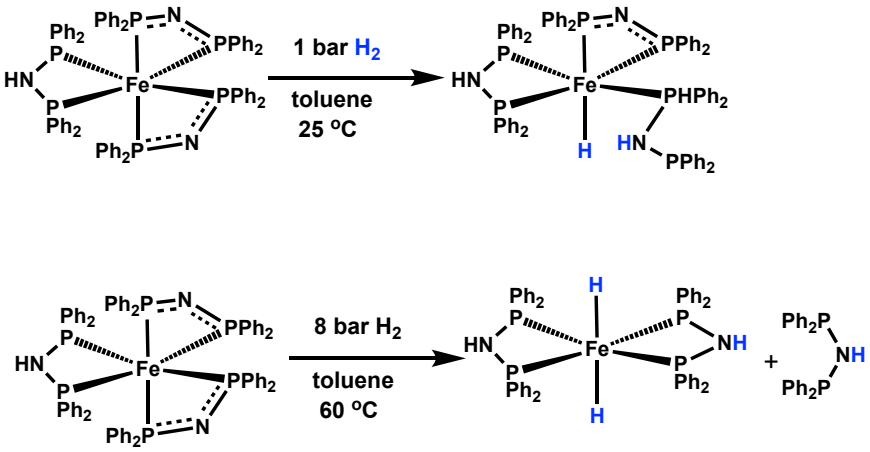

Figure 1.9. Hemilabile ligand cooperation of a bridging phosphinoamine ligand assists hydrogen activation at Fe.

Hemilabile ligands can act as an internal base and also provide stability to catalytic intermediates through coordination of its substitutionally labile ligands. One such example is a palladium catalyst supported by a 1,1'-bis(*tert*-butyl(pyridine-2-yl)phosphanyl)ferrocene ligand

for the methoxycarbonylation of alkenes, Figure 1.10.[28,37] In this study, Dong and coworkers showed experimentally and computationally that the pendent pyridyl moieties of the Pd catalyst both reversibly bind to stabilize the catalytic intermediate Pd acyl species, and also act as an internal base to deprotonate methanol prior to the methanolysis of the Pd-acyl, which was determined to be the rate determining step. Notably, this work utilizes a hemilabile ligand as both a stabilizer of highly reactive intermediates, and as an internal base to facilitate methanolysis of the Pd-acyl.

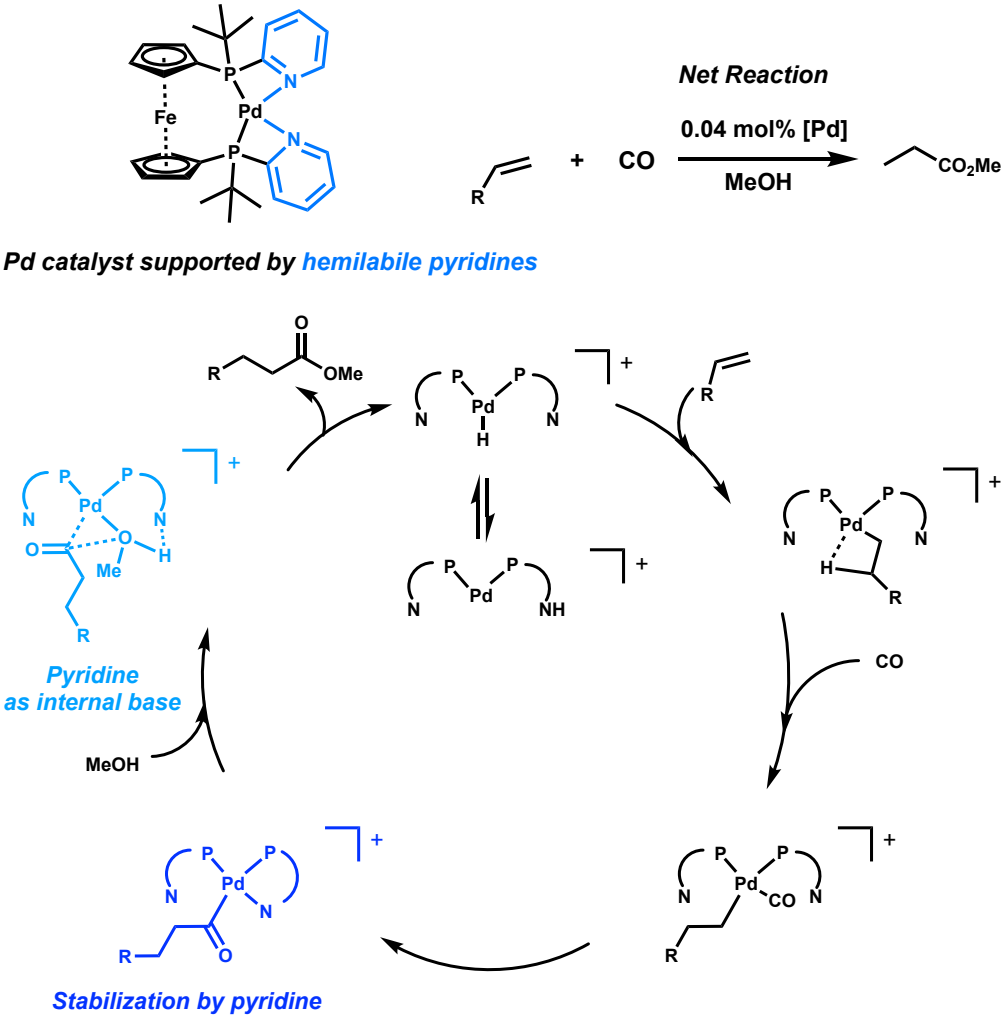

Figure 1.10. Hemilabile ligand scaffold stabilizing intermediates and acting as internal base.

Pincer Crown Ether Complexes

Inspired by the wide utility of hemilabile ligands within organometallic transformations, we sought to explore this utility within our own pincer crown ether hemilabile scaffold, shown in Figure 1.11. Macrocycles containing weak donor ligands, such as crown ethers, are suitable targets to incorporate into ligand scaffolds and impart hemilability, where their denticity to the metal center can be modulated through non-covalent interactions with the addition Lewis acidic cations.[38–40] Prior to the work reported herein, our group had reported the synthesis of this macrocycle-containing hemilabile scaffold on iridium, shown in Figure 1.11. It was found that in the binding of the pendent macrocycle to the Ir center could be modulated between κ^3 to κ^5 coordination modes. This phenomenon was found to impart the ability to tune the rates of catalysis of isomerization[41] and hydrogen activation in the presence of Lewis acidic cations (Figure 1.11),[38] as well as trigger substrate binding[39] and influence activity towards methanol carbonylation.[42]

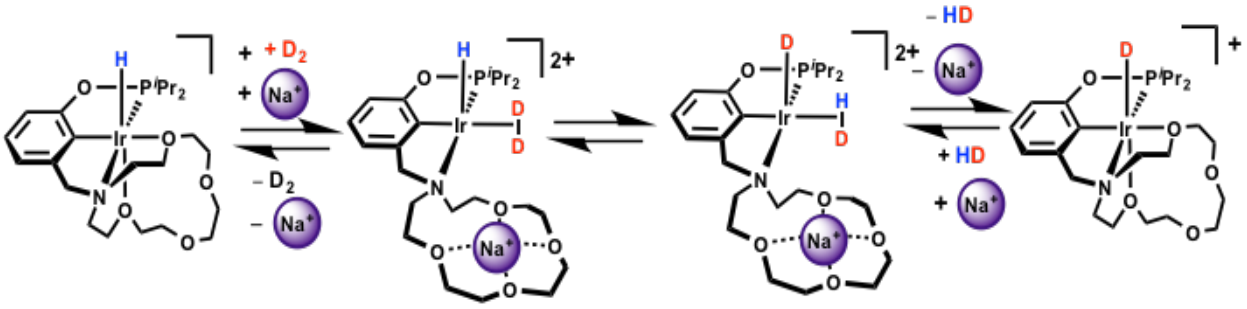

Figure 1.11. Allosteric control of hemilabile macrocycle binding. HD exchange promoted in the presence of Lewis acidic cations.

As cited earlier and described in the chemistry of Dong and coworkers, hemilabile ligands can serve dual purposes in catalytic reactions—stabilizing reactive intermediates and facilitating catalysis through proton shuttling. We envisioned that we could expand the utility of

our pincer ligand scaffold's controllable denticity in a similar manner. One could imagine both the stabilization of high valent and highly reactive metal centers through donation of the pendent macrocycle upon oxidation, as well as possibly leveraging the potential hemilability of the pendent amine arm itself as an internal base in catalytic transformations. Since the denticity of our pincer ligand scaffold on Ir and Ni complexes had been shown to be modulated in the presence of cations in solution, one could also imagine utilizing the "switchability" of our catalyst systems to study fundamental reactions such as reductive elimination, by stabilizing the products of oxidative addition through macrocycle ether donation, and triggering reductive elimination through the addition of cations in solution, Figure 1.12.

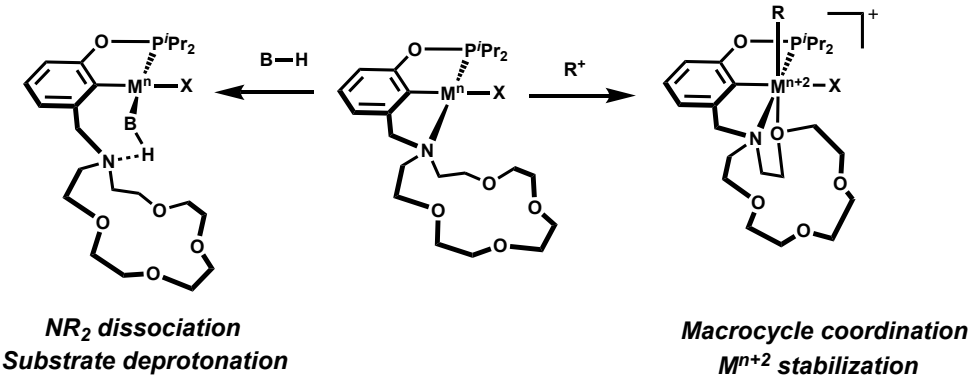

Figure 1.12. Hemilability of pincer crown ether ligand scaffold to stabilize high valent intermediates and serve as an internal base.

This Work

We chose to focus our study on the preparation of new macrocycle-containing pincer complexes based on palladium to explore our ligand scaffold's potential in reactive intermediate stabilization, and in internal base-assisted catalysis. A rich history of high-value palladium catalyzed reactions,[43–45] along with a growing field in the study of high valent Pd^{IV} intermediates in cross-coupling reactions,[46–48] seemed apropos for our ligand scaffold. Additionally, precedence for the lability of the pendent amine in other reported PCN palladium pincer

complexes,[49] along with precedence of intramolecular base-assisted Pd catalyzed reactions,[27,50–53] added further applications that we could envision with tunable Pd pincer crown ether catalysts.

Chapter 2 describes the synthesis of these novel aminophosphinite pincer palladium complexes, detailing the challenges and considerations in their preparation, as well as their preliminary reactivity with oxidants. Palladium pincer complexes of three different aminophosphinte ligand scaffolds of the form (NCOP)Pd(X) (where X = Cl, Br, I, OAc, and CF_3) were prepared, along with their cationic analogues.

The three different aminophsophinite ligand scaffolds varied in their amine substitution, where the aza-15-crown-5 ether, bis(methoxy)diethylamine, and diethylamine analogs were prepared. Of note, preparation of the diethylamine analogue of the $[\kappa3\text{-}(15c5NCOP)Ir(H)]^+$ complex was inaccessible prior to this work. It was found that the installation of a methoxy group on the phenyl backbone of the aminophosphinite pincer ligand was essential for ensuring tridentate NCOP pincer Pd metalation, as well as to prevent activation of the phenyl backbone of the pincer *ortho* to the phosphinite. A screen of preliminary reactivity of ($^{15c5}N^{MeO}COP$)Pd(X) complexes with electrophilic R^+ reagents did not generate Pd^{IV} species. Either no reactivity is observed, or partial halide abstraction towards the formation of a mono-halide bridging Pd dimers is observed.

Chapter 3 pivots to explore the reactivity of two cationic palladium complexes with olefins, as a comparative study to interrogate the role of hemilabile ligands and their interactions with external lithium salt additives. The isomerization of 1-hexene by palladium supported by 15-aza-crown-5 ether and diethylamine-substituted aminophosphinite pincer ligand scaffolds is explored. These complexes display markedly different reactivity with olefins than our group's previously reported pincer crown ether Ir-H complexes, where the dimerization of olefins that

are highly substituted or contain acidic allylic protons is observed, while clean isomerization without subsequent dimerization is observed in the presence of linear 1-hexene.

Interestingly, the activity of [($^{15c5}N^{MeO}$COP)Pd]$^+$ towards isomerization is increased in the presence of Li^+, whereas the activity of [($^{Et}N^{MeO}$COP)Pd]$^+$ is hindered in the presence of Li^+. We propose that this chemistry is proceeding through a π-allyl mechanism, necessitating the dissociation of the pendent amine to deprotonate substrate and form the Pd-allyl.

Chapter 4 diverges from the chemistry of pincer crown ether palladium complexes and hemilability altogether for a detailed study on the polymerization and oligomerization of 5-ethylidene2-norbornene (ENB) by "activatorless" Pd and Ni catalysts. These catalysts are capped with labile mesitylene ligands that are readily displaced in solution by monomer or phosphine co-ligands.[54,55] Polymerizations in the presence of terminal olefin chain transfer agents are explored with and without added phosphine co-ligands. Both the activity of these catalysts and their product distribution are determined by the added phosphine co-ligand and chain transfer agent in solution.

Notably, both Pd and Ni catalysts suffer from low activity in the homopolymerization of ENB without any added co-ligand or chain transfer agent, relative to the polymerization of unsubstituted norbornene. The addition of co-ligand phosphines dramatically improves the reactivity of both Pd and Ni catalysts towards ENB homopolymerization. The addition of the chain transfer agent 1-hexene is tolerated by both systems, and modulates the molecular weight of the product polymers and oligomers as a function of the concentration of 1-hexene. The introduction of a smaller chain transfer agent, ethylene, results in decreased activity of the Pd systems, where decomposition of the catalyst is observed. In the Ni system, ethylene increases its activity towards the oligomerization of ENB, and the chain length of the oligomers can be

modulated by changing the identity of the added phosphine in solution, or by increasing the pressure of ethylene.

CHAPTER 2 – SYNTHESIS OF PALLADIUM PINCER COMPLEXES SUPPORTED BY AN AMINOPHOSPHINITE LIGAND SCAFFOLD

Introduction

Palladium catalysis has become a ubiquitous tool in chemical synthesis. Cross-coupling reactions catalyzed by palladium were recognized with a Nobel Prize in 2010 and have been applied in ton-scale syntheses of pharmaceuticals.[44,56] The centerpiece of palladium catalysis is a two-electron chemical redox transformation, where oxidative addition of a substrate increases the Pd formal oxidation state by two, while reductive coupling often releases product while decreasing the metal oxidation state by two, Figure 2.1.[56] Much of the lucrative chemistry in industry relies on $Pd^{II/0}$ catalytic systems and it is most studied to date.[57]

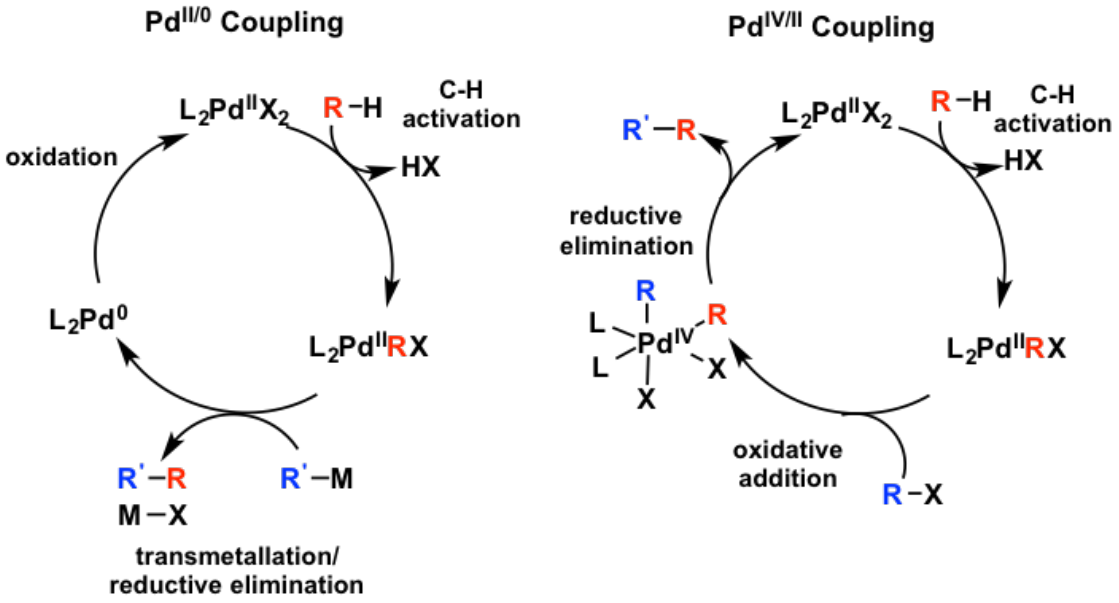

Figure 2.1. $Pd^{II/0}$ and $Pd^{IV/II}$ cross coupling requires different metal complex geometries.

While palladium catalytic cycles most commonly utilize Pd^0 and Pd^{II} oxidation states, catalytic cycles that move between Pd^{II} and Pd^{IV} have increasingly been proposed in some cross-coupling mechanisms.[58,59] Proposed Pd^{IV} catalytic intermediates are increasingly prevalent in the literature, and ligand scaffolds capable of supporting high valent Pd are desired to further understand these transformations.[46,48,59,60] Catalysis involving relatively high-valent intermediates could offer improved air and moisture tolerance and perhaps facilitate rapid chemical steps along coupling process.[57] A key feature of the $Pd^{II/IV}$ cycle is an oxidative addition to reach Pd^{IV} prior to the reductive elimination of the coupled product (Figure 2.1).

We hypothesized that our hemilabile aminophosphinite pincer ligand scaffold[38] with a pendent macrocycle could support palladium complexes in both Pd^{II} and Pd^{IV} oxidation states, and hopefully allow for studying high valent intemediates in $Pd^{II/IV}$ cycles, via stabilization of high valent intermediates through crown ether donation to the metal center.

The aminophosphinite pincer ligand developed by our group,[38,61] abbreviated as ^{15c5}NCOP-H, combines a rigid and strongly donating pincer ligand with several weak and potentially hemilabile donors of the pendent 15-aza-crown-5 ether macrocycle, which would be explored in the context of cation-modulated oxidative addition and reductive elimination. When this work began, however, relatively few NCOP palladium pincer complexes had been prepared,[62–72] and no pincer-crown ether palladium complexes were known.

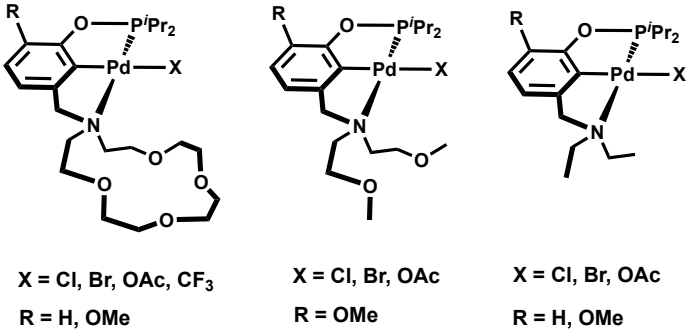

Figure 2.2. Palladium pincer complexes supported by three distinct aminophosphinite pincer ligands of different hemilability.

This chapter describes the preparation of Pd^{II} complexes of C_s symmetry supported by three different aminophosphinite pincer ligands, Figure 2.2. Non-equivalent axial ligands on Pd would break the symmetry of complex, and be indicative of Pd^{IV} formation under oxidative conditions. A reactivity screen of these novel neutral Pd^{II} complexes with electrophilic alkyl and halide reagents will also be discussed.

Synthesis of Neutral (NCOP)Pd^{II}X Complexes

Synthesis of (^{15c5}NCOP)Pd^{II}Br

Synthesis of ^{15c5}NCOP-H ligand was performed following the literature procedure (^{31}P{^{1}H} NMR δ 147).[61] Metalation was achieved by allowing ^{15c5}NCOP-H to react with $PdBr_2$

in the presence of base, affording (^{15c5}NCOP)Pd (Br) as a yellow-orange solid in 60% yield (Scheme 2.1)**.**

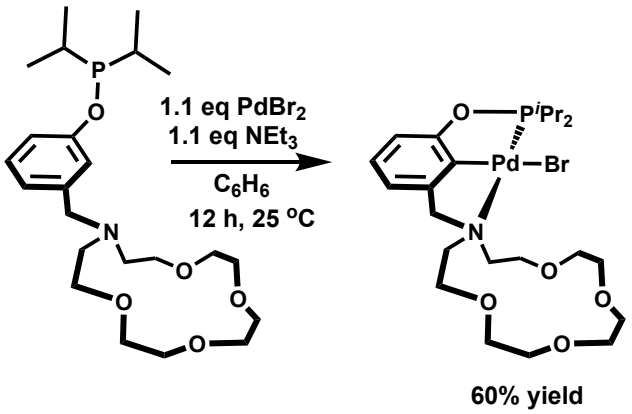

Scheme 2.1. Synthesis of (^{15c5}NCOP)Pd(Br).

Diagnostic ^{1}H NMR resonances indicated C_s symmetry in solution. These proposed cyclometalated complexes have convenient ^{1}H and ^{31}P NMR handles to probe cyclometalation, axial-ligand coordination, and oxidation state of the metal (Figure 2.3). The free ligand ^{15c5}NCOP-H has a ^{31}P{^{1}H} NMR resonance at δ 147. In analogous Ni^{II} systems, (^{15c5}NCOP)Ni^{II}(Br),[61] the ^{31}P{^{1}H} NMR resonance shifts approximately 50 ppm downfield from the free ligand upon cyclometalation (δ 200). The aromatic region in the ^{1}H NMR spectrum is also diagnostic, where two doublets and one triplet corresponding to the ligand-backbone are expected. The isopropyl methyl and methine resonances in the ^{1}H NMR spectrum are indicative of the symmetry of the molecule, where a square-planar (NCOP)Pd^{II}(X) or a (NCOP)$Pd^{IV}(X)_3$ complex with equivalent axial ligands should be C_s symmetric in solution.

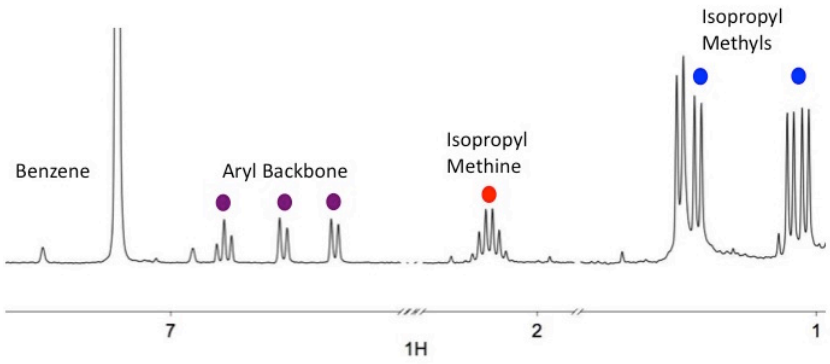

Figure 2.3. The diagnostic ^{1}H NMR resonances of (^{15c5}NCOP)Pd^{II}(Br) that is C_s symmetric in solution, showing the aryl backbone protons (purple), isopropyl methine protons (red) and isopropyl methyl protons (blue).

A diagnostic ^{31}P{^{1}H} NMR singlet at δ 203, consistent with an analogous cyclometalated Ni^{II} species,[61] as well as phosphorus chemical shifts typical of phosphines chelated to a metal center in a five-memberd ring,[73] provided evidence for a cyclometalated phosphorus-containing species. In the ^{1}H NMR spectrum, expected resonances corresponding to the aryl backbone δ 6.86 (t, J = 7.7 Hz, 1H), δ 6.70 (d, J = 8.0 Hz, 1H), and δ 6.57 (d, J = 7.5 Hz, 1H), a septet corresponding to the isopropyl methine protons (δ 2.13, J = 7.1 Hz, 2H), and two doublets of doublets corresponding to the isopropyl methyl protons (δ 1.34, J = 18.8, 7.1 Hz, 6H, and δ 1.05, J = 15.8, 7.0 Hz, 6H) provided evidence for the formation of (^{15c5}NCOP)Pd^{II}(Br).

Synthesis of (^{15c5}NCOP)Pd (Cl)

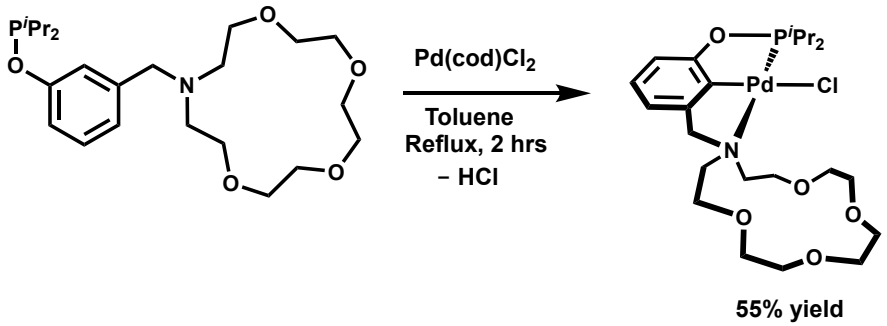

Scheme 2.2. Synthesis of (^{15c5}NCOP)Pd (Cl).

The complex (^{15c5}NCOP)Pd (Cl) is prepared by refluxing the ligand ^{15c5}NCOP-H in toluene for two hours (Scheme 2.2). The crude light yellow to colorless oil can be extracted into toluene, layered with pentane, and crystallized at –30 ^{o}C to afford colorless crystals in 55% yield. Diagnostic aryl backbone resonances of two doublets (6.58 J = 7.5 Hz, and 6.72 J = 7.9 Hz), as well as one triplet of doublets 6.87 (J = 7.8, 1.0 Hz) in the ^{1}H NMR spectrum and a singlet in the ^{31}P{^{1}H} NMR spectrum (δ 201) confirm a cyclometalated structure, and a C_s symmetry in solution, like the bromide analogue (^{15c5}NCOP)Pd (Br).

Since our goal in utilizing these complexes was to leverage allosteric tuning of the pendent hemilabile macrocycle with cations in solution, we wanted to quantify the binding affinity of the neutral chloride complex to Li^+ cations in acetonitirile. The binding affinity of (^{15c5}NCOP)Pd (Cl) to Li^+ was measured in CD_3CN according to previous methods. [39] The K_a was determined to be 294±16 M^{-1}, the strongest interactions with cations of group 10 pincer crown ether complexes synthesized. Figure 2.4 shows the relationship of the natural log of the binding affinity to Li^+ versus the Allred-Rochow electronegativity parameter[74] of each metal center. The observed linear correlation shows that the complex with the least electronegative

metal center, (^{15c5}NCOP)Pd(Cl), has the strongest interactions with Li^+, and suggests that complexes with more electronegative metal centers, such as the nickel analogue (^{15c5}NCOP)Ni(Cl) have lower binding affinities to Li^+ because the organometallic fragment withdraws more electron density from the pendent amine and the ether oxygen atoms.[39,75] Encouraged by the strong binding affinity of the palladium complex to Li^+, we pursued other palladium analogues to further expand our library of pincer crown ether palladium complexes.

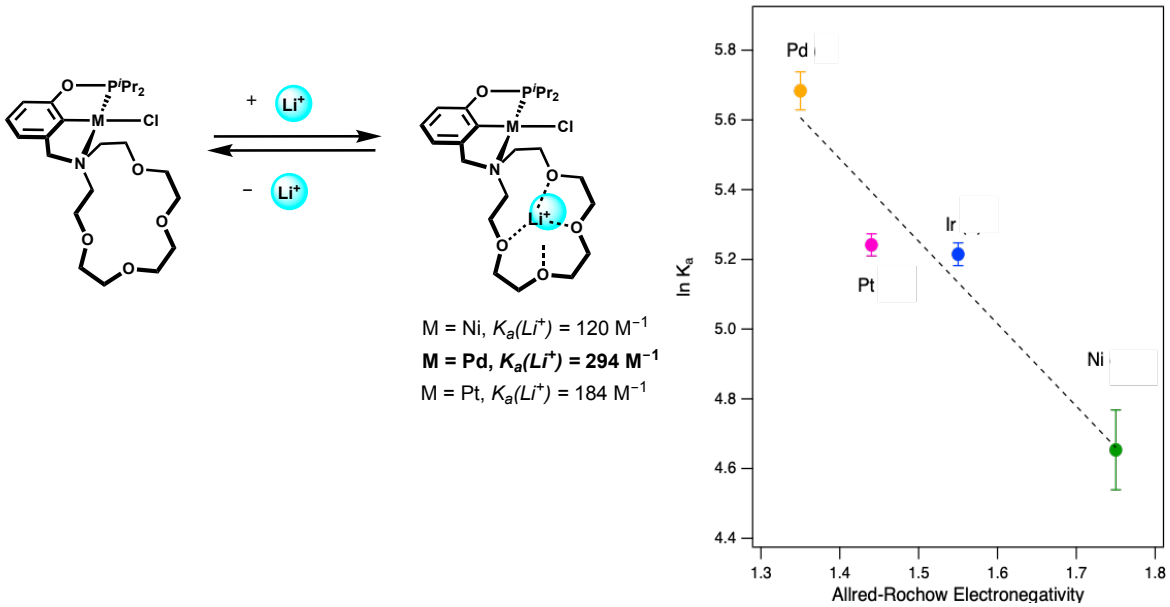

Figure 2.4. Natural log of LiOTf binding affinity of group 10 chloride complexes (^{15c5}NCOP)Ni(Cl), (^{15c5}NCOP)Pt(Cl), and (^{15c5}NCOP)Pd(Cl) along with the isoelectronic (^{15c5}NCOP)Ir(CO) vs. metal Allred-Rochow electronegativity parameter.

Synthesis of (^{15c5}NCOP)Pd(OAc)

The reaction of ^{15c5}NCOP-H and $Pd(OAc)_2$ in acetonitrile was undertaken in an attempt to prepare (^{15c5}NCOP)Pd (OAc) (Figure 2.5). While base was required to achieve cyclometalation of ^{15c5}NCOP-H with $PdBr_2$, an acetate group could act as an internal base (the pK_a of acetic acid in acetonitrile is 23.5),[76] so no additional base was employed.

The reaction afforded a mixture of one major product and one trace cyclometalated product. The major product contained a singlet (δ 6.71, 1H), a doublet (δ 6.72, J = 8.2 Hz, 1H), and doublet of doublets (δ 7.12, J = 7.7, 4.4 Hz, 1H) in the aromatic region of the ^{1}H NMR spectrum, and a singlet (δ 195) in the ^{31}P{^{1}H} NMR spectrum. A 2D COSY NMR experiment showed correlation between the protons at δ 6.72 and δ 7.12, consistent with cyclometallation of Pd on an undesired position of the aryl ring. We tentatively assigned the major product as Pd^{II} bridging acetate dimer (Figure 2.5. Bridging acetate dimers of Pd^{II} are common, especially when Pd centers are supported by a bidentate ligand.[77,78] Specifically, this type of metalation was observed for a very similar system based on an aminophosphinite pincer ligand scaffold bearing bulky triphenylphosphine ligands.[71] The bidentate binding mode is not desired for our purposes, because the aza-crown ether moiety is not coordinated to Pd and is too far away to participate as a hemilabile ligand. The trace product contained a triplet (δ 6.94, J = 7.8 Hz, 1H) and two doublets (δ 6.68, J = 8.4 Hz, 1H, and δ 6.58, J = 8.0 Hz, 1H) in the baseline of the aromatic region of the ^{1}H NMR spectrum, and a ^{31}P{^{1}H} NMR resonance (δ 198) consistent with the expected product (^{15c5}NCOP)Pd(OAc).

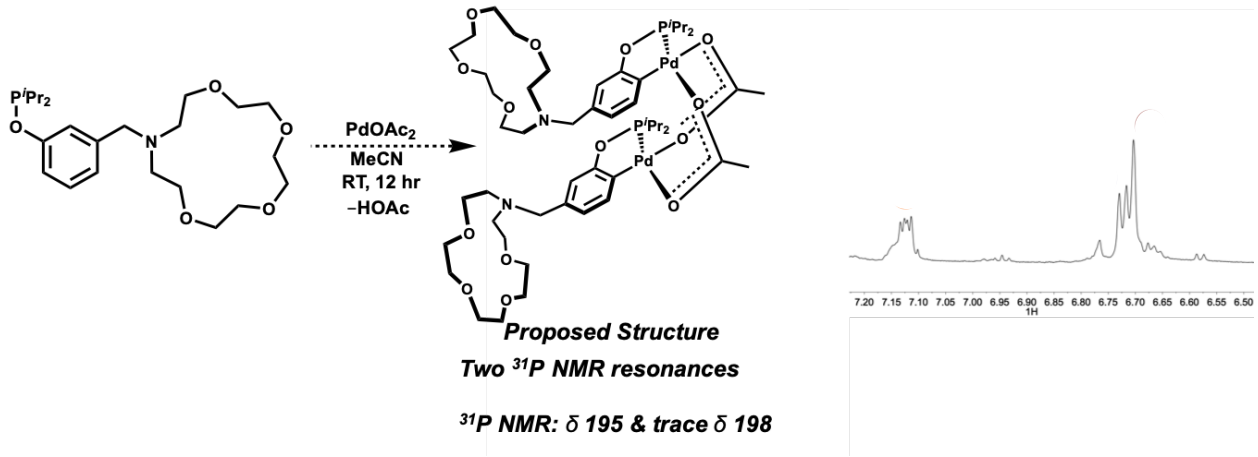

Figure 2.5. Attempted preparation of (^{15c5}NCOP)Pd(OAc) and ^{1}H NMR spectrum of the aromatic region of the product.

An alternative route to (^{15c5}NCOP)Pd(OAc) was sought via salt metathesis of (^{15c5}NCOP)Pd(Br) with AgOAc,[71] where acetate coordination would be driven by precipitation of insoluble AgBr (Scheme 2.3). Surprisingly, the expected product of salt metathesis, (^{15c5}NCOP)Pd(OAc), was observed in a 1:1 ratio with the proposed dimeric Pd species by ^{1}H NMR spectroscopy. This observation suggested that there must be adventitious protons in solution, given that the proposed dimeric Pd species contains an extra proton relative to both the cyclometalated starting material (^{15c5}NCOP)Pd(Br) and the expected cyclometalated product (^{15c5}NCOP)Pd(OAc).

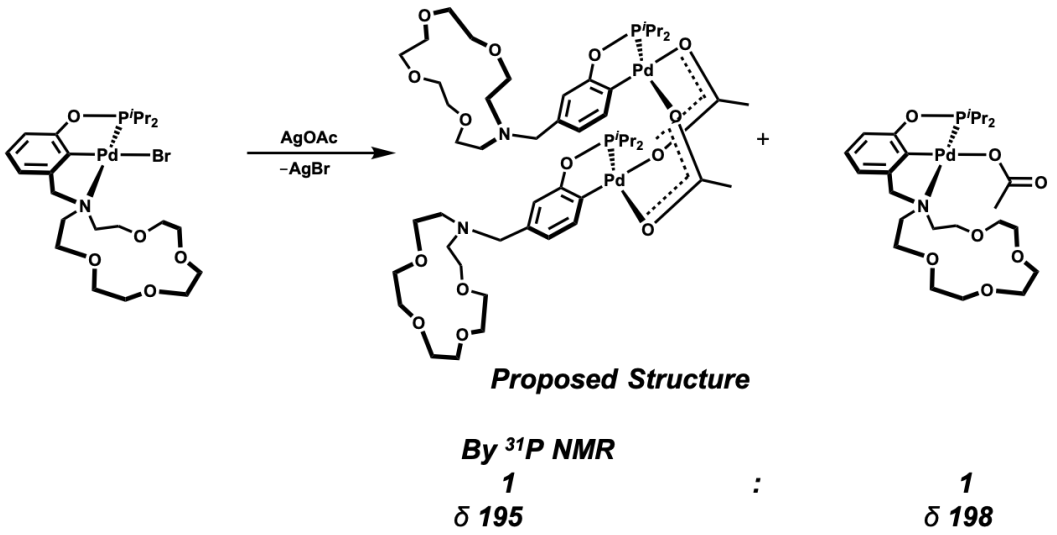

Scheme 2.3. Salt metathesis of (^{15c5}NCOP)Pd(Br) with AgOAc.

Suspicious that adventitious protons may be facilitating remetalation chemistry on the pincer ligand backbone under the salt metathesis conditions with AgOAc, we employed the use of excess base in the reaction (Scheme 2.4). After adding excess triethylamine (7 equivalents) to a solution of (^{15c5}NCOP)Pd(Br), one equivalent of AgOAc was added to achieve full conversion to the expected cyclometalated (^{15c5}NCOP)Pd(OAc) by ^{1}H NMR and ^{31}P{^{1}H} NMR spectroscopy (δ 198). A triplet (δ 6.94, J = 7.8 Hz, 1H) and two doublets (δ 6.68, J = 8.4 Hz, 1H, and δ 6.58, J = 8.0 Hz, 1H) were observed in the aromatic region of the ^{1}H NMR spectrum, consistent with the expected cyclometalated product (^{15c5}NCOP)Pd^{II}(OAc).

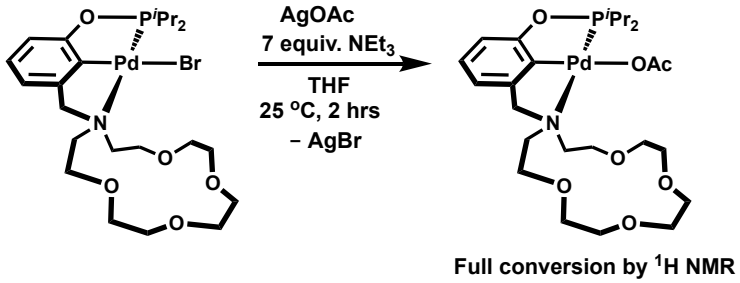

Scheme 2.4. Modified preparation of (^{15c5}NCOP)Pd(OAc).

Synthetically Blocking Ancillary Ligand Reactivity

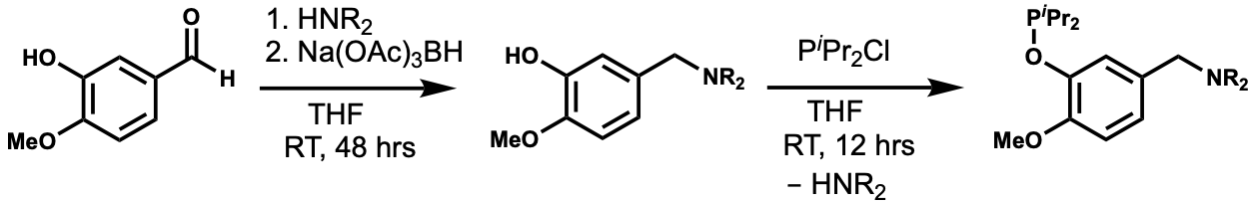

Scheme 2.5. Preparation of methoxy-blocked aminophosphinite pincer ligands. HNR_2 = aza-15-crown-5, $HNEt_2$, $HN(CH_2CH_2OCH_3)_2$.

The observation of undesired ligand reactivity at the aromatic C–H bond *para* to the aza-crown ether highlighted the need to redesign the ligand scaffold for its further implementation in synthesis and catalysis. In order to protect the reactive aromatic position, we prepared a new methoxy-blocked aminophosphinite ligand $^{15c5}N^{MeO}$COP-H in hopes that the installation of the methoxy blocking group would prevent unwanted cyclometallation to form bidentate chelates and any other potential backbone activation. The methoxy-blocked aminophosphinite ligand, $^{15c5}N^{MeO}$COP-H ($^{31}P\{^1H\}$ NMR δ 153), was prepared in a two-step synthesis from 3-hydroxy-4-methoxybenzaldehyde (Scheme 2.5).[61]

Synthesis of ($^{15c5}N^{MeO}$COP)Pd^{II}(OAc) and ($^{15c5}N^{MeO}$COP)Pd^{II}(Br)

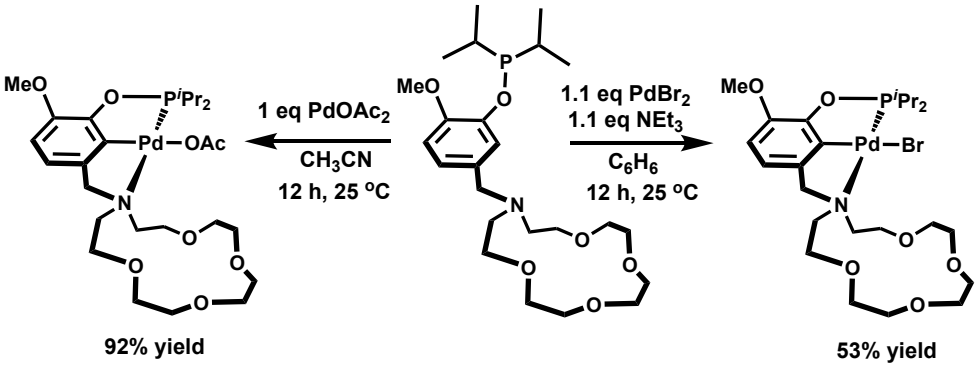

Scheme 2.6. Synthesis of ($^{15c5}N^{MeO}$COP)Pd(OAc) and ($^{15c5}N^{MeO}$COP)Pd(Br).

The cyclometallated acetate complex (^{15c5}N^{MeO}COP)Pd(OAc) was obtained in 92% yield after allowing the ^{15c5}N^{MeO}COP-H ligand to stir in acetonitrile in the presence of $Pd(OAc)_2$ at room temperature for twelve hours ($^{31}P\{^1H\}$ NMR δ 199) (Scheme 2.6). Two doublets (δ 6.65, J = 8.1 Hz, 1H; δ 6.60, J = 8.0 Hz, 1H) corresponding to the aryl backbone were observed in the aromatic region of the ^{1}H NMR spectrum, and are slightly upfield of the aromatic resonances of the unblocked complex as might be expected from a more electron rich arene backbone. Notably, no base was required to achieve the desired metalation product, unlike the synthesis of (^{15c5}NCOP)Pd(OAc) with the unblocked ligand. Light yellow crystals of (^{15c5}N^{MeO}COP)Pd(OAc) suitable for X-ray diffraction were grown from the slow evaporation of pentane (Figure 2.6). (^{15c5}N^{MeO}COP)Pd(OAc) co-crystallized with acetic acid that interacted via hydrogen bonding to the acetate ligand on Pd . This result led to employing an aqueous treatment to remove any excess acetic acid by washing the product with deionized water, and extracting into dichloromethane. The absence of acetic acid was confirmed by ^{1}H NMR spectroscopy post-aqueous workup.

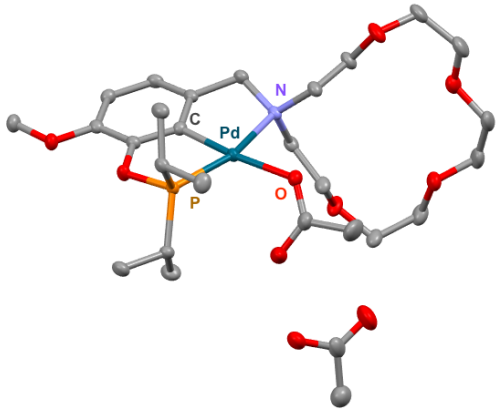

Figure 2.6. Structure of (^{15c5}N^{MeO}COP)Pd(OAc)•HOAc is presented with thermal ellipsoids shown at 50% probability density. Hydrogen atoms are omitted for clarity.

The bromide complex (^{15c5}N^{MeO}COP)Pd(Br) ($^{31}P\{^1H\}$ NMR δ 205) was prepared by adding a solution of ^{15c5}N^{MeO}COP-H ligand and triethylamine in benzene to $PdBr_2$. The reaction

mixture was allowed to stir for twelve hours, after which it was dried *in vacuo* and washed with pentane to afford a yellow solid in 53% yield (Figure 2.7). Two doublets (δ 6.71, J = 8.2 Hz, 1H, and δ 6.63, J = 8.2 Hz, 1H) corresponding to the aryl backbone were observed in the aromatic region of the ^{1}H NMR spectrum. Two doublet of doublets (δ 1.43, J = 19.1, 7.2 Hz, 6H, and δ1.32, J = 16.0, 7.0 Hz, 6H) corresponding to the isopropyl methyl protons, consistent with a square-planar cyclometalated species, were observed. Amber-orange crystals of (^{15c5}N^{MeO}COP)Pd(Br) that were suitable for X-ray diffraction were grown by layering a concentrated solution of (^{15c5}N^{MeO}COP)Pd(Br) in toluene with pentane (Figure 2.7).

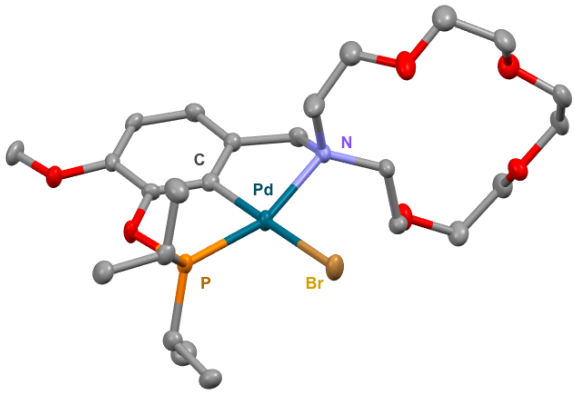

Figure 2.7. Structure of (^{15c5}N^{MeO}COP)Pd(Br) is presented with thermal ellipsoids shown at 50% probability density. Hydrogen atoms are omitted for clarity.

Synthesis of (15c5N^{MeO}COP)Pd^{II}(Cl)

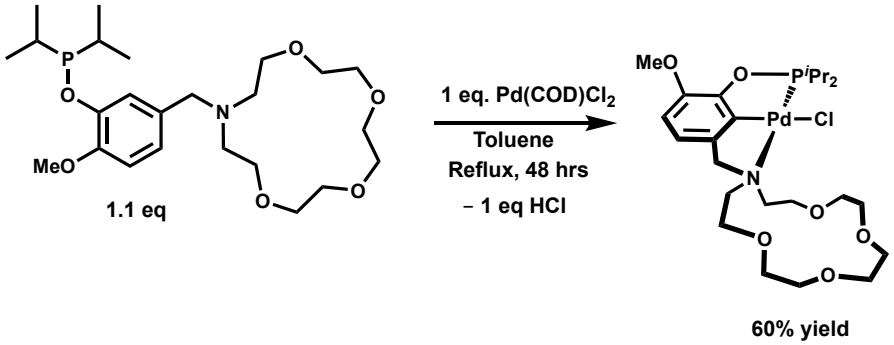

Scheme 2.7. The synthesis of (^{15c5}N^{MeO}COP)Pd(Cl).

A palladium chloride complex of the methoxy-blocked pincer-crown ether ligand was prepared in 60% yield by refluxing of (cod)Pd(Cl)$_2$ in the presence of 1.1 equivalents of ^{15c5}N^{MeO}COP-H ligand in toluene for 48 hours (Scheme 2.7). The ^{1}H NMR spectrum features two doublets δ 6.66 and δ 6.58 in the aromatic region, as well as a heptet and two sets of doublets of doublets in the aliphatic region, consistent with a cyclometalated pincer complex of C$_s$ symmetry in solution. The ^{31}P{^{1}H} NMR spectrum contains a singlet δ 203.

Synthesis of (^{15c5}N^{MeO}COP)Pd(CF$_3$)

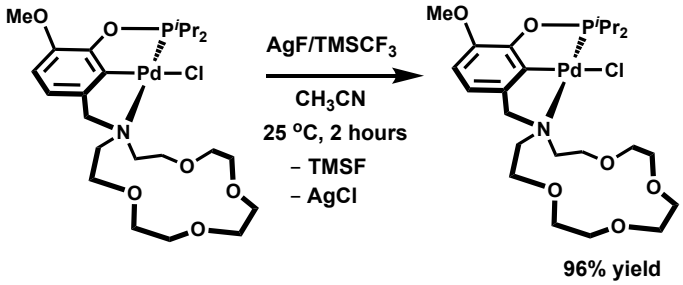

Scheme 2.8. Synthesis of (^{15c5}N^{MeO}COP)Pd(CF$_3$).

The trifluoromethyl complex (^{15c5}N^{MeO}COP)Pd(CF$_3$) was synthesized by salt metathesis of (^{15c5}N^{MeO}COP)Pd(Cl) with AgCF$_3$ (generated *in situ* from AgF and TMSCF$_3$)[79] in acetonitrile

(Scheme 2.8). Two doublets (δ 6.70, J = 7.9 Hz, δ 6.59, J = 8.2 Hz) corresponding to the aromatic backbone, as well as a septet (δ 2.37, J = 6.9) corresponding to the isopropyl methines can be observed in the ^{1}H NMR spectrum, consistent with C_s symmetry in solution. A quartet (δ 200.7, J = 9.1 Hz) is observed in the ^{31}P NMR spectrum, consistent with fluorine-phosphorus coupling due to incorporation of the trifluoromethyl group in the primary coordination sphere. In the ^{19}F NMR spectrum, a resonance at δ –21.51 ($J^{P\text{-}F}$ = 7.5 Hz) corresponds to the Pd—CF_3, similar to previously reported POCOP Ni and Pd trifluoromethyl complexes.[79]

Diversifying the N-donor on the Aminophosphinite Pincer Ligand Scaffold

Synthesis of (^{MeOEt}N^{MeO}COP)Pd(Cl) and of (^{Et}N^{MeO}COP)Pd(Cl)

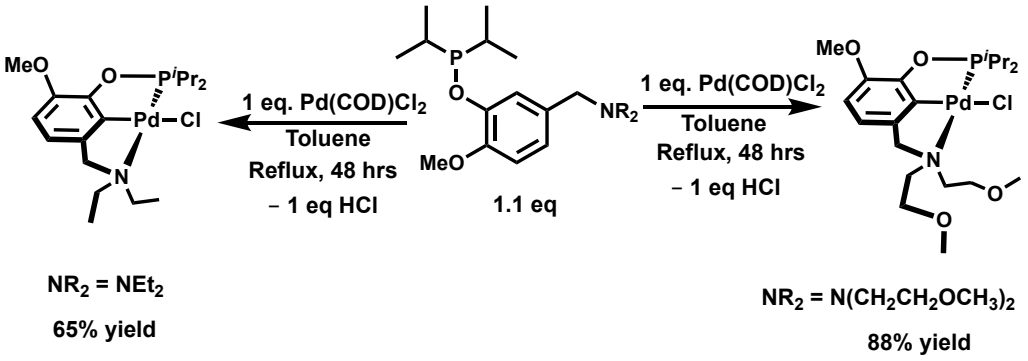

Scheme 2.9. The synthesis of (^{Et}N^{MeO}COP)Pd(Cl) and (^{EtMeO}N^{MeO}COP)Pd(Cl).

The amine substituents are expected to play a critical role in catalysis, so a series varying the structure of the amine donor was developed. To complement the complexes with ligands containing a 15-aza-crown-5 ether macrocycle, a diethylamine analogue lacking ether functionality and a bis(methoxy)diethylamine analogue with non-cyclic ethers were prepared (Scheme 2.9).

Two chloride complexes supported by these aminophosphinite ligands were prepared according to the same procedure as the macrocycle-containing analogue, Scheme 2.9. Both complexes displayed C_s symmetry in solution, consistent with cyclometalated species and the macrocycle-containing analogues. X-ray quality crystals of (^{MeOEt}NCOP)Pd(Cl) were grown in hexane at -35 °C.

Synthesis of Cationic (NCOP)Pd^{II} Complexes

Synthesis of [($^{15c5}N^{MeO}$COP)Pd]$^+$

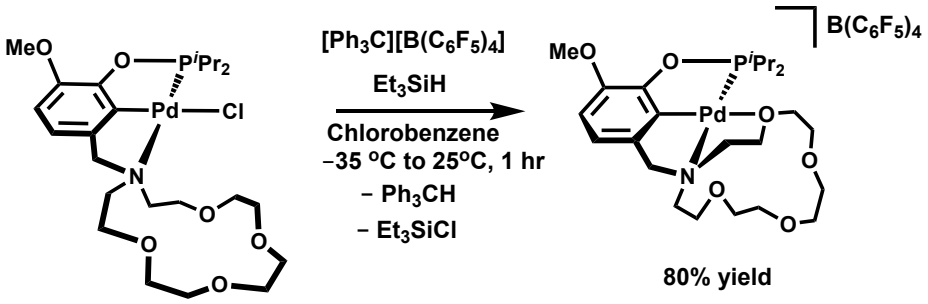

Scheme 2.10. Synthesis of [($^{15c5}N^{MeO}$COP)Pd][B(C$_6$F$_5$)$_4$].

Halide abstraction from the chloride, bromide, or acetate complexes ($^{15c5}N^{MeO}$COP)Pd(X) proved challenging. Attempts with salts of sodium, potassium, thallium, and trityl cation resulted in either partial conversion of simple salt interaction with the crown ether macrocycle without halide abstraction. Halide abstraction obtained using $AgPF_6$, however, leads to the formation of a cationic Pd(II) species, determined by high-resolution mass spectrometry and NMR spectroscopy. The presence of persistent silver impurities was confirmed by ICP-MS (inductively-coupled mass spectrometry) to a Pd:Ag ratio of 2.4:1, hampering utilization of this procedure.

The only method discovered for clean halide abstraction from ($^{15c5}N^{MeO}$COP)Pd(Cl) relied on *in situ* generated [Et$_3$Si]$^+$, Scheme 2.10.[80–82] Silylium cation is generated via the

addition of a slight excess of triethylsilane (1.1 equivalents) to a solution of trityl tetrakis(pentafluorophenyl)borate in chlorobenzene. A solution of neutral ($^{15c5}N^{MeO}COP$)Pd(Cl) is then added dropwise to the solution of $[Et_3Si][B(C_6F_5)_4]$ and stirred at room temperature for two hours, dried *in vacuo*, and washed several times with pentane to remove the triphenylmethane byproduct. The palladium-containing product is then dissolved in ether, filtered through a short alumina plug, and dried *in vacuo* to give a white powder $[(^{15c5}N^{MeO}COP)Pd][B(C_6F_5)_4]$ in 80 % yield, and confirmed by mass spectrometry.

Critically, slightly more than one equivalent of silylium must be generated *in situ* to ensure complete halide abstraction. Initial attempts to prepare the cationic species with less than one equivalent of silylium cation resulted in a broad, C_s symmetric palladium species in solution by ^{1}H NMR spectroscopy. We suspected that we may be forming bridging mono-halide dimers resulting from one cationic species coordinating to one neutral chloride species, $[Pd^{II}\text{-}X\text{-}Pd^{II}]^+$, as observed in two previous reports of aminophosphinite-supported palladium pincer complexes, Figure 2.8.[49,64] To test this hypothesis, a 1:1 mixture of the neutral ($^{15c5}N^{MeO}COP$)Pd^{II}(Cl) and the cationic $[(^{15c5}N^{MeO}COP)Pd][B(C_6F_5)]$ was dissolved in CD_2Cl_2 and analyzed by ^{1}H and $^{31}P\{^1H\}$ NMR spectroscopy. Only one broad species was observed, matching the spectra of the partial halide abstractions and those of the unknown Pd species generated in the presence of only 0.5 equivalents silylium cation.

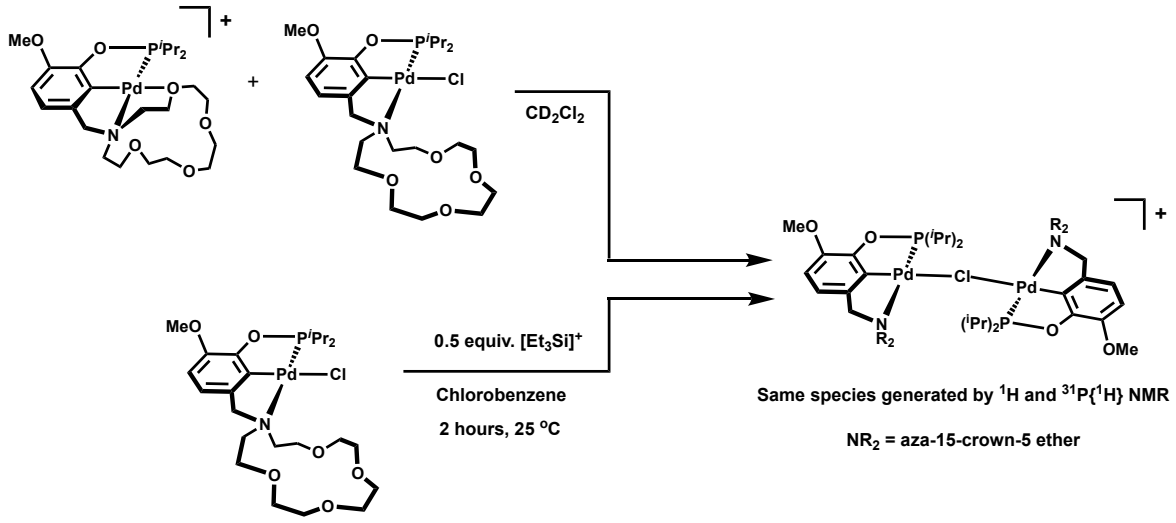

Figure 2.8. Proposed formation of bridging $[Pd^{II}\text{-Cl-}Pd^{II}]^+$ species.

Synthesis of [(MeOEtNMeOCOP)Pd]+

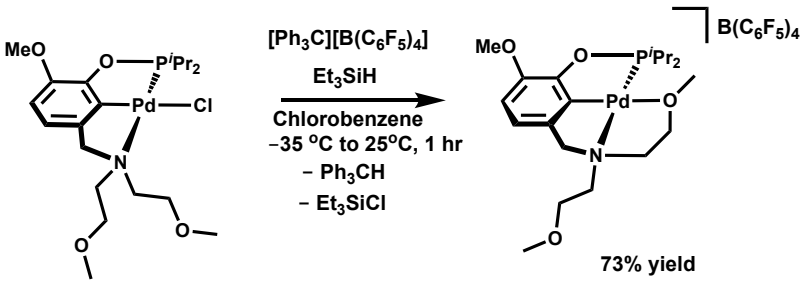

Scheme 2.11. Synthesis of $[(^{MeOEt}N^{MeO}COP)Pd][B(C_6F_5)_4]$.

Halide abstraction from $(^{MeOEt}N^{MeO}COP)Pd(Cl)$ by *in situ* generated $[Et_3Si]^+$ proceeds cleanly to form the cationic species $[(^{MeoEt}N^{MeO}COP)Pd][BAr^{F20}{}_4]$ in 73% yield, Scheme 2.11. High-resolution mass spectrometry electron spray ionization (HRMS-ESI) confirmed a cationic species. Similarly to the macrocycle-containing species, a 1:1 ratio of the cationic $[(^{MeoEt}N^{MeO}COP)Pd][BAr^{F20}{}_4]$ and the neutral $^{MeOEt}N^{MeO}COP)Pd(Cl)$ complexes generates one broad, C_s symmetric species in solution, characterized by ^1H NMR and $^{31}P\{^1H\}$ NMR spectroscopy, and proposed to be a bridging mono-chloride cationic dimer, $[Pd^{II}\text{-Cl-}Pd^{II}]^+$.

Synthesis of [($^{Et}N^{MeO}$COP)Pd]$^+$

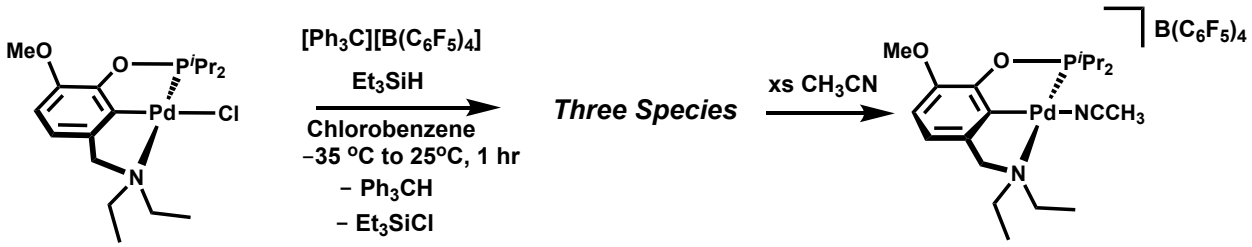

Scheme 2.12. Halide abstraction of ($^{Et}N^{MeO}$COP)Pd(Cl) with silylium cation generated *in situ*.

Halide abstraction of the diethylamino-substituted chloride complex ($^{Et}N^{MeO}$COP)Pd(Cl) by $[Et_3Si]^+$ yields three species in the ^{1}H NMR spectrum that appear to be in dynamic exchange, Scheme 2.12. With no intramolecular ether donors, we suspect that there is competitive binding of the Pd center by any available donors in solution. It is very sensitive to Lewis basic donors in solution, and the speciation changes in solution in the presence of excess ether, thf, or acetonitrile. Addition of excess acetonitrile (approximately 100 equiv.) converts the mixture to a single species assigned as the cationic acetonitrile complex. By HRMS-ESI, a sample in methylene chloride and acetonitrile contained *m/z* 430.11362 and *m/z* 471.14028, corresponding to the cationic complex with no ligand *trans* to the phenyl backbone, and to a cationic nitirile species, respectively. Additionally, an *m/z* 897.19674 is also observed, corresponding to a bridging cationic mono-chloride dimer. This species is stable to filtration over alumina in ether, and can be stored as an off-white solid at –35 °C. Notably, two other bridging dimers of aminophosphinite palladium complexes have been reported, one a bridging chloride dimer,[49] and the other a bridging hydride species.[64] Synthetic attempts to generate one cationic species in solution in the absence of acetonitrile were unsuccessful. Synthetic modifications such as increasing the reaction time, lowering the reaction temperature, changing the order of addition of

palladium to silylium cation, or reactions in excess silylium (2 equiv.) all resulted in a mixture of three cationic species by ^{1}H NMR, including the bridging halide dimer by mass spectrometry.

Attempts to Synthesize Pd^{IV} Complexes

With an arsenal of neutral pincer crown ether palladium complexes in hand, their reactivity with electrophilic alkyl reagents was probed to see if Pd^{IV} could be accessed with our aminophosphinite ligand scaffold. Complexes of Pd^{IV} have been known since 1986, with the first reported high valent structure by Canty and coworkers of a bipyridine supported *fac*-[(bpy)Pd$(CH_3)_3$(I)] octahedral complex.[83] While some Pd^{IV} complexes can be isolated,[47,83–85] many undergo C-C or C-X reductive elimination to form more stable Pd^{II} species or decomposition products. The high valent intermediates can either be observed spectroscopically at low temperature,[86–90] or are proposed intermediates in catalytic reactions.[91–94] Notably, two examples of Pd^{IV} CNN[95] and NCN[96] pincer complexes were reported by van Koten and coworkers from the oxidation of neutral Pd^{II} species with Cl_2 or $PhICl_2$. While both Pd^{IV} species could be characterized spectroscopically, both underwent facile decomposition at room temperature. We were encouraged by an example from Willis and coworkers[36] that showed the preparation of a Pd^{IV} methyl complex that was stabilized by a hemilabile cyclic thioether (Figure 1.8) This reported complex was stable to reductive elimination, and we hoped that our macrocycle-containing pincer scaffold might stabilize Pd^{IV} in a similar fashion. Below is a summary of our attempts to access Pd^{IV} with a selection of electrophilic reagents previously reported to be successful in oxidizing Pd^{II} to attain high valent Pd^{IV}.[46]

Addition of Methyl Iodide to ($^{15c5}N^{MeO}$COP)Pd(X)

In the presence of excess (6 equiv.) methyl iodide, halide complexes ($^{15c5}N^{MeO}$COP)Pd(X) (X = Cl, Br or OAc), converted quantitatively to the corresponding ($^{15c5}N^{MeO}$COP)Pd(I) and an equivalent of MeX (X = Cl, Br or OAc) by ^{1}H NMR spectroscopy, respectively, in deuterated dichloromethane (Figure 2.9). The reaction solutions for all three complexes with methyl iodide became a darker yellow upon conversion to ($^{15c5}N^{MeO}$COP)Pd(I) ($^{31}P\{^{1}H\}$ NMR δ 208)**.** The identity of ($^{15c5}N^{MeO}$COP)Pd(I) as a bright yellow product was confirmed by its independent synthesis from ($^{15c5}N^{MeO}$COP)Pd^{II}(Br) and five equivalents of potassium iodide, with a $^{31}P\{^{1}H\}$ NMR resonance at δ 208, and the precipitation of potassium bromide as a by-product.

Addition of Trimethyloxonium Tetrafluoroborate to ($^{15c5}N^{MeO}$COP)Pd(X)

The addition of trimethyloxonium tetrafluoroborate, $[Me_3O][BF_4]$, to ($^{15c5}N^{MeO}$COP)Pd^{II}(Cl) ($^{31}P\{^{1}H\}$ NMR s, δ 205) in dichloromethane led to the production of approximately half an equivalent of MeCl and dimethyl ether by ^{1}H NMR spectroscopy, as well as the full conversion to a new palladium species with fluxional behavior apparent by ^{1}H and $^{31}P\{^{1}H\}$ NMR spectroscopy (Figure 2.9). The NMR spectra are consistent with a square-planar Pd^{II} complex of C_s symmertry. Interestingly, this product Pd complex matched the ^{1}H NMR spectrum of halide abstractions performed with only 0.5 eq silylium in solution, and is proposed to be a a bridging mono-halide cationic dimer, $[Pd^{II}\text{-X-}Pd^{II}]^{+}$. No Pd^{IV} intermediates or products were observed by ^{1}H NMR spectroscopy, where a break in the C_s symmetry would be expected upon coordination of the electrophilic methyl to Pd in the axial position.

Addition of other electrophilic reagents to ($^{15c5}N^{MeO}$COP)Pd(X)

No reaction was observed upon treatment of ($^{15c5}N^{MeO}$COP)Pd(X) with bis(4-methylphenyl)iodonium hexafluorophosphate, $[(CH_3C_6H_4)_2I][PF_6]$, in CD_2Cl_2 at 25 °C. Treatment of $^{15c5}N^{MeO}$COP)Pd(X) with an electrophilic trifluoromethyl source (CF_3^+), 3,3-dimethyl-1-(trifluoromethyl)-1,2-benziodoxole (Togni's reagent) also gave no reaction at 25 °C in CD_2Cl_2. Finally, treatment of ($^{15c5}N^{MeO}$COP)Pd(X) with X^+ sources, such as hypervalent iodonium salt $PhI(OAc)_2$ and Br_2, were also unsuccessful in preparing Pd^{IV} species, and resulted in no reaction and decomposition, respectively.

While the production of CH_3X from the addition of $[Me_3O][BF_4]$ to the neutral ($^{15c5}N^{MeO}$COP)Pd(X) complexes could be accessed through Pd^{IV} intermediates, halide abstraction by the electrophilic reagent could not be discounted. We next explored accessing Pd^{IV} complexes from our trifluoromethyl precursor, to ($^{15c5}N^{MeO}$COP)Pd(CF_3), since there is precedent in the literature for the stabilization of high valent palladium and nickel trifluoromethyl complexes,[97,98] and because we hoped we could circumvent formation of bridging dimers of the ($^{15c5}N^{MeO}$COP)Pd(CF_3), since CF_3 should be a poor bridging ligand to a cationic Pd center in a bridging dimer species.

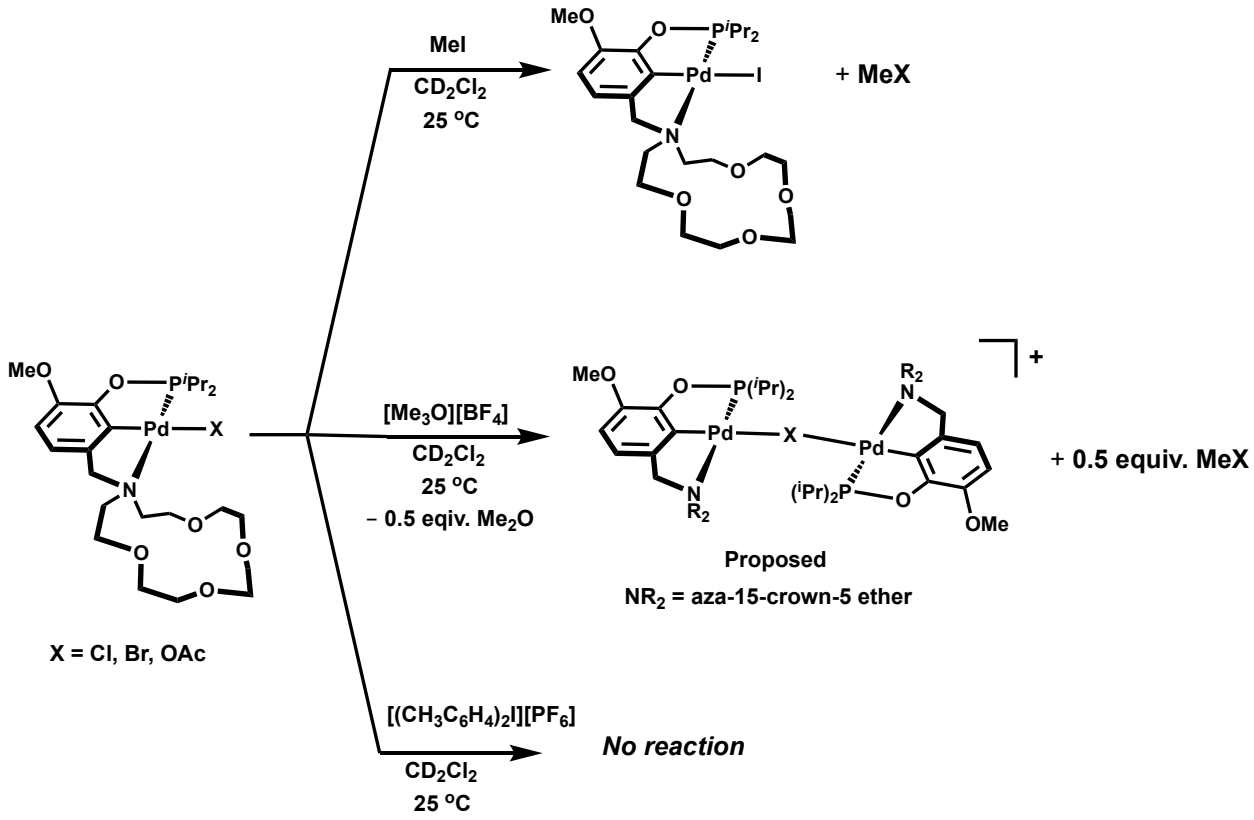

Figure 2.9. Reactivity of ($^{15c5}N^{MeO}$COP)Pd(X) complexes with alkyl electrophiles.

Attempts to synthesize Pd(IV) from ($^{15c5}N^{MeO}$COP)Pd(CF_3)

The trifluoromethyl complex ($^{15c5}N^{MeO}$COP)Pd(CF_3) was considered likely to be less likely to undergo direct electrophilic attack than halide complexes, motivating reactivity explorations with a range of electrophiles.

In deuterated methylene chloride, no changes were observed in the ^{1}H, $^{31}P\{^{1}H\}$, or $^{19}F\{^{1}H\}$ spectra of ($^{15c5}N^{MeO}$COP)Pd(CF_3) after a week at room temperature in the presence of methyl iodide. This is a distinctly different outcome than the addition of methyl iodide to other ($^{15c5}N^{MeO}$COP)Pd(X), which slowly converted to the iodide complex and produced one equivalent of MeX.

Like the ($^{15c5}N^{MeO}$COP)Pd(X) halides, no reactivity was observed with the trifluoromethyl ($^{15c5}N^{MeO}$COP)Pd(CF_3) in the presence of the hypervalent iodonium salt, [$(CH_3C_6H_4)_2I$][PF_6]. No aryl-CF_3 coupling or new Pd species were detected by NMR spectroscopy, even after two weeks in solution at 25 ºC.

The addition of [Me_3O][BF_4] to ($^{15c5}N^{MeO}$COP)Pd(CF_3), however, results in the formation of a new Pd species in the ^1H and $^{31}P\{^1H\}$ NMR spectra, along with the production of MeF detected by a quartet in the ^{19}F NMR spectrum (δ –270) and a singlet $^{19}F\{^1H\}$ NMR spectrum (δ –270). No $^{19}F\{^1H\}$ resonance corresponding to a Pd-CF_3 fragment was detected, and this new Pd species contains no P-F coupling in the $^{31}P\{^1H\}$ NMR spectrum (δ 199), indicative of loss of the CF_3 ligand.

Precedent in the literature has demonstrated the production of a carbonyl complex, (POCOP)Pd(CO) from a trifluoromethyl complex (POCOP)Pd(CF_3) via fluoride abstraction by Lewis acidic boranes in the presence of trace protons.[79] The borane is proposed to first abstract F^- from the CF_3 ligand to form a Pd carbene. In the presence of trace water, it is proposed to then form a carbonyl Pd complex with the loss of HF. While more characterization is necessary to determine the outcome of this reaction, we tentatively propose that [Me_3O][BF_4] may be acting as an F^- abstractor, making a carbene complex *in situ* to form a Pd carbonyl complex and methyl fluoride, as shown in Figure 2.10.

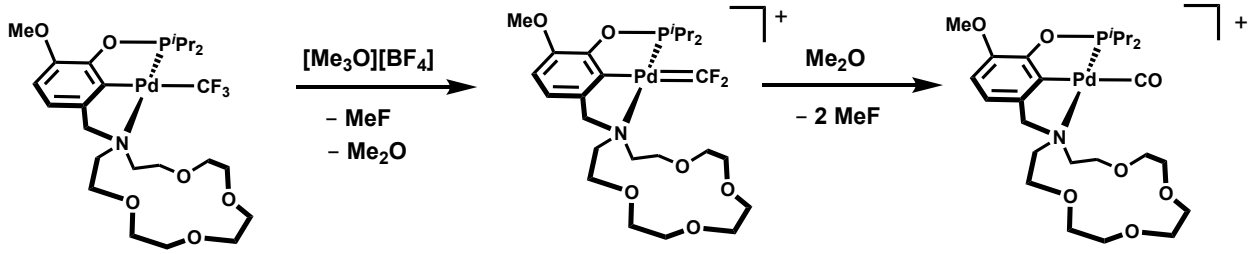

Figure 2.10. Proposed F^- abstraction to form ($^{15c5}N^{MeO}COP$)Pd(CO) complex.

Summary and Conclusions:

A series of neutral palladium pincer complexes supported by three distinct aminophosphinite ligands of varying hemilability was prepared. It was found that the neutral chloride complex, (^{15c5}NCOP)Pd(Cl) had the highest binding affinity for Li^+ (294 M^{-1}) of group 10 pincer crown ether complexes. Installation of a methoxy group on the pincer ligand backbone proved essential for ensuring productive metalation, as well as to prevent ancillary ligand activation. The halide abstraction of these neutral complexes to afford their cationic analogues has also been described, and required the use of *in situ* generated silylium. Incomplete halide abstraction resulted in bridging cationic dimers of [Pd^{II}-X-Pd^{II}] configuration, as shown in mass spectrometry. Attempts to synthesize or observe Pd^{IV} complexes from neutral ($^{15c5}N^{MeO}COP$)Pd(X) and ($^{15c5}N^{MeO}COP$)Pd(CF_3) complexes were unsuccessful, and instead the formation of bridging [Pd^{II}-X-Pd^{II}] cationic dimers was observed. This work has produced a library of novel aminophosphinite-supported palladium complexes, paving the groundwork for future reactivity and catalytic studies.

Experimental Section

General Considerations

All reactions were performed under an inert nitrogen atmosphere, utilizing standard vacuum line and glovebox techniques unless otherwise noted. All NMR-scale reactions were prepared in a glovebox and monitored in Teflon-sealed NMR tubes. Organic solvents were dried and degassed with argon using a Pure Process Technology solvent system and stored over 3 Å molecular sieves. Under standard glovebox operating conditions, pentane, diethyl ether, benzene, toluene, and tetrahydrofuran were used without purging, so traces of those solvents were present in the atmosphere and in the solvent bottles. High resolution mass spectra were collected on a ThermoScientific Q Exactive HF-X with a mass range of 50 to 4,000 Da, and resolution up to 100,000 at *m/z* 400 at 1 Hz, >750,000 at *m/z* 400 at slower scan repetition rates. ^{1}H NMR spectra were recorded on 400, 500, or 600 MHz spectrometers. NMR characterization data are reported at 25 °C, unless specified otherwise. All of the NMR solvents were purchased from Cambridge Isotopes Laboratories. Methylene chloride-d_2 (CD_2Cl_2) was freeze− pump−thaw-degassed three times, dried by passage through a small column of activated alumina, and stored over 3 Å molecular sieves. ^{1}H chemical shifts are reported in parts per million relative to residual protio solvent resonances. ^{Et}NCOP-H, ^{15c5}NCOP-H, were synthesized according literature procedures.[61] $NaBAr^{F}_{4}$ and $LiBAr^{F}_{4}*(Et_2O)_3$ were prepared according to literature procedure.[99] All of the other reagents were commercially available and used without further purification. Single-crystal X-ray diffraction data were collected on a Bruker Smart Apex-II diffractometer at 100 ± 2 K with Cu Kα radiation (λ = 1.54175 Å). Diffraction profiles were integrated using the SAINT software program. Absorption corrections were applied using SADABS. The structure was solved using direct methods and refined using the XL refinement package via the least-squares method.

Hydrogen atoms were generated theoretically and refined isotropically with fixed thermal factors.

Synthesis of (^{15c5}NCOP)Pd(Br)

A 20 mL vial was charged with $PdBr_2$ (71.0 mg, 0.267 mmol), ^{15c5}NCOP (98.2 mg, 0.222 mmol), and triethylamine (32.0 uL, 0.230 mmol) in benzene (5 mL). The yellow solution turned amber after stirring for three hours at room temperature. The reaction was allowed to stir at room temperature overnight, and was concentrated after 24 hours to a yellow-orange oil. The crude product was extracted with ether, filtered, and dried *in vacuo* to afford a yellow-orange powder (103.0 mg, 74% yield). ^{1}H NMR (400 MHz, Methylene Chloride-d_2) δ 6.95 (td, J = 7.8, 1.3 Hz, 1H), 6.70 (d, J = 7.5 Hz, 1H), 6.60 (d, J = 7.9 Hz, 1H), 4.45 (s, 2H), 4.14 (ddd, J = 11.3, 6.7, 4.6 Hz, 2H), 4.04 – 3.86 (m, 2H), 3.78 – 3.50 (m, 16H), 3.41 (dddd, J = 13.5, 6.5, 4.9, 1.4 Hz, 2H), 2.39 (dq, J = 14.1, 7.0 Hz, 2H), 1.49 – 1.34 (m, 7H), 1.34 – 1.13 (m, 9H). ^{31}P{^{1}H} NMR (162 MHz, Chloroform-d) δ 203.05

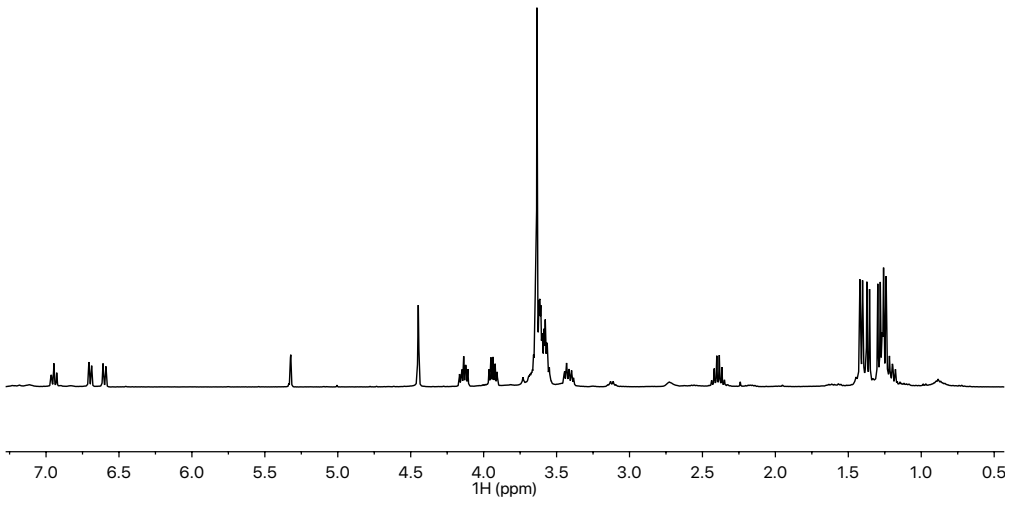

Figure 2.11. ^{1}H NMR spectrum of (^{15c5}NCOP)Pd(Br) in CD_2Cl_2.

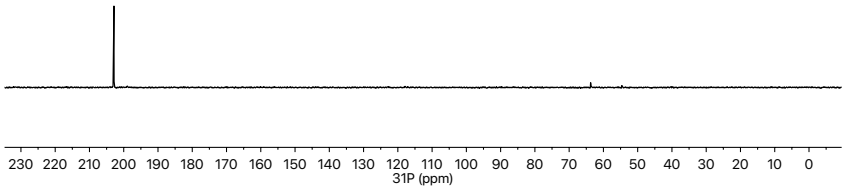

Figure 2.12. $^{31}P\{^{1}H\}$ NMR spectrum of (^{15c5}NCOP)Pd*(*Br*)* in $CDCl_3$.

Synthesis of $^{15c5}N^{MeO}$COP-H

A 20 mL vial was charged with $^{15c5}N^{MeO}$COH (155.7 mg, 0.438 mmol) and triethylamine (70 uL, 0.502 mmol) in THF (3 mL), and was placed in a freezer at -35 ^{o}C for 10 minutes. Another vial of THF (3 mL) was also placed in the freezer for 10 minutes. To the second vial, diisopropylchlorophosphine was added (70 uL, 0.438 mmol). To the ligand solution was added the diisopropylphosphine solution, and the reaction mixture was allowed to warm up to room temperature. The reaction was allowed to stir at room temperature overnight, and was subsequently concentrated, extracted with ether, filtered through a short glass plug, and dried *in vacuo* to reveal a colorless oil (191.8 mg, 92% yield). ^{1}H NMR (400 MHz, Benzene-d_6) δ 7.60 (s, 1H), 6.96 (dd, J = 8.2, 2.1 Hz, 1H), 6.62 (d, J = 8.2 Hz, 1H), 3.66 (t, J = 6.0 Hz, 4H), 3.58 – 3.46 (m, 11H), 3.42 (d, J = 11.2 Hz, 8H), 2.88 (t, J = 6.1 Hz, 4H), 1.90 (pd, J = 7.1, 2.5 Hz, 2H), 1.30 (dd, J = 10.5, 7.0 Hz, 6H), 1.08 (dd, J = 15.4, 7.2 Hz, 6H). ^{31}P{^{1}H} NMR (162 MHz, Benzene-d_6) δ 152.82.

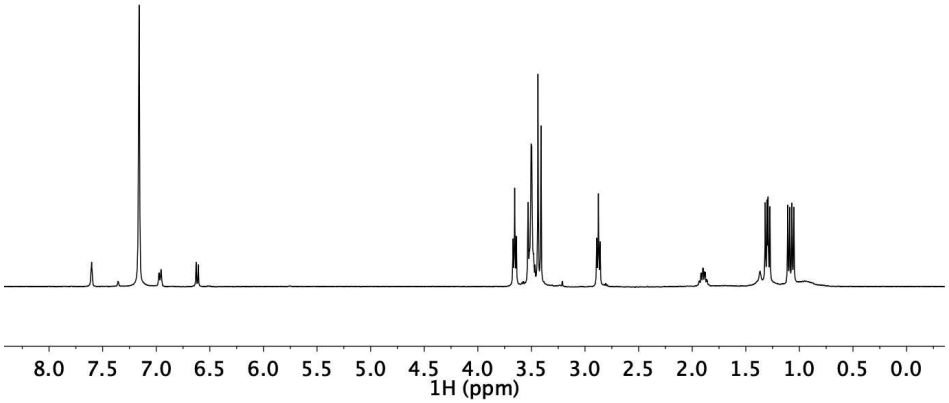

Figure 2.13. ^{1}H NMR spectrum of $^{15c5}N^{MeO}COP\text{-}H$ in C_6D_6.

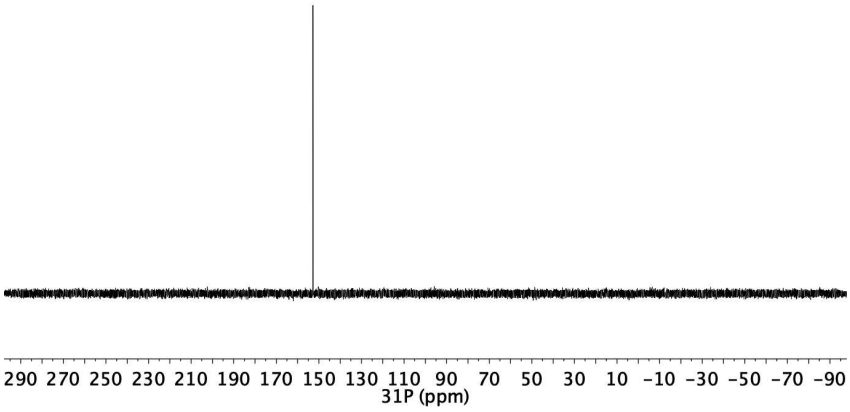

Figure 2.14. $^{31}P\{^{1}H\}$ NMR spectrum of $^{15c5}N^{MeO}COP\text{-}H$ in C_6D_6.

Synthesis of $^{Et}N^{MeO}COH$

This ligand was prepared according to the same procedure to prepare $^{15c5}N^{MeO}COH$.[100] Isovanillin (105.3 mg, 0.657 mmol) and triethylamine (70 uL, 0.657 mmol) were dissolved in THF (15 mL) and allowed to stir at room temperature under nitrogen. Triacetoxyborohydride was added in four portions over the course of twenty-four hours (152.8 mg, 0.720 mmol). The crude product was isolated and purified according to the methods described for the preparation of $^{15c5}N^{MeO}COH$ to yield a colorless waxy solid (80.0 mg, 58% yield). ^{1}H NMR (400 MHz, Chloroform-*d*) δ 6.93 (d, *J* = 1.9 Hz, 1H), 6.86 – 6.72 (m, 2H), 3.88 (s, 3H), 3.50 (s, 2H), 2.53 (q, *J* = 7.1 Hz, 4H), 1.05 (t, *J* = 7.1 Hz, 6H).

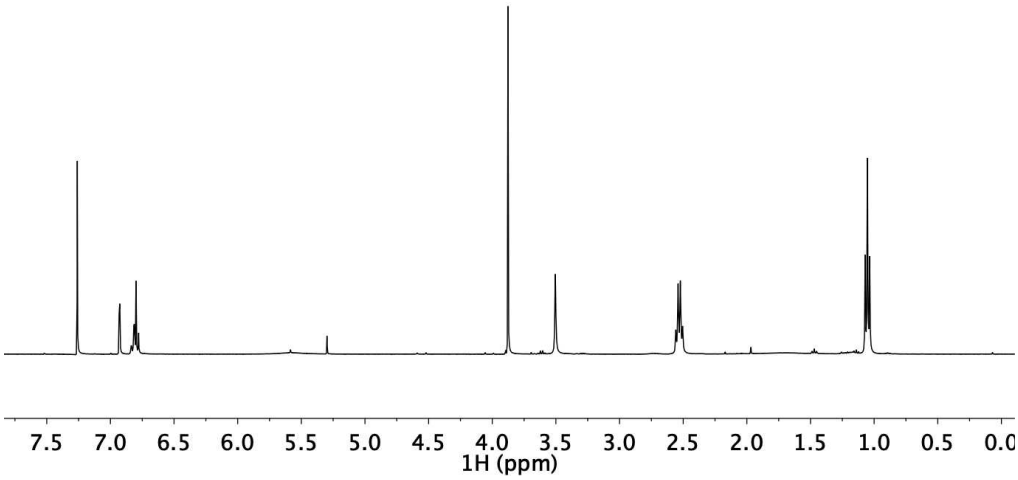

Figure 2.15. ^{1}H NMR spectrum of $^{Et}N^{MeO}COH$ in $CDCl_3$.

Synthesis of $^{Et}N^{MeO}$COP-H

This ligand was prepared according to the same method for the preparation of $^{15c5}N^{MeO}$COP-H.[100] The reaction was carried out using $^{Et}N^{MeO}$COH (65.9 mg, 0.315 mmol), triethylamine (48 uL, 0.347 mmol), and diisoproplyphosphine (50 uL, 0.315 mmol). The product was isolated and purified according to the methods described by the preparation for $^{15c5}N^{MeO}$COP-H, as a colorless waxy solid (60.0 mg, 60% yield). ^{1}H NMR (400 MHz, Benzene-d_6) δ 7.65 (s, 1H), 6.99 (dd, J = 8.2, 2.0 Hz, 1H), 6.64 (d, J = 8.2 Hz, 1H), 3.46 (s, 2H), 3.42 (s, 3H), 2.45 (q, J = 7.1 Hz, 5H), 1.89 (pd, J = 7.1, 2.6 Hz, 2H), 1.29 (dd, J = 10.4, 7.0 Hz, 7H), 1.07 (dd, J = 15.5, 7.2 Hz, 7H), 0.98 (t, J = 7.1 Hz, 8H). ^{31}P{^{1}H} NMR (162 MHz, Methylene Chloride-d_2) δ 155.71.

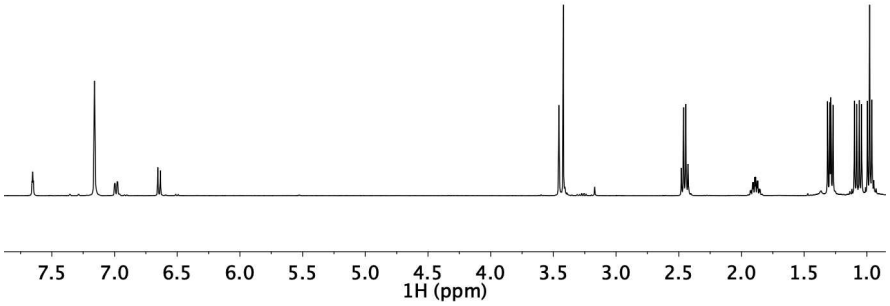

Figure 2.16. ^{1}H NMR spectrum of $^{Et}N^{MeO}$COP-H in CD_2Cl_2.

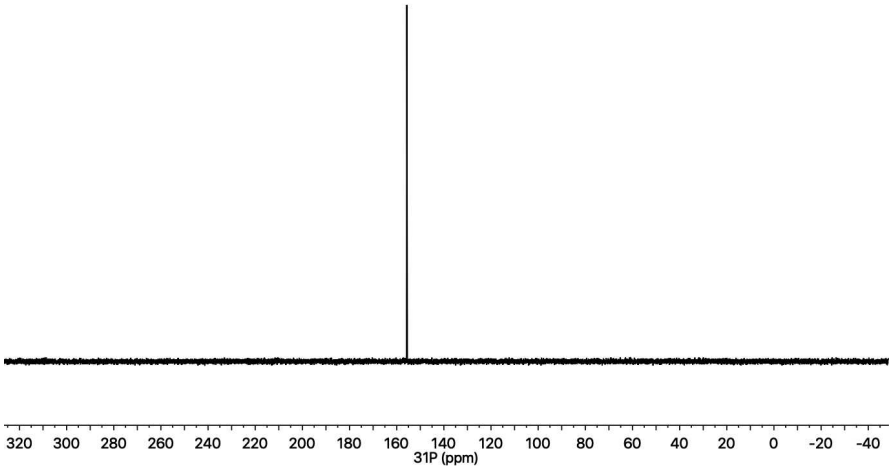

Figure 2.17. $^{31}P\{^{1}H\}$ NMR spectrum of $^{Et}N^{MeO}$COP-H in CD_2Cl_2.

Synthesis of $^{MeOEt}N^{MeO}COH$

This ligand was prepared according to the same procedure to prepare $^{15c5}N^{MeO}COH$.[100] Isovanillin (439.3 mg, 2.89 mmol) and *bis*(methoxy)ethylamine (409 μL, 2.78 mmol) were dissolved in THF (25 mL) and allowed to stir at room temperature under nitrogen. Triacetoxyborohydride was added in four portions over the course of twenty-four hours (900 mg, 4.2 mmol). The crude product was isolated and purified according to the methods described for the preparation of $^{15c5}N^{MeO}COH$ to yield a colorless waxy solid (520 mg, 1.93 mmol, 67% yield). ^{1}H NMR (400 MHz, Chloroform-*d*) δ 6.93 (d, J = 1.5 Hz, 1H), 6.79 (s, 2H), 3.87 (s, 3H), 3.62 (s, 2H), 3.48 (t, J = 6.1 Hz, 4H), 3.33 (s, 6H), 2.73 (t, J = 6.1 Hz, 4H). $^{13}C\{^{1}H\}$ NMR (151 MHz, Methylene Chloride-d_2) δ 145.77, 145.74, 145.48, 145.46, 120.37, 115.09, 115.05, 110.35, 110.34, 71.09, 59.07, 58.46, 55.95.

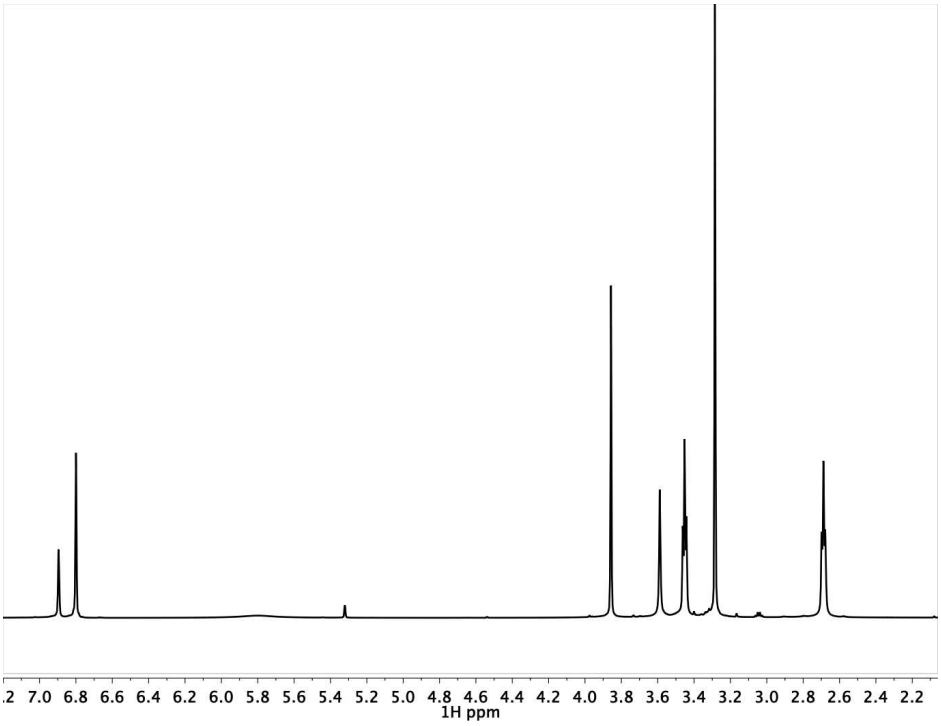

Figure 2.18. ^{1}H NMR spectrum of $^{MeOEt}N^{MeO}COH$ in CD_3Cl.

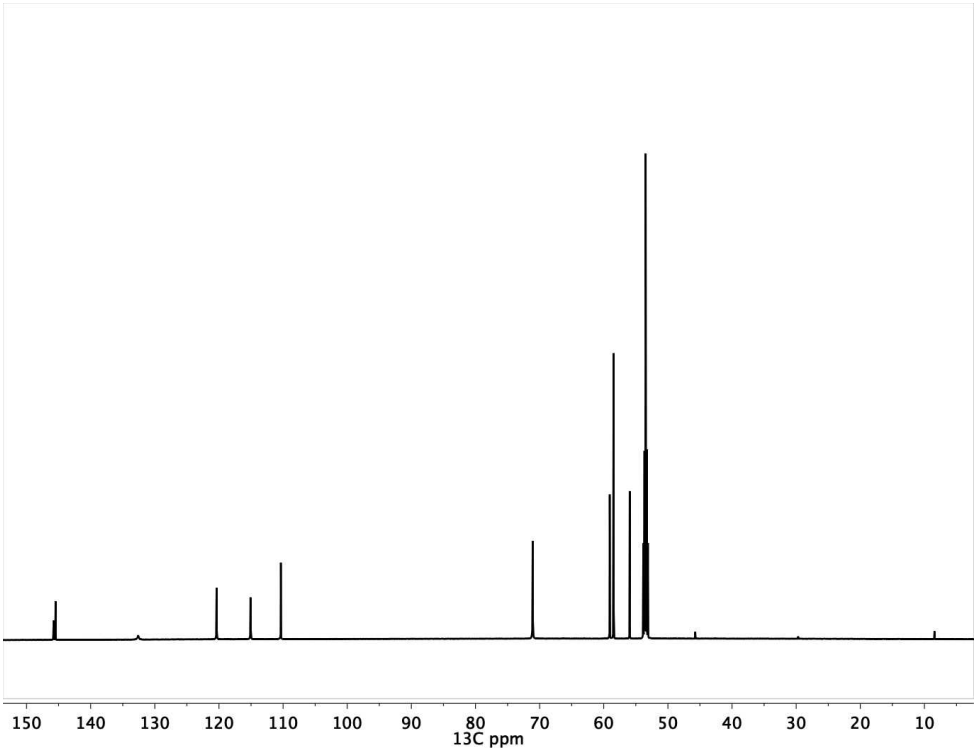

Figure 2.19. $^{13}C\{^{1}H\}$ NMR spectrum of $^{MeOEt}N^{MeO}COH$ in CD_2Cl_2.

Synthesis of $^{MeOEt}N^{MeO}$COP-H

This ligand was prepared according to the same method for the preparation of $^{15c5}N^{MeO}$COP-H.[100] The reaction was carried out using $^{EtMeO}N^{MeO}$COH (34.3 mg, 0.127 mmol), triethylamine (19.5 μL, 0.140 mmol), and diisoproplyphosphine (20.5 μL, 0.128 mmol). The product was isolated and purified according to the methods described by the preparation for $^{15c5}N^{MeO}$COP, as a colorless waxy solid (0.06 mmol, 47% yield). ^{1}H NMR (400 MHz, Chloroform-d) δ 6.81 (d, J = 8.2 Hz, 1H), 3.84 (s, 3H), 3.64 (s, 2H), 3.48 (t, J = 6.2 Hz, 4H), 3.34 (s, 6H), 2.74 (t, J = 6.2 Hz, 4H), 1.97 (h, J = 7.3 Hz, 2H), 1.33 – 0.99 (m, 15H). ^{13}C{^{1}H} NMR ^{31}P NMR (400 MHz, CDCl3) δ 156.52.

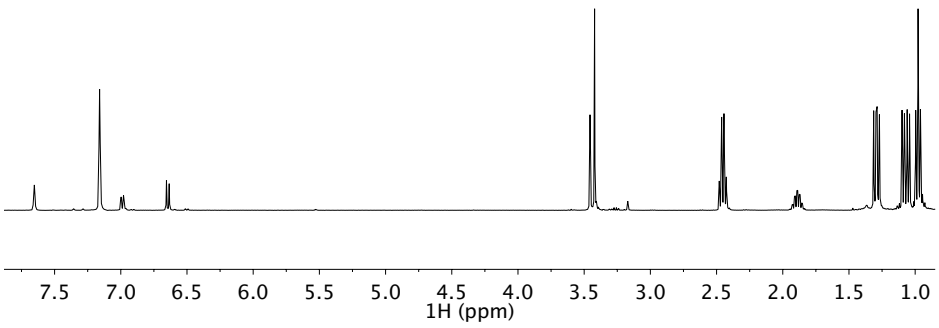

Figure 2.20. ^{1}H NMR spectrum of $^{MeOEt}N^{MeO}$COP-H in CD_2Cl_2.

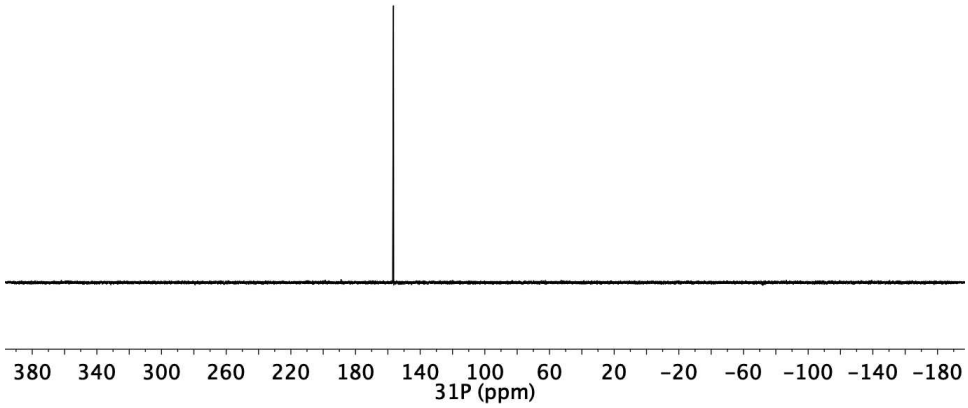

Figure 2.21. $^{31}P\{^{1}H\}$ NMR spectrum of $^{MeOEt}N^{MeO}$COP-H in CD_2Cl_2.

Synthesis of ($^{15c5}N^{MeO}$COP)Pd(OAc)

A 20 mL vial was charged with palladium acetate (38.2 mg, 0.170 mmol) and $^{15c5}N^{MeO}$COP (75.3 mg, 0.160 mmol) in acetonitrile (3 mL). The orange solution was allowed to stir for 24 hours at room-temperature, and was subsequently dried *in vacuo* to a light-yellow oil. The product was extracted in ether, and washed and triturated with pentane to yield a light-yellow powder (100 mg, 0.157 mmol, 92% yield). ^{1}H NMR (400 MHz, Methylene Chloride-d_2) δ 6.65 (d, J = 8.1 Hz, 1H), 6.60 (d, J = 8.2 Hz, 1H), 4.27 (s, 2H), 4.12 (dt, J = 11.5, 5.9 Hz, 2H), 3.96 (dt, J = 11.2, 5.7 Hz, 2H), 3.80 (s, 3H), 3.65 (q, J = 6.6 Hz, 14H), 3.47 – 3.26 (m, 4H), 2.64 (h, J = 7.1 Hz, 3H), 1.91 (s, 3H), 1.41 – 1.21 (m, 12H). ^{31}P{^{1}H} NMR (162 MHz, Methylene Chloride-d_2) δ 200.27.

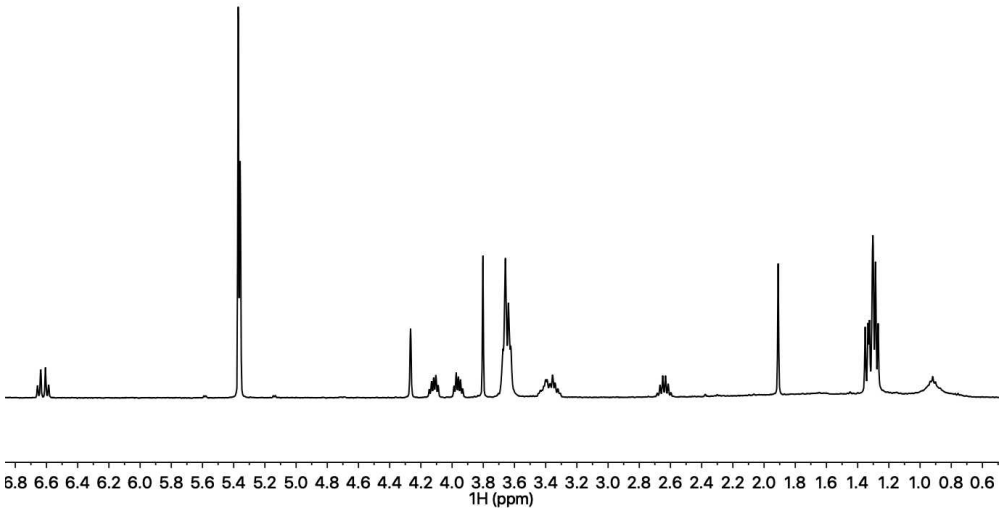

Figure 2.22. ^{1}H NMR spectrum of ($^{15c5}N^{MeO}$COP)Pd(OAc) in CD_2Cl_2.

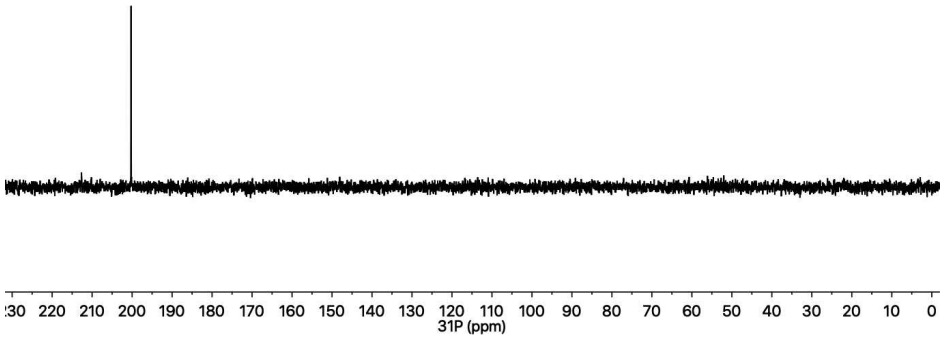

Figure 2.23. $^{31}P\{^{1}H\}$ NMR spectrum of ($^{15c5}N^{MeO}$COP)Pd(OAc) in CD_2Cl_2.

Synthesis of ($^{15c5}N^{MeO}$COP)Pd(Br)

This complex was prepared according to the procedure for the unblocked (^{15c5}NCOP)Pd(Br) described above. The ligand ($^{15c5}N^{MeO}$COP-H) (60.6 mg, 0.127 mmol), $PdBr_2$ (38.5 mg, 0.140 mmol), and triethylamine (18.0 uL, 0.127 mmol) were dissolved in benzene (7 mL) and allowed to stir at room-temperature overnight. The amber solution was dried *in vacuo*, extracted into ether, filtered, and dried *in vacuo* to yield a yellow powder, (43.8 mg, 53 % yield). ^{1}H NMR (400 MHz, Benzene-d_6) δ 6.57 (d, J = 8.1 Hz, 1H), 6.45 (d, J = 8.1 Hz, 1H), 4.35 (s, 2H), 4.17 (ddd, J = 11.3, 6.9, 4.5 Hz, 2H), 3.94 (dt, J = 11.0, 5.3 Hz, 2H), 3.76 (dq, J = 13.9, 4.6 Hz, 2H), 3.59 (dt, J = 12.8, 5.8 Hz, 2H), 3.47 – 3.38 (m, 7H), 3.32 (dtd, J = 17.6, 8.7, 8.2, 4.7 Hz, 9H), 2.17 (dq, J = 14.1, 7.1 Hz, 2H), 1.35 (dd, J = 19.0, 7.2 Hz, 6H), 1.09 (dd, J = 15.9, 6.9 Hz, 6H). ^{31}P{^{1}H} NMR (162 MHz, Benzene-d_6) δ 204.25.

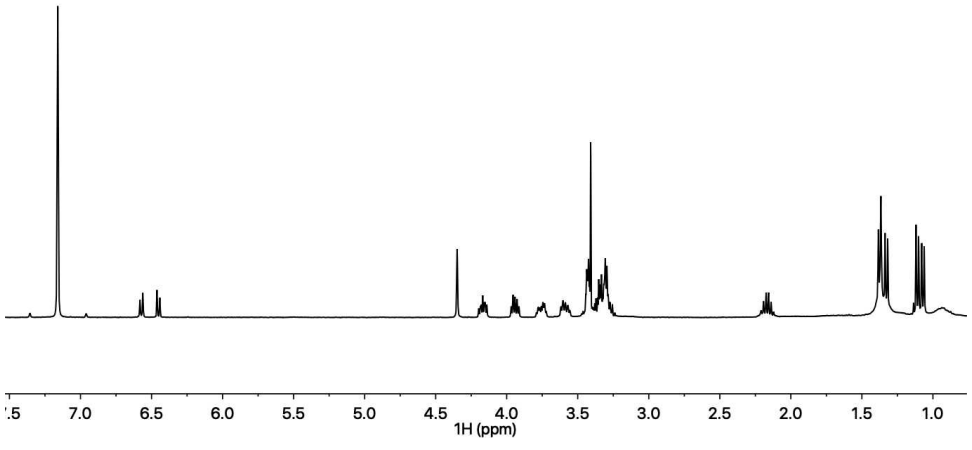

Figure 2.24. ^{1}H NMR spectrum of ($^{15c5}N^{MeO}$COP)Pd(Br) in C_6D_6.

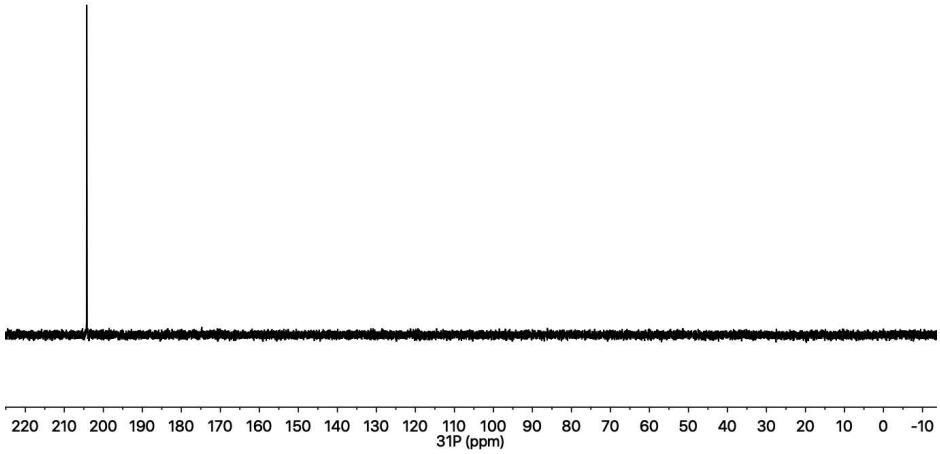

Figure 2.25. $^{31}P\{^{1}H\}$ NMR spectrum of ($^{15c5}N^{MeO}$COP)Pd(Br) in C_6D_6.

Synthesis of ($^{15c5}N^{MeO}$COP)Pd(Cl)

To a Schlenk flask was added Pd(cod)Cl_2 (85.4 mg, 0.299 mmol, 1 eq) and ($^{15c5\text{-}MeO}$NCOP) ligand (155.1 mg, 0.329 mmol, 1.1 eq) in toluene (20 mL), and a stir bar. The reaction mixture was refluxed under nitrogen for 48 hours, turning from a bright yellow solution to pale yellow. The crude reaction was allowed to cool and dried *in vacuo*, and washed with ether. ($^{15c5\text{-}MeO}$NCOP)PdCl was extracted into dichloromethane, filtered, dried *in vacuo*, and recrystallized from toluene/pentane diffusion at -35 °C to yield a pale yellow-to-off-white crystalline powder (110 mg, 0.180 mmol, 60% yield). ^{1}H NMR (600 MHz, Methylene Chloride-d_2) δ 6.66 (d, J = 8.1 Hz, 1H), 6.58 (d, J = 8.1 Hz, 1H), 4.32 (s, 2H), 4.14 (ddd, J = 11.4, 6.6, 4.9 Hz, 2H), 3.92 (dq, J = 11.8, 6.3, 5.9 Hz, 2H), 3.77 (s, 3H), 3.69 – 3.59 (m, 11H), 3.59 – 3.53 (m, 2H), 3.47 (dtd, J = 14.1, 5.5, 3.8 Hz, 2H), 3.34 (septet, J = 13.5, 6.7, 5.1, 1.4 Hz, 2H), 2.50 – 2.28 (m, J = 7.1 Hz, 2H), 1.37 (dd, J = 19.1, 7.2 Hz, 6H), 1.28 (dd, J = 15.9, 7.0 Hz, 7H). ^{13}C NMR (151 MHz, Methylene Chloride-d_2) δ 116.91, 110.33, 70.52, 70.46, 70.26, 68.65, 66.66, 57.70, 56.18, 53.84, 53.66, 53.48, 53.30, 53.12, 29.27, 29.10, 17.20, 17.16, 16.62. ^{31}P{^{1}H} NMR (162 MHz, Methylene Chloride-d_2) δ 203.14.

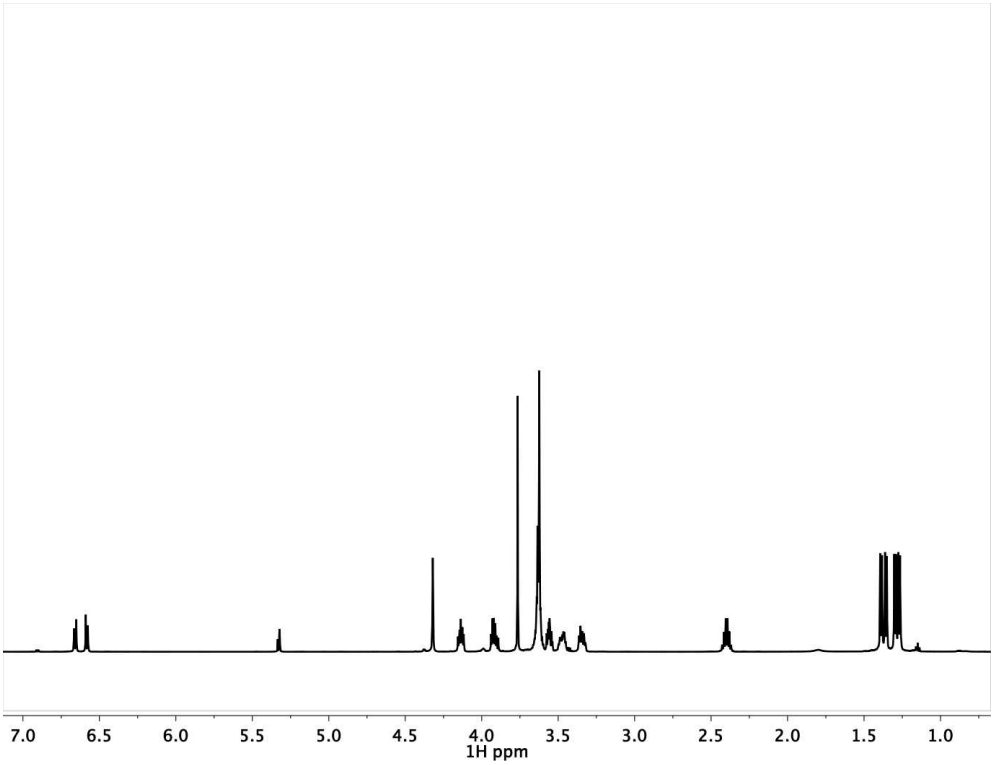

Figure 2.26. ^{1}H NMR spectrum of ($^{15c5}N^{MeO}COP$)Pd(Cl) in CD_2Cl_2.

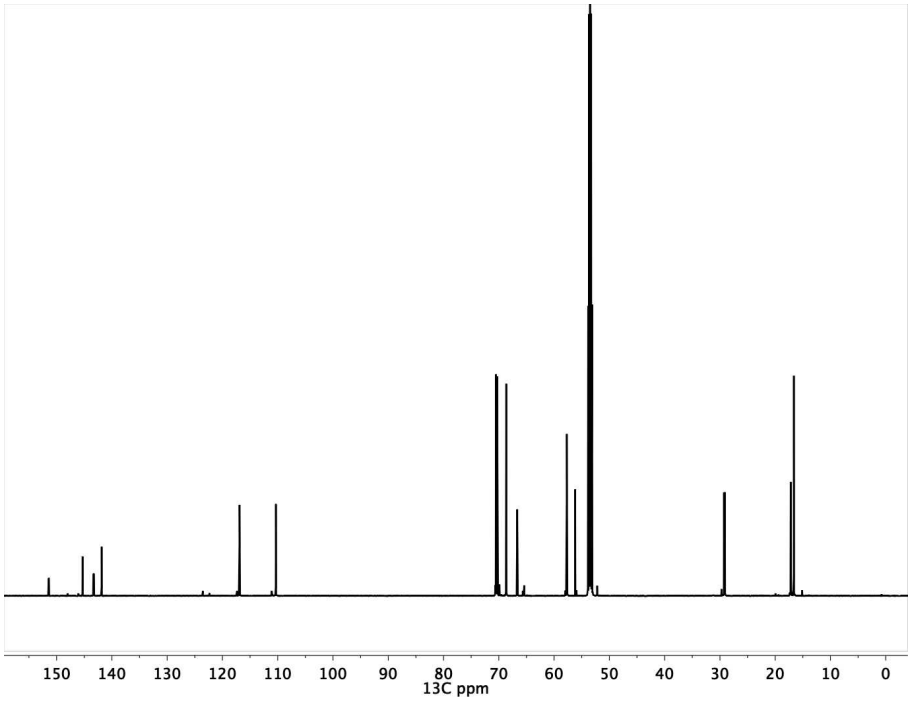

Figure 2.27. $^{13}C\{^{1}H\}$ NMR spectrum of ($^{15c5}N^{MeO}COP$)Pd(Cl) in CD_2Cl_2.

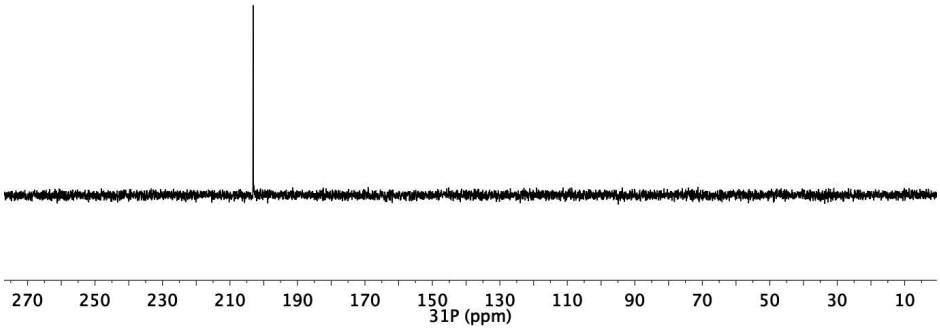

Figure 2.28. $^{31}P\{^{1}H\}$ NMR spectrum of ($^{15c5}N^{MeO}COP$)Pd(Cl) in CD_2Cl_2.

Synthesis of ($^{Et}N^{MeO}$COP)Pd(Cl)

This complex was prepared according to the procedure for ($^{15c5}N^{MeO}$COP)Pd(Cl). The ligand ($^{Et}N^{MeO}$COP) (61.0 mg, 0.187 mmol) and Pd(cod)Cl_2 (50.7 mg, 0.177 mmol) were dissolved in toluene (10 mL) and refluxed for 48 hours. The crude reaction was allowed to cool and dried *in vacuo*, and washed with ether. ($^{Et}N^{MeO}$COP)PdCl was extracted into dichloromethane, filtered, dried *in vacuo* to yield a pale yellow-to-off-white crystalline powder (53.6 mg, 0.115 mmol, 65% yield). (AS-2-182) ^{1}H NMR (600 MHz, Methylene Chloride-d_2) δ 6.64 (d, J = 8.2 Hz, 1H), 6.58 (d, J = 8.2 Hz, 1H), 4.06 (s, 2H), 3.77 (s, 3H), 3.28 (dqd, J = 12.4, 7.3, 1.4 Hz, 2H), 2.73 (dp, J = 13.2, 6.8 Hz, 2H), 2.49 – 2.33 (m, J = 7.1 Hz, 2H), 1.48 – 1.34 (m, 13H), 1.29 (dd, J = 15.8, 7.0 Hz, 7H). ^{13}C NMR (151 MHz, Methylene Chloride-d_2) δ 115.79, 110.24, 56.17, 55.39, 55.37, 53.83, 53.65, 53.47, 53.29, 53.11, 29.34, 29.17, 17.14, 17.10, 16.59, 13.09. ^{31}P{^{1}H} NMR (162 MHz, Methylene Chloride-d_2) δ 201.28.

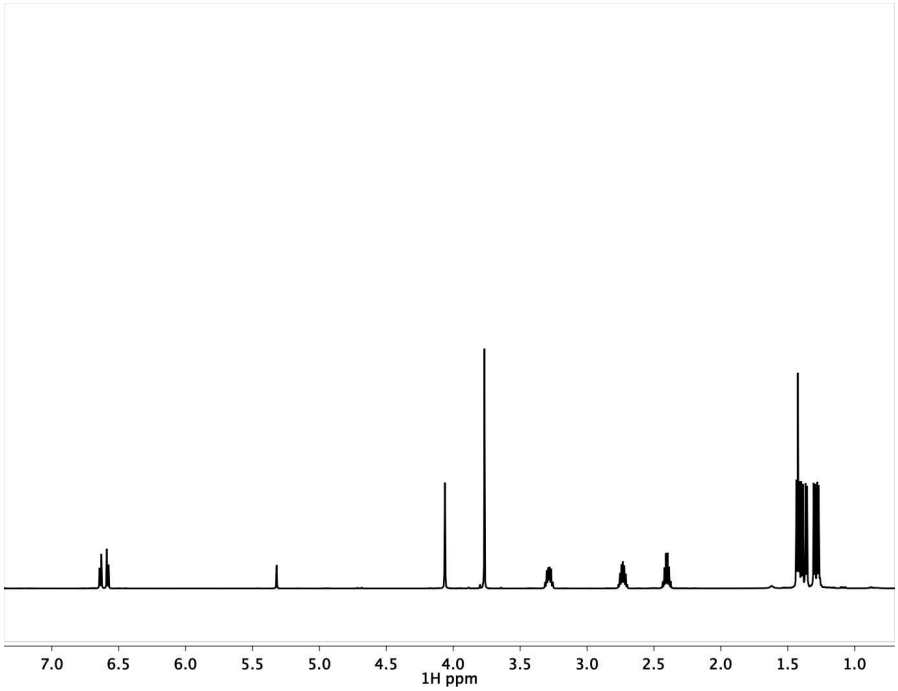

Figure 2.29. ^{1}H NMR spectrum of ($^{Et}N^{MeO}$COP)Pd(Cl) in CD_2Cl_2.

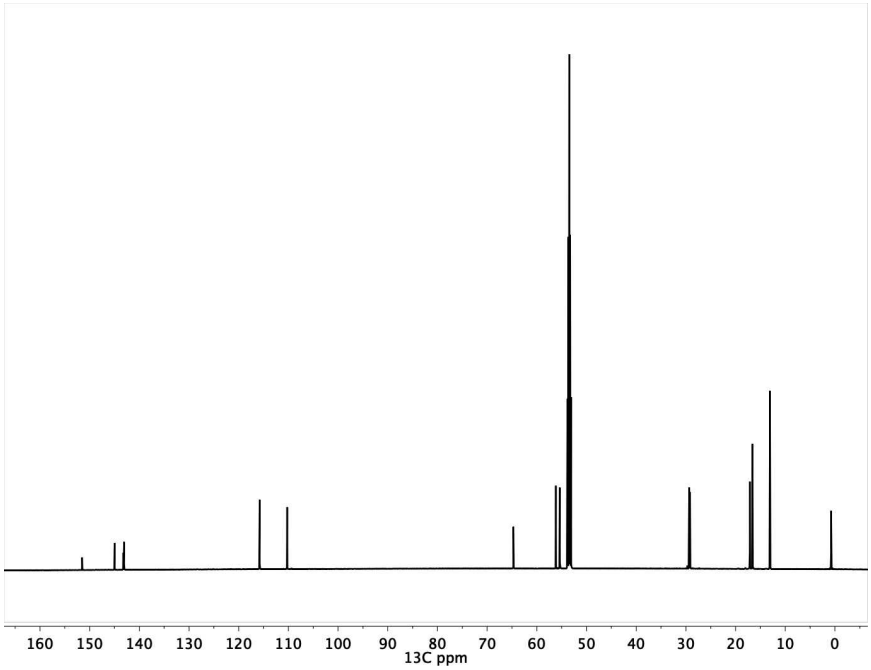

Figure 2.30. ^{13}C{^{1}H} NMR spectrum of ($^{Et}N^{MeO}$COP)Pd(Cl) in CD_2Cl_2.

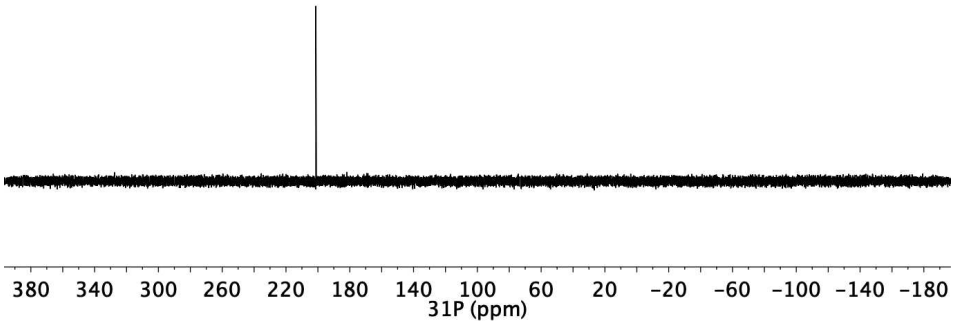

Figure 2.31. $^{31}P\{^{1}H\}$ NMR spectrum of ($^{Et}N^{MeO}$COP)PdCl in CD_2Cl_2.

Synthesis of ($^{MeOEt}N^{MeO}$COP)Pd(Cl)

This complex was prepared according to the procedure for ($^{15c5}N^{MeO}$COP)Pd(Cl).[101] The ligand ($^{MeOEt}N^{MeO}$COP) (182.2 mg, 0.470 mmol) and Pd(cod)Cl_2 (123.0 mg, 0.431 mmol) were dissolved in toluene (48 mL) and refluxed for 48 hours. The crude reaction was allowed to cool, filtered and dried *in vacuo* to a light yellow solid. The crude product was dissolved in hexane (50 mL) and allowed to recrystallize at -35 °C to yield the product as a pale yellow crystals (0.380, 88% yield). ^{1}H NMR (500 MHz, Methylene Chloride-d_2) δ 6.65 (q, J = 8.2 Hz, 1H), 4.37 (s, 1H), 4.00 (hept, J = 5.3 Hz, 2H), 3.81 (s, 1H), 3.42 (ddd, J = 12.8, 8.1, 3.1 Hz, 1H), 3.28 (s, 2H), 3.09 – 2.97 (m, 1H), 2.44 (qd, J = 13.9, 6.0 Hz, 1H), 1.49 – 1.33 (m, 5H), 1.32 (d, J = 7.0 Hz, 2H), 0.92 (t, J = 6.9 Hz, 0H).^{13}C NMR ^{31}P{^{1}H} NMR (500 MHz, Methylene Chloride-d_2) δ 202.14.

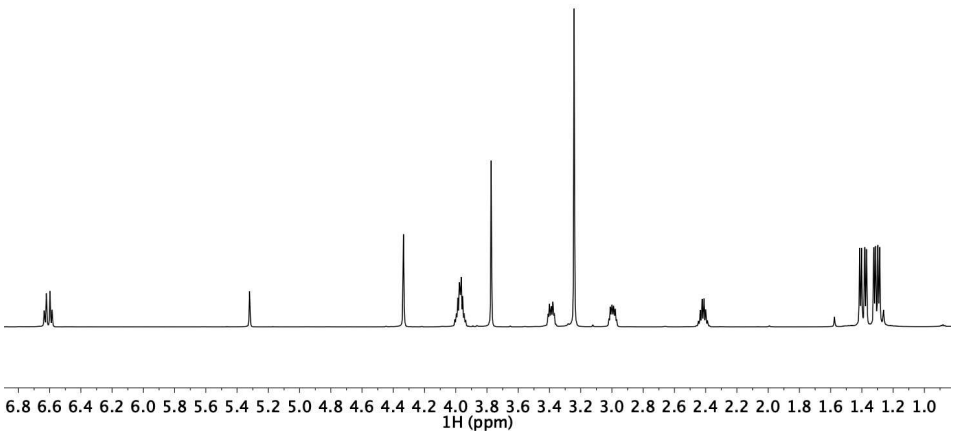

Figure 2.32. ^{1}H NMR spectrum of ($^{MeOEt}N^{MeO}$COP)PdCl in CD_2Cl_2.

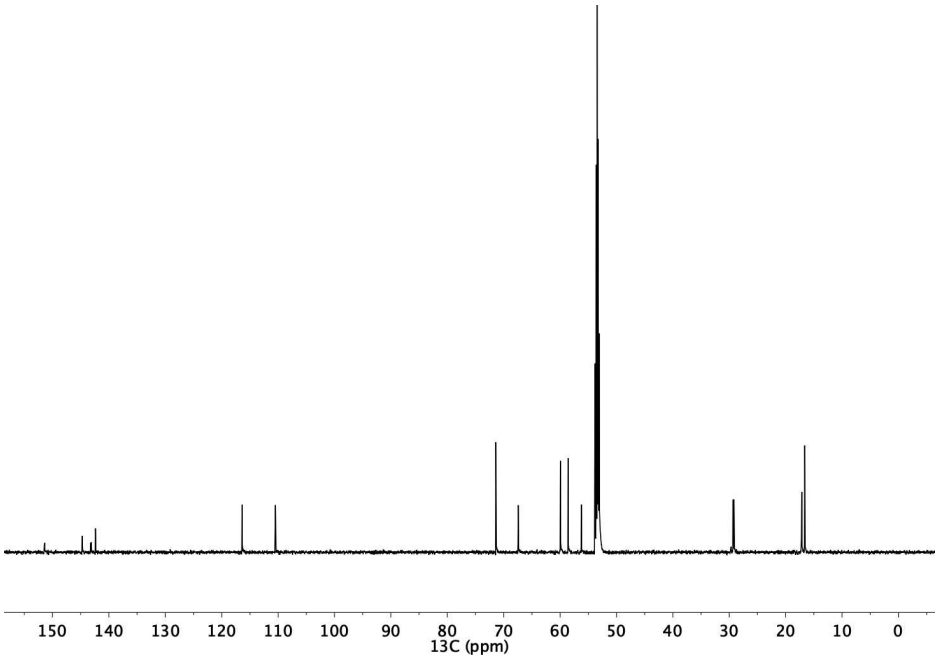

Figure 2.33. $^{13}C\{^{1}H\}$ NMR spectrum of ($^{MeOEt}N^{MeO}COP$)Pd(Cl) in CD_2Cl_2.

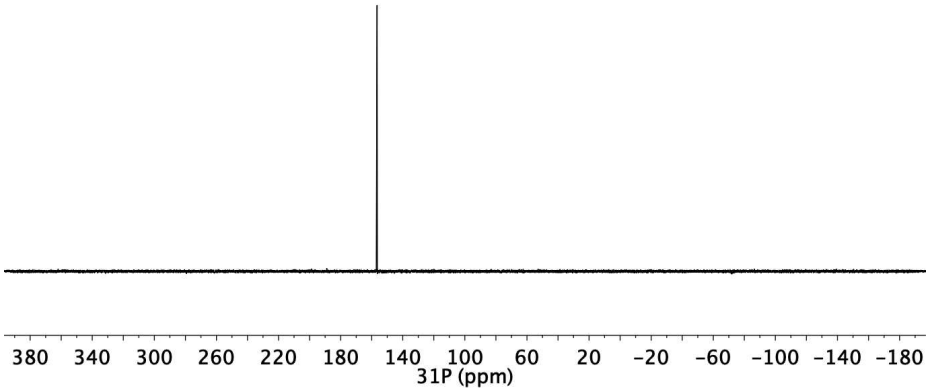

Figure 2.34. $^{31}P\{^{1}H\}$ NMR spectrum of ($^{MeOEt}N^{MeO}COP$)Pd(Cl) in CD_2Cl_2.

Synthesis of ($^{15c5}N^{MeO}$COP)Pd(CF_3)

A 20 mL vial was charged with AgF (4.4 mg, 0.0273 mmol) and acetonitrile (1 mL), to which was added $TMSCF_3$ (4.0 uL, 0.0271 mmol). The solution turned into a dark grey slurry, and was allowed to stir for thirty-minutes. To the AgF/$TMSCF_3$ solution, a solution of ($^{15c5}N^{MeO}$COP)Pd(Cl) (8.9 mg, 0.0145 mmol) in acetonitirile (1 mL) was added. The reaction was allowed to stir at room temperature for two hours, was subsequently concentrated, and extracted into ether and filtered. The ether filtrate was dried *in vacuo* to reveal a white powder (9.0 mg, 0.0139 mmol, 96 % yield). ^{1}H NMR (600 MHz, Methylene Chloride-d_2) δ 6.71 (d, J = 8.0 Hz, 1H), 6.61 (d, J = 8.0 Hz, 1H), 4.49 (s, 2H), 3.98 (hept, J = 5.8, 5.4 Hz, 5H), 3.80 (s, 3H), 3.66 (dq, J = 12.0, 4.5, 4.1 Hz, 8H), 3.63 – 3.59 (m, 5H), 3.56 (dt, J = 14.4, 5.2 Hz, 2H), 3.44 (dt, J = 13.8, 5.4 Hz, 3H), 2.56 – 2.31 (m, J = 7.5, 6.9 Hz, 2H), 1.30 (ddd, J = 26.8, 17.4, 7.1 Hz, 15H).^{13}C{^{1}H} NMR (151 MHz, Methylene Chloride-d_2) δ 153.09 (d, J = 13.2 Hz), 152.30 (q, J = 15.5 Hz), 150.87 (d, J = 7.7 Hz), 150.62 (d, J = 13.3 Hz), 143.02, 142.90, 142.60, 116.60, 110.89, 70.64, 70.51, 70.31, 69.29, 67.33, 58.19, 56.12, 29.06, 28.88, 17.45, 17.41, 16.59. ^{31}P NMR (202 MHz, Methylene Chloride-d_2) δ 200.74 (q, J = 8.2 Hz). ^{19}F{^{1}H} NMR (376 MHz, Methylene Chloride-d_2) δ -21.51 (d, J = 7.5 Hz).

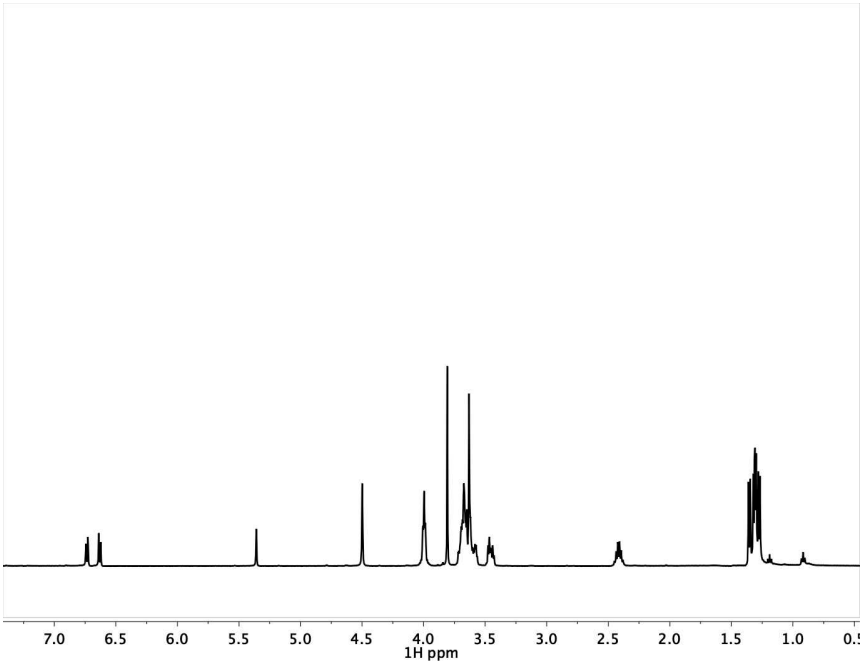

Figure 2.35. ^{1}H NMR spectrum of ($^{15c5}N^{MeO}COP$)Pd(CF_3) in CD_2Cl_2.

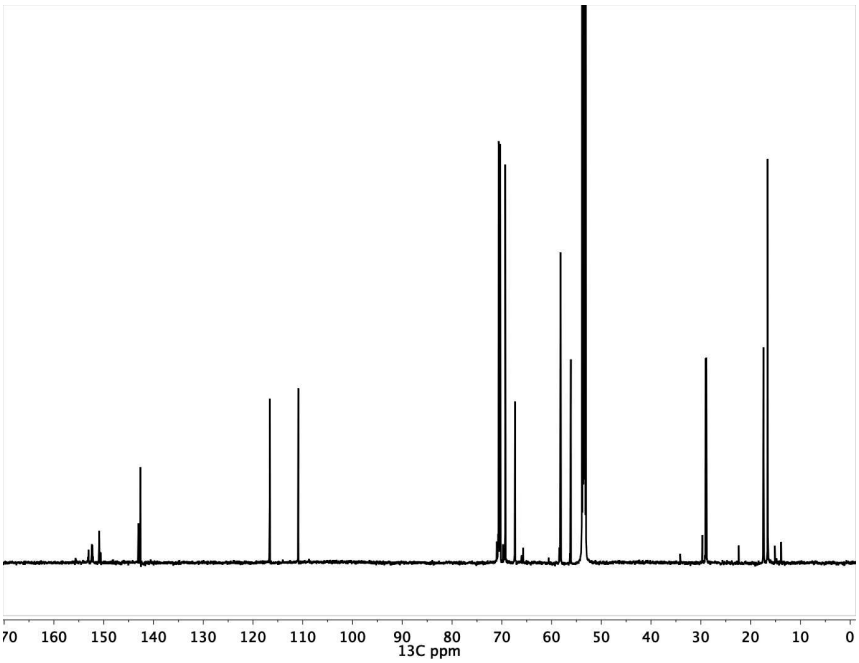

Figure 2.36. $^{13}C\{^{1}H\}$ NMR spectrum of ($^{15c5}N^{MeO}COP$)Pd(CF_3) in CD_2Cl_2.

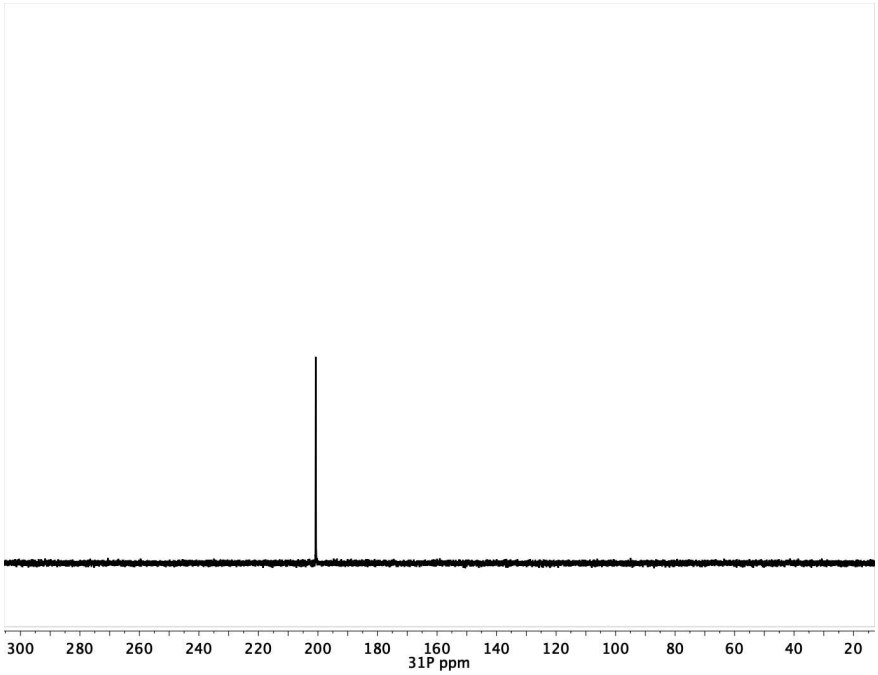

Figure 2.37. $^{31}P\{^{1}H\}$ NMR spectrum of ($^{15c5}N^{MeO}$COP)Pd(CF_3) in CD_2Cl_2.

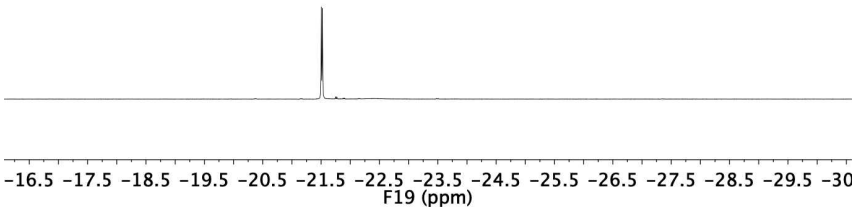

Figure 2.38. $^{19}F\{^{1}H\}$ NMR spectrum of ($^{15c5}N^{MeO}$COP)Pd(CF_3) in CD_2Cl_2.

Synthesis of [($^{15c5}N^{MeO}$COP)Pd]$^+$

A 20 mL vial was charged with ($^{15c5}N^{MeO}$COP)Pd(Cl) (30 mg, 0.0490 mmol) in C_6H_5Cl (3 mL). In a separate vial, trityl tetrakis(pentafluorophenyl)borate (47.4 mg, 0.0514 mmol) was dissolved in C_6H_5Cl (2 mL). Triethylsilane (8.6 µL, 0.0539 mmol) was added to the bright yellow trityl tetrakis(pentafluorophenyl)borate solution, and allowed to stir at room temperature for ten minutes, over which time the solution turned colorless, indicating the *in situ* formation of silylium cation. The ($^{15c5}N^{MeO}$COP)Pd(Cl) solution was then added to the $[CPh_3][B(C_6F_5)_4]$/Et_3SiH solution at room temperature, and the reaction was allowed to stir at room temperature for one hour. The reaction solution was dried *in vacuo* to a peach solid, and washed rigorously with pentane. The crude product was then dissolved in ether, and filtered through a short alumina plug to yield a white powder (49.4 mg, 80% yield), and was characterized via ^1H and ^{31}P NMR. ^1H NMR (400 MHz, Methylene Chloride-d_2) δ 6.69 (q, J = 8.3 Hz, 2H), 4.49 (d, J = 9.9 Hz, 2H), 4.24 (s, 2H), 3.90 (ddd, J = 16.3, 10.7, 6.3 Hz, 5H), 3.83 (s, 4H), 3.75 (dd, J = 13.7, 10.3 Hz, 6H), 3.69 (s, 5H), 3.64 – 3.45 (m, 5H), 3.35 (dd, J = 13.5, 3.5 Hz, 2H), 2.41 (dq, J = 13.7, 6.9 Hz, 2H), 1.46 – 1.23 (m, 12 H). $^{13}C\{^1H\}$ NMR (151 MHz, Methylene Chloride-d_2) δ 137.00, 117.96, 111.24, 69.92, 69.30, 68.02, 67.66, 60.26, 53.78, 53.60, 53.42, 53.24, 53.06, 29.36, 29.20, 16.78, 16.74, 16.56. $^{31}P\{^1H\}$ NMR (162 MHz, Methylene Chloride-d_2) δ 197.93.

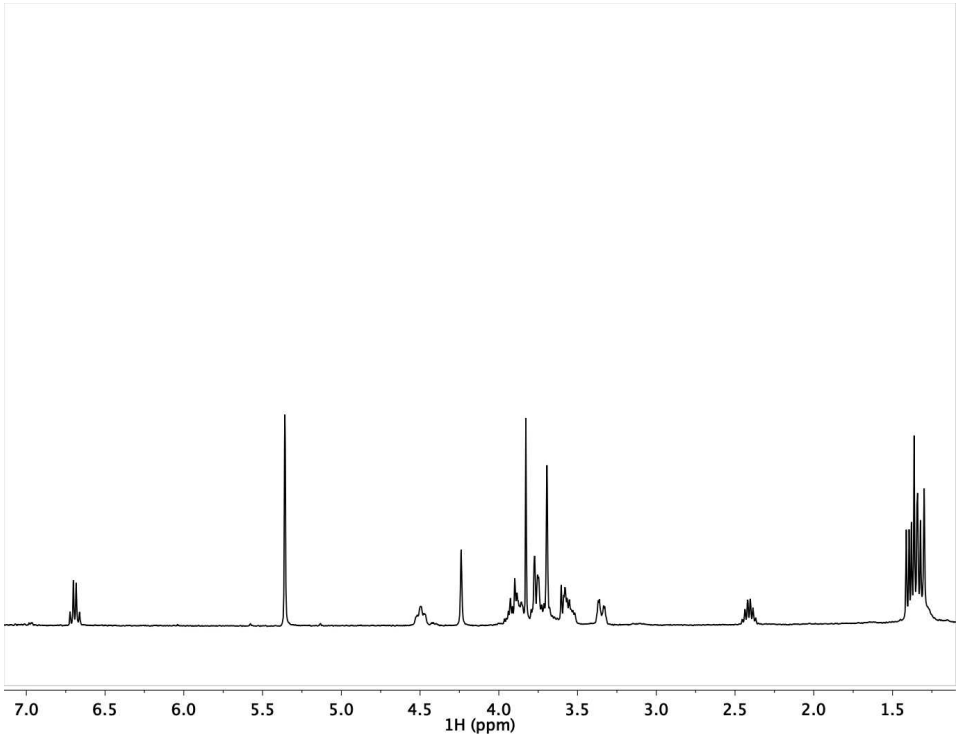

Figure 2.39. ^{1}H NMR spectrum of [($^{15c5}N^{MeO}$COP)Pd][$B(C_6F_5)_4$] in CD_2Cl_2.

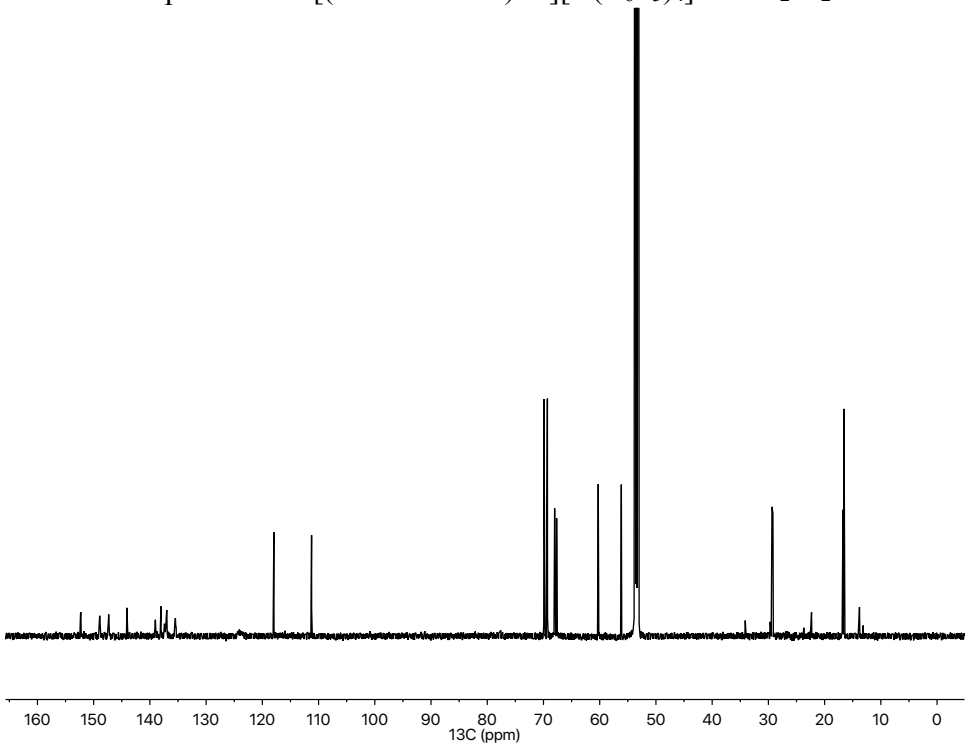

Figure 2.40. $^{13}C\{^{1}H\}$ NMR spectrum of [($^{15c5}N^{MeO}$COP)Pd][$B(C_6F_5)_4$] in CD_2Cl_2.

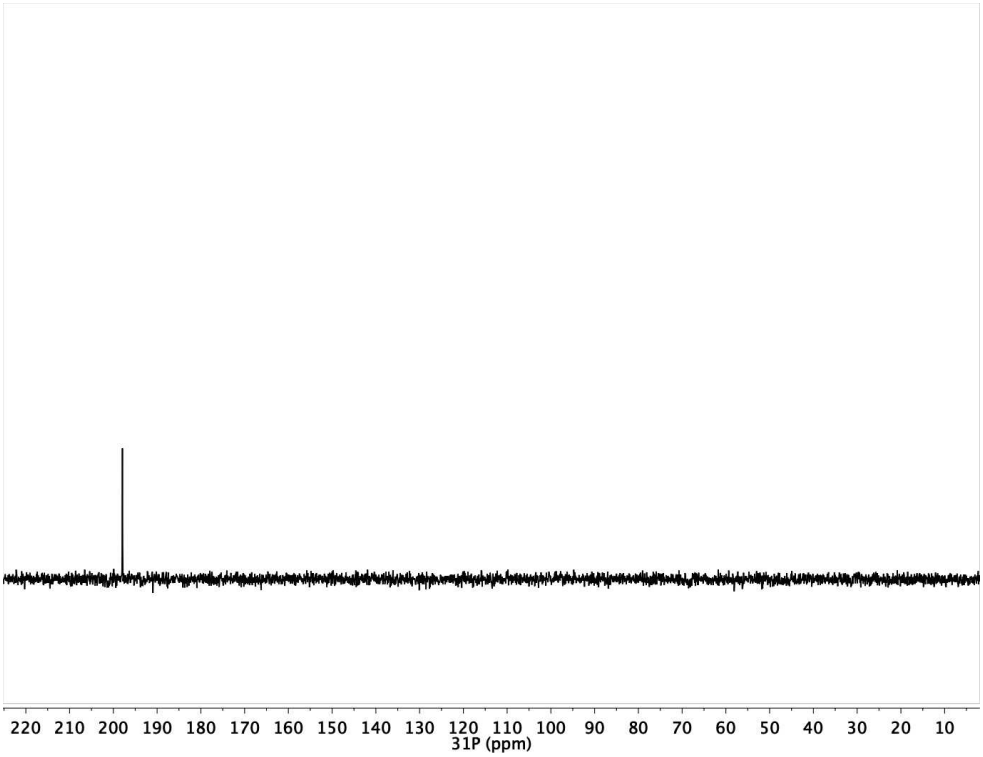

Figure 2.41. $^{31}P\{^{1}H\}$ NMR spectrum of $[(^{15c5}N^{MeO}COP)Pd][B(C_6F_5)_4]$ in CD_2Cl_2.

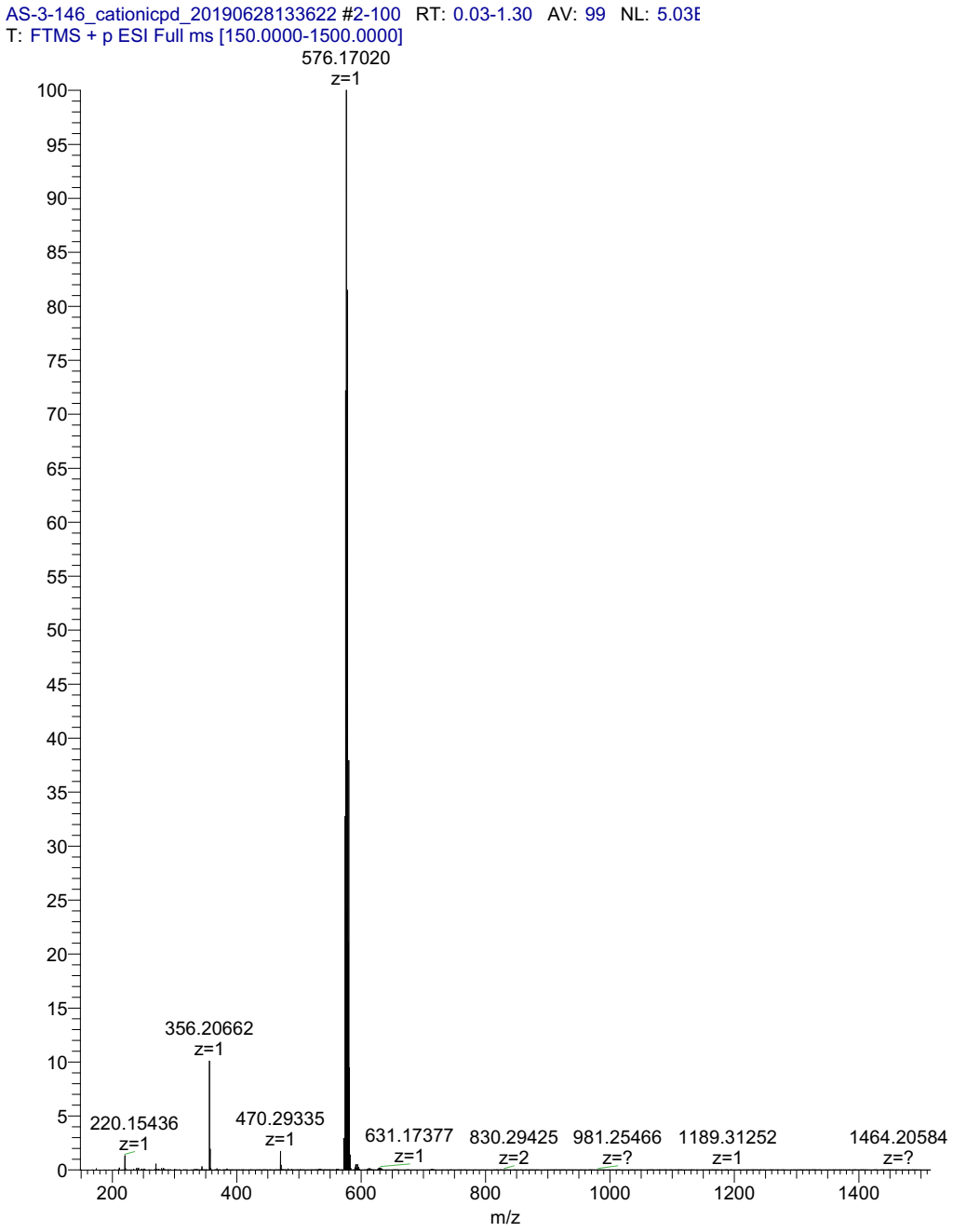

Figure 2.42. Mass spectrum of $[(^{15c5}N^{MeO}COP)Pd][B(C_6F_5)_4]$ in positive mode.

The addition of neutral ($^{15c5}N^{MeO}$COP)Pd(Cl) to [($^{15c5}N^{MeO}$COP)Pd][$B(C_6F_5)_4$

To probe the possible formation of bridging chloride dimers in solution, a 1:1 ratio of ($^{15c5}N^{MeO}$COP)Pd(Cl) (2.3 mg, 0.0037 mmol) and [($^{15c5}N^{MeO}$COP)Pd][$B(C_6F_5)_4$ (4.8 mg, 0.0037 mmol) was dissolved in CD_2Cl_2 and transferred to a Teflon-sealed NMR tube. Only one, new C_s symmetric species was observed in solution by ^{1}H NMR spectroscopy. ^{1}H NMR (400 MHz, Methylene Chloride-d_2) δ 6.69 (t, J = 6.3 Hz, 2H), 4.31 (s, 2H), 4.25 – 3.26 (m, 27H), 2.44 (dp, J = 14.0, 7.3 Hz, 2H), 1.52 – 1.13 (m, 18H).

The addition of 0.5 equivalents $[Et_3Si]^+$ to ($^{15c5}N^{MeO}$COP)Pd(Cl)

A 20 mL vial was charged with ($^{15c5}N^{MeO}$COP)Pd(Cl) (7.4 mg, 0.012 mmol) in C_6H_5Cl (0.5 mL). In a separate vial, trityl tetrakis(pentafluorophenyl)borate (5.6 mg, 0.0061 mmol) was dissolved in C_6H_5Cl (2 mL). Triethylsilane (1.0 µL, 0.0061 mmol) was added to the bright yellow trityl tetrakis(pentafluorophenyl)borate solution, and allowed to stir at room temperature for ten minutes, over which time the solution turned colorless, indicating the *in situ* formation of silylium cation. The ($^{15c5}N^{MeO}$COP)Pd(Cl) solution was then added to the $[CPh_3][BAr^{F20}]$/Et_3SiH solution at room temperature, and the reaction was allowed to stir at room temperature for one hour. The reaction solution was dried *in vacuo* to a peach solid, and washed rigorously with pentane. The crude product was analyzed by ^{1}H NMR spectroscopy. ^{1}H NMR (400 MHz, Methylene Chloride-d_2) δ 6.81 – 6.53 (m, 2H), 4.32 (s, 2H), 4.24 – 3.29 (m, 26H), 2.42 (hept, J = 7.0 Hz, 2H), 1.55 – 1.19 (m, 14H).

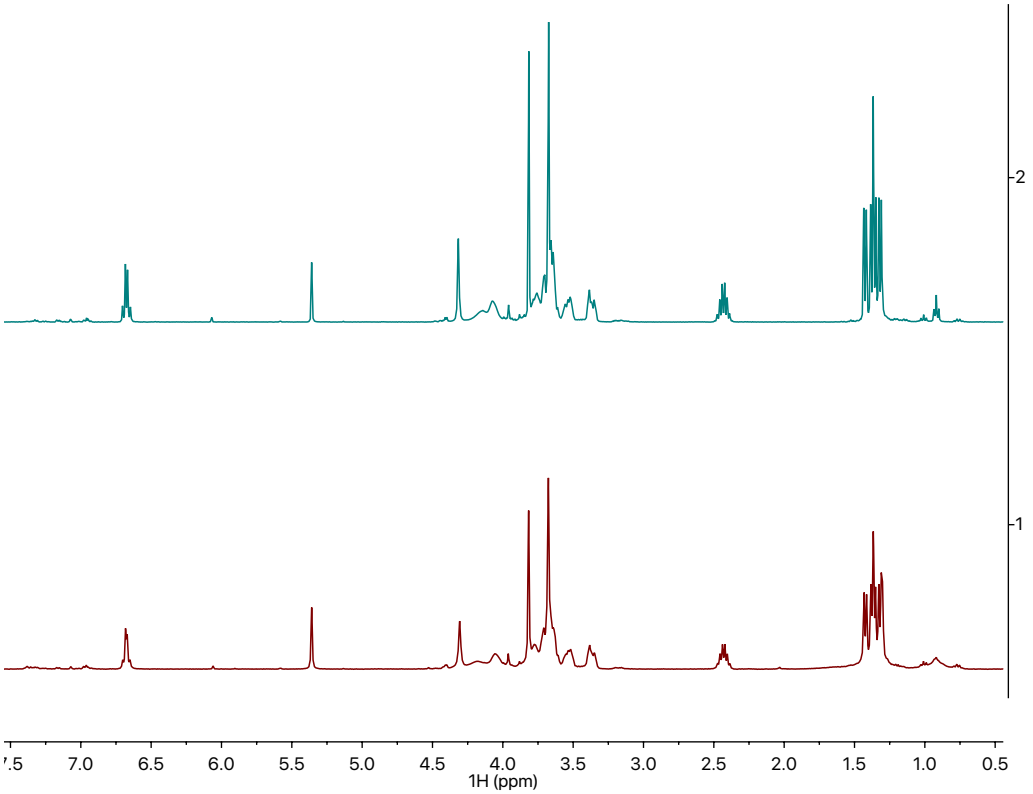

Figure 2.43. ^{1}H NMR spectra of a 1:1 mixture of ($^{15c5}N^{MeO}$COP)Pd(Cl) and [($^{15c5}N^{MeO}$COP)Pd][B(C_6F_5)$_4$

Synthesis of [($^{Et}N^{MeO}$COP)Pd]$^+$

A 20 mL vial was charged with ($^{Et}N^{MeO}$COP)Pd(Cl) (30.0 mg, 0.0643 mmol) in C_6H_5Cl (4 mL). In a separate vial, trityl tetrakis(pentafluorophenyl)borate (62.3 mg, 0.0676 mmol) was dissolved in C_6H_5Cl (2 mL). Triethylsilane (11.3 μL, 0.0707 mmol) was added to the bright yellow trityl tetrakis(pentafluorophenyl)borate solution, and allowed to stir at room temperature for ten minutes, over which time the solution turned colorless, indicating the *in situ* formation of silylium cation. The ($^{Et}N^{MeO}$COP)Pd(Cl) solution was then added to the $[CPh_3][B(C_6F_5)_4]$/Et_3SiH solution at room temperature, and the reaction was allowed to stir at room temperature for one hour. Ether (~ 1 mL) was then added to the reaction solution, and it was dried *in vacuo* to a peach solid. The crude product was and washed rigorously with pentane, dissolved in ether, and then filtered through a short alumina plug to yield a white powder (53.4 mg, 75% yield), and was characterized via ^1H and ^{31}P NMR. ^1H NMR (500 MHz, Methylene Chloride-d_2) δ 6.85 – 6.61 (m, 2H), 4.13 (s, 2H), 3.83 (d, J = 5.1 Hz, 3H), 3.03 (dtdd, J = 58.9, 29.1, 13.1, 6.8 Hz, 4H), 2.57 – 2.33 (m, 2H), 1.56 – 1.45 (m, 6H), 1.37 (ddd, J = 24.9, 15.0, 6.9 Hz, 14H). $^{31}P\{^1H\}$ NMR (202 MHz, Methylene Chloride-d_2) δ 318.07, 200.59, 199.80, -70.14.

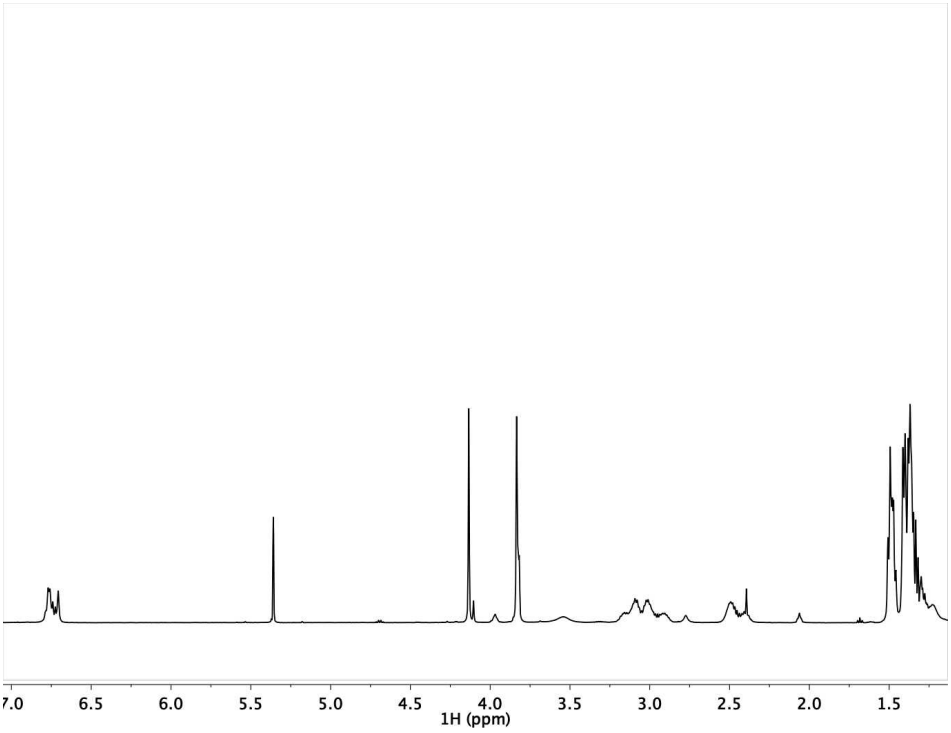

Figure 2.44. ^{1}H NMR spectrum of [($^{Et}N^{MeO}$COP)Pd][$B(C_6F_5)_4$] species in CD_2Cl_2.

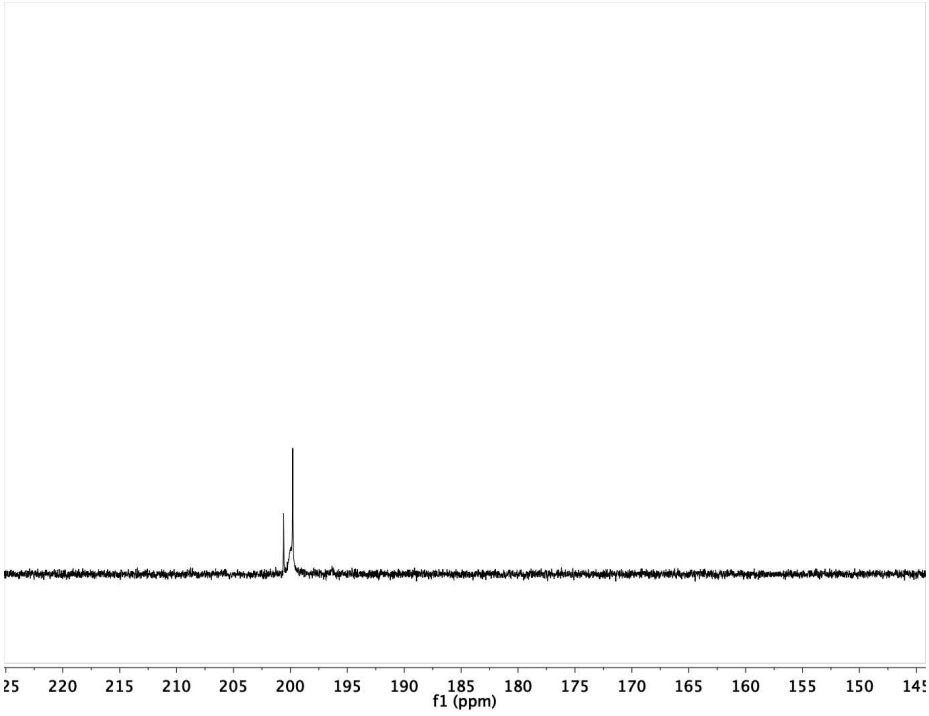

Figure 2.45. $^{31}P\{^{1}H\}$ NMR spectrum of [($^{Et}N^{MeO}$COP)Pd][$B(C_6F_5)_4$] species in CD_2Cl_2.

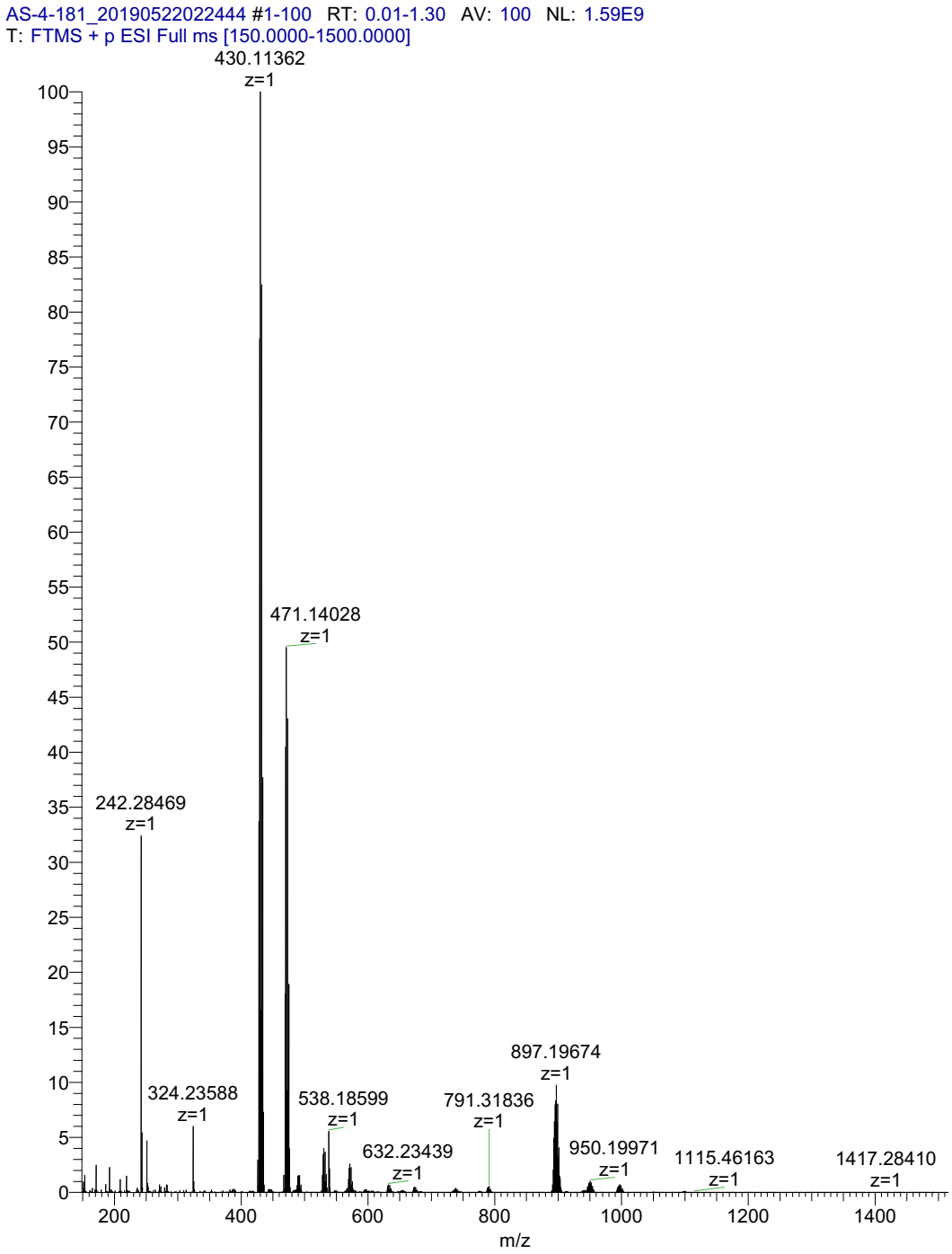

Figure 2.46. Mass spectrum of [($^{Et}N^{MeO}$COP)Pd][B(C_6F_5)$_4$] species in positive mode. .

Synthesis of [($^{MeOEt}N^{MeO}$COP)Pd]$^+$

A 20 mL vial was charged with ($^{EtMeO}N^{MeO}$COP)Pd(Cl) (21.8 mg, 0.0414 mmol) in C_6H_5Cl (3 mL). In a separate vial, trityl tetrakis(pentafluorophenyl)borate (37.5 mg, 0.0407 mmol) was dissolved in C_6H_5Cl (2 mL). Triethylsilane (6.5 µL, 0.0407 mmol) was added to the bright yellow trityl tetrakis(pentafluorophenyl)borate solution, and allowed to stir at room temperature for ten minutes, over which time the solution turned colorless, indicating the *in situ* formation of silylium cation. The ($^{EtMeO}N^{MeO}$COP)Pd(Cl) solution was then added to the $[CPh_3][B(C_6F_5)_4]$/Et_3SiH solution at room temperature, and the reaction was allowed to stir at room temperature for one hour. The reaction solution was dried *in vacuo* to a peach solid, and washed rigorously with pentane. The crude product was then dissolved in ether, and filtered through a short alumina plug to yield a white powder (34.8 mg, 0.0299 mmol, 73% yield), and was characterized via NMR spectroscopy. ^{1}H NMR (400 MHz, Methylene Chloride-d_2) δ 6.71 (s, 2H), 4.33 (s, 2H), 4.11 – 3.93 (m, 3H), 3.84 (d, J = 4.7 Hz, 6H), 3.52 (s, 11H), 3.36 (d, J = 13.6 Hz, 3H), 2.43 (q, J = 7.1 Hz, 2H), 1.48 – 1.23 (m, 29H). ^{31}P{^{1}H} NMR (162 MHz, Methylene Chloride-d_2) δ 197.9.

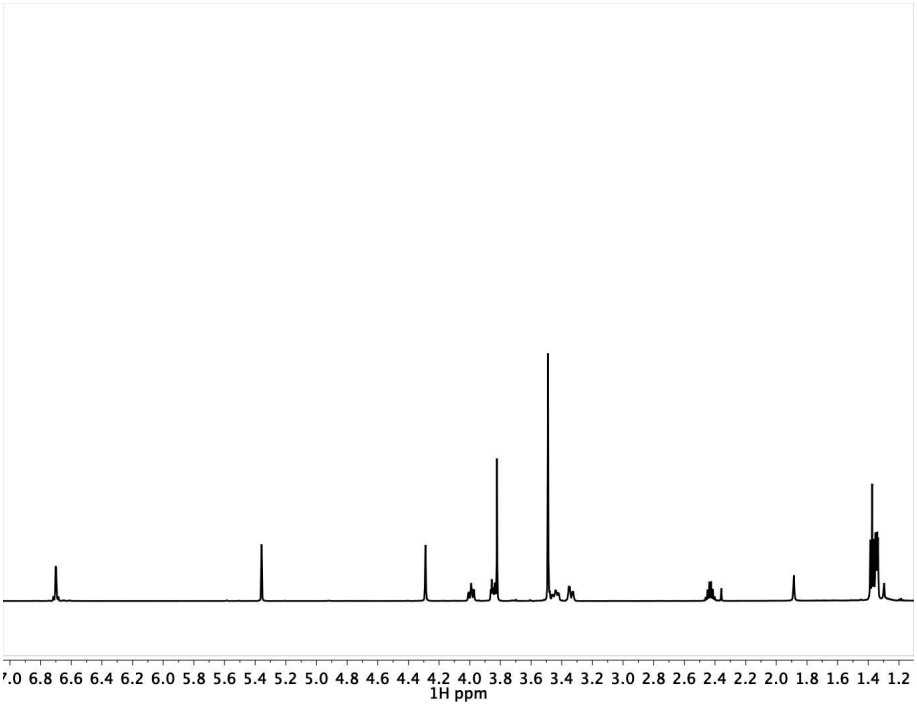

Figure 2.47. ^{1}H NMR spectrum of [($^{MeOEt}N^{MeO}$COP)Pd][$B(C_6F_5)_4$] in CD_2Cl_2.

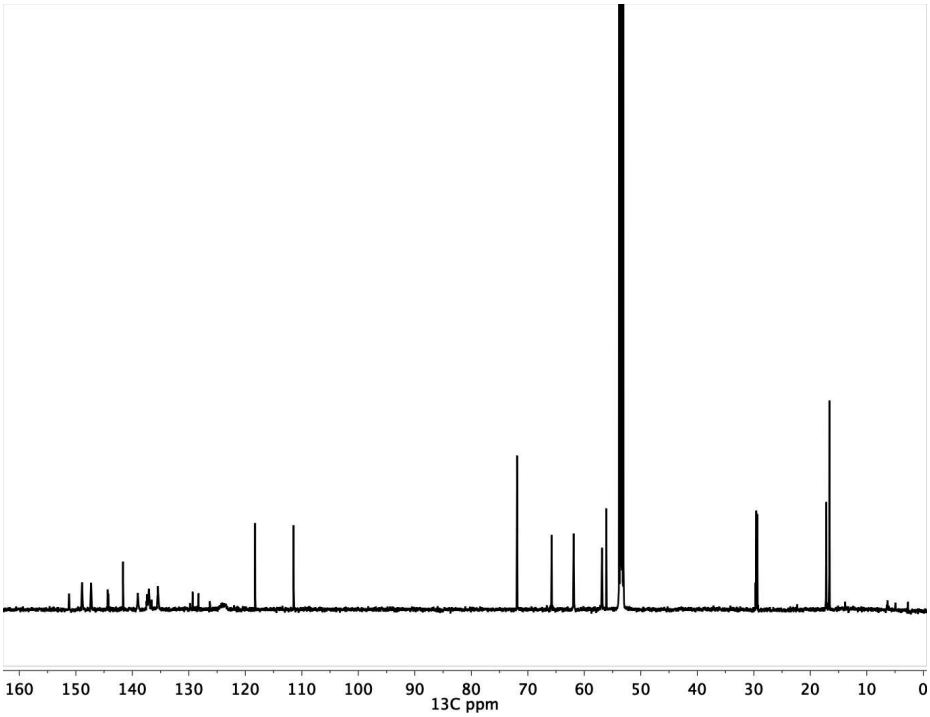

Figure 2.48. $^{13}C\{^{1}H\}$ NMR spectrum of [($^{MeOEt}N^{MeO}$COP)Pd][$B(C_6F_5)_4$] in CD_2Cl_2.

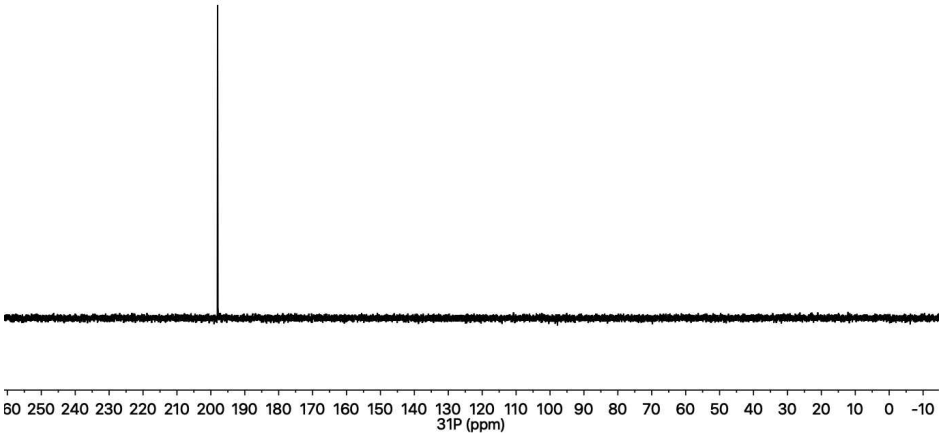

Figure 2.49. $^{31}P\{^{1}H\}$ NMR spectrum of [($^{MeOEt}N^{MeO}$COP)Pd][$B(C_6F_5)_4$] in CD_2Cl_2.

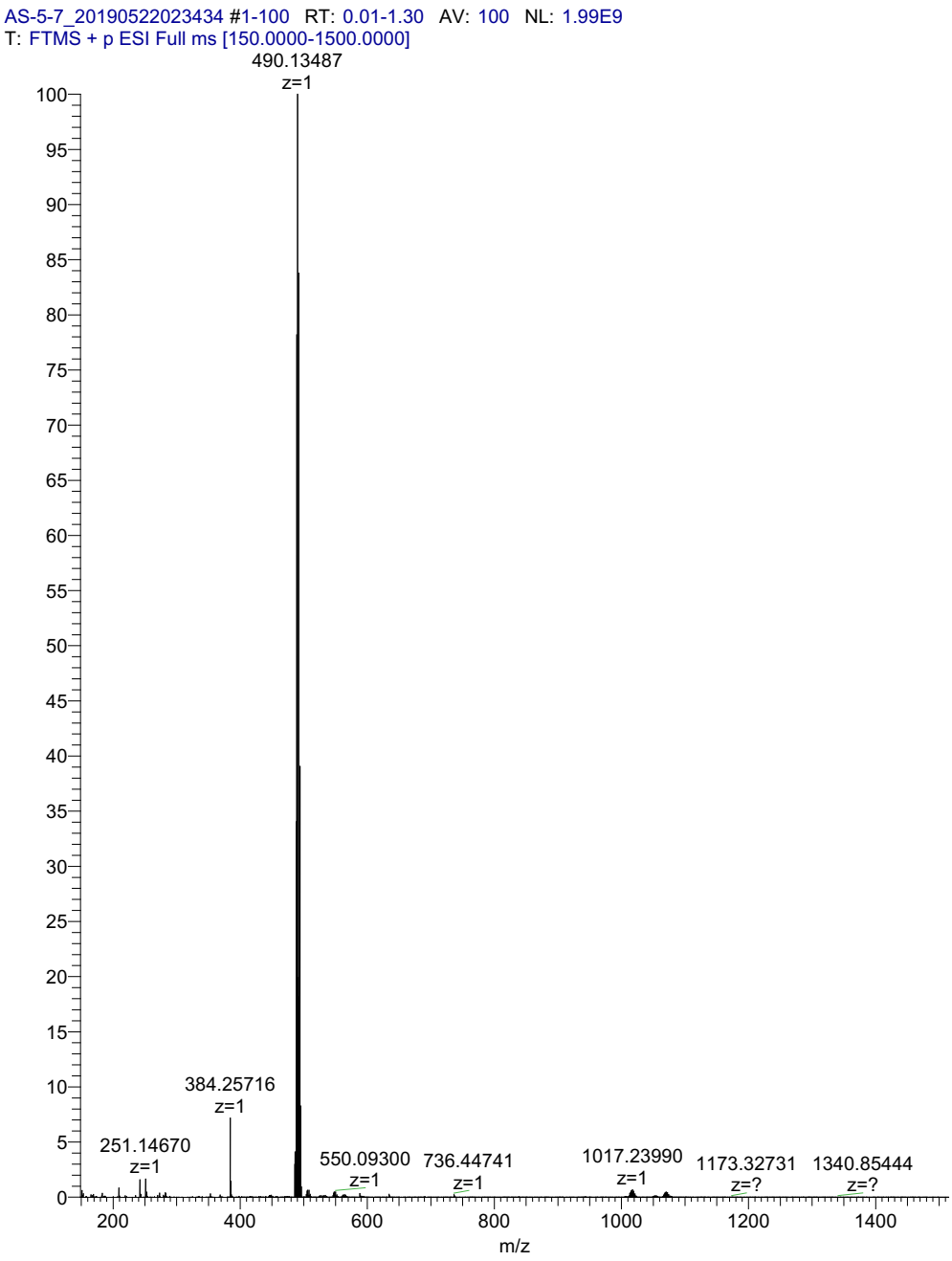

Figure 2.50. Mass spectrum of [($^{MeOEt}N^{MeO}$COP)Pd][$B(C_6F_5)_4$] in positive mode.

The addition of trimethyloxonium tetrafluoroborate to ($^{15c5}N^{MeO}$COP)Pd(Cl)

In a nitrogen glovebox, a Teflon-sealed NMR tube was charged with ($^{15c5}N^{MeO}$COP)Pd(Cl) (7.7 mg, 0.013 mmol) and [Me_3O][BF_4] (2.8 mg, 0.020 mmol) in CD_2Cl_2 (500 μL). The reaction was monitored at 25 °C by ^{1}H NMR spectroscopy. The production of 0.5 equiv. chloromethane, 0.5 equiv. dimethyl ether, and one new Pd species with C_s symmetry was observed after 24 hours. ^{1}H NMR (400 MHz, Methylene Chloride-d_2) δ 6.68 (q, J = 8.3 Hz, 2H), 4.32 (s, 2H), 4.09 (s, 4H), 3.89 – 3.34 (m, 20H), 3.30 (s, 2H), 3.05 (s, 1H), 2.43 (tt, J = 15.1, 7.5 Hz, 2H), 1.52 – 1.21 (m, 14H).

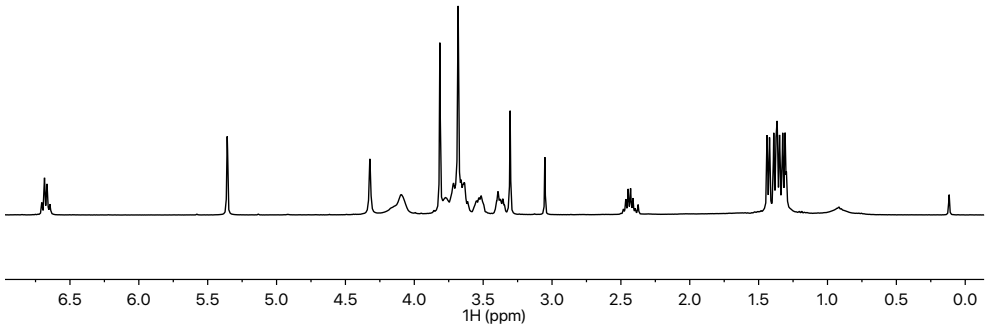

Figure 2.51. ^{1}H NMR spectrum of the products from the addition of [Me_3O][BF_4] to ($^{15c5}N^{MeO}$COP)Pd(Cl).

The addition of trimethyloxonium tetrafluoroborate to ($^{15c5}N^{MeO}$COP)Pd(CF_3)

In a nitrogen glovebox, a Teflon-sealed NMR tube was charged with ($^{15c5}N^{MeO}$COP)Pd(CF_3) (3.9 mg, 0.0060 mmol) and [Me_3O][BF_4] (2.6 mg, 0.018 mmol) in CD_2Cl_2 (500 μL). The reaction was monitored at 25 °C by ^{1}H NMR spectroscopy. The production of fluoromethane and one new Pd species with C_s symmetry was observed after 24 hours by NMR spectroscopy

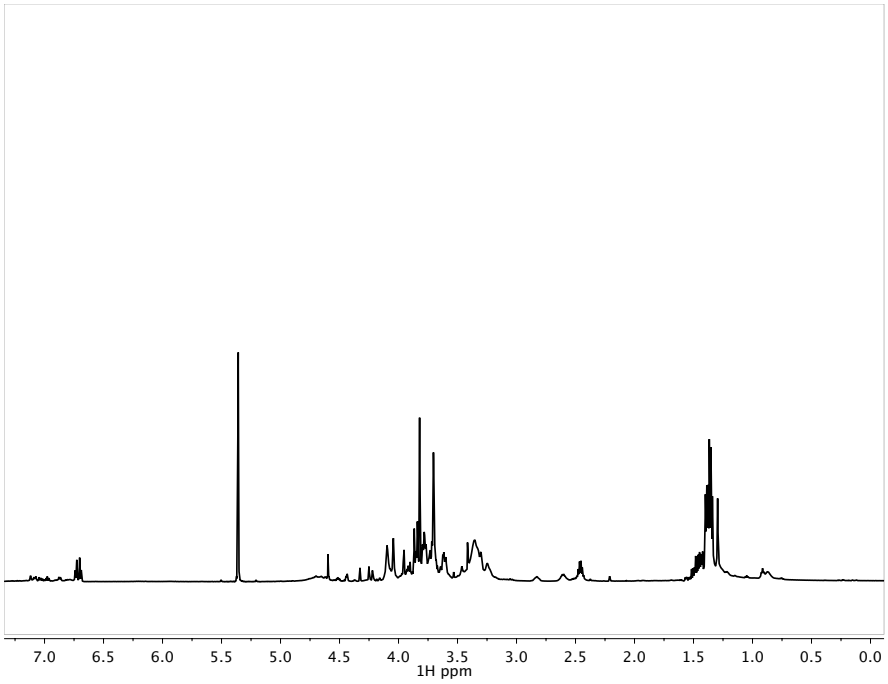

Figure 2.52. ^{1}H NMR spectrum of product from the addition of [Me_3O][BF_4] to ($^{15c5}N^{MeO}$COP)Pd(CF_3).

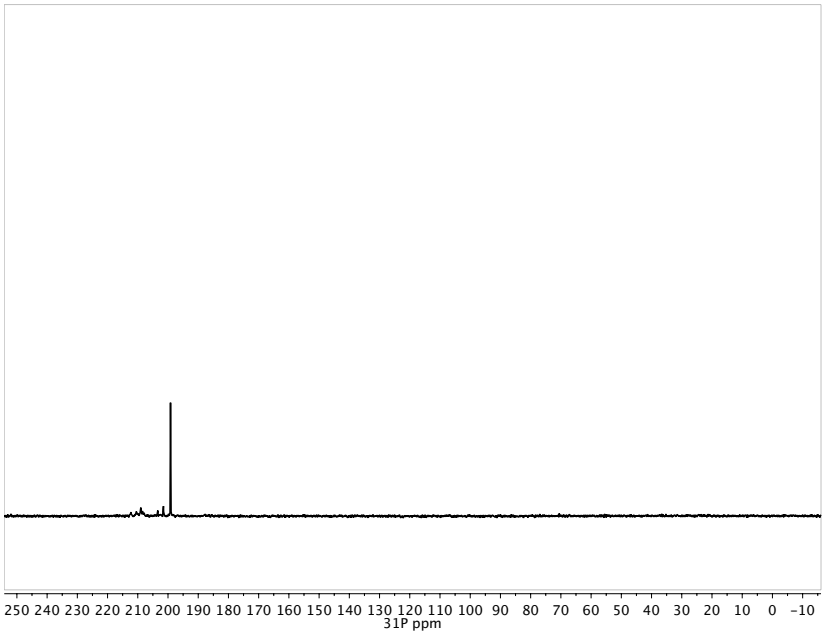

Figure 2.53. $^{31}P\{^{1}H\}$ NMR spectrum of product from the addition of $[Me_3O][BF_4]$ to $(^{15c5}N^{MeO}COP)Pd(CF_3)$.

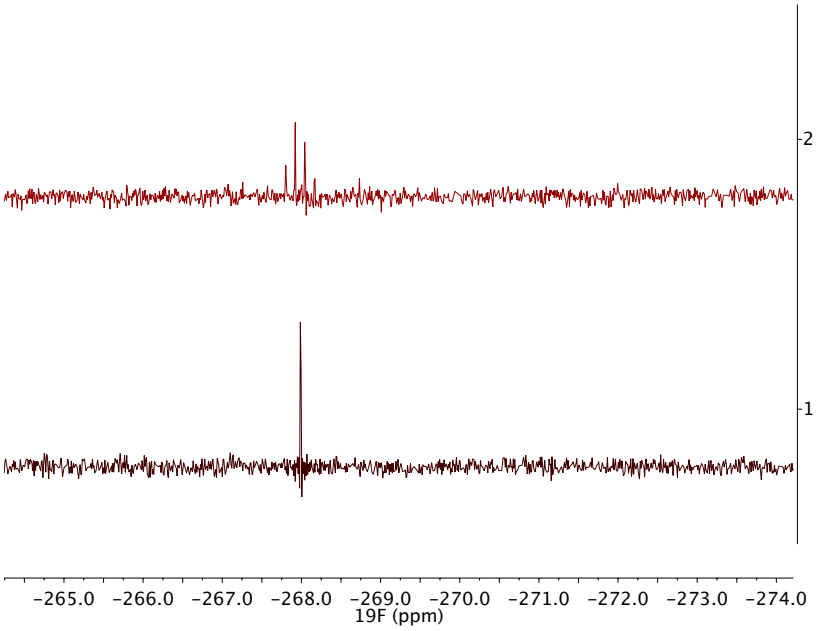

Figure 2.53. ^{19}F NMR (top) and $^{19}F\{^{1}H\}$ NMR spectra of CH_3F generated from the addition of $[Me_3O][BF_4]$ to $(^{15c5}N^{MeO}COP)Pd(CF_3)$.

CHAPTER 3 – POSITIONAL OLEFIN ISOMERIZATION BY CATIONIC PALLADIUM PINCER COMPLEXES

Introduction

Olefin isomerization remains an important reaction in pharmaceutical chemistry, the fragrance and pesticides industries, as well as in petrochemical synthesis, such as the Shell higher olefin process.[102] Three common pathways for olefin isomerization include an alkyl mechanism,[103–107] a radical pathway,[108,109] and a π-allyl mechanism that can either be base-assisted,[14,30,110,111] or proceed through formal C-H activation at the metal center, Scheme 3.1.[102,112] While olefins comprise a powerful functionality that can be readily elaborated in organic synthesis, the selective installation of unsaturation stereoselectively is challenging.[106] Thus, isomerization of a pre-existing olefin to a desired position in a substrate is desirable to garner synthetic diversity. Controllable catalysts with tunable rates are an attractive option to acquire products other than those driven by thermodynamics.

Scheme 3.1. Distinct mechanisms of olefin isomerization.

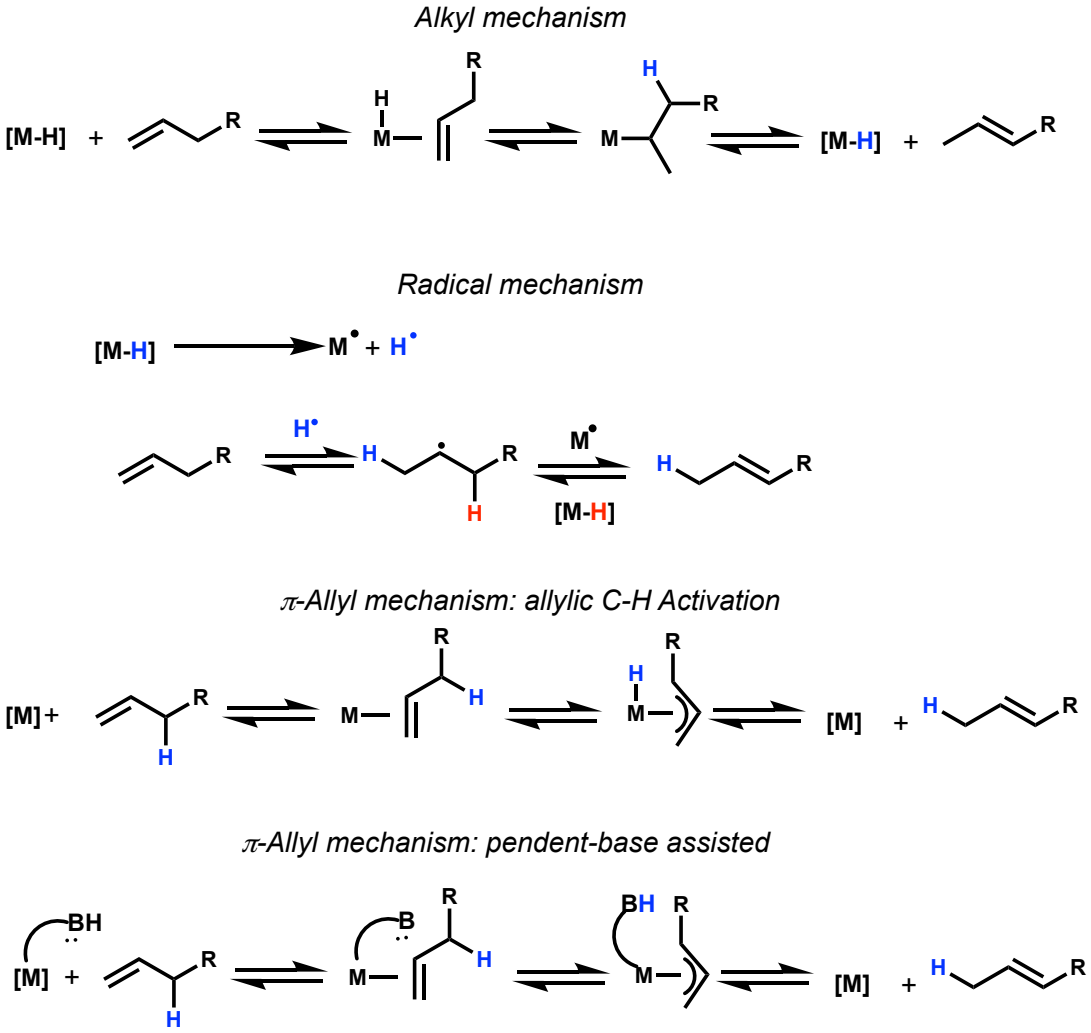

Our group has reported the olefin isomerization of allylbenzene by Ir-H pincer crown ether complexes that proceed via hydride insertion.[41] In this work, Kita and Miller found that the κ^3-(^{15c5}NCOP)Ir(H)(Cl) complex was inert towards olefin isomerization, however it was active upon abstraction of the chloride ligand towards the isomerization of allylbenzene (TOF 2,750 h^{-1}). The rate of isomerization could be tuned over two orders of magnitude via the addition of Li^+ cations. Accelerating the catalyst to achieve rapid turnover at room temperature enabled high

yields of β-methyl styrene with >99% *E* selectivity. At higher temperatures, the selectivity is eroded due to shifting thermodynamic distributions.

The iridium system is proposed to follow an insertion-elimination mechanism for olefin isomerization, Figure 3.1. In the absence of cations, the reaction is first order in allylbenzene and Ir and a pre-equilibrium of allylbenzene binding to Ir is proposed, and the hemilabile macrocycle is proposed to facilitate substrate binding. With increasing concentrations of Li^+ salt, the reaction becomes zero-order in allylbenzene.

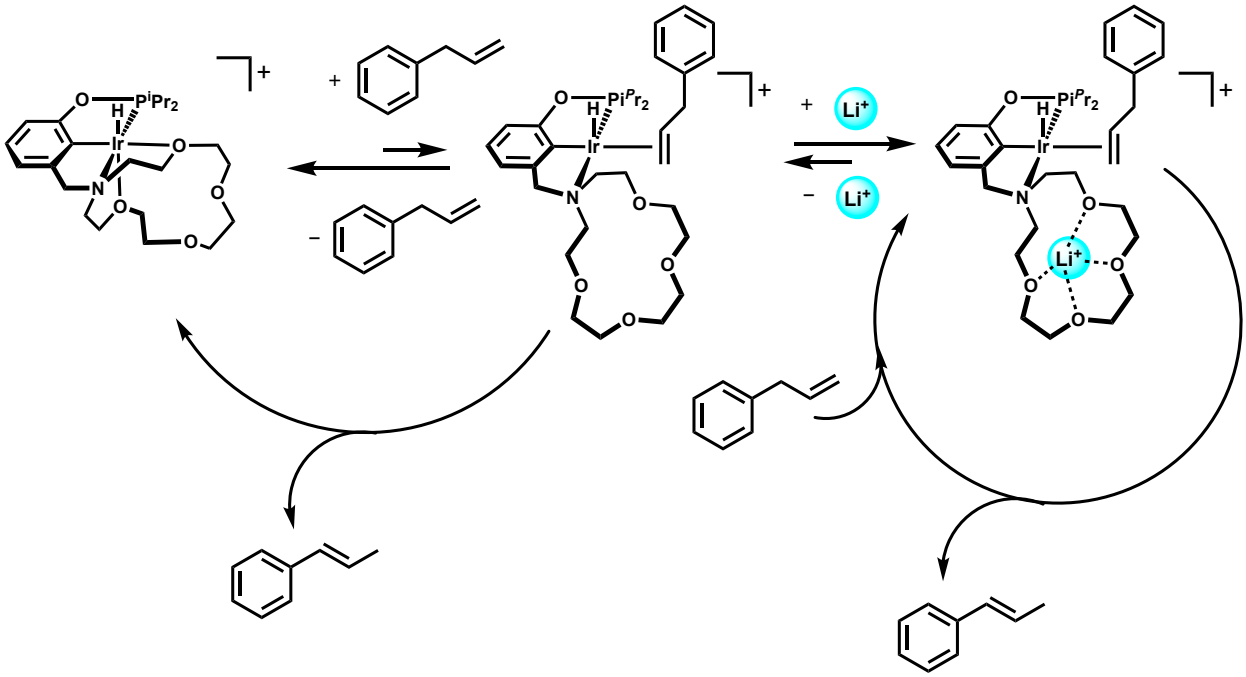

Figure 3.1. Hemilabile "pincer crown ether" ligand controls binding of allylbenzene.

A key feature of the mechanism of cation promotion is the ability of cation–macrocycle interactions to facilitate substrate binding. This hypothesis is supported by an analogous cationic Ni pincer complex reported by Smith and Miller,[39] which displayed triggered substrate-binding of electron-poor pentafluorophenylnitirile in methylene chloride. Neither the nitrile nor Li^+ salts

show evidence of interaction with nickel independently, but together they effect displacement of the ether donor of the pendent macrocycle and formation of a cationic nitrile complex.

Interest in exploring macrocyclic compounds of Pd is further enhanced by thermodynamic studies that indicate a particularly strong binding affinity for Li^+ cations.[101] The LiOTf binding affinity of pincer-crown ether complexes of iridium, nickel, palladium, and platinum were compared in acetonitrile, with the complex of the most electronegative metal, nickel, was found to have the weakest Li^+ binding affinity (120 M^{-1}), whereas the complex of the least electronegative metal, palladium, had the highest Li^+ binding affinity (294 M^{-1}). This observation is proposed to be imparted by inductive effects of the metal center,[74,101] where the more electronegative metal centers draw electron density from the crown ether binding pocket, dampening their Lewis basicity towards cations in solution.

Since Li^+ cations had the highest binding affinity with macrocyclic ethers appended to palladium, we hypothesized that a cationic pincer crown ether palladium complex may be a good candidate for cation-modulated catalysis. We therefore set out to study cation-promoted olefin isomerization at palladium. To interrogate the role of the macrocycle in any cation promotion, we chose to compare the reactivity of two different cationic palladium complexes, Figure 3.2: one supported by a pincer-crown ether ligand containing a pendent macrocycle; and another supported by a simple dialkylamine-based ligand lacking pendent ether donors altogether. At the start of this work, synthetic efforts to prepare an iridium complex supported by dialkylamine-based pincer ligand had been unsuccessful. Thus, the palladium system would enable this important comparison.

We expected $[(^{15c5}N^{MeO}COP)Pd]^+$ to be a stable catalyst that would have tunable rates of isomerization in the presence of Li^+ cations. The diethylamine analogue, $[(^{Et}N^{MeO}COP)Pd]^+$ was

expected to bind substrate readily, but it would lack catalytic rate modulation through the addition of cation additives, and also possibly lack stability due to the absence of a pendent ligand.

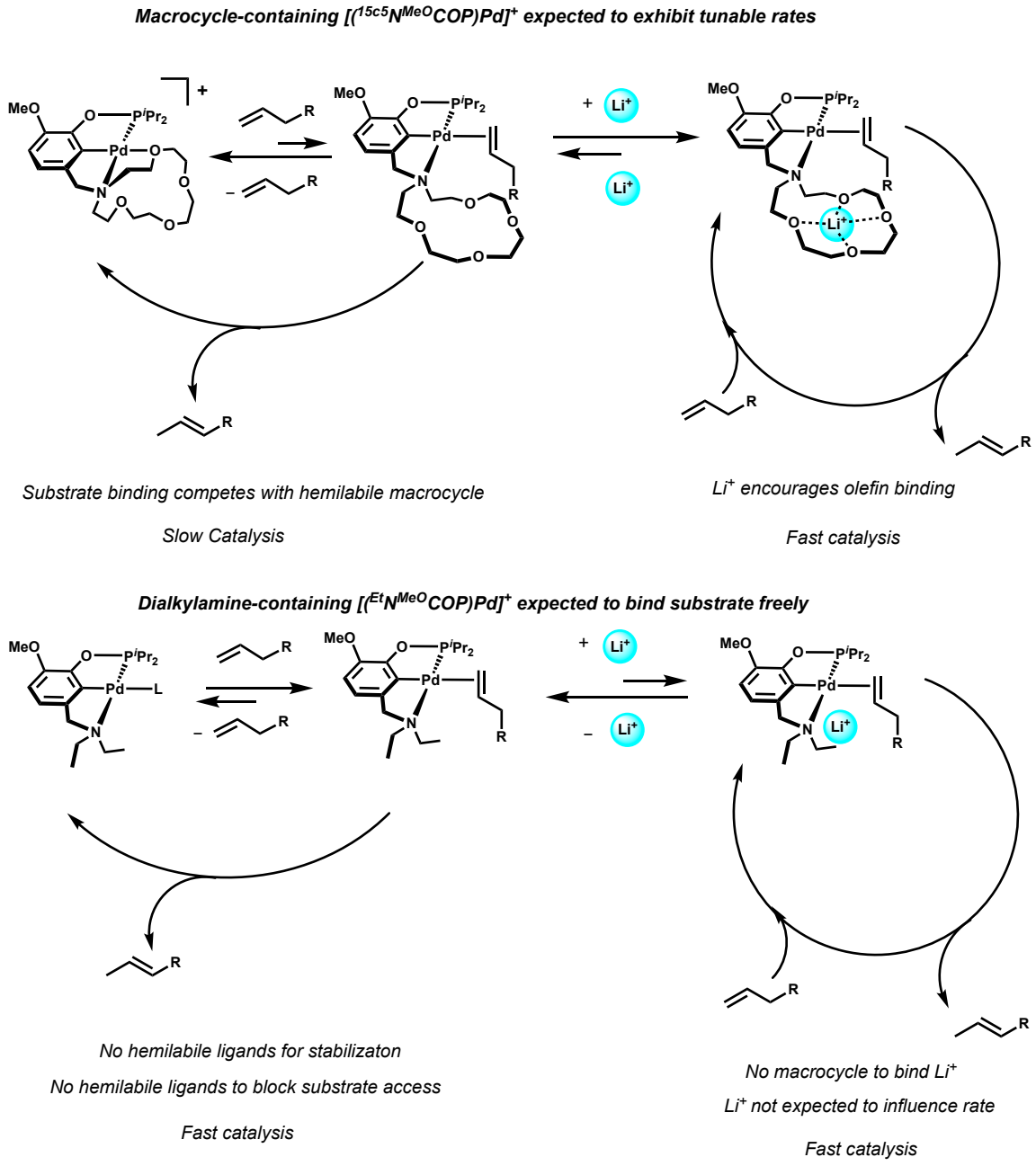

Figure 3.2. Cationic Pd complexes in this study and expected olefin binding reactivity.

The cationic palladium complexes were expected to exhibit significant differences from the related iridium pincer-crown ether complexes. First, the Pd complexes are square planar, whereas the iridium complexes are octahedral, such that the Pd complexes have a single macrocyclic ether donor while the Ir complexes have two. Thus, we wondered if the mechanism of olefin binding might be different, perhaps changing the way that cations influence the reaction. Second, the Pd complexes do not feature a metal hydride ligand, while the Ir complexes do contain a hydride. Given that these cationic palladium complexes contain no hydrides, we hypothesized that the $[(NCOP)Pd]^+$ species would isomerize olefins through a π-allyl mechanism. This could proceed either via a Pd^{IV} allyl hydride (after allylic C–H activation), or via a Pd(II) allyl (after allylic deprotonation by the amine in the pincer ligand).

Described herein are reactivity studies of $[(^{15c5}N^{MeO}COP)Pd]^+$ with allylbenzene, 2,3-dimethyl-1-butene, and 1-hexene. Proposed carbocationic rearrangements of allylbenzene and 2,3-dimethyl-1-butene precluded detailed kinetic analysis of these substrates. No coupling chemistry was observed with linear 1-hexene, however, so this substrate allowed for a comparative study with the dialkylamine-containing $[(^{Et}N^{MeO}COP)Pd]^+$ to interrogate the role of the hemilabile macrocycle of $[(^{15c5}N^{MeO}COP)Pd]^+$ in isomerization.

Results and Discussion

Preliminary Reactivity Studies

To begin our assessment of olefin isomerization, allylbenzene was selected as a prototypical substrate.[112] Investigating this substrate would allow for direct comparison to the Ir pincer-crown ether system.

The reactivity of the macrocycle-containing complex $[(^{15c5}N^{MeO}COP)Pd][PF_6]$ with allylbenzene was first explored in the absence of salt in CD_2Cl_2. No change to the catalyst

structure was observed by ^{1}H NMR spectroscopy. No isomerization of allylbenzene to β-methylstyrene was observed, even after one week at room temperature. This was somewhat surprising, given that the Ir pincer-crown ether system does slowly isomerize allylbenzene in the absence of salts.[41] No other reaction was observed, including no decomposition of the catalyst.

When the same reaction of allylbenzene and [(^{15c5}N^{MeO}COP)Pd][PF_6] is performed in the presence of LiBAr$^{F}_{4}$, consumption of allylbenzene in eight hours was observed by ^{1}H NMR spectroscopy, along with formation of the expected isomerization product, β-methylstyrene, Figure 3.3. Despite the initial promise of this cation-modulated reactivity, we were surprised to see that the β-methylstyrene product was consumed soon after it was formed, accompanied by the production of a plethora of products with signals in the aliphatic region of ^{1}H NMR spectra. ^{1}H NMR spectroscopic analysis after a work-up procedure led to the characterization of two cyclodimerized indans. These products appear to be derived from Friedel-crafts-type dimerization of β-methylstyrene.[113–115] No dimerization or other C–C coupled products were observed in the previously reported Ir system, regardless of cation identity or concentration in solution.[41] A possible explanation for the observed dimerization of β-methylstyrene could be trace protons or water in solution, made more Brønsted acidic from coordination to the added Li^{+} in solution.[114] To support that this observed dimerization chemistry was not merely due to the presence of added Li^{+} in solution, a control reaction under the same standard conditions with no Pd catalyst and only Li^{+} was run – neither isomerization nor dimerization of allylbenzene was observed, even after a week at room temperature.

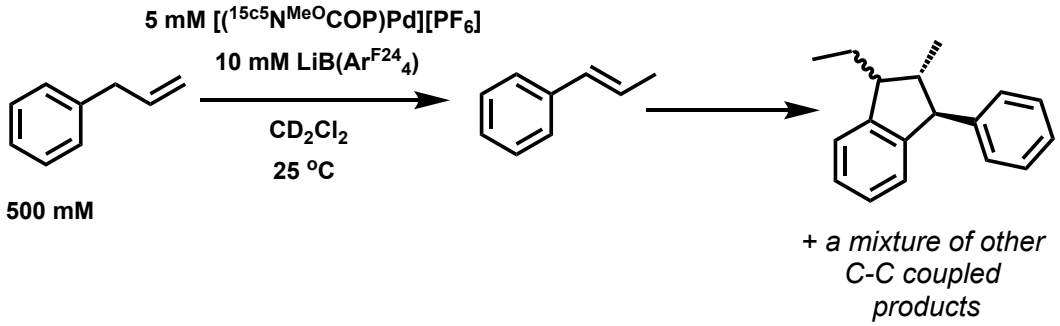

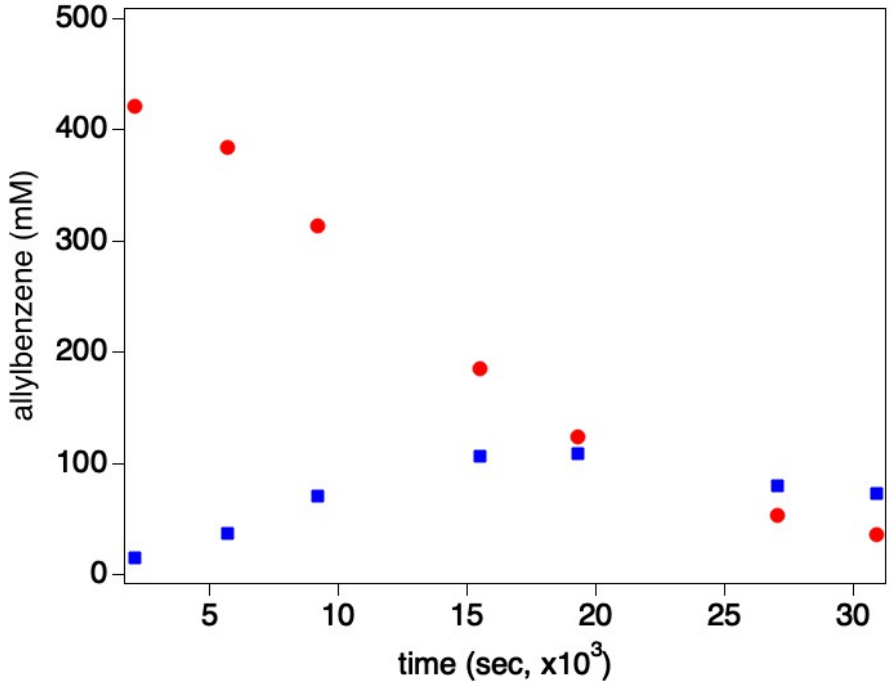

Figure 3.3. The consumption of allylbenzene (red dots) and β-methylstyrene (blue squares) in the presence of [($^{15c5}N^{MeO}$COP)Pd][PF_6] (5 mM) and $LiBAr^F_4$ (10 mM).

The reactivity of [($^{15c5}N^{MeO}$COP)Pd][$B(C_6F_5)_4$] with 2,3-dimethyl-1-butene was next investigated, Figure 3.4. No isomerization of 2,3-dimethyl-1-butene was observed in the absence of Li^+ cations over eight hours. In the presence of one equivalent of Li^+, on the other hand, isomerization of 2,3-dimethyl-1-butene to 2,3-dimethyl-2-butene proceeded to full conversion at room temperature in thirty minutes. The product was not stable to the reaction conditions, however, with extended reaction times leading to production of dimers and trimers of 2,3-

dimethyl-2-butene according to gas chromatography-mass spectrometry (GC-MS) analysis. Notably, the isomerization and dimerization chemistry of 2,3-dimethyl-1-butene are only observed in the presence of the Pd catalyst and Li salt – neither one of these components reacts with 2,3-dimethyl-1-butene in the absence of the other.

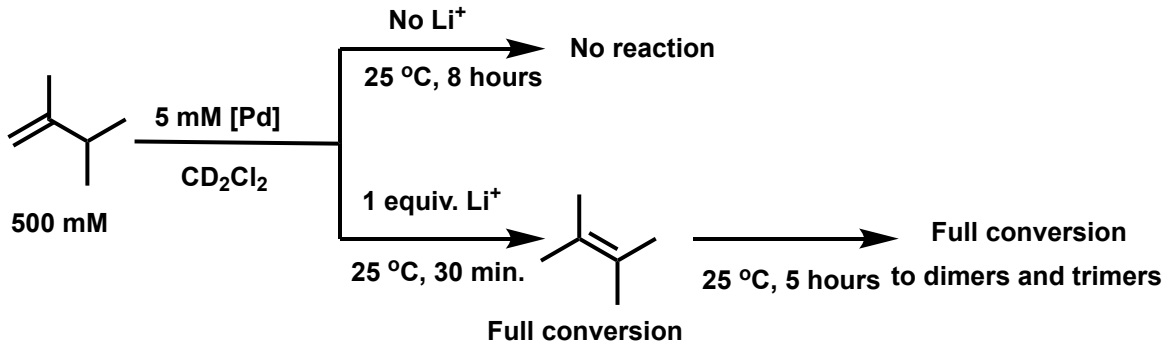

Figure 3.4. Isomerization of 2,3-dimethylbutene.

Both the allylbenzene and 2,3-dimethyl-1-butene reactions display the hallmarks of carbocation chemistry. The carbocationic rearrangement of substituted olefins by weakly ligated cationic Pd^{II} was reported by Sen and coworkers in 1988.[115] Sen notes that the electron affinity of Pd^{II} is actually comparable to that of other main group Lewis acids, such as Zn^{2+} or Hg^{2+}, and is notably twice that of isoelectronic metal ions Ir^{I} and Rh^{I}. However, since Pd^{II} has a smaller electron promotion energy than Zn^{II} or Hg^{II} cations, it can bind olefinic substrates much more tightly through more efficient back-bonding.

If the [($^{15c5}N^{MeO}$COP)Pd][$B(C_6F_5)_4$] catalyst was isomerizing 2,3-dimethyl-1-butene through a π-allyl mechanism, but was electrophilic enough to dimerize the product of isomerization, 2,3-dimethyl-2-butene, we postulated that in the presence of base, isomerization to 2,3-dimethyl-1-butene would proceed, but not the subsequent dimerization. To assess this hypothesis, a separate experiment monitoring the isomerization of 2,3-diemethyl-1-butene with

catalytic amounts of [($^{15c5}N^{MeO}$COP)Pd][$B(C_6F_5)_4$], Li($B(C_6F_5)_4$, and 2,6-ditertbutylpyridine was monitored by ^{1}H NMR spectroscopy. The isomerization of 2,3-dimethyl-1-butene to 2,3-dimethyl-2-butene was observed over twenty-four hours to reach 50% conversion, however no dimerization of the olefins was observed.[116] Additionally, the formation of Pd black was observed. In a separate experiment, one equivalent of ditertbutylpyridine was added to [($^{15c5}N^{MeO}$COP)Pd][$B(C_6F_5)_4$] in CD_2Cl_2. The production of Pd black and decomposition of the catalyst was observed.

To avoid complications from side reactions, we sought olefins that would be less susceptible to carbocationic chemistry as model substrates for isomerization.

Isomerization of 1-hexene with [($^{15c5}N^{MeO}$COP)Pd][$B(C_6F_5)_4$]

To investigate the rate of isomerization with [($^{15c5}N^{MeO}$COP)Pd][$B(C_6F_5)_4$], we first looked at its activity in the presence of 1-hexene with no added Li^+ in methylene chloride. No isomerization of 1-hexene was observed by ^{1}H NMR spectroscopy in the presence of [($^{15c5}N^{MeO}$COP)Pd][$B(C_6F_5)_4$], even after one week at room temperature, Figure 3.5. Further, no changes were observed in the ^{1}H NMR spectrum to indicate any change in catalyst concentration, structure, or olefin binding in the presence of 1-hexene.

However, in the analogous reaction under standard conditions with the added 1 equivalent of $LiBAr^F{}_4$, slow isomerization of 1-hexene to *cis* and *trans* 2-hexene and 3-hexene was observed over the course of five days by ^{1}H NMR spectroscopy, with a calculated TOF of 0.51 h^{-1}. No further carbocation-type reactions were observed.

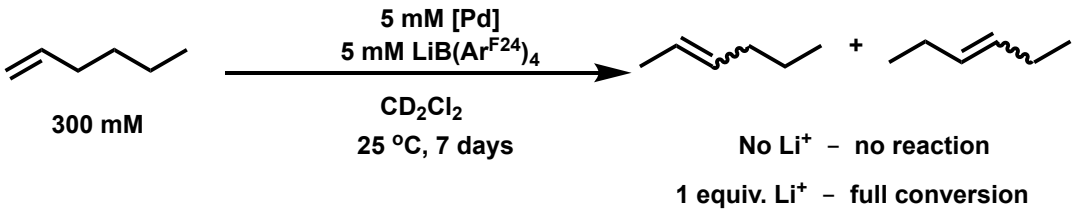

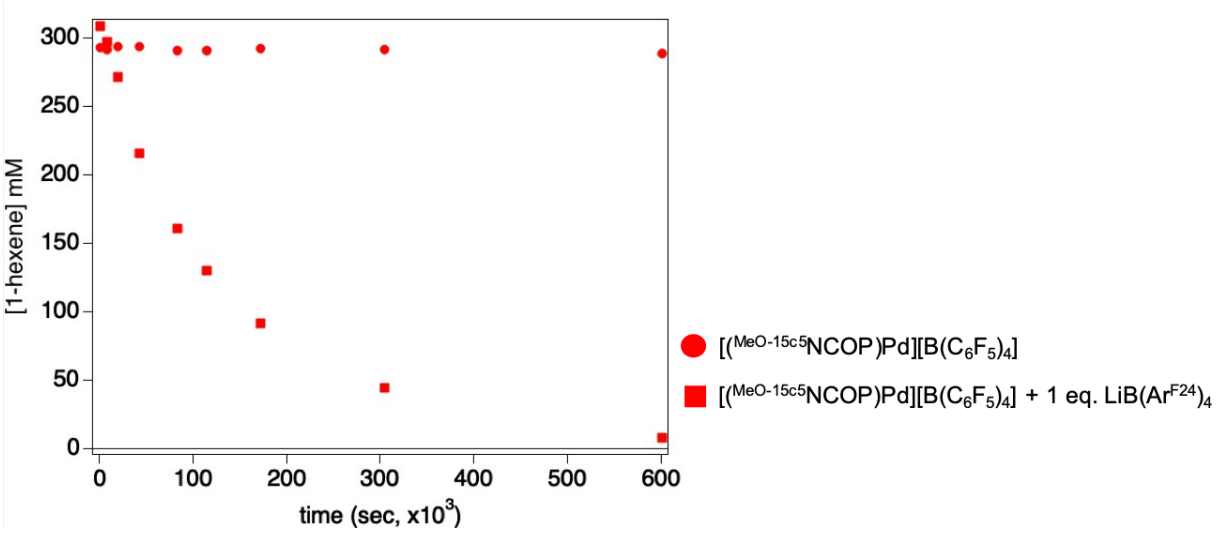

Figure 3.5. Isomerization of 1-hexene in the presence of [($^{15c5}N^{MeO}$COP)Pd][$B(C_6F_5)_4$].

In order to gain insight into catalyst stability and reproducibility, four different isomerization reactions of varying initial [1-hexene] using two different batches of Pd catalyst in the presence of 1 eq $LiBAr^F_4$ were monitored via ^{1}H NMR spectroscopy. The raw data was then "time-adjusted" utilizing reaction progress kinetic analysis (RPKA)[117] to create a visual comparison of reactions starting at different initial concentrations of 1-hexene. RPKA provides insight into catalyst stability: if the time-adjusted data overlay, it suggests that a catalyst is well-behaved and not subject to product inhibition; however, if the data do not overlay, it suggests that the catalyst is either decomposing or becoming deactivated by the accumulating product. As can be seen in Figure 3.6, the data from all initial concentrations of 1-hexene overlay after time-adjustment, suggesting that [($^{15c5}N^{MeO}$COP)Pd][$B(C_6F_5)_4$] is neither deactivated by substrate nor decomposing during the reaction.

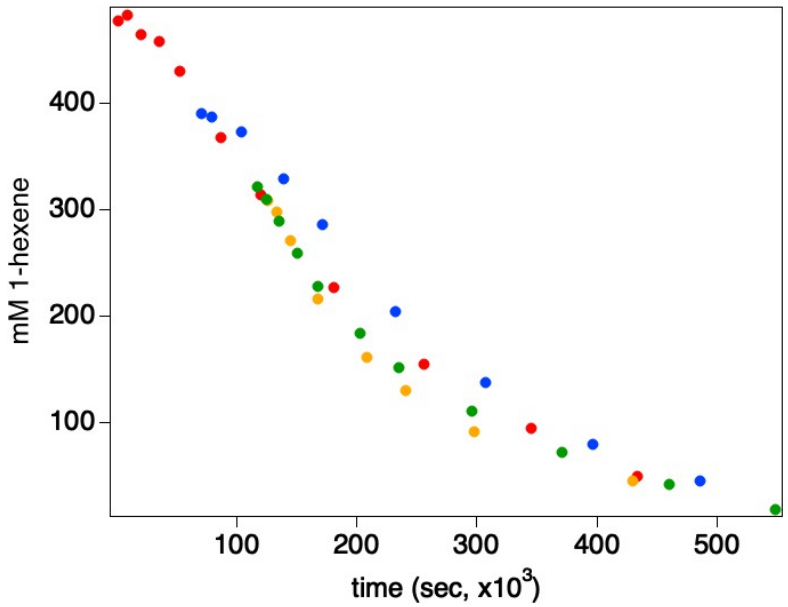

Figure 3.6. Time-adjusted overlay of the isomerization of 1-hexene by $[(^{15c5}N^{MeO}COP)Pd][B(C_6F_5)_4]$ (5 mM) and $LiBAr^{F}{}_4$ (5 mM) shows catalyst robustness and lack of product inhibition.

We next determined the order in 1-hexene utilizing variable time normalization analysis (VTNA).[118,119] This analysis is done by plotting the abscissa axis normalized for time (Σ[1-hexene]$^{\beta}\Delta$t) for reactions starting at different concentrations of 1-hexene, against the concentration of product, where β in the abscissa axis represents the order of 1-hexene in the reaction. Overlay of the data suggests that the correct order of substrate has been determined. As displayed in Figure 3.7, the order in 1-hexene was determined to be first order. It was also determined that this reaction proceeded first order in 1-hexene by plotting the natural log of the concentration of 1-hexene vs. time, which had a linear fit.

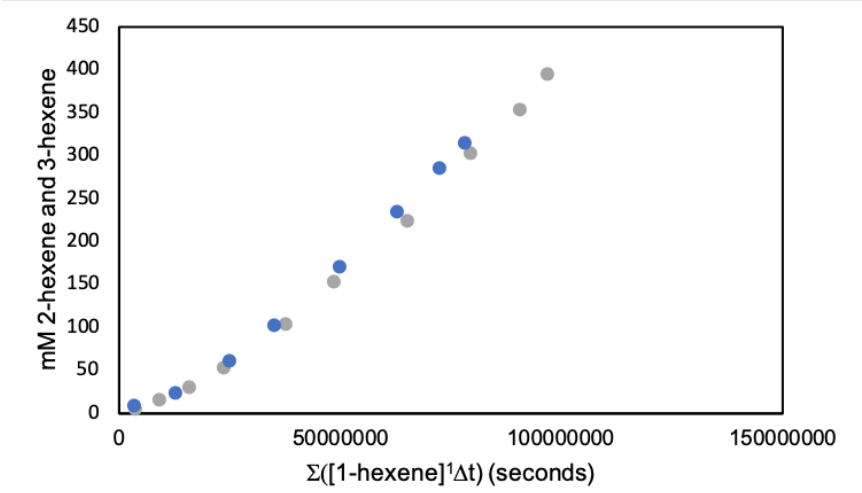

Figure 3.7. VTNA treatment to determine order in 1-hexene by [($^{15c5}N^{MeO}$COP)Pd][$B(C_6F_5)_4$] (5 mM) and $LiBAr^{F24}{}_4$ (5 mM).

The order in Pd catalyst was also determined utilizing VTNA treatment of the isomerization kinetics in the presence of [($^{15c5}N^{MeO}$COP)Pd][$B(C_6F_5)_4$] and one equivalent of $LiBAr^F{}_4$. The isomerization of 1-hexene was examined at two different catalyst concentrations: 5 mM Pd and 5 mM Li^+, as well as 2.5 mM Pd and 2.5 mM Li^+. Reasonable overlay of the two reactions plotted in first order for the Pd catalyst and Li^+ are consistent with one discrete molecular Pd complex catalyzing the reaction in the presence of one equivalent of Li^+, Figure 3.8.

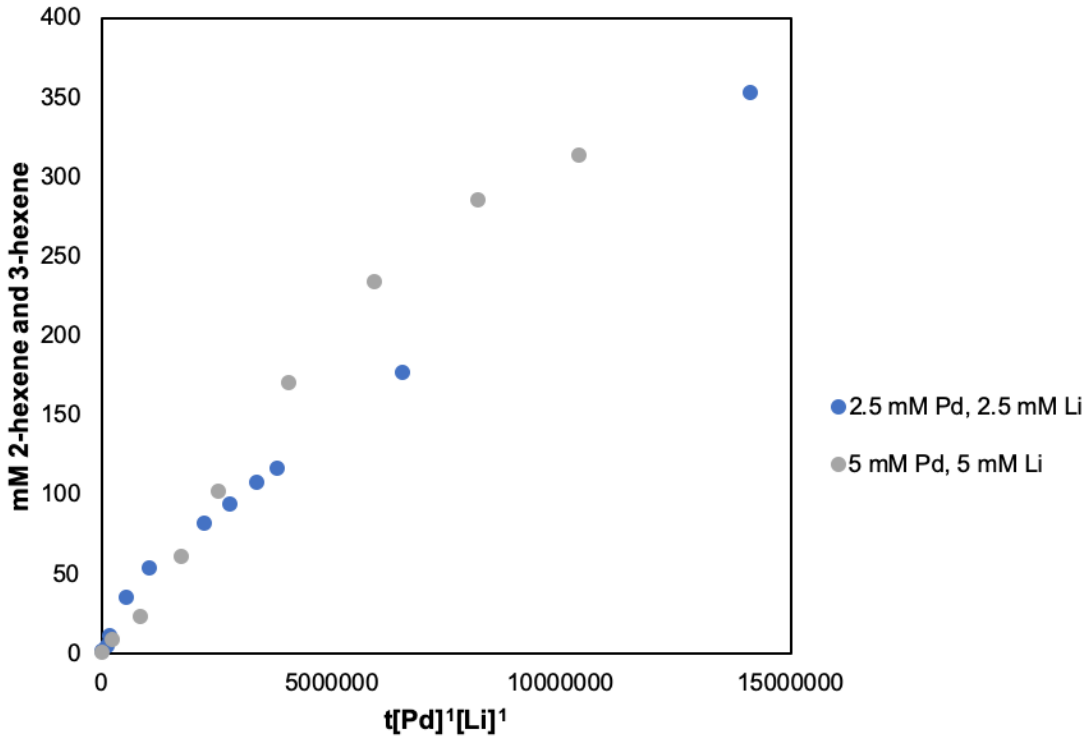

Figure 3.8. VTNA normalization to determine the order in [(^{15c5}N^{MeO}COP)Pd][B(C_6F_5)$_4$] catalyst, assuming first order in Li^+.

Isomerization of 1-hexene with [(^{Et}N^{MeO}COP)Pd][B(C_6F_5)$_4$]

The isomerization reactivity of the diethylamine-substituted [(^{Et}N^{MeO}COP)Pd][B(C_6F_5)$_4$] species was explored next. Isomerization of 1-hexene proceeded over the course of fifteen hours in the presence of [(^{Et}N^{MeO}COP)Pd][B(C_6F_5)$_4$] with no added salt (TOF 3.4 h^{-1}), significantly faster than [(^{15c5}N^{MeO}COP)Pd][B(C_6F_5)$_4$] with Li^+ (TOF 0.51 h^{-1}). This is significant, since as stated above, no isomerization of 1-hexene was observed with the macrocycle-containing [(^{15c5}N^{MeO}COP)Pd][B(C_6F_5)$_4$] catalyst in the absence of Li^+. This observation is consistent with the hypothesis that Li^+ is required to labilize the crown ether from [(^{15c5}N^{MeO}COP)Pd][B(C_6F_5)$_4$] to allow substrate binding, whereas in the diethylamine-substituted [(^{Et}N^{MeO}COP)Pd][B(C_6F_5)$_4$], no hemilabile ligand blocks substrate access and Li^+ is not expected to be required.

Time adjusted kinetics were also pursued with this system in order to determine the catalyst's robustness. Five isomerizations under the standard reaction conditions with varying initial concentrations of 1-hexene and two different batches of Pd catalyst were monitored via ^{1}H NMR spectroscopy. The results are shown in Figure 3.9 below, highlighting the robustness of this catalyst system in the absence of Li^{+} cations.

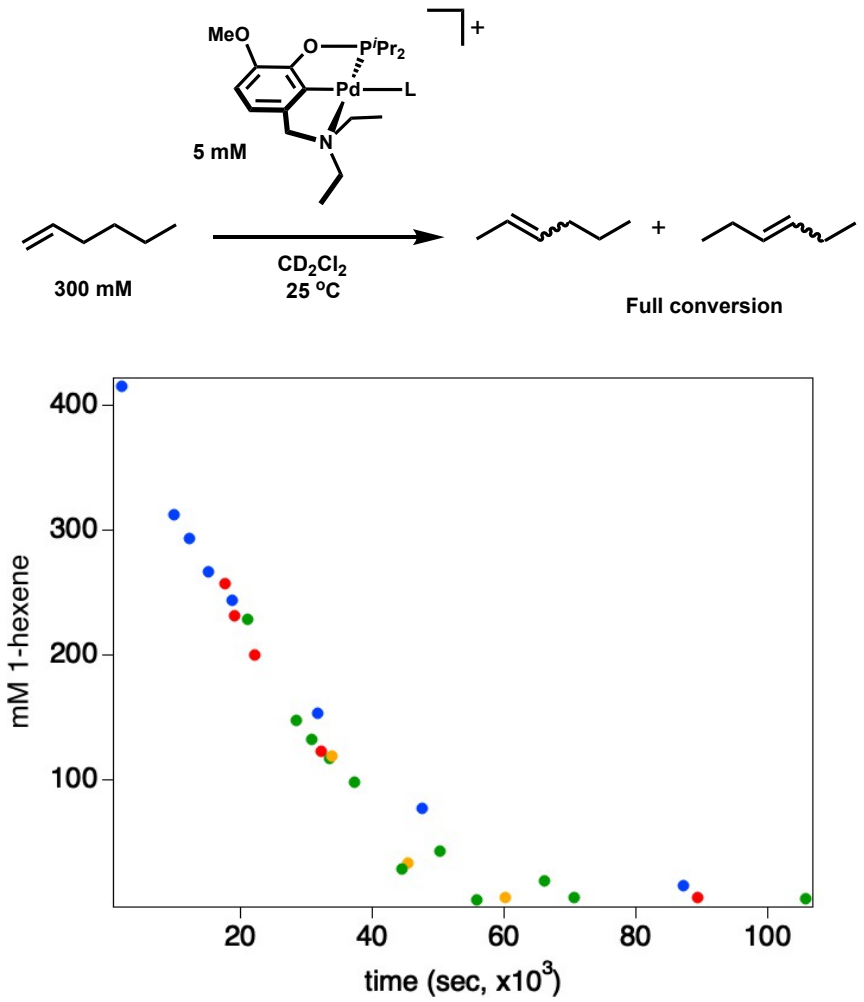

Figure 3.9. Time-adjusted overlay of the isomerization of 1-hexene by [($^{Et}N^{MeO}$COP)Pd][B(C_6F_5)$_4$] (5 mM) shows catalyst robustness and lack of product inhibition.

The isomerization of 1-hexene in the presence of [($^{Et}N^{MeO}$COP)Pd][B(C_6F_5)$_4$] was calculated to be nearly first order in 1-hexene (0.8) utilizing VTNA treatment of the kinetics,

Figure 3.10. Classic treatment of the kinetics, plotting the natural log of the concentration of 1-hexene versus time supported first order kinetics in 1-hexene.

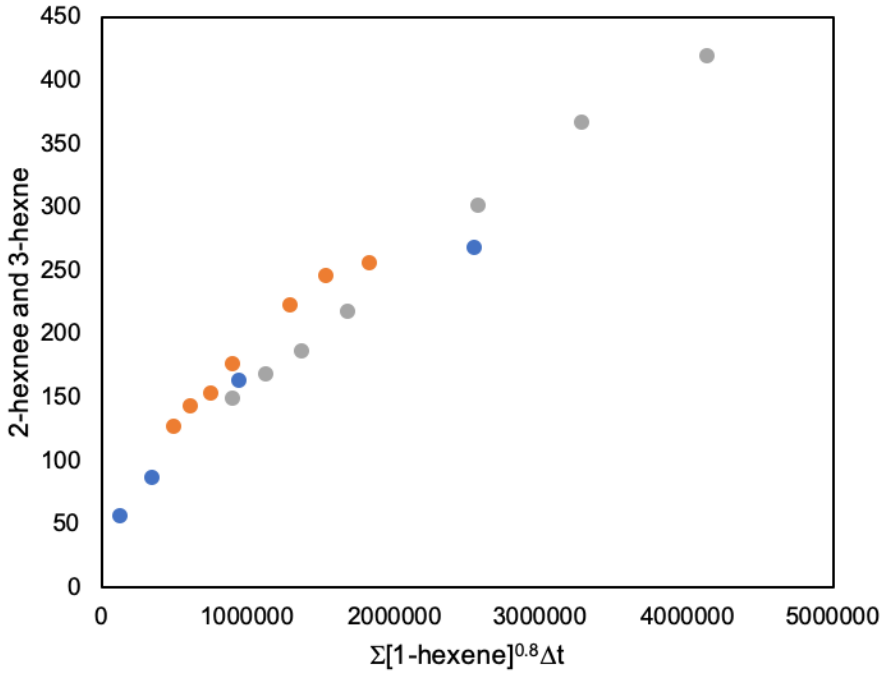

Figure 3.10. VTNA treatment of the isomerization of 1-hexene by [($^{Et}N^{MeO}$COP)Pd][$B(C_6F_5)_4$] to determine the order in 1-hexene.

In the presence of one equivalent of $LiBAr^F{}_4$, isomerization of 1-hexene proceeded to complete conversion over the course of four days (TOF 0.68 h^{-1}), approximately five times slower than in the case with no added salt (TOF 3.4 h^{-1}), Figure 3.11.

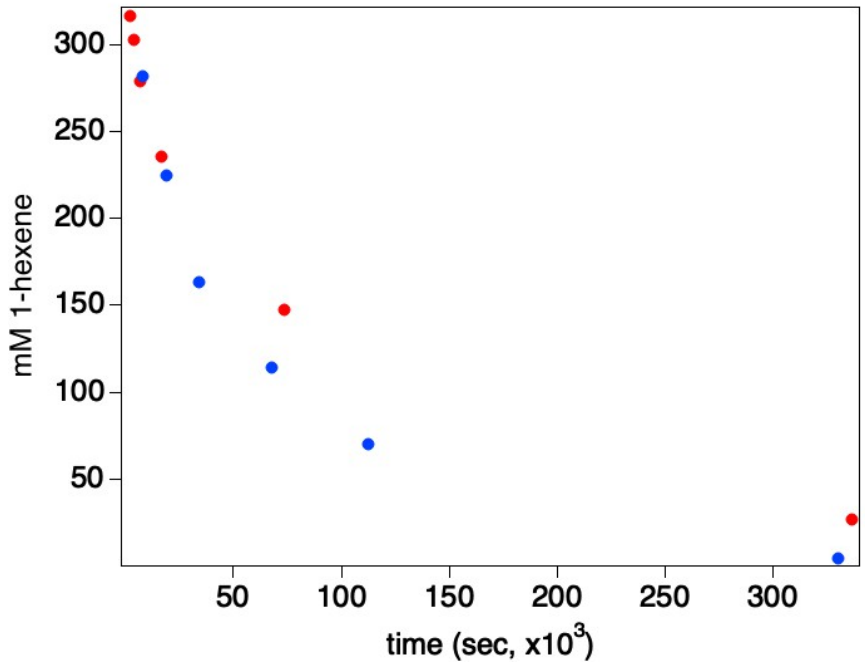

Figure 3.11. Time-adjusted overlay of the isomerization of 1-hexene by [($^{Et}N^{MeO}$COP)Pd][$B(C_6F_5)_4$] (5 mM) and $LiBAr^F_4$ (5 mM) shows catalyst robustness and lack of product inhibition.

The order in 1-hexene in the presence of [($^{Et}N^{MeO}$COP)Pd][$B(C_6F_5)_4$] and $LiBAr^F_4$ was determined utilizing VTNA treatment of the kinetics, where there was reasonable overlay to support first order kinetics in 1-hexene, as seen in Figure 3.12. Treating the data classically in plotting the natural log of the concentration of 1-hexene versus time, first order kinetics in 1-hexene are more apparent, Figure 3.13.

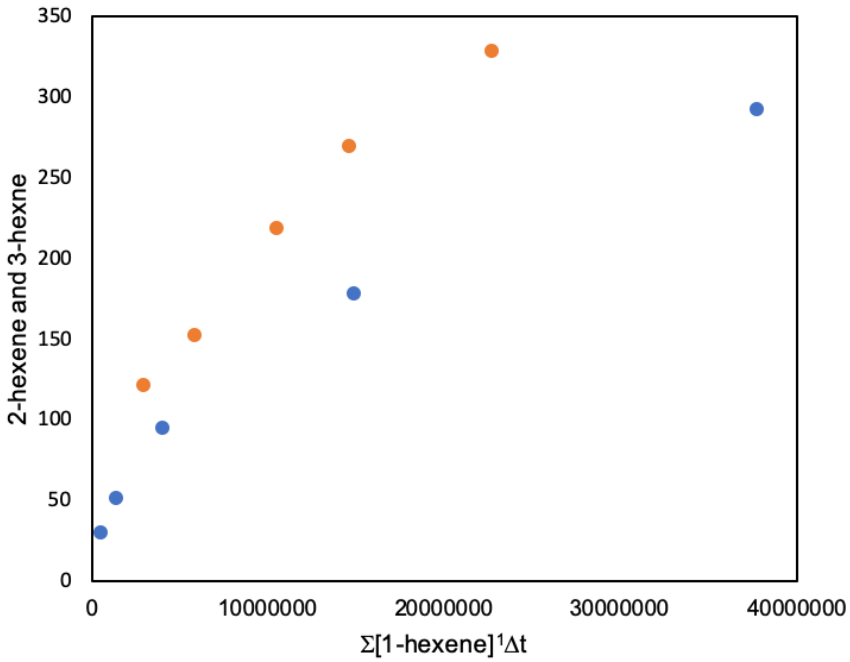

Figure 3.12. VTNA treatment to determine the order of 1-hexene in the presence of [($^{Et}N^{MeO}$COP)Pd][B(C_6F_5)$_4$] and one equivalent LiBAr$^F_4$.

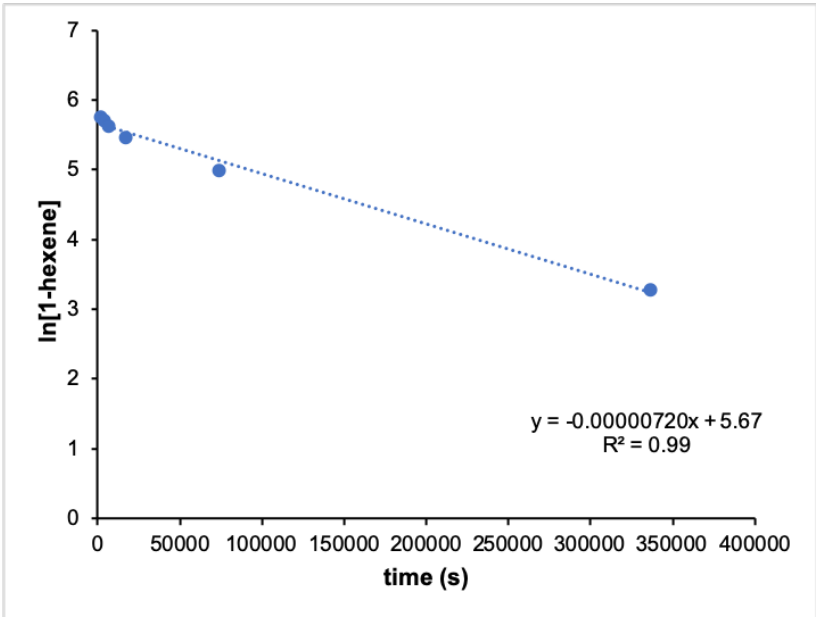

Figure 3.13. Classic treatment to determine the order of 1-hexene in the presence of [($^{Et}N^{MeO}$COP)Pd][B(C_6F_5)$_4$] and one equivalent LiBAr$^F_4$.

The slower isomerization of 1-hexene in the presence of Li^+ and $[(^{Et}N^{MeO}COP)Pd][B(C_6F_5)_4]$, again, is distinctly different than the isomerization of 1-hexene with the macrocycle-containing catalyst, $[(^{15c5}N^{MeO}COP)Pd][B(C_6F_5)_4]$, which is activated towards isomerization in the presence of Li^+, whereas no reactivity with olefin is observed in its absence. Interestingly, isomerization of 1-hexene proceeds at approximately the same rate with both the macrocyle-containing $[(^{15c5}N^{MeO}COP)Pd][B(C_6F_5)_4]$ (TOF 0.51 h^{-1}) and the dialkylamine-containing $[(^{Et}N^{MeO}COP)Pd][B(C_6F_5)_4]$ (TOF 0.68 h^{-1}) in the presence of Li^+. Since the isomerization of 1-hexene proceeds approximately five times faster (TOF 3.4 h^{-1}) with $[(^{Et}N^{MeO}COP)Pd][B(C_6F_5)_4]$ in the absence of Li^+, the comparison of the two catalysts supports two mechanistic possibilities: one, that Li^+ is required in the macrocycle-containing system to allow substrate binding, and two, that Li^+ impedes the isomerization of 1-hexene through some other mechanistic pathway in the dialkylamine-containing system.

One hypothesis for the slower kinetics of the dialkylamine-containing $[(^{Et}N^{MeO}COP)Pd][B(C_6F_5)_4]$ in the presence of Li^+ was the presence of more Lewis basic donors in solution that would compete with 1-hexene binding due to the addition of three extra equivalents of ether that come with the added $LiBAr^F{}_4$ salt. However, no differences in rates were observed for the isomerization of 1-hexene in the presence of $[(^{Et}N^{MeO}COP)Pd][B(C_6F_5)_4]$ and two different ether concentrations (40 mM and 80 mM). Another possibility for the slower kinetics in the presence of Li^+ could be that the basicity of the pincer's diethylamine moiety is reduced in the presence of Lewis acidic Li^+ cations, which would be consistent with a π-allyl mechanism.

Summary and Outlook

The reactivity of macrocycle-containing complex [(^{15c5}N^{MeO}COP)Pd][B(C_6F_5)$_4$] and the acyclic, diethylamine-containing complex [(^{Et}N^{MeO}COP)Pd][B(C_6F_5)$_4$] were examined with a variety of olefins. In the absence of Li^+ in solution, the macrocycle-containing [(^{15c5}N^{MeO}COP)Pd]$^+$ does not react with olefins in solution; however, in the presence of Li^+, isomerization of allylbenzene and 2,3-dimethyl-1-butene and their subsequent dimerization were observed. The dimerization of 2,3-dimethyl-1-butene could be suppressed in the presence of base, however its isomerization only proceeded to 50% conversion along with the production of Pd black. Linear 1-hexene was isomerized in the presence of [(^{15c5}N^{MeO}COP)Pd][B(C_6F_5)$_4$] and Li^+, and no dimerization was observed, even in the absence of base.

The dialkylamine-containing complex [(^{Et}N^{MeO}COP)Pd][B(C_6F_5)$_4$] isomerized 1-hexene even in the absence of Li^+. This supports the hypothesis that without pendent ethers to block coordination of substrate, no Li^+ is needed to open a coordination site on Pd. While we expected Li^+ in solution to have minimal effect on the rate of isomerization in the presence of [(^{Et}N^{MeO}COP)Pd][B(C_6F_5)$_4$], the isomerization actually proceeded five times slower with one equivalent of added Li^+. We tentatively propose that this may be due to Li^+ coordination to the pendent amine, which would decrease its basicity and be expected to retard the formation of a Pd-allyl if proceeding through a base-assisted π-allyl mechanism, Scheme 3.2.

While there are some similarities to the previously reported Ir-H system, there are also marked differences. Unlike the Ir-H catalyst, macrocycle-containing [(^{15c5}N^{MeO}COP)Pd][B(C_6F_5)$_4$] is not active towards olefin isomerization in the absence of Li^+, while slow isomerization of allylbenzene proceeds in the presence of [κ^5-(^{15c5}NCOP)Ir(H)]$^+$ even with no added cations. Isomerization of three different olefins, allylbenzene, 2,3-dimethyl-1-

butene, and 1-hexene, proceeds in the presence of catalytic amounts of Li^+ and [($^{15c5}N^{MeO}$COP)Pd][$B(C_6F_5)_4$]. In the case of allylbenzene and 2,3-dimethyl-1-butene, total consumption of the isomerized products to generate conjugated dimers is observed. This reactivity has not been reported with the Ir-H system, and is a hallmark of carbocationic rearrangement chemistry at cationic Pd.

This work lays the foundation for investigations into macrocycle-containing [($^{15c5}N^{MeO}$COP)Pd][$B(C_6F_5)_4$] reactivity towards olefins, as well as comparative reactivity of the dialkylamine-containing [($^{Et}N^{MeO}$COP)Pd][$B(C_6F_5)_4$]. Dialkylamine aminophosphinite scaffolds could not previously be accessed on Ir, and this work provides an opportunity to interrogate the role of the macrocycle in catalysis relative to non-macrocycle containing analogues.

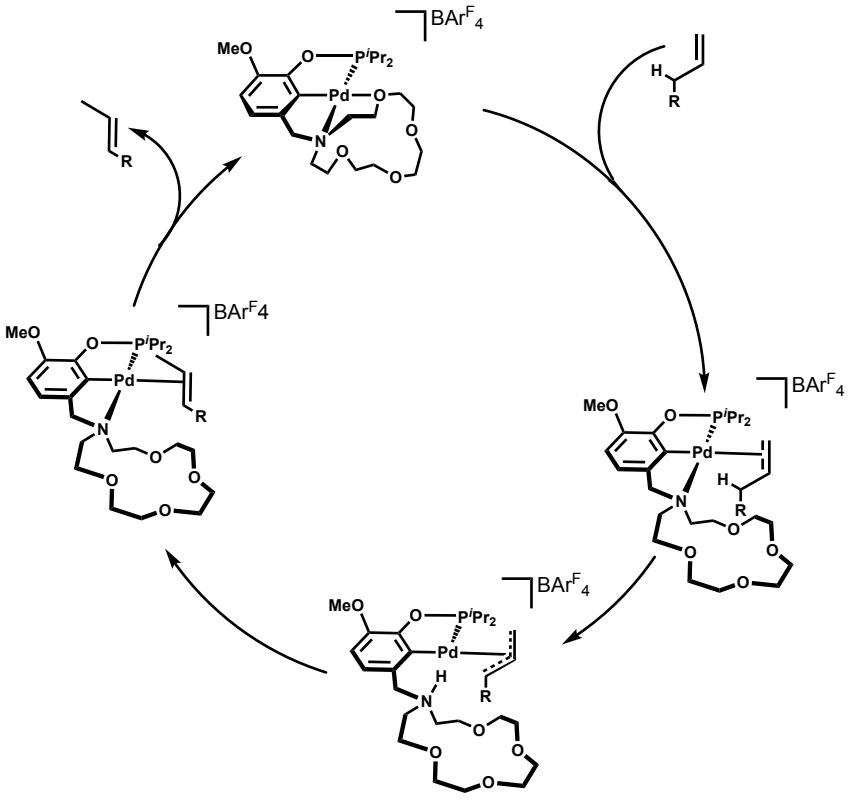

Scheme 3.2. Proposed internal base-assisted isomerization by [($^{15c5}N^{MeO}$COP)Pd][$B(C_6F_5)_4$].

Experimental

General Considerations

All reactions were performed under an inert nitrogen atmosphere, utilizing standard vacuum line and glovebox techniques unless otherwise noted. All NMR-scale kinetic reactions were prepared in a glovebox and monitored in Teflon-sealed NMR tubes. Organic solvents were dried and degassed with argon using a Pure Process Technology solvent system and stored over 3 Å molecular sieves. Under standard glovebox operating conditions, pentane, diethyl ether, benzene, toluene, and tetrahydrofuran were used without purging, so traces of those solvents were present in the atmosphere and in the solvent bottles. Mass spectra from gas-chromatography mass-spectrometry were collected on a ThermoScientific Exactive GC, with a mass range of 30 to 700 Da, and resolution up to 50,000 at *m/z* 272. ^{1}H NMR spectra were recorded on 400, 500, or 600 MHz spectrometers. NMR characterization data are reported at 25 °C, unless specified otherwise. All of the NMR solvents were purchased from Cambridge Isotopes Laboratories. Methylene chloride-*d*2 (CD_2Cl_2) was freeze− pump−thaw-degassed three times, dried by passage through a small column of activated alumina, and stored over 3 Å molecular sieves. ^{1}H chemical shifts are reported in parts per million relative to residual proteo solvent resonances. [($^{Et}N^{MeO}$COP)Pd[$B(C_6F_5)_4$] and [($^{15c5}N^{MeO}$COP)Pd[$B(C_6F_5)_4$] were synthesized according to procedures detailed in Chapter 2. $LiBAr^F_4 \bullet 3Et_2O$ was prepared according to literature procedure. Allylbenzene, 2,3-dimethyl-1-butene, 1-hexene, and mesitylene were freeze− pump−thaw-degassed three times, dried by passage through a small column of activated alumina, and stored over 3 Å molecular sieves. All of the other reagents were commercially available and used without further purification.

Isomerization of allylbenzene

A stock solution of [($^{15c5}N^{MeO}$COP)Pd][PF_6] (10.0 mg, 0.0138 mmol) and hexamethylbenzene (10.0 mg, 0.0616 mmol) in CD_2Cl_2 (1.70 mL) was prepared. A second solution of $LiBAr^F{}_4$ (11.0 mg, 0.0126 mmol) in CD_2Cl_2 (1.00 mL) was prepared. Two Teflon-sealed NMR tubes were charged with 300 μL each of the Pd/hexamethylbenzene stock solution. To one of the tubes, was added 200 μL of the $LiBAr^{F24}{}_4$ solution. To the other tube was added 200 μL CD_2Cl_2. To each tube was added allylbenzene (33 μL, 0.249 mmol). The tubes were allowed to sit at 25 °C and the reactions were monitored by ^{1}H NMR spectroscopy. The reaction containing $LiBAr^F{}_4$ was dried *in vacuo* after total consumption of β-methylstyrene, re-dissolved in pentane, and run through a short silica plug. Cyclized indans were isolated from the mixture of β-methylstyrene dimers.

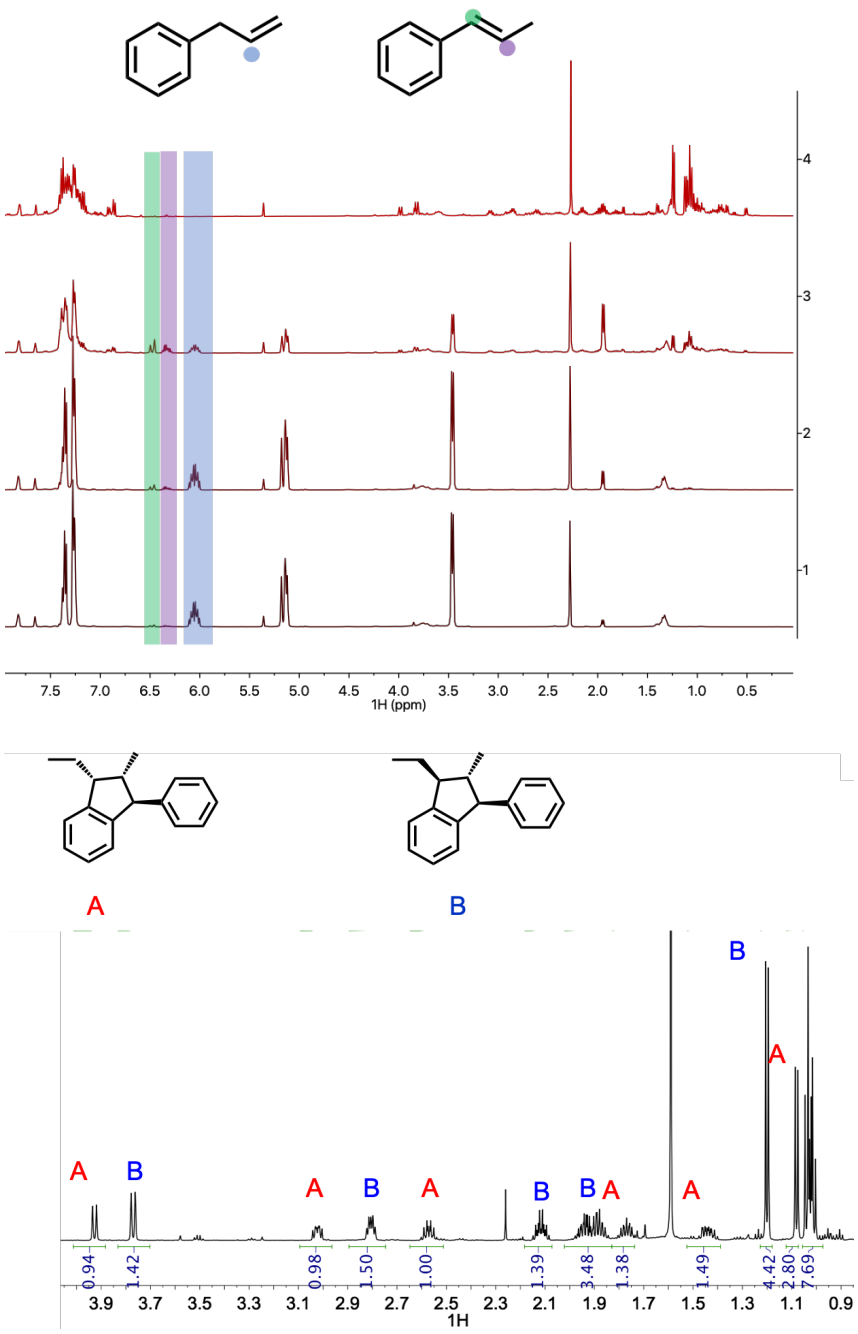

Figure 3.14. A representative ^{1}H NMR in CD_2Cl_2 stack of the isomerization of allylbenzene by [($^{15c5}N^{MeO}$COP)Pd][PF_6] and $LiBAr^{F24}{}_4$ (top), and the ^{1}H NMR spectrum of two isolated indans in $CDCl_3$ (bottom).

Isomerization of 2,3-dimethyl-1-butene

A stock solution of [($^{15c5}N^{MeO}$COP)Pd][$B(C_6F_5)_4$] (13.3 mg, 0.0106 mmol) and mesitylene (10 μL, 0.0719 mmol) in CD_2Cl_2 (1.30 mL) was prepared. A second solution of $LiB(C_6F_5)_4$ (10.6 mg, 0.0121 mmol) in CD_2Cl_2 (1.00 mL) was prepared. Four Teflon-sealed NMR tubes were charged with 300 μL each of the Pd/mesitylene stock solution. To two of the tubes, was added 200 μL of the $LiB(C_6F_5)_4$ solution. To one of these tubes was added ditertbutylpyridine (0.5 μL, 0.002 mmol). To the remaining two tubes was added 200 μL CD_2Cl_2. To one of these tubes was added ditertbutylpyridine (0.5 μL, 0.002 mmol). To each tube was added 2,3-dimethyl-1-butene (30 μL, 0.248 mmol). The tubes were allowed to sit at 25 °C and the reactions were monitored by ^{1}H NMR spectroscopy.

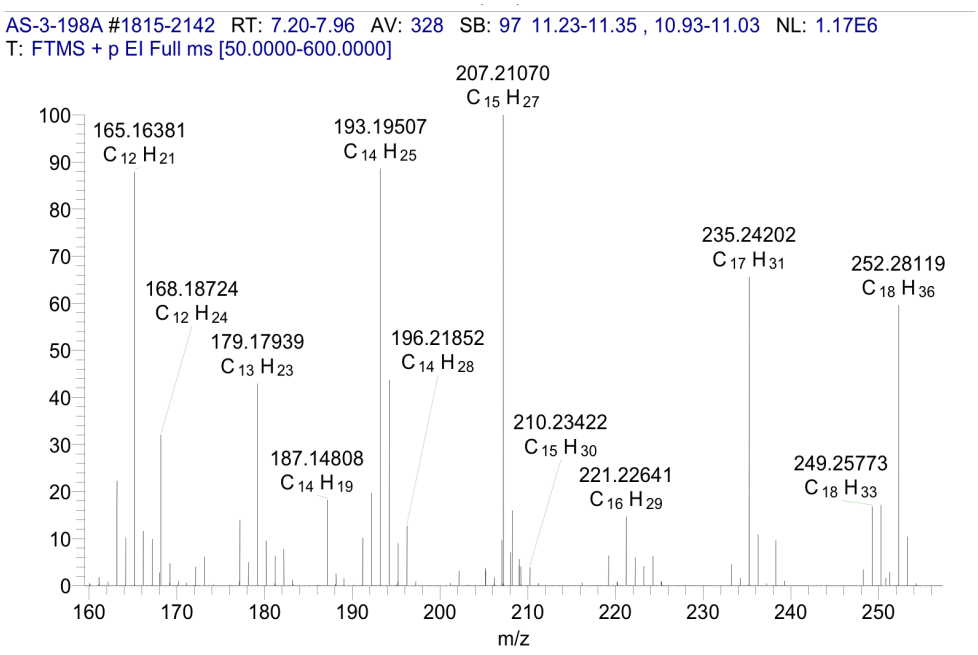

Figure 3.15. Mass spectrum of dimers (*m/z* 168.18724) and trimers (*m/z* 252.28119) of 2,3-dimethyl-1-butene obtained in the presence of [($^{15c5}N^{MeO}$COP)Pd][$B(C_6F_5)_4$] and $LiB(C_6F_5)_4$.

General procedure for the isomerization of 1-hexene

A 12.5 mM stock solution of [($^{15c5}N^{MeO}$COP)Pd][$B(C_6F_5)_4$] in CH_2Cl_2 was prepared, and 200 μL aliquots were added to 4 mL vials and dried *in vacuo*. Similarly, a 12.5 mM stock solution of $LiBAr^F_4$ in CH_2Cl_2 was prepared. Aliquots (200 μL) were added separate 4 mL vials and dried *in vacuo*. A stock solution of mesitylene (50 mM) and diethyl ether (70 mM) was prepared in CD_2Cl_2. To each dried sample of Pd catalyst was added 500 μL of the mesitylene/ether/CD_2Cl_2 stock solution, followed by the addition of 1-hexene (30 μL, 0.239 mmol). The solutions were quickly mixed, and then transferred to Teflon-sealed NMR tubes. For reactions following the kinetics in the presence of $LiBAr^F_4$, the solutions were quickly transferred to the vials containing the dried $LiBAr^F_4$ after mixing, and then transferred to Teflon-sealed NMR tubes. The final concentrations of reagents in each tube were 5 mM Pd, 5 mM Li^+, 50 mM mesitylene, 70 mM diethyl ether, and 500 mM 1-hexene. The reactions were monitored at 25 ^oC by ^1H NMR spectroscopy.

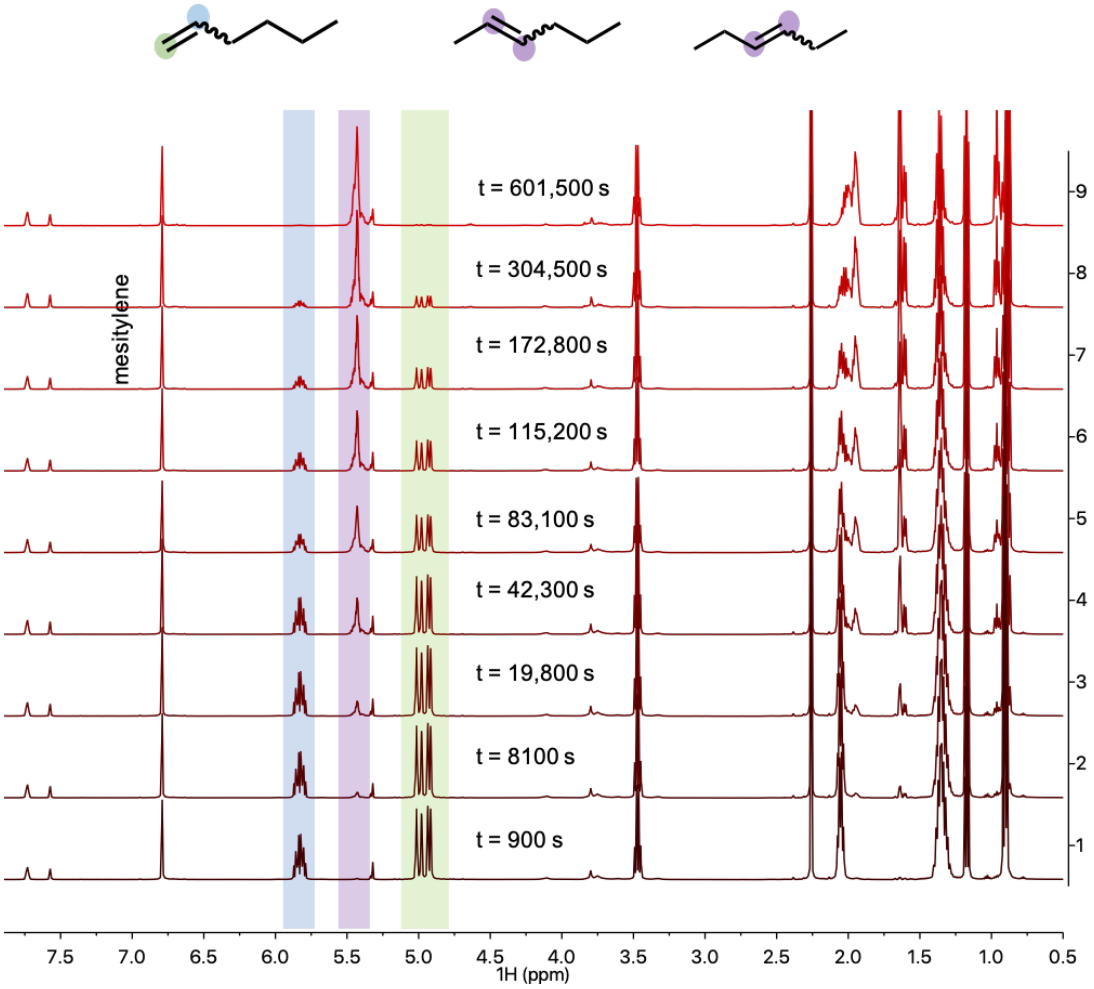

Figure 3.16. Representative ^{1}H NMR spectra in CD_2Cl_2 from *in situ* monitoring of the isomerization of 1-hexene.

CHAPTER 4 – OLIGOMERIZATION AND POLYMERIZATON OF ETHYLIDENE NORBORNENE BY CATIONIC PALLADIUM AND NICKEL ALLYL CATALYSTS

Introduction

Oligomers derived from alkenes have found industrial application in a range of materials and commodity chemical streams, including surfactants, lubricants, resins, and adhesives.[120,121] The physical properties of low molecular weight oligomers are particularly affected by their chain length, where even the addition of a few monomer units can have significant impact on a material's glass transition temperature.[122] Selective formation of oligomers of a given chain length is challenging, and distinct strategies are likely required for effective control over the chain-length of oligomers derived from different monomers.

The controlled oligomerization of norbornene derivatives via a coordination-insertion mechanism poses a challenge because catalysts operating by this mechanism produce extremely high molecular weight poly(norbornene).[123–129] High molecular weights are the result of exceptionally slow β-hydride elimination relative to chain propagation in the metal bicyclic alkyl intermediates. Various methods[121,130] have been reported for production of norbornene-based oligomers, particularly those based on dicyclopentadiene, which find applications including resins.[131,132] However, such methods frequently suffer from poor control of molecular weights, low yields, and harsh reaction conditions. In addition, the scope of monomers examined has been somewhat limited.

Several features of 5-ethylidene-2-norbornene (ENB) motivated a study to develop and operationally-simple methods for coordination-insertion oligomerization. First, ENB is readily available since it is used as a crossing-linking agent in ethylene propylene diene monomer (EPDM) rubber production.[133,134] ENB is easily prepared by Diels-Alder reaction of 1,3 butadiene with cyclopentadiene to yield 2-vinylnorbornene which is then isomerized to an E:Z isomeric mixture (5:1). Second, the oligomerization of ENB is greatly underexplored relative to norbornene itself and dicyclopentadiene; the rigid bicyclic repeat units of oligomeric ENB should provide similar physical properties to oligomeric norbornene and DCPD. Third, the ethylidene functionality contained in every repeat unit would facilitate incorporation of a range of functional groups into these oligomers including, for example, hydroxy, epoxy, halo and carbonato groups.[135,136] Hydroxy-functionalized oligomers should exhibit enhanced solubility in polar or even aqueous solvents while introduction of halides could enhance optoelectronic properties. Generation of functionalized oligomers is noteworthy in light of the general problem confronted by metal-catalyzed oligomerization/polymerization of functionalized olefins where Lewis basic groups can inhibit catalysis through coordination to the electrophilic catalyst. [137] [138,139]

To access ENB-derived oligomers of low molecular weight, we envisioned a strategy that would increase the rate of chain termination in an active ENB polymerization catalyst. The polymerization of norbornenes typically proceeds by one of three distinct mechanisms: ring opening metathesis polymerization (ROMP), cationic initiation, or coordination-insertion, Scheme 4.1.[126,140,137]

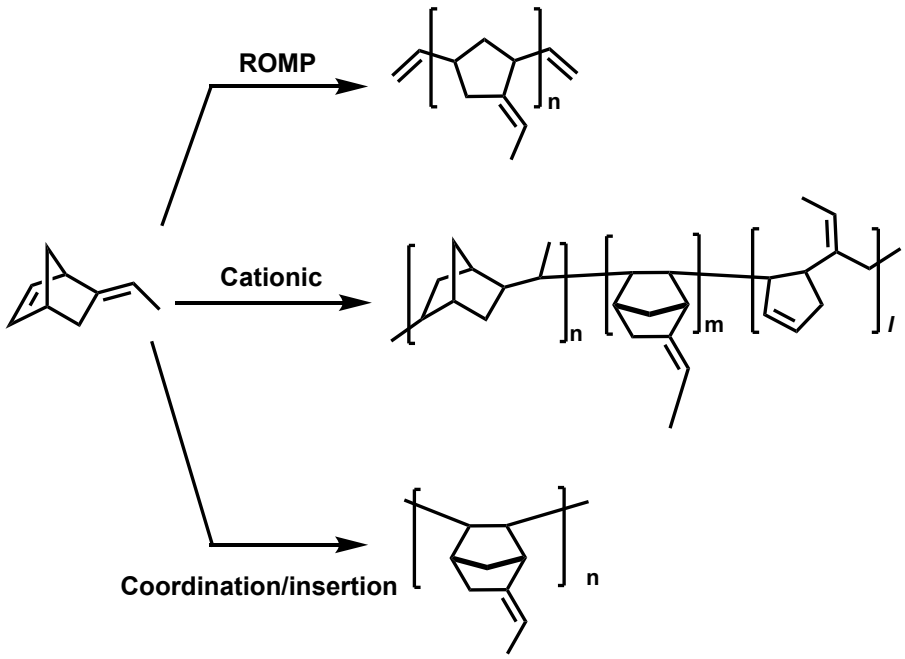

Scheme 4.1. Three different mechanisms produce three distinct ENB polymer structures. Only coordination/insertion polymerizaiton maintains both the bicyclic structure and vinylic functionality.

ROMP produces ring-opened materials with unsaturated linkages and a cyclopentane core, eliminating the potential advantages of materials properties gained with rigid bicyclic cores. Cationic polymerization has been reported to create linkages indiscriminately, including crosslinking through the ethylidene unit, generating insoluble and nonuniform materials.[141] Consequently, norbornene (NB) polymerizations that proceed via cationic mechanisms often are unwieldy and do not allow for facile control over product molecular weight.[123,137] Therefore, only the coordination/insertion mechanism maintains the bicyclic structure and vinylic functionality of ENB.[123] To achieve controlled access to ENB-derived oligomers of low molecular weight, we pursued a strategy that would increase the rate of chain termination relative to the rate of propagation in an active ENB polymerization catalyst.

Goodall and coworkers,[142–144] Brookhart and coworkers,[54,55] and others[126–129] have shown that cationic Ni and Pd complexes are excellent coordination/insertion catalysts for the polymerization of norbornene. Comparatively little work has been reported on metal-catalyzed polymerizations of ENB.[140,141,145–148]

Goodall has pioneered a strategy in which α-olefins can function as chain transfer agents in the coordination/insertion polymerization of norbornenes and thus modulate the molecular weights of the resultant polymers.[143,149,150] α-Olefin insertion into an intermediate metal-bicyclic alkyl metal complex yields a linear alkyl metal species that readily undergoes β-elimination to provide a polymer bearing an olefinic end group, Scheme 4.2. The effectiveness of the α-olefin chain transfer reagent in reducing molecular weights will depend on the relative rates of insertion of the α-olefin versus the norbornene monomer. Goodall has shown that α-olefins can effectively curtail growing NB polymer chains during polymerization by well-studied Ni(II)-allyl-derived catalysts,[142] but the production of oligomers with molecular weights less than 5,000 Da remains a significant challenge as very high α-olefin:norbornene feeds are required in that system.

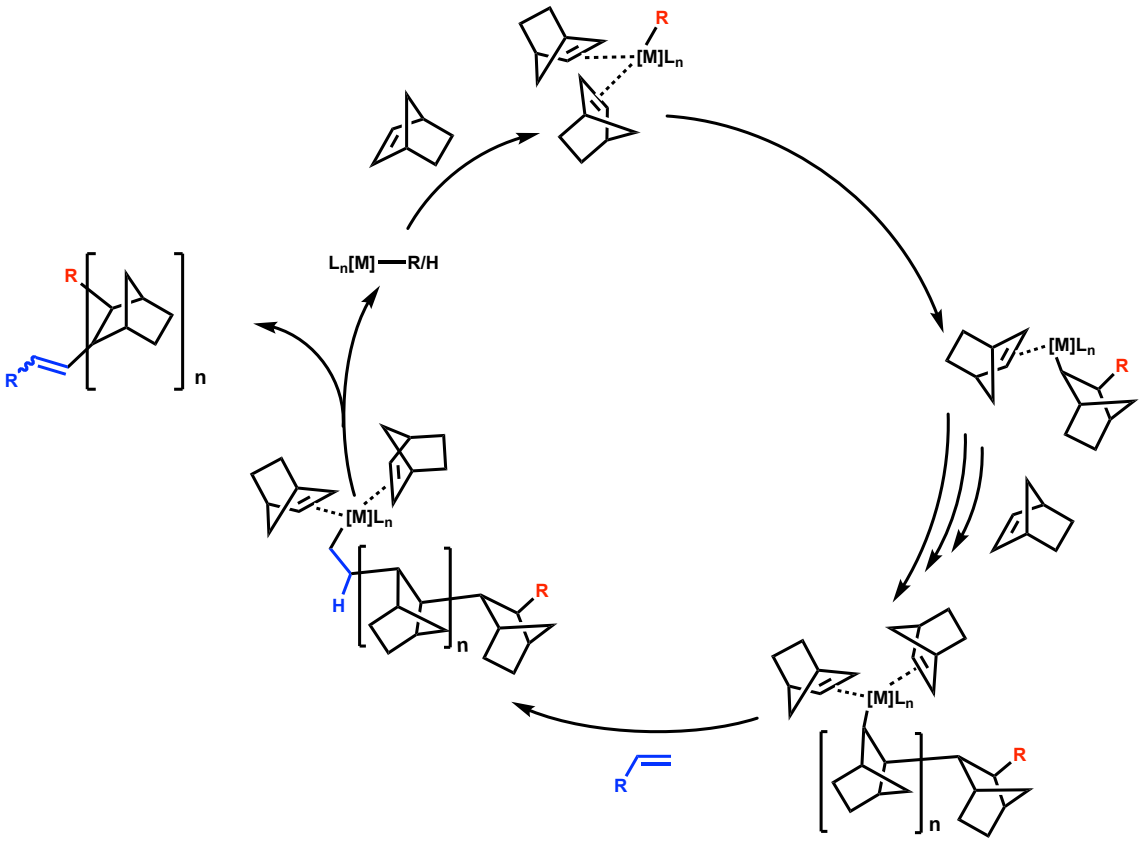

Scheme 4.2. Chain transfer of α-olefins clips growing polyNB chain via chain transfer.

In order to alter the reactivity ratios of α-olefin:ENB to favor light oligomers, we targeted binding a bulky ligand to the Ni(II) or Pd(II) center, which we reasoned would produce a catalyst with a less accessible active site and therefore enhance the relative reactivity of the less encumbered α-olefin and result in easier access to low M_n (number-average molecular weight) oligomers. [149,150] We therefore paired known mesitylene-capped cationic Ni and Pd allyl catalysts[54] with bulky tertiary phosphine supporting ligands and used α-olefins as chain transfer agents to target controlled generation of low molecular weight oligomers derived from ENB.

The catalyst system reported here generates ENB-derived oligomers with molecular weights ranging from 270 Da (dimers) to polymers >100,000 Da in a controlled fashion. The Ni

and Pd systems offer complementary reactivity patterns, enabling access to low molecular weight materials with high glass transition temperatures.

Results and Discussion

Homopolymerization of Ethylidene Norbornene by Cationic Palladium Catalysts

The targeted approach to low molecular weight norbornene-derived oligomers requires a catalyst that undergoes well-behaved coordination/insertion polymerization of ENB. The palladium precatalyst [(mes)Pd(allyl)][PF_6] was selected for initial studies because it does not require an activator and can be used in conjunction with various tertiary phosphine ligands. After synthesizing the precatalyst [(mes)Pd(allyl)][PF_6] according to literature methods,[54] the homopolymerization of ENB was investigated to establish the viability of this catalyst system for later use with α-olefin chain transfer agents.

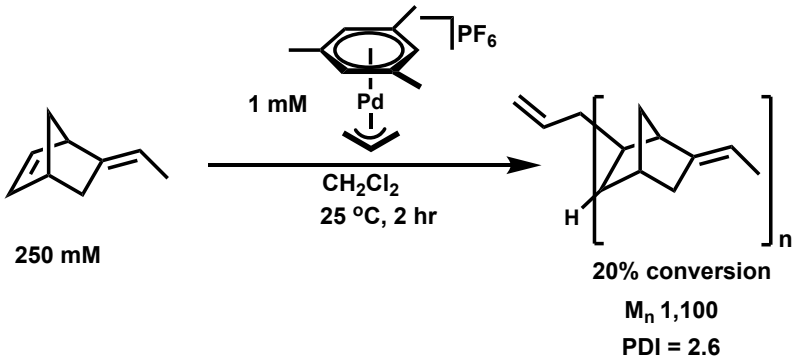

Scheme 4.3. Homopolymerization of ENB (250 mM) catalyzed by [(mes)Pd(allyl)][PF_6] (1 mM) in CH_2Cl_2 at 25 °C ± 1 °C for two hours, and quenched with methanol.

A solution of 250 mM ENB in CH_2Cl_2 was charged under nitrogen with 1 mM [(mes)Pd(allyl)][PF_6], and was allowed to stir at room temperature for two hours, Scheme 4.3. After two hours, a 100 μL aliquot of the reaction was removed, transferred to an NMR tube, and diluted with 400 μL $CDCl_3$. To this NMR tube was added 10 μL mesitylene as an internal

standard, and 10 μL methanol to quench the reaction, and the conversion of ENB was determined via ^{1}H NMR spectroscopy against the mesitylene internal standard. For bulk analysis including gel permeation chromatography (GPC), the polymer was precipitated with methanol, washed vigorously with additional methanol, and dried *in vacuo*. The product was analyzed by GPC in THF. We found the homopolymerization of ENB with [(mes)Pd(allyl)][PF_6] proceeded to very low conversion (~20%), with the resulting polymer having an M_n of ~1100, and a large (polydispersity index) PDI of 2.6, indicating poor catalyst control.

The arene-capped palladium precatalyst was then examined in the presence of tertiary phosphine ligands. Adding [(mes)Pd(allyl)][PF_6] and one equivalent of P^{t}Bu$_3$ to a 250 mM ENB solution in CH_2Cl_2 resulted in complete conversion to high molecular weight polymer (M_n ~42,000, PDI 1.3) after 2 hours (Scheme 4.4). Encouraged by the improved catalytic control afforded by P^{t}Bu$_3$, several other tertiary phosphine ligands were screened, as summarized in Scheme 4.4. The effect of different supporting ligands in solution with [(mes)Pd(allyl)][PF_6] was investigated using three phosphines of increasing cone angles: PEt_3 (132 ^{o}), PPh_3 (145 ^{o}), and P^{t}Bu$_3$ (182 ^{o}). All reactions with one equivalent of added PR_3 proceeded to full conversion within 2 hours at room temperature. The M_n values of the resultant polymers were ca. 42,000 Da for the Pd/P^{t}Bu$_3$ catalyst system, 22,000 Da for Pd/PPh_3, and 140,000 Da for Pd/PEt_3, respectively.

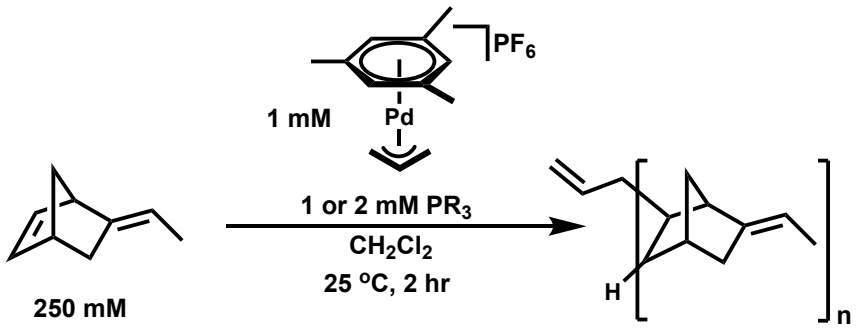

	P^tBu_3 (182 °)	PPh_3 (145 °)	PEt_3 (132 °)
1 mM	M_n 42,000 Da PDI 1.3	M_n 22,000 Da PDI 2.7	M_n 140,000 Da PDI 1.2
2 mM	M_n 42,000 Da PDI 1.2	nr	nr

Scheme 4.4. Homopolymerization of ENB (250 mM) catalyzed by [(mes)Pd(allyl)][PF_6] (1 mM) and PR_3 (1 or 2 mM) mixture in CH_2Cl_2 at 25 °C ± 1 °C for two hours. Reactions were quenched with methanol, and analyzed by NMR spectroscopy and GPC. The table shows the M_n of the resultant polymer materials. All reactions proceeded to full conversion, unless otherwise denoted "nr" for "no reaction." Reactions were quenched, precipitated, and washed with methanol, and dried in vacuo. Products were analyzed by NMR spectroscopy and GPC.

No poly(ENB) was observed when [(mes)Pd(allyl)][PF_6] was used in conjunction with two equivalents of PPh_3 or PEt_3, presumably due to a second equivalent of PR_3 binding to Pd and thus blocking substrate access to the metal center. On the other hand, the conversion and polymer molecular weights were nearly identical regardless of whether one or two equivalents of P^tBu_3 was added. These findings suggest that P^tBu_3 is too bulky to allow for two phosphines to coordinate to Pd, whereas binding a second equivalent of PEt_3 or PPh_3 poisons the catalyst. Therefore, subsequent studies focused on P^tBu_3 as a supporting ligand.

To avoid complications from free ligand in solution, a well-defined phosphine-substituted palladium catalyst was examined. The methyl complex (P^tBu_3)PdMeCl was previously shown by

Nozaki and co-workers to undergo chloride abstraction by $NaBAr^F_4$ *in situ* to yield an active cationic catalyst for the homopolymerization of norbornene.[151] Homopolymerization of ENB with the (P^tBu_3)PdMeCl/$NaBAr^F_4$ catalyst system showed analogous reactivity to the [(mes)Pd(allyl)][PF_6]/P^tBu_3 catalyst system, likely indicating access to the same active species. Four parallel homopolymerization reactions using (P^tBu_3)PdMeCl/$NaBAr^F_4$ (1 mM) and variable concentrations of ENB (250 – 1000 mM) were carried out in CH_2Cl_2 at room temperature. Complete conversion of ENB occurred within five minutes under these conditions, on the basis of ^{1}H NMR spectroscopic monitoring. Methanol was added to the reaction solutions to quench the reaction and precipitate polymer. To remove the Pd catalyst, the precipitated polymers were dissolved in toluene at room temperature, filtered through a short glass plug, and dried *in vacuo* to afford off-white powders. The resulting polymers are soluble in toluene, dichloromethane, and tetrahydrofuran, allowing for solution characterization by NMR spectroscopy and GPC.

The ^{1}H NMR spectra of the ENB-derived polymers feature a broad resonance at δ 5.2 that corresponds to an intact ethylidene unit, and integrates roughly 1:12 against the broad aliphatic resonances between δ 1.0 – 3.1, as would be expected for the ENB homopolymer. Broad resonances in the $^{13}C\{^1H\}$ NMR spectrum at δ 147 and δ 112 also indicated retention of the ethylidene units throughout the homopolymer. Little or no cross-linking is apparent, on the basis of the materials' high solubility in aromatic solvents as well as the spectroscopic detection of ethylidene units. The GPC chromatogram showed that each of the four polymers had narrow PDI values ca. 1.1, and M_n increased with increasing initial concentration of ENB (Figure 4.1). The molecular weight increased with increased concentration of monomer, Figure 4.1, consistent with well-behaved (highly controlled) polymerization.

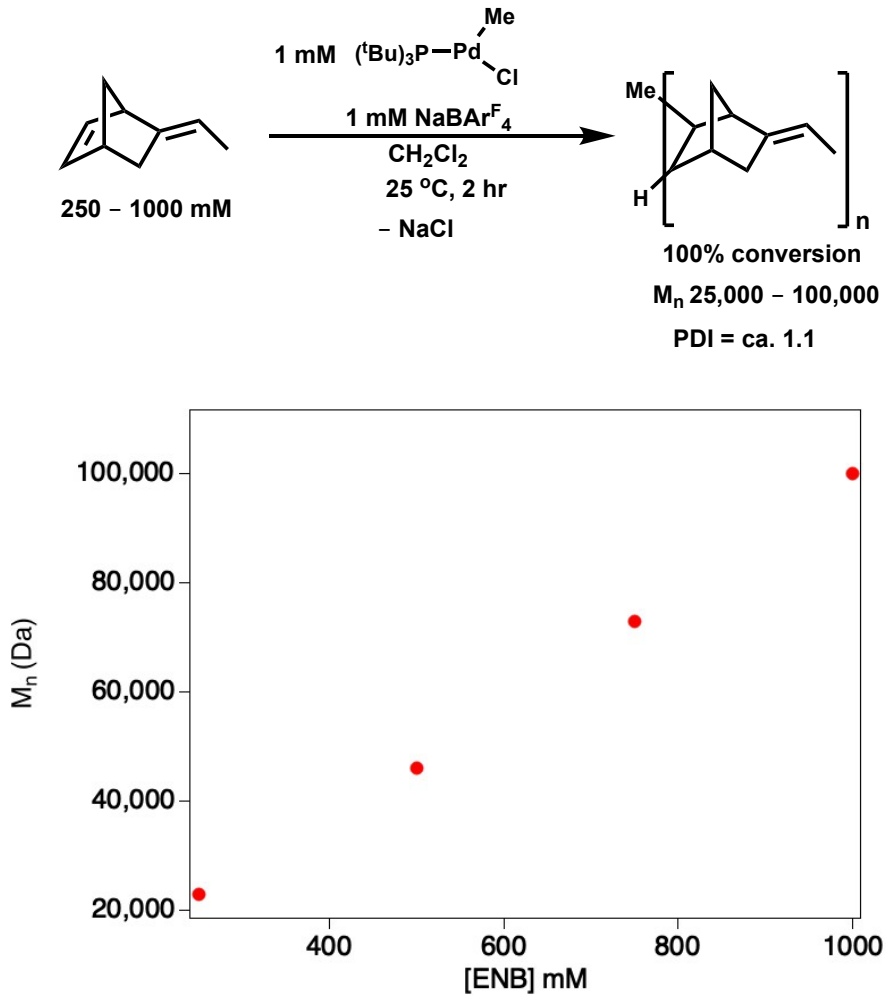

Figure 4.1. Number-averaged molecular weight (M_n) as a function of ENB concentration in the homopolymerization of ENB by (P^tBu_3)PdMeCl/NaBAr$^F_4$. Conditions: 250 – 1000 mM ENB, 1 mM (P^tBu_3)PdMeCl/NaBAr$^F_4$, two hours at 25 °C ± 1 °C under nitrogen.

The controlled character of this homopolymerization was further corroborated by monitoring the M_n as a function of conversion. Dichloromethane solutions containing 250 mM ENB and 1 mM (P^tBu_3)PdMeCl were initiated with 1 mM $NaBAr^F{}_4$ and quenched at different times over the course of ten minutes (See Experimental Section). The M_n increases linearly as a function of percent conversion, again suggesting a highly controlled polymerization, Figure 4.2.

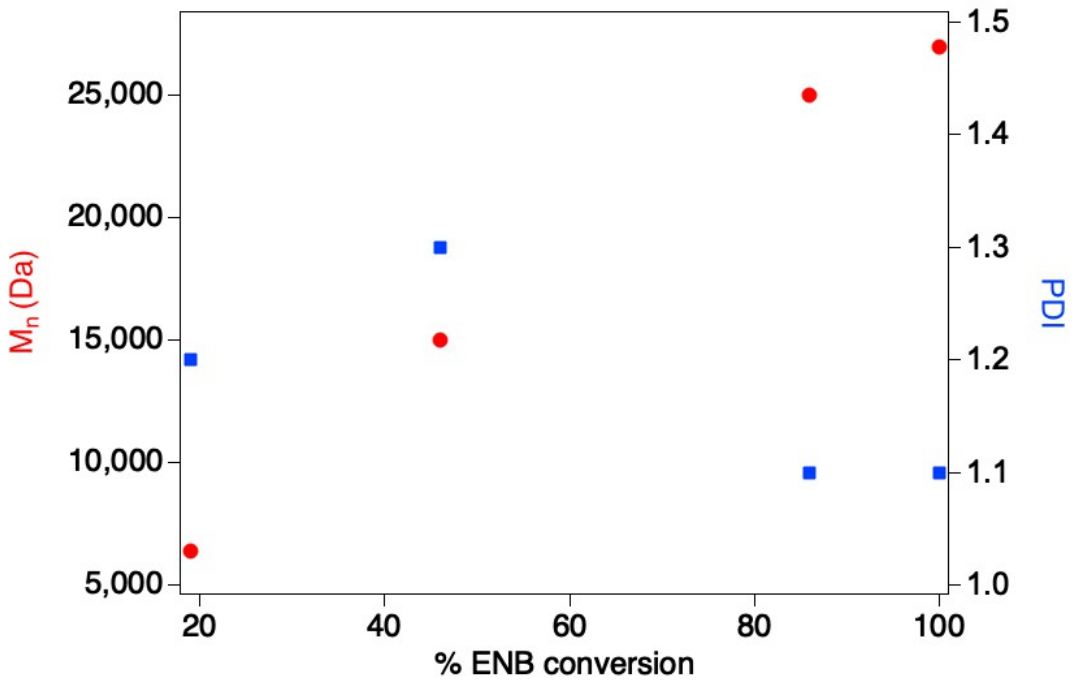

Figure 4.2. Polymer M_n values increase linearly with conversion. Red circles denote the relationship of M_n as a function of % conversion, and blue circles show the relationship between PDI and % conversion. Conditions: 250 mM ENB, 1 mM (P^tBu_3)PdMeCl/$NaBAr^F{}_4$, two hours at 25 °C ± 1 °C under nitrogen.

Controlling Molecular Weight in Palladium-Catalyzed Ethylidene Norbornene Enchainment

With a well-defined ENB polymerization system in hand, we targeted α-olefins as chain transfer agents. Whereas the bulky, geometrically constrained metal-bicyclic metal alkyl complex formed upon ENB insertion does not undergo β-hydride elimination rapidly (as evidenced by the controlled homopolymerization to high molecular weight), the flexible linear metal alkyl complex formed upon α-olefin insertion was expected to undergo extremely rapid β-hydride elimination from the cationic Pd center. This elimination process would terminate the poly(norbornene) chain producing a polymer bearing a single terminal alkene unit, as well generate a metal hydride species that can re-enter the catalytic cycle. This strategy has proved fruitful in the case of high molecular weight parent norbornene polymerizations.[144,149,150]

A liquid α-olefin, 1-hexene was selected as an initial chain transfer agent because the concentration can be varied easily, enabling investigations into the effect of the concentration of chain transfer agent on polymer molecular weight.

Four polymerizations of ENB (250 mM) catalyzed by (P^tBu_3)PdMeCl/$NaBAr^F_4$ (1 mM) were run in the presence of 30, 50, 80, and 250 mM 1-hexene. All four polymerizations proceeded to full conversion of ENB within two hours at room temperature. The standard workup was followed by NMR and GPC analysis. As shown in Figure 4.3, a decrease in M_n was observed as the concentration of 1-hexene in solution increased from 30 mM to 250 mM. The PDI increased with increasing 1-hexene concentration, consistent with increased chain transfer at high α-olefin concentrations. Of note, when the concentration of 1-hexene is 250 mM (a 1:1 ratio of CTA (chain transfer agent):monomer) the M_n of the hexene-terminated polymer was 10,000

Da, approximately half the M_n of the ENB homopolymer prepared in the absence of chain-transfer agent (M_n ~25,000 Da).

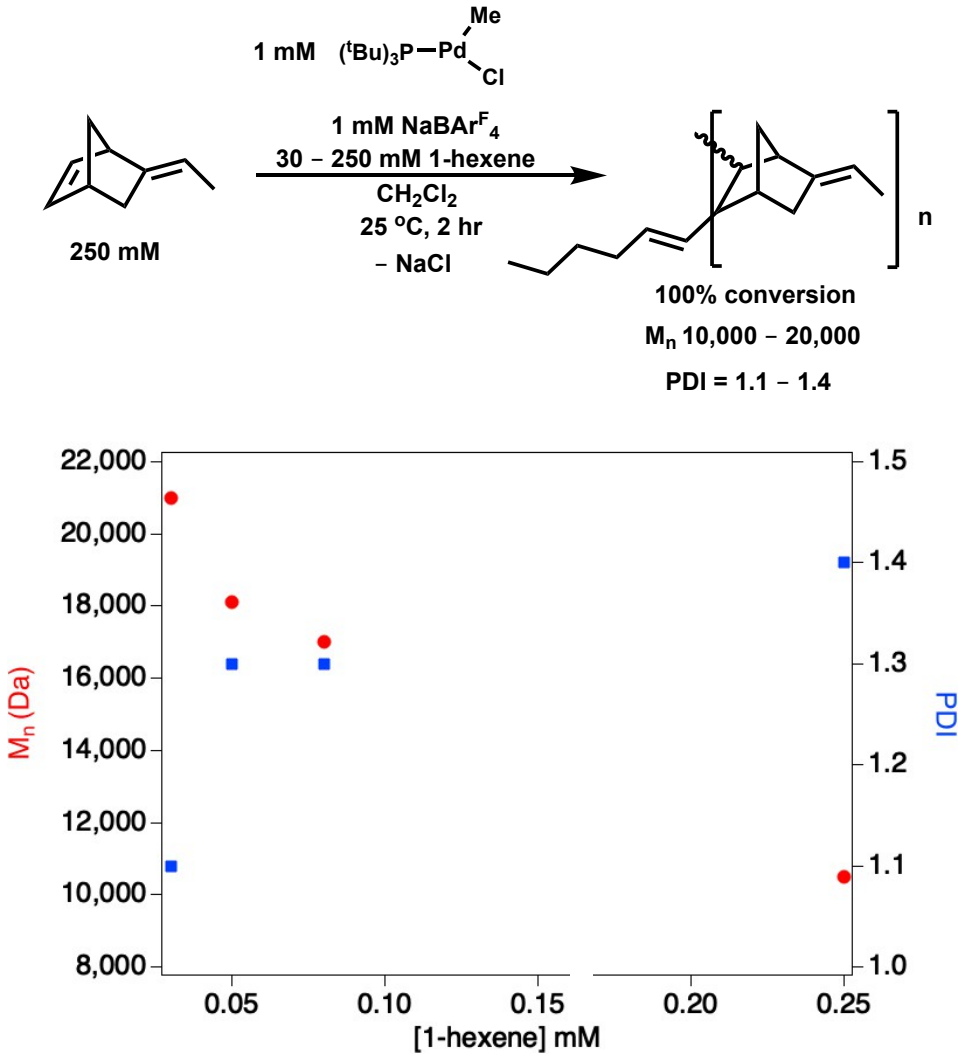

Figure 4.3. M_n increases with decreasing [1-hexene]. Red circles denote the relationship of M_n as a function of initial concentration of 1-hexene, and blue circles show the relationship between PDI and the initial concentration of 1-hexene. Conditions: 250 mM ENB, 1 mM (P^tBu_3)PdMeCl/$NaBAr^F_4$, and 30, 50, 80, or 250 mM 1-hexene, two hours at 25 °C ± 1 °C under nitrogen.

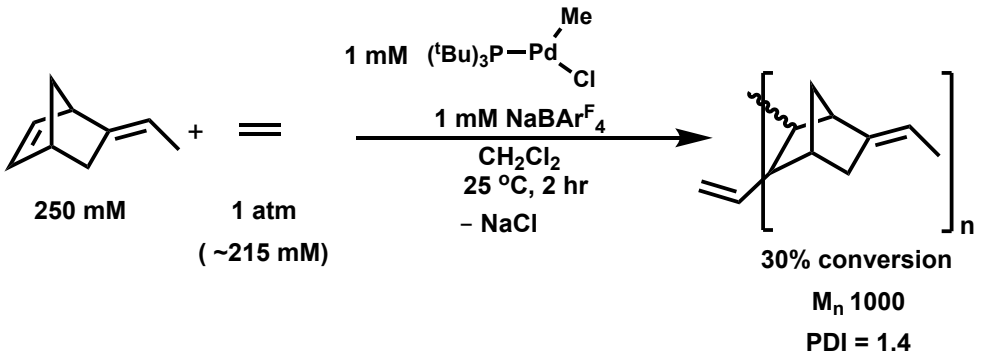

Scheme 4.5. Ethylene as a chain transfer reagent leads to low ENB conversion. Conditions: 250 mM ENB, 1 mM (P^tBu3)PdMeCl/$NaBAr^F_4$, and 1 atm C_2H_4, two hours at 25 °C ± 1 °C.

We hypothesized that the less bulky chain transfer agent, ethylene, would insert more rapidly into the Pd-alkyl intermediate than 1-hexene and thus be more efficient to curtail chain growth to give lower molecular weight oligomers. A CH_2Cl_2 solution of (P^tBu_3)PdMeCl and $NaBAr^F_4$ was added to an ethylene-saturated CH_2Cl_2 solution (~215 mM C_2H_4 based on an independent measurement, see Experimental) containing 250 mM ENB, and the reaction was allowed to stir for two hours at room temperature, Scheme 4.5. The yellow reaction solution turned dark brown, presumably due to the formation of Pd black. This observation stands in contrast to ENB homopolymerizations and ENB/1-hexene oligomerizations, which retained a yellow color throughout the polymerization reaction without any visible formation of Pd black. Consistent with catalyst decomposition, only ~30% conversion of ENB was observed. The resulting ethylene-terminated oligomer did, however, feature a significantly lower molecular weight (M_n ~ 1,000, PDI ~1.4) than the homopolymer prepared under a nitrogen atmosphere (M_n ~ 25,000, PDI ~1.1) and the hexene-terminated oligomer prepared with 250 mM 1-hexene (M_n ~ 10,000, PDI ~ 1.4). The ethylene-derived vinylic chain-ends were apparent by ^1H NMR spectroscopy and by MS-APCI (mass spectrometry-atmospheric pressure chemical ionization).

Oligomeric ENB fragments containing a C_2H_4 fragment plus a proton could be observed from dimers (*m/z* 269.22) to 16-mers (*m/z* 1951.54).

The role of ethylene in promoting catalyst decomposition was probed in the absence of ENB. When a Teflon-sealed NMR tube containing (P^tBu_3)PdMeCl and $NaBAr^F_4$ in CD_2Cl_2 was charged with 1 atm ethylene, an immediate color change from bright yellow to dark brown was observed within a few seconds of the ethylene addition. The ^1H NMR spectrum revealed decomposition of the Pd catalyst, as reflected by the presence of free P^tBu_3.

Despite a promising reduction in M_n under ethylene, the low conversion (30%) and catalyst decomposition led us to consider alternative catalysts for accessing ENB-derived oligomers with molecular weights under 1,000 Da. Cationic allyl Ni complexes were pursued to achieve low molecular weight oligomers and to afford an opportunity to compare the reactivity trends in structurally analogous first-row and second-row transition metal catalysts.

Homopolymerization of Ethylidene Norbornene by [(mes)Ni(Me-allyl)][BAr^F_4]

The nickel precatalyst [(mes)Ni(Me-allyl)][BAr^F_4], a close analogue of the cationic palladium system under study, was pursued on the basis of promising polymerization of 1,3-dienes,[55] and its known activity towards the formation of butenes in the presence of ethylene. Like the palladium system, [(mes)Ni(Me-allyl)][BAr^F_4] enables facile screening of supporting ligands.

The homopolymerization of ENB by [(mes)Ni(Me-allyl)][BAr^F_4] was pursued initially. A flask was charged with 250 mM ENB in CH_2Cl_2, followed by addition of 1 mM catalyst. The reaction was allowed to stir at room temperature for two hours, after which it was quenched with methanol, followed by the standard workup, NMR analysis, and GPC analysis. The reaction was quenched with methanol and dried *in vacuo*. Surprisingly, only 10% of the ENB was consumed,

producing a material of M_n = 2,200 Da. The low conversion could possibly be attributed to chelation of the diolefin monomer to Ni, which has been suggested for other similar catalysts based on palladium.[140]

To test this hypothesis, a homopolymerization of norbornene (NB) with [(mes)Ni(Me-allyl)][BAr^F_4] was then carried out under general conditions. Polymer precipitated within 10 minutes after charging the reaction tube with the Ni catalyst, but the reaction was allowed to stir for a total of two hours at room temperature per standard conditions, after which it was quenched with methanol and worked up according to standard procedures. Total consumption of NB was observed by ^{1}H NMR spectroscopy; however, the product polymer was insoluble in chlorinated, alkane, and ether solvents, preventing further physical characterization.

Notably, the homopolymerization of ENB with [(mes)Pd(allyl)][PF_6] also went to low conversion, only consuming 20% of the monomer. However, NB was also found to be totally consumed in the presence [(mes)Pd(allyl)][PF_6], similarly precipitating polymer shortly after the reaction was initiated with the addition of Pd. Similarly, this product was not soluble, and prevented further physical characterization. These results show that both [(mes)Ni(Me-allyl)][BAr^F_4] and [(mes)Pd(allyl)][PF_6] are much more active towards the homopolymerization of NB, a monomer with only one olefinic group, than ENB, a diolefin. Although not definitive, these observations support that chelation of ENB to Ni or Pd may explain their lower activities with ENB relative to unsubstituted NB.

Since the activity of [(mes)Pd(allyl)][PF_6] towards ENB increased in the presence of phosphines, the influence of tertiary phosphine supporting ligands on the activity of [(mes)Ni(Me-allyl)][BAr^F_4] was examined. Under the general conditions described above, but in the presence of 1 equiv P^tBu_3, ENB underwent 61% conversion to low molecular weight

oligomers (M_n = 1,100). Improved activity was also observed in the presence of 1 equiv PPh_3 or PEt_3, as shown in Table 4.1. The M_n values ranged from 1,100 to 7,400 Da, without clearly correlating with the steric bulk of the phosphine ligand (Table 4.1).

Table 4.1. Influence of PR_3 identity and concentration of ENB homopolymer M_n (Da). Conditions: 250 mM ENB, 1 mM [(mes)Ni(Me-allyl)][BAr^F_4] and PR_3 (1 or 2 mM) mixture in CH_2Cl_2 at 25 °C ± 1 °C for two hours.

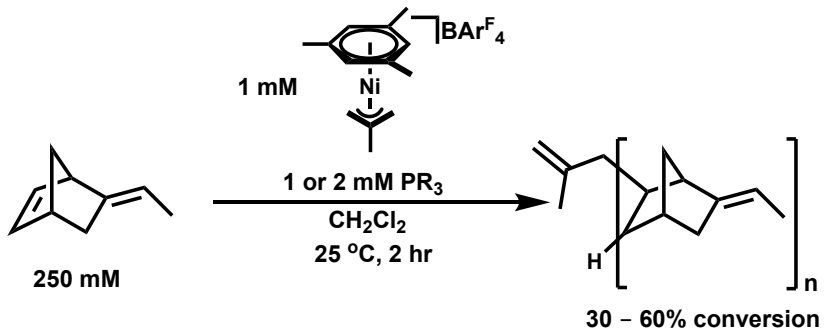

Concentration PR_3	P^tBu_3	PPh_3	PEt_3
1 mM	M_n 1,100, M_w 2,000 61% conversion	M_n 7,400, M_w 11,000 55% conversion	M_n 4,900, M_w 1,500 56% conversion
2 mM	M_n 1,200, M_w 2,100 52% conversion	M_n 330, M_w 360 30% conversion	M_n 1,500, M_w 1,500 30% conversion

The same experiments were also carried out with two equivalents of phosphine ligand. The bulkiest phosphine, P^tBu_3, showed similar activity with either 1 or 2 equivalents of added phosphine. A second equivalent of the sterically smaller phosphines, on the other hand, reduces

the conversion of ENB from 60% to 30%, while also leading to shorter oligomers. The palladium-based catalysts exhibited similar reactivity trends: 1 equivalent of PR_3 improved activity (higher conversion), and 2 equivalents of PR_3 were only tolerated for the bulky ligand P^tBu_3.

Controlling Molecular Weight in Nickel-Catalyzed Ethylidene Norbornene Enchainment

Despite the poor ENB homopolymerization reactivity, [(mes)Ni(Me-allyl)][BAr^F_4] was explored in the presence of ethylene as a possible chain transfer agent. A solution of 250 mM ENB in CH_2Cl_2 under 1 atm ethylene was charged with [(mes)Ni(Me-allyl)][BAr^F_4] and allowed to stir at room temperature for two hours, Scheme 4.6. Spectroscopic analysis revealed full conversion of ENB, a stark contrast to the analogous reaction in the absence of ethylene. Quenching with methanol and drying *in vacuo* afforded white powder with $M_n \sim 900$ Da, as determined by GPC. The ^{1}H NMR spectrum featured broad resonances centered around δ 5.0 and δ 5.2 corresponding to intact ethylidene units, as well as a broad resonance at δ 5.8 corresponding to the vinyl chain-end. By atmospheric-pressure chemical-ionization mass spectrometry (MS-APCI), masses corresponding to ethylene-capped ENB dimers (269.23) up to decamers (*m/z* 1258.01) were observed. An analogous reaction with unsubstituted NB showed that full conversion of NB was also achieved to produce ethylene-terminated oligomers, albeit with an M_n of 2000 Da – twice the M_n of the ENB oligomers produced under the same conditions, (See Experimental Section). This result is consistent with NB inserting faster relative to ENB prior to ethylene insertion. Although ENB chelation is suspected to impede Ni catalysis in homopolymerizations, high conversions in the presence of ethylene may be due to its displacement of ethylidene unit of ENB.

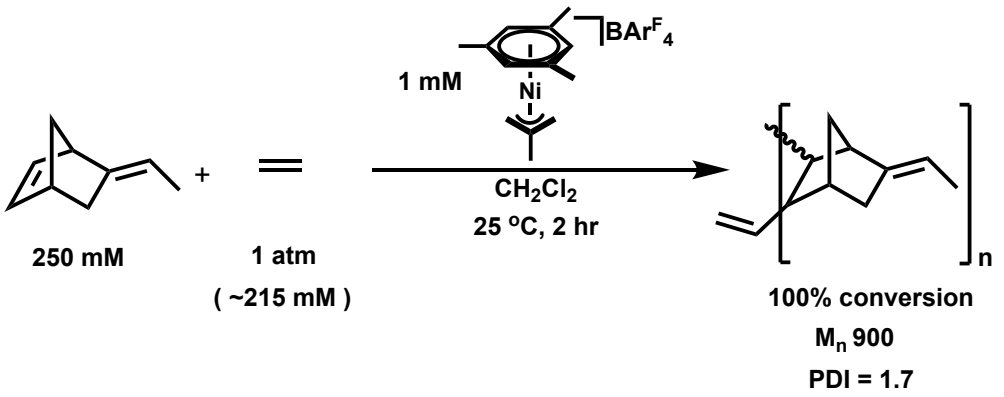

Scheme 4.6. Quantitative production of oligomers (M_n 900 Da) in the presence of 1 atm C_2H_4. Conditions: 250 mM ENB, 1 mM [(mes)Ni(Me-Allyl)][BAr^F_4], 1 atm C_2H_4, stirred for two hours at 25 ºC ± 1 ºC.

With a promising initial reaction in hand, we sought to vary conditions to tune the average molecular weight of the oligomer. The average degree of oligomerization should be sensitive to the ENB/C_2H_4 ratio, with lower ratios favoring more chain termination and thus smaller oligomers. To test this theory, the initial concentration of ENB was changed from 250 mM to 125 mM, with room temperature nickel-catalyzed oligomerization proceeding cleanly to produce an oligomeric material with M_n ~ 740 Da in high yield (See Experimental Section).

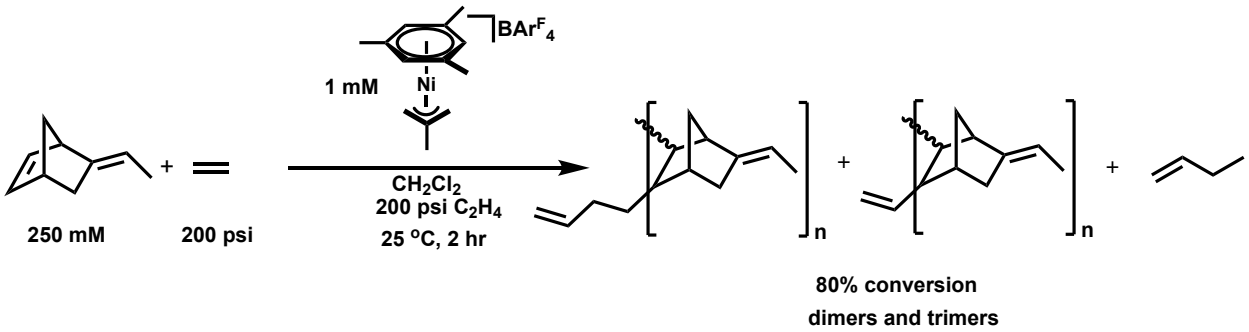

Scheme 4.7. Increased C_2H_4 pressure decreases ENB oligomer chain length. Conditions: 250 mM ENB, 1 mM [(mes)Ni(Me-allyl)][BAr^F_4], 200 psi C_2H_4, stirred for two hours at 25 °C ± 1 °C.

To increase the concentration of ethylene, a nickel-catalyzed oligomerization was carried out at 0 °C in an ethylene-saturated solution under 1 atm ethylene. The reaction again proceeded in high yield, but no significant change in the number-averaged molecular weight was observed relative to the room temperature conditions (M_n = 900 Da). Operating at elevated ethylene pressure would also increase the concentration of the chain transfer agent relative to ENB. To this end, a Parr reactor was charged with an ethylene-saturated 250 mM ENB solution in CH_2Cl_2, followed by addition of [(mes)Ni(Me-allyl)][BAr^F_4], and immediate pressurization to 200 psi ethylene, Scheme 4.7. After stirring for two hours at room temperature, the reaction proceeded to ca. 80% conversion of ENB. Approximately 350 mM 1-butene was apparent by ^{1}H NMR spectroscopy, formed via ethylene dimerization that is not significant at 1 atm ethylene under these conditions. The M_n value of this oligomeric material produced was too low to be detected by GPC, showing that the elevated ethylene pressure successfully shortened the chain length compared to the reaction under 1 atm ethylene. By mass spectrometry, the major species were ethylene-capped dimers of ENB (m/z 269.23), while the second most abundant species were butene-capped trimers of ENB (m/z 417.35). We propose that the butene-coupled oligomers are the product of a second insertion of ethylene into the growing ENB chain prior to β-hydride

elimination, due to the lack of evidence for internal olefin chain-ends in the $^{13}C\{^{1}H\}$ NMR and ^{1}H NMR spectra.

To better understand the role of chain transfer agent in Ni ENB polymerizations, a concentration dependence with 1-hexene was studied. Under a nitrogen atmosphere, four vials were charged with ENB in dichloromethane (250 mM) and varying amounts of 1-hexene (30 mM, 50 mM, 80 mM, and 250 mM, respectively). The vials were then charged with 1 mM [(mes)Ni(Me-allyl)][BAr^{F}_{4}] and allowed to stir at room temperature for two hours before standard workup and characterization. GPC analysis of the four materials shows that shorter oligomers are produced with increasing initial concentrations of 1-hexene, where the lowest molecular weight oligomers ($M_n \sim 1000$ Da) result from the highest ratio of chain transfer agent to monomer (1-hexene:ENB ~1:1). A broad resonance at δ 5.2 in the ^{1}H NMR spectrum corresponds to intact ethylidene units and a broad resonance from δ 1.0 - 3.0 corresponds to the oligomers' bicyclic aliphatic backbone. Another broad singlet around δ 0.9 corresponding to a methyl group on the hexene chain-end is observed in the ^{1}H NMR spectrum. The ratio of the terminal methyl resonance to the broad aliphatic resonances increases with decreasing oligomer weight, as would be expected. The $^{13}C\{^{1}H\}$ NMR spectrum reveals that the hexene chain-end contains an internal olefin rather than a terminal olefin (δ 130).

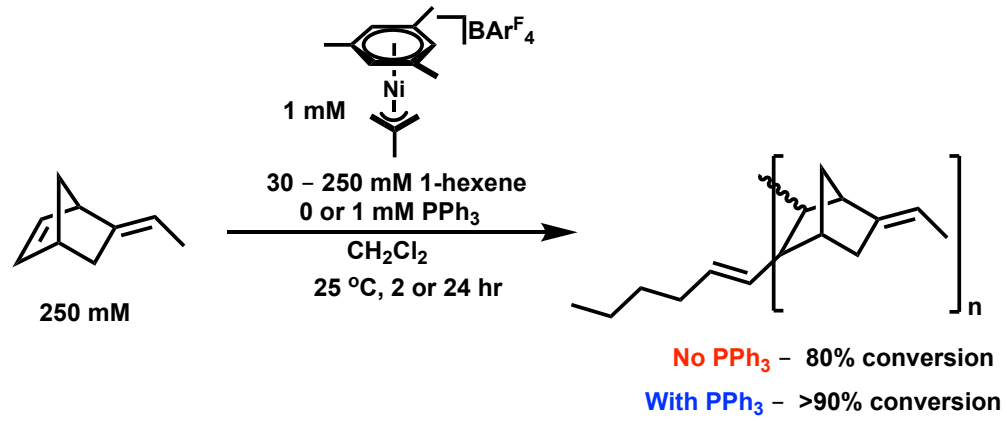

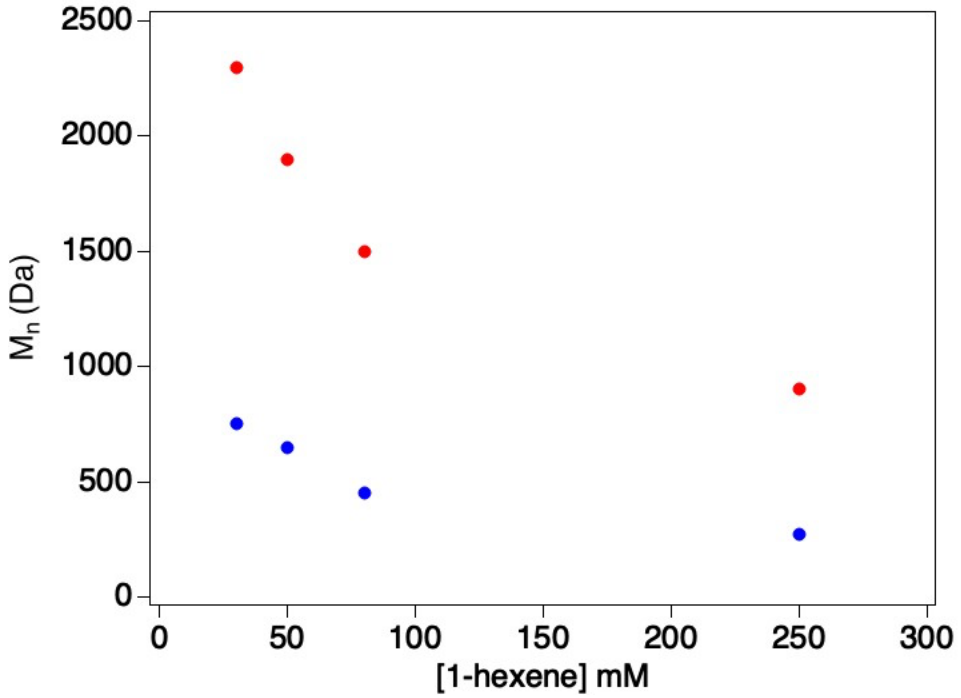

Figure 4.4. M_n decreases with increasing [1-hexene] (red circles), and shorter oligomers are obtained in the presence of a PPh_3 co-ligand (blue circles). Conditions: 250 mM ENB, 1 mM [(mes)Ni(Me-allyl)][BAr^F_4] and 0 or 1 mM PPh_3. 30, 50, 80, or 250 mM 1-hexene in CH_2Cl_2, stirred for two hours at 25 °C ± 1 °C.

Figure 4.4 shows the relationship between oligomer M_n and the initial concentration of 1-hexene, which illustrates that increasing the concentration of 1-hexene produces materials with

lower M_n. Interestingly, these reactions only achieved ca. 50% conversion (in contrast to the nearly quantitative conversion seen with ethylene). Binding and insertion of 1-hexene may be slow relative to the smaller ethylene. Allowing reactions containing 30 mM or 80 mM 1-hexene to stir at room temperature for twenty-four hours led to increased ENB conversion (~80%), maintaining the same distribution of oligomers (See Experimental Section).

Table 4.2. Concentration of dimer increases with increasing PR_3 cone angle.

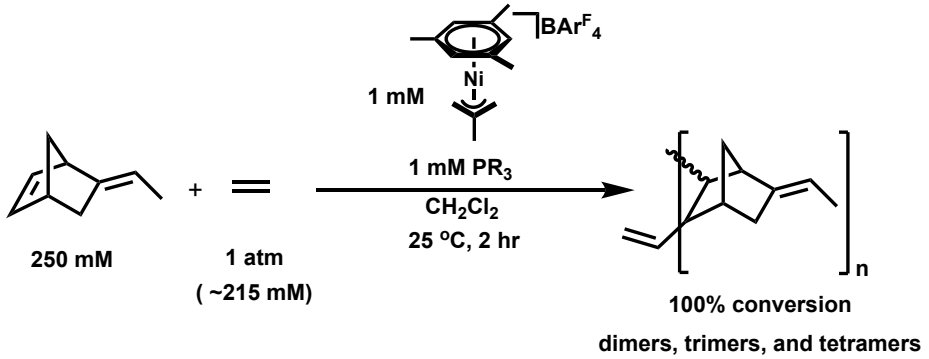

additive	Conversion	M_n (Da) GPC	M_w (Da) GPC	*m/z* MS-APCI
1 mM PPh_3 (145°)	100%	<500	<500	269.22507
1 mM $PMePh_2$ (136°)	100%	<500	<500	389.31867
1 mM PEt_3 (132°)	77%	<500	<500	389.31867

Including phosphine supporting ligands during ethylene-terminated oligomerization by [(mes)Ni(Me-allyl)][BAr$^F_4$] leads to high yields of light ENB-derived oligomers. An ethylene-saturated CH_2Cl_2 solution containing 250 mM ENB under 1 atm ethylene was treated with

[(mes)Ni(Me-allyl)][BAr^F_4] and 1 equiv PR_3 (PR_3 = PPh_3, $PMePh_2$, PEt_3). As shown in Table 4.2, all of the reactions proceeded to high conversion and produced tacky oligomeric materials with molecular weights below the molecular weight cutoff of the GPC columns. MS-APCI analysis revealed the materials to be predominantly composed of ethylene-coupled dimers and trimers of ENB. When the smaller ligand $PMePh_2$ was utilized, mostly trimers were produced; when the larger ligand PPh_3 was utilized there were substantially more dimers than trimers.

Chain termination with 1-hexene was investigated next for the Ni/PR_3 ENB oligomerization catalyst system. Parallel reactions were carried out in CH_2Cl_2 containing 250 mM ENB, varying amounts of 1-hexene, and the [(mes)Ni(Me-Allyl)][BAr^F_4]/PPh_3 catalyst system (1 mM of each catalyst component). The reactions proceed to approximately 60-70% conversion after 2 hours (See Experimental Section). Nearly quantitative conversion of ENB was observed in reactions that were allowed to stir at room temperature for 24 hours. The reactions were quenched with methanol, and dried *in vacuo*, and analyzed by NMR spectroscopy, mass spectrometry, and GPC. The resulting materials produced from this catalyst system closely resembled those produced in the presence of PR_3 by NMR spectroscopy. Notable features in the ^1H NMR and $^{13}C\{^1H\}$ NMR spectra indicate a hexene chain-end. Furthermore, MS-APCI spectra of these materials revealed masses corresponding to hexene-terminated oligo(ENB). By GPC analysis, the materials produced in the presence of PPh_3 were significantly lighter than those produced without phosphine, Figure 4.4, where all had M_n < 1,000 Da (Figure 4.4). These results suggest that chain transfer occurs more readily in the presence of bulky PR_3 co-ligands to make shorter oligomers.

Figure 4.4 (above) shows that higher initial concentrations of 1-hexene give rise to oligomers with lower M_n (blue circles), just as observed without added phosphine co-ligand (red

circles). In the presence of PPh_3, however, the oligomer M_n values are reduced by approximately a factor of three relative to the oligomers produced by the allyl Ni catalyst alone. This appears to be the result of to a change in the relative binding affinity of ENB vs. 1-hexene to favor α-olefin association and chain termination at the bulkier catalyst containing a PR_3 ligand.

Comparing Catalytic Reactivity Trends of the Nickel and Palladium Systems

The nickel- and palladium-based catalyst systems exhibit a few distinct reactivity patterns. One similarity is that both the arene-capped Ni and Pd allyl catalysts exhibit low activity for ENB homopolymerization alone, but give improved ENB conversion in the presence of a tertiary phosphine supporting ligand. The products of the PR_3-supported homopolymerization are distinct, however: the Pd system produces high molecular weight polymers with narrow polydispersity and behaves as a highly controlled catalyst system. Depending on the ratio of catalyst to monomer, poly(ENB) was prepared with M_n between 22,000 and 136,000 Da. In contrast, the Ni system does not homopolymerize ENB in a controlled manner, instead producing oligomers with broader polydispersity and short chains (M_n between 4,900 and 7,400 Da).

In the presence of ethylene, the palladium catalysts rapidly decompose to Pd black, even in the presence of PR_3. Conversely, the activity of the cationic allyl Ni catalyst increases in the presence of ethylene, giving quantitative conversion of ENB to low molecular weight oligomers with oligomer chain length depending on the ratio of monomer to ethylene in the system.

The positive influence of phosphine supporting ligands in the nickel system was surprising, given that many Ni(allyl)(halide) dimers are unstable in the presence of phosphine ligands[152] at room-temperature, and that previous reports suggested that Ni-catalyzed norbornene polymerization is inhibited by PR_3. The order of reagent addition is important with respect to

catalyst stability: addition of PR_3 to CH_2Cl_2 solutions of $[(mes)Ni(Me\text{-}allyl)]^+$ leads to decomposition, but that addition of PR_3 to a CH_2Cl_2 solution of ENB followed by addition of $[(mes)Ni(Me\text{-}allyl)]^+$ leads to clean and controlled reactivity.

Physical properties of ENB-derived materials

Part of the motivation for preparing ENB-derived oligomers and polymers with controllable molecular weight is the promise of unusual and valuable materials properties provided by the rigid bicyclic cores of hydrocarbon chains. Varying the chain length and chain end composition through a combination of chain transfer agents and PR_3 supporting ligands was aimed at providing access to materials with a wide range of physical properties. As described by the Flory-Fox equation,[122] the glass transition temperature (T_g) of a given polymer is related to its M_n. As the chain length and molecular weight of a polymer increases, it approaches its theoretical maximum T_g. Given our ability to prepare oligomers and high polymers ranging from M_n ca. 270 to 100,000 Da, we selected several ENB oligomers and homopolymers for T_g determination.

Ten ENB-derived materials were selected for detailed characterization. Four ethylene-terminated ENB oligomers prepared with the Ni catalyst system with varying M_n (400, 800, 1,000 and 1,700 Da) were examined. The shortest ethylene-terminated oligomer, M_n 400 Da, is a viscous, sticky material, whereas the longest ethylene-terminated material (M_n 1,700 Da) appears as a white, powdery solid. The white powder became a transparent, colorless, brittle film upon heating to 200 ^oC and cooling back to 25 ^oC. Four analogous hexene-terminated materials prepared with the Ni catalyst system were also examined (M_n 600, 1000, 1900, and 2500 Da). The shortest hexene-terminated oligomer is a tacky paste, whereas the longest hexene-terminated oligomer is a white powder that transforms into a transparent, brittle material upon melting and

cooling. Finally, one hexane-terminated ENB polymer (M_n 20,000 Da) and one ENB homopolymer (M_n 25,000 Da) prepared with the (P^tBu_3)PdMeCl catalyst were examined. Both of these materials appear as off-white powders that can be solution-cast out of dichloromethane as transparent films.

Differential Scanning Calorimetry (DSC) was performed on the ten ENB-derived materials to determine the T_g of each material. Figure 4.5 shows the relationship between T_g and M_n. In the low molecular weight range, increasing the polymer chain length results in an increase in the glass transition temperature. The T_g values span a wide range, with the lowest molecular weight material (mostly ENB tetramer, M_n 400 Da) having a T_g below room temperature (–18 ^oC) and the highest molecular weight polymers (M_n ~ 25,000 Da) having T_g of approximately 178 ^oC. The T_g value of the high molecular weight polymer is similar to T_g values reported for similar high molecular weight polymers of norbornene derivatives.[123,141] The thermal measurements correlate with the physical properties of the materials, with the low T_g materials appearing as viscous pastes at room temperature and the high T_g materials melting into hard, transparent films.

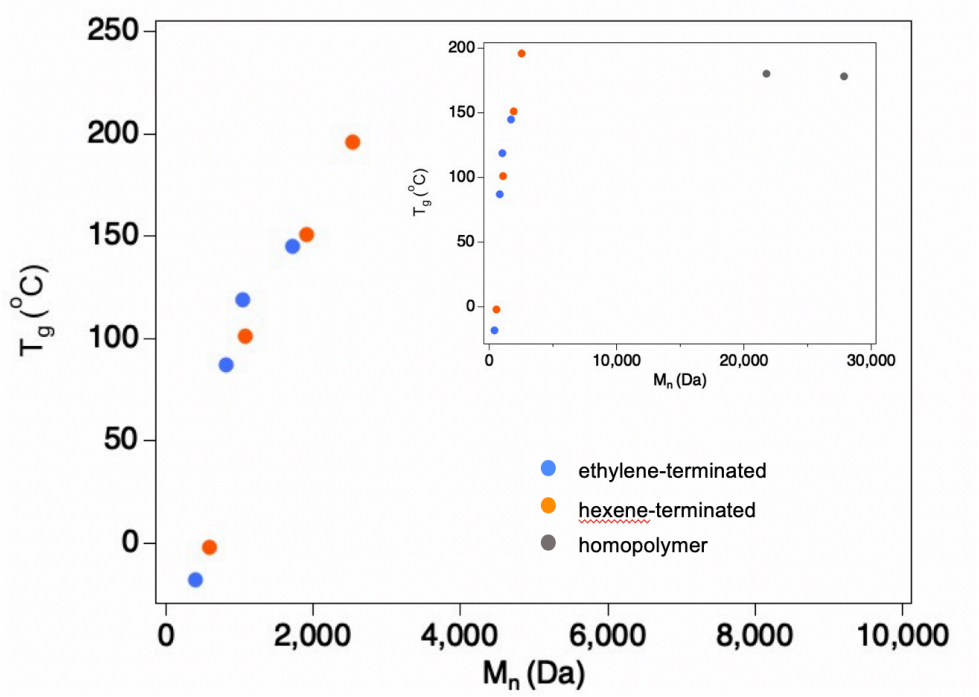

Figure 4.5. The T_g of ENB oligomers increases with increasing chain length. Ethylene-terminated oligomers (blue circles), hexene-terminated oligomers (orange circles), and ENB homopolymer (grey circles) were (M_n ranging from 400 to 25,000 Da). See Experimental Section for details.

To examine the influence of the ethylidene units on the physical properties, hydrogenation of one of the oligomeric samples and one of the polymeric samples was carried out. Hydrogenation of these ENB-derived materials could (a) provide materials that are more robust towards oxidative degradation and (b) modify T_g values through the removal of the unsaturated units. The ENB-derived materials (M_n of either 500 or M_n = 25,000 Da) were each dissolved in CH_2Cl_2, sparged with hydrogen at 0 ºC, and treated with five 1 mM portions of [(cod)Ir(PCy_3)(py)][PF_6] over the course of one hour.[153] Both materials were found to be ca. 99% hydrogenated on the basis of ^{1}H NMR and $^{13}C\{^1H\}$ NMR spectroscopy, with almost all olefin resonances replaced by new aliphatic resonances corresponding to a terminal methyl group

derived from the ethylidene unit. The T_g of the hydrogenated materials did not differ from their unsaturated parent materials (See Experimental Section).

Conclusions

A series of Ni and Pd catalyst systems were developed that convert ENB to materials ranging in molecular weights from dimers (ca. 270 Da) to higher polymer (>100,000 Da) polymers. These reactions proceed in high yields at room temperature in the presence of bulky tertiary phosphine co-ligands, with molecular weights controlled by α-olefin chain transfer agents. Notably, oligomers ranging in molecular weight 270 – 2,000 Da can be controllably and selectively prepared using the catalyst [(mes)Ni(Me-allyl)][BAr^F_4] in the presence of ethylene, where the molecular weight of the oligomer is controlled by the relative ratio of ethylene to monomer in solution, and the identity of the added phosphine co-ligand (or lack thereof). The present catalyst system is noteworthy for offering a convenient method for controlled oligomerization of cycloolefins with $M_n < 2{,}000$ Da.

The monomer ENB is much less reactive than norbornene, presumably due to unproductive metal coordination by the ethylidene unit poses. By introducing bulky phosphine ligands, the present catalyst systems achieved high conversion of ENB with controlled molecular weights. ENB-derived materials may be particularly interesting for applications in post-functionalization. Pd and Ni polymerization catalysts are often deactivated by polar or Lewis basic functional groups. The present catalyst systems produce materials with an unsaturated ethylidene unit throughout the chains, providing an entry to post-functionalization to introduce a wide range otherwise-inaccessible of functional groups.

Experimental Section

General Considerations

All reactions were performed under an inert nitrogen atmosphere, utilizing standard vacuum line and glovebox techniques unless otherwise noted. All NMR-scale reactions were prepared in a glovebox and monitored in Teflon-sealed NMR tubes. Organic solvents were dried and degassed with argon using a Pure Process Technology solvent system and stored over 3 Å molecular sieves. Under standard glovebox operating conditions, pentane, diethyl ether, benzene, toluene, and tetrahydrofuran were used without purging, so traces of those solvents were present in the atmosphere and in the solvent bottles.

Gel permeation chromatography (GPC) was performed on a Waters 2695 separations module liquid chromatograph equipped with either four Waters Styragel HR columns (WAT044225, WAT044231, WAT044237, and WAT054460) arranged in series or two Agilent Resipore columns (PL1113-6300) maintained at 35 °C. Tetrahydrofuran was used as the mobile phase at a flow rate of 1.0 mL/min. Molecular weight and dispersity data are reported relative to polystyrene standards. All molecular weight and dispersity data are reported with a normalized RI signal. Glass-transition temperatures (T_g) of dried polymer samples were measured using differential scanning calorimetry (DSC) on a TA Instruments Discovery DSC. All T_g values were obtained from a second heating scan after the thermal history was removed. All heating and cooling rates were 10 °C/min. Decomposition onset temperatures (T_d) of dried polymer samples were measured by thermal gravimetric analysis (TGA) on a TA Instruments Q5000 Thermogravimetric Analyzer. Polymer samples were heated from ambient temperatures to 500 °C at a heating rate of 10 °C/min. Values of T_d (temperature at 5% weight loss) were obtained from wt % vs. temperature (°C) plots).

High resolution mass spectra were collected on a ThermoScientific Q Exactive HF-X with a mass range of 50 to 4,000 Da with an atmospheric-pressure chemical- ionization probe, and resolution up to 100,000 at *m/z* 400 at 1 Hz, >750,000 at *m/z* 400 at slower scan repetition rates. Oligomer samples were analyzed by atmospheric pressure chemical ionization mass spectrometry in methylene chloride/methanol mixtures. Oligomer samples with M_n exceeding 1,000 as determined by GPC could not be successfully ionized and analyzed using this mass spectrometry technique.

^1H, $^{13}C\{^1H\}$, and $^{31}P\{^1H\}$ NMR spectra were recorded on 400, 500, or 600 MHz spectrometers. NMR characterization data are reported at 25 °C, unless specified otherwise. All of the NMR solvents were purchased from Cambridge Isotopes Laboratories. Methylene chloride-*d*2 (CD_2Cl_2) was freeze− pump−thaw-degassed three times, dried by passage through a small column of activated alumina, and stored over 3 Å molecular sieves. ^1H chemical shifts are reported in parts per million relative to residual protio solvent resonances. Metal complexes [(mes)Ni(Me-Allyl)][BAr^F_4], [(mes)Pd(allyl)][PF_6], and (P^tBu_3)PdMeCl were prepared according literature procedures.[54] $NaBAr^F_4$ was also prepared according to literature procedure.[99] 5-ethylidene-2-norbornene was purchased from Sigma Aldrich and freeze−pump−thaw-degassed three times, and stored at −35 °C under nitrogen. All of the other reagents were commercially available and used without further purification.

Conversions were determined by ^1H NMR spectroscopy. Samples to determine % conversion were prepared by removing a 100 μL aliquot from a reaction prior to quenching. The aliquot was then diluted with 400 mL $CDCl_3$, and 10 μL mesitylene was added as an internal standard, along with 10 μL methanol to quench the sample. Conversion was determined by

relative integration of the known concentration of mesitylene against the resonance for the *endo* olefin of 5-ethylidene-2-norbornene, as seen in Figure 4.6.

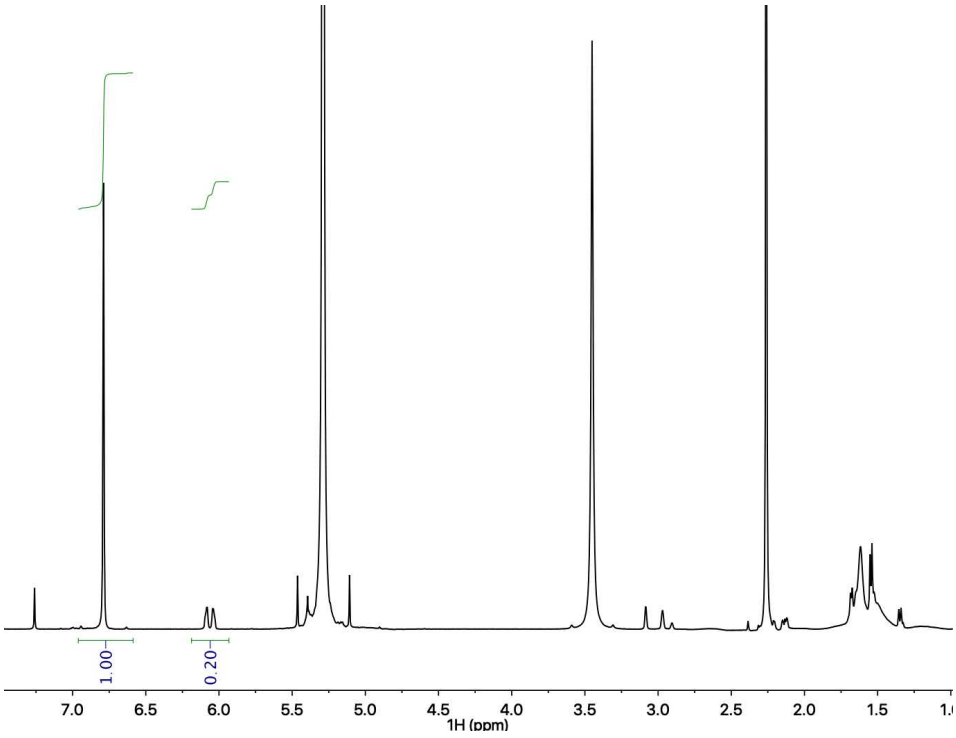

Figure 4.6. Representative ^{1}H NMR spectrum to determine the conversion of 5-ethylidene-2-norbornene.

Procedure for ENB polymerization by [(mes)Pd(allyl)][PF_6] and [(mes)Pd(allyl)][PF_6] + P^tBu_3

In a nitrogen glovebox, two septum capped reaction tubes were charged with dichloromethane and 5-ethylidene-2-norbornene (151 μL, 1.1 mmol) such that the total volume of the tubes would be a total of 4.4 mL each (250 mM ENB). To a separate vial was added [(mes)Pd(allyl)][PF_6] (4.1 mg, 0.0099 mmol) and dichloromethane (800 μL) . A solution of P^tBu_3 in dichloromethane (10 mg, 0.049 mmol in 2 mL) was prepared. To one of the reaction tubes was added 178 uL of the P^tBu_3 solution (0.0044 mmol). To each of the reaction tubes was then added 400 μL of the [(mes)Pd(allyl)][PF_6] solution (0.0044 mmol each). The tubes were capped, and allowed to stir outside of the box at room-temperature for two hours. Conversion of monomer was determined by removing an aliquot from the reactions prior to quenching, and analyzing by ^{1}H NMR spectroscopy with respect to a mesitylene internal standard. The tubes were subsequently quenched with methanol and the reactions were dried *in vacuo* and analyzed by GPC.

Table 4.3. GPC characterization of ENB homopolymers obtained using $[(mes)Pd(allyl)]^+$.

PR_3	Catalyst	Conversion	M_n (Da)	M_w (Da)	PDI
-	$[(mes)Pd(allyl)]^+$	23%	1,100	3,000	2.6
P^tBu_3	$[(mes)Pd(allyl)]^+$	100%	39,000	49,000	1.3
-	$(P^tBu_3)PdMeCl$ /$NaBAr^F_4$	100%	23,000	26,000	1.1

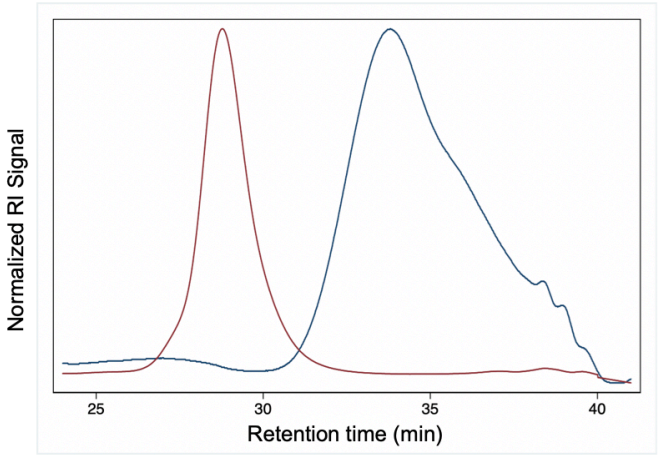

Figure 4.7. GPC trace overlay of ENB homopolymerizations by $[(mes)Pd(allyl)][PF_6]$ alone (blue trace) and with P^tBu_3 (red trace).

Procedure for norbornene polymerization by [(mes)Pd(allyl)][PF_6]

In a nitrogen glovebox, a septum-capped reaction tube was charged with norbornene (103 mg, 1.1 mmol) and 4 mL dichloromethane. To a separate vial was added [(mes)Pd(allyl)][PF_6] (4.1 mg, 0.0099 mmol) and dichloromethane (800 uL) . To the reaction tube containing norbornene was then added 400 uL of the [(mes)Pd(allyl)][PF_6] solution (0.0044 mmol). The tube was capped, and allowed to stir outside of the box at room temperature for two hours. Precipitation of polymer was observed less than five minutes after addition the [(mes)Pd(allyl)][PF_6] solution. Conversion of monomer was determined by removing an aliquot from the reactions prior to quenching, and analyzing by ^{1}H NMR spectroscopy with respect to a mesitylene internal standard. By ^{1}H NMR, the reaction went to full conversion. The tube was subsequently quenched with methanol and the reaction was dried *in vacuo.* The isolated white powder product (95 mg, 92% yield) was insoluble in toluene, pentane, THF, and chlorinated solvents, and precluded solution characterization.

Reaction of ENB with [(mes)Pd(allyl)][PF_6] in the presence of 1 atm C_2H_4

In a glovebox, a Schlenk flask was charged with ENB (300 μL, 2.2 mmol) in dichloromethane (8.3 mL). The flask was removed from the glovebox and ethylene was bubbled through the solution for approximately two minutes. The mixture was allowed to stir at 25 ºC for approximately 10 minutes under ethylene flow. Meanwhile, in the glovebox, a septum-capped vial was charged with [(mes)Pd(allyl)][PF_6] (3.9 mg, 0.0094 mmol) and dichloromethane (200 μL). The catalyst solution was added to the ENB solution via syringe under a positive pressure of ethylene. The reaction turned from yellow to dark grey within a few minutes, and the reaction was allowed to stir at 25 ºC for two hours. An aliquot of the reaction was removed via syringe and the conversion of monomer was measured by ^{1}H NMR spectroscopy against an internal mesitylene standard, and determined to be 6%. The reaction was subsequently quenched with methanol, dried *in vacuo*, and analyzed by GPC.

Reaction of ENB and [(mes)Pd(allyl)][PF_6] with P^tBu_3 in the presence of 1 atm C_2H_4

In a glovebox, a Schlenk flask was charged with 5-ethylidene-2-norbornene (300 μL, 2.2 mmol) and dichloromethane (8.1 mL). A separate vial was charged with P^tBu_3 (10.0 mg, 0.049 mmol) and dichloromethane (2 mL). To the Schlenk flask was added 180 μL of the P^tBu_3 solution (0.0094 mmol). The flask was removed from the glovebox, purged with ethylene on a Schlenk line for approximately two minutes, and allow to stir at 25 ºC for 10 minutes under ethylene flow. Meanwhile, in the glovebox, a septum-capped vial was charged with [(mes)Pd(allyl)][PF_6] (8.0 mg, 0.019 mmol) and dichloromethane (400 μL). To the Schlenk flask was added 200 μL of the catalyst solution (0.0094 mmol) under a positive pressure of ethylene. The reaction turned from yellow to dark grey over time, and the reaction was allowed to stir at 25 ºC for two hours. An

aliquot of the reaction was removed via syringe and the conversion of monomer was measured by ^{1}H NMR spectroscopy against an internal mesitylene standard, and determined to be 41%. The reaction was subsequently quenched with methanol, dried *in vacuo*, and analyzed by GPC.

Table 4.4. GPC characterization of polymer obtained via chain transfer with C_2H_4 using $[(mes)Pd(allyl)]^+$ catalyst.

Additive	**PR_3**	**Conversion**	**M_n** (Da)	**M_w** (Da)	**PDI**
1 atm C_2H_4	-	6%	500	920	1.8
1 atm C_2H_4	1 eq P^tBu_3	41%	2,200	3,200	1.5

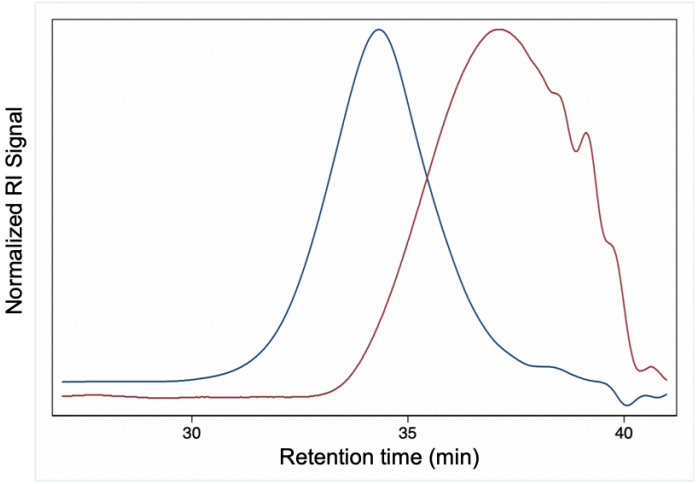

Figure 4.8. Overlay of GPC traces of polymer obtained via chain transfer with C_2H_4 using $[(mes)Pd(allyl)]^+$ catalyst alone (red trace) and with P^tBu_3 (blue trace).

General procedure for PR_3 screening in the polymerization of ENB by [(mes)Pd(allyl)][PF_6]

In a nitrogen glovebox, six septum-capped reaction tubes were charged with ENB (151 μL, 1.1 mmol) and 4 mL dichloromethane. A dichloromethane solution of the appropriate tertiary phosphine (P^tBu_3, PPh_3, or PEt_3) was added (either 1 mM or 2 mM final phosphine concentration). A separate vial was charged with [(mes)Pd(allyl)][PF_6] and dichloromethane, and an aliquot of this solution was added to the reaction such that the final concentrations were 1 mM catalyst, 250 mM ENB. The tubes were allowed to stir at 25 ºC for two hours outside of the glovebox. Aliquots of the tubes were taken to determine monomer conversion by ^{1}H NMR spectroscopy against a mesitylene internal standard. The reactions were quenched with methanol, dried *in vacuo*, and analyzed by GPC.

Table 4.5. GPC characterization of polymer obtained via of homopolymerizations of ENB by $[(mes)Pd(allyl)]^+$ and PR_3

additive	Conversion	M_n (Da)	M_w (Da)	PDI
1 eq P^tBu_3	100%	42,000	55,000	1.3
2 eq P^tBu_3	100%	42,000	52,000	1.2
1 eq PPh_3	100%	22,000	59,000	2.7
2 eq PPh_3	0%	-	-	-
1 eq PEt_3	100%	140,000	170,000	1.2
2 eq PEt_3	1 %	-	-	-

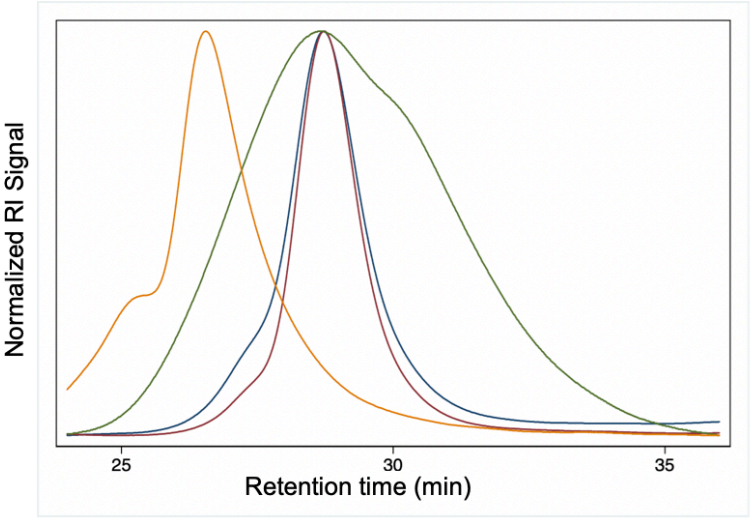

Figure 4.9. GPC overlay of ENB homopolymers obtained using $[(mes)Pd(allyl)]^+$ and 1 equiv. PEt_3 (yellow), 1 equiv. PPh_3 (green), 1 equiv. P^tBu_3 (blue), and 2 equiv. P^tBu_3 (red).

General procedure for reaction of (P^tBu_3)PdMeCl/$NaBAr^F_4$ with ENB

In a nitrogen glovebox, a septum capped reaction tube was charged with the desired amount of ENB and 4 mL dichloromethane. Separately, a scintillation vial was charged with $NaBAr^F_4$ (0.018 mmol) and a dichloromethane solution of (P^tBu_3)PdMeCl (0.018 mmol Pd). An aliquot of the catalyst solution was injected into the septum-capped reaction tube by syringe to initiate the reaction. At initiation, the 4.4 mL reaction mixture contained 1 mM of the (P^tBu_3)PdMeCl/$NaBAr^F_4$ catalyst system and ENB varying between 250 mM and 1000 mM. The tubes were allowed to stir at 25 ºC for two hours outside of the glovebox, at which point an aliquot (100.0 uL) was removed. The aliquot was diluted with $CDCl_3$, and methanol (10.0 uL) and mesitylene (10.0 uL) were added to the aliquot. The monomer conversion was determined by integration of remaining ENB resonances relative to a mesitylene internal standard in ^{1}H NMR spectra. Methanol (10 mL) was added to the bulk reaction solution to quench and precipitate any oligomeric or polymeric materials and the resulting powders were isolated by filtration and dried *in vacuo*.

Table 4.6. GPC characterization of ENB homopolymers obtained using different initial ENB concentrations.

[monomer] (mM)	[Catalyst]	Conversion	M_n (Da)	M_w (Da)	PDI
250	1 mM	100%	23,000	26,000	1.1
500	1 mM	100%	46,000	50,000	1.1
750	1 mM	100%	73,000	77,000	1.1
1000	1 mM	100%	100,000	108,000	1.1

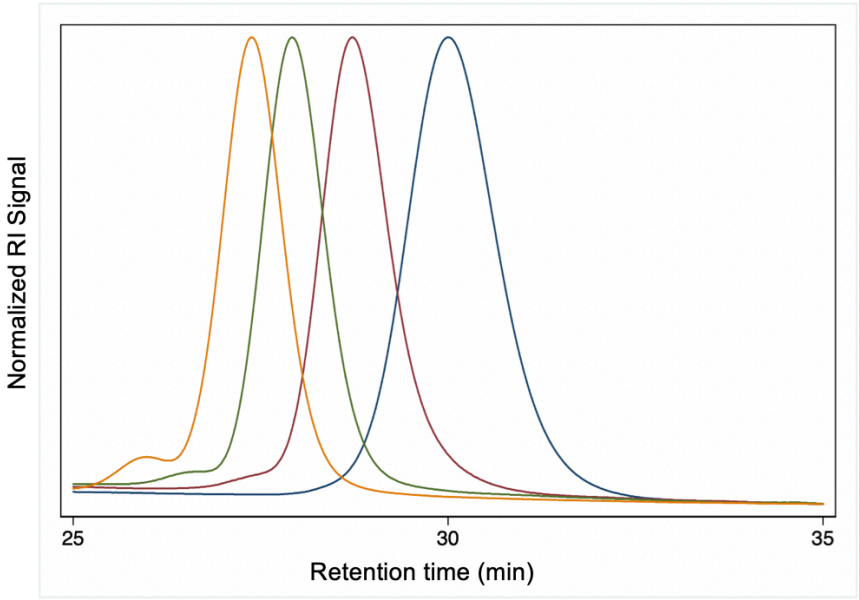

Figure 4.10. GPC overlay of ENB homopolymers produced from different initial ENB concentrations: 1000 mM (yellow), 750 mM (green), 500 mM (red), and 250 mM (blue).

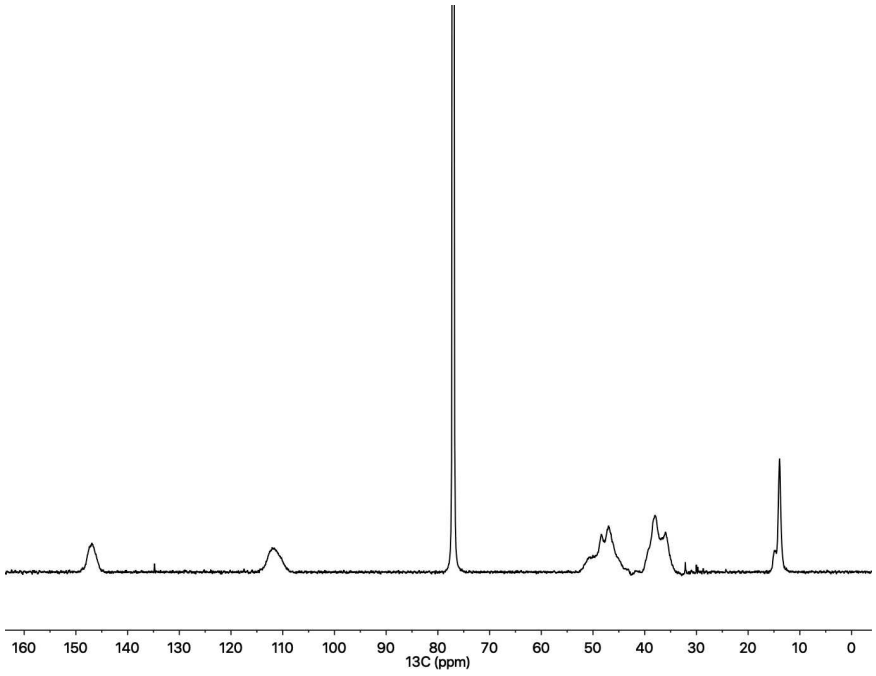

Figure 4.11. $^{13}C\{^{1}H\}$ NMR spectrum of ENB homopolymer (M_n 23,000) from (P^tBu_3)PdMeCl/$NaBAr^F_4$ system in $CDCl_3$.

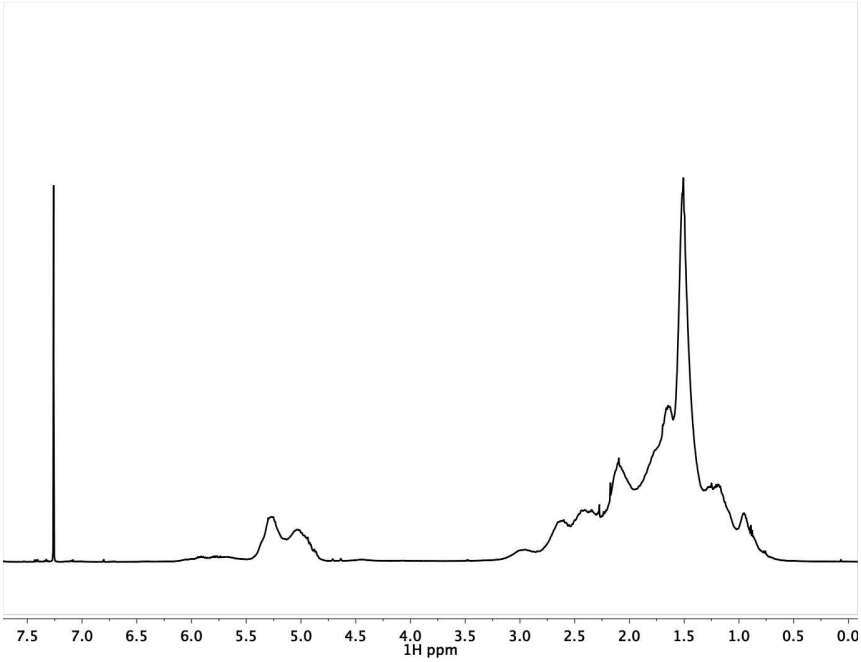

Figure 4.12. ^{1}H NMR spectrum of ENB homopolymer (M_n 23,000) from (P^tBu_3)PdMeCl/$NaBAr^F_4$ system in $CDCl_3$.

Time course of ENB homopolymerization by (P^tBu_3)PdMeCl/$NaBAr^F_4$

In a nitrogen glovebox, four septum-capped reaction tubes were charged with ENB (151 μL, 1.1 mmol) and 4 mL dichloromethane. Separately, a scintillation vial was charged with $NaBAr^F_4$ (16.0 mg, 0.018 mmol) and a dichloromethane solution of (P^tBu_3)PdMeCl (1.6 mL, 11.3 mM, 0.018 mmol Pd). To each septum-capped reaction tube, 400 μL of the catalyst solution was added by syringe, leading to a final concentration of 1 mM (P^tBu_3)PdMeCl/$NaBAr^F_4$ and 250 mM ENB in 4.4 mL dichloromethane. The reactions were allowed to stir at 25±1 ºC for 30 seconds, 1 minute, 5 minutes, and 10 minutes, respectively, before being quenched with methanol (1 mL). The monomer conversion was determined by integration of remaining ENB resonances relative to a mesitylene internal standard in ^{1}H NMR spectra. The samples were precipitated out of methanol and then dried *in vacuo*. The molecular weights were determined by gas permeation chromatography (GPC). The data is consistent with controlled (living) polymerization.

Table 4.7. GPC characterization of ENB homopolymers obtained at different reaction times.

Time (mins)	**Conversion**	**M_n**	**M_w**	**PDI**
0.5	19%	6,400	7,600	1.2
1	46%	15,000	20,000	1.3
5	86%	25,000	28,000	1.1
10	100%	27,000	30,000	1.1

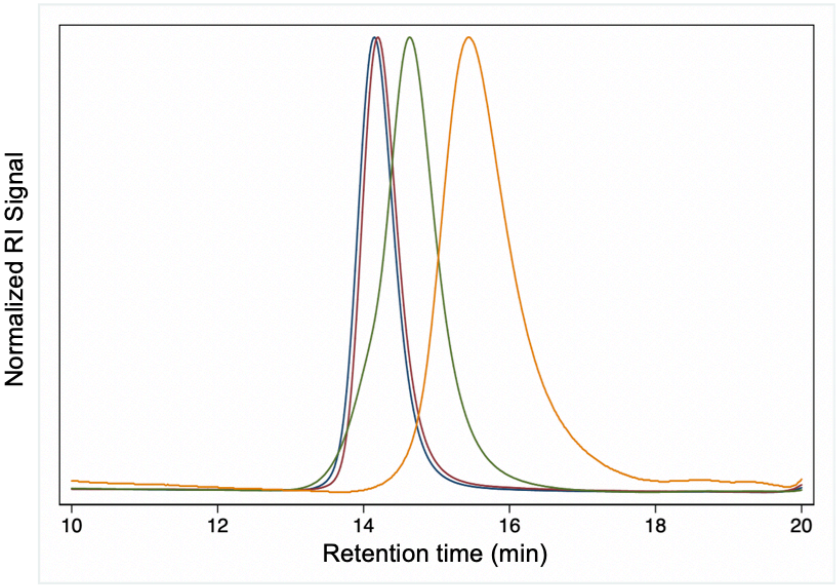

Figure 4.13. GPC overlay of ENB homopolymers obtained at varying reaction times: yellow (0.5 min), green (1 min), red (5 min), blue (10 min).)

General procedure for the polymerization of ENB by (P^tBu_3)PdMeCl/$NaBAr^F{}_4$ in the presence of 1-hexene

In a nitrogen glovebox, four septum-capped reaction tubes were charged with ENB (151 μL, 1.1 mmol), the desired amount of 1-hexene, and 4 mL dichloromethane. Separately, a vial was charged with $NaBAr^F{}_4$ (16.0 mg, 0.018 mmol) and a solution of (P^tBu_3)PdMeCl (1.6 mL, 11.3 mM, 0.018 mmol Pd). To each septum-capped reaction tube was added 400 μL of the catalyst solution by syringe, leading to a final concentration of 1 mM (P^tBu_3)PdMeCl/$NaBAr^F{}_4$, 250 mM ENB, and between 30 and 250 mM 1-hexene. The reactions were allowed to stir at room-temperature for two-hours outside of the glovebox, and were subsequently quenched with methanol. Full conversion of monomer was determined by ^{1}H NMR spectroscopy relative to a mesitylene internal standard. Quantitative yields of polymer powder were precipitated out of methanol and dried *in vacuo*.

Table 4.8. GPC characterization of hexene-terminated ENB polymers (M_n 10,500 – 21,000 Da).

[hexene] (mM)	[Catalyst]	Conversion	M_n (Da)	M_w (Da)	PDI
250	1 mM	100%	10,500	15,000	1.4
~80	1 mM	100%	17,000	21,000	1.3
50	1 mM	100%	18,100	23,000	1.3
~30	1 mM	100%	21,000	23,000	1.1

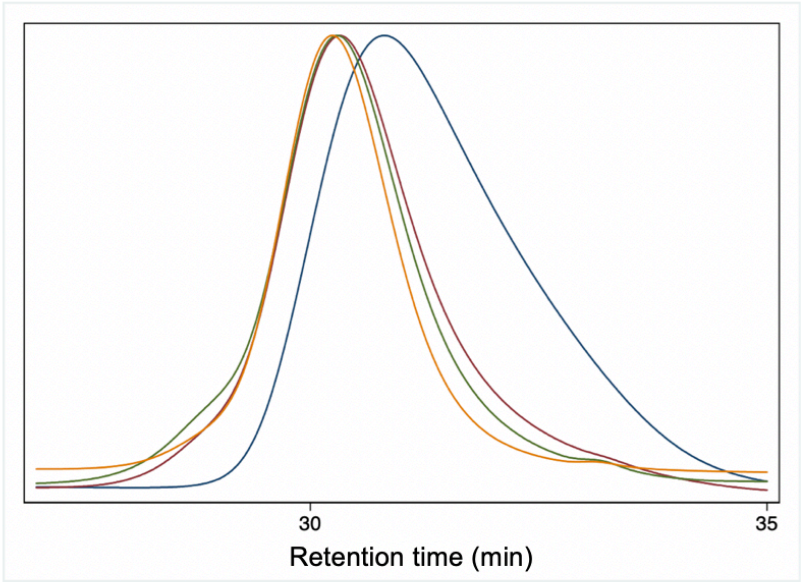

Figure 4.14. GPC overlay of hexene-terminated ENB polymers produced from different initial concentrations of 1-hexene: blue (250 mM), red (80 mM), green (50 mM), yellow (30 mM).

Procedure for determining concentration of ethylene in dichloromethane at 25 °C

In a nitrogen glovebox, a screw-cap NMR tube was charged with CD_2Cl_2 (1 mL), hexamethylbenzene (14.8 mg, mmol) as an internal standard. Due to the marginal solubility of hexamethylbenzene in dichloromethane at that concentration, *bis*(pentamethyl)cyclopentadienyl iron(II) (11.9 mg, 0.0733 mmol) was also added as an internal standard and was fully soluble. Ethylene was then purged through the solution in the tube for approximately two minutes, and a ^{1}H NMR spectrum was acquired. The final volume of the solution was approximately 800 uL after sparging with ethylene, making the final concentration of *bis*(pentamethyl)cyclopentadienyl iron (II) approximately 90 mM. The concentration of ethylene in solution, at 25 °C, was measured to be 220 mM.

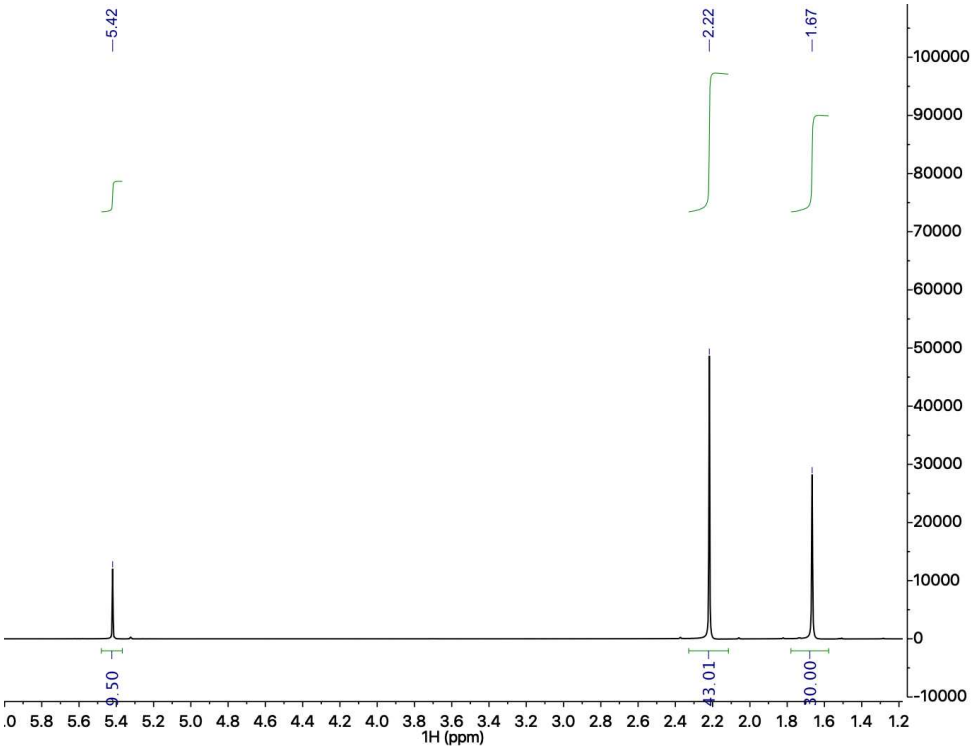

Figure 4.15. ^{1}H NMR spectrum to determine concentration of ethylene in CD_2Cl_2 at 25 °C.

Reaction of ENB with (P^tBu_3)PdMeCl/$NaBAr^F_4$ in the presence of 1 atm C_2H_4

In a nitrogen glovebox, a Schlenk flask was charged with ENB (605 μL, 4.5 mmol) and dichloromethane (16.6 mL) before ethylene was purged through the solution for approximately two minutes. The flask was allowed to stir at room temperature under 1 atm ethylene for approximately fifteen minutes. Meanwhile, in the glovebox, a septum-capped glass vial was charged with $NaBAr^F_4$ (17.3 mg, 0.021 mmol) and a solution of (P^tBu_3)PdMeCl (6.5 mg, 0.018 mmol) in dichloromethane (400 uL). All 400 μL of the catalyst solution was added to the stirring ENB solution under a positive pressure of ethylene via syringe. The reaction mixture quickly changed color from yellow to dark grey. After stirring for two hours at 25 ºC under 1 atm ethylene, a 100 μL aliquot of the reaction was obtained to determine conversion of monomer via ^{1}H NMR spectroscopy with respect to an internal mesitylene standard. The monomer was determined to be 28% converted relative to a mesitylene internal standard by ^{1}H NMR spectroscopy. The reaction solution was quenched with methanol (10 mL) immediately after removing the aliquot to determine conversion, and white polymer was precipitated out of methanol and was dried *in vacuo* (160 mg, 30% yield). The polymer was analyzed by GPC.

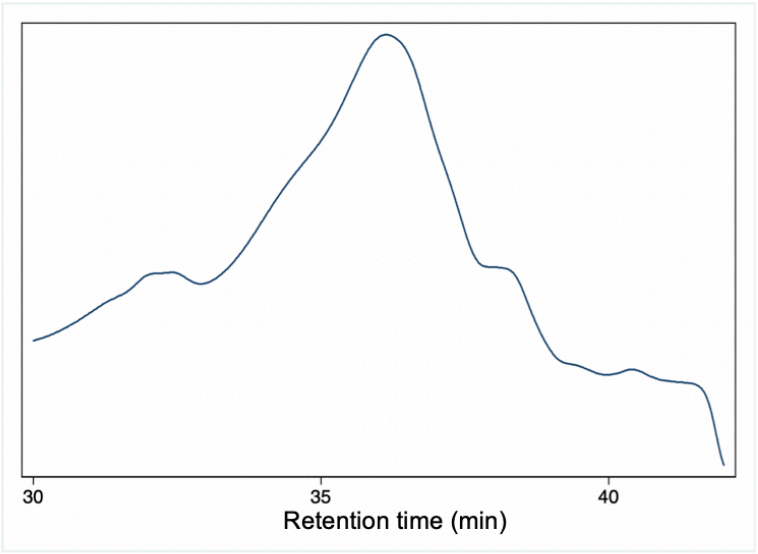

Figure 4.16. GPC trace of ENB polymer obtained via chain transfer with C_2H_4 in (P^tBu_3)PdMeCl/$NaBAr^F{}_4$ system.

The addition of C_2H_4 to (P^tBu_3)PdMeCl/$NaBAr^F{}_4$ in CD_2Cl_2

A Teflon-sealed NMR tube was charged with (P^tBu_3)PdMeCl (4.1 mg, 0.011 mmol) and $NaBAr^F{}_4$ (10.8 mg, 0.012 mmol) in approximately 500 μL CD_2Cl_2. The tube was quickly attached to a Schlenk-line via its Teflon cap, and was quickly charged with ethylene after evacuating the headspace of the cap to remove oxygen. The yellow solution immediately turned dark brown upon the addition of ethylene. A ^1H NMR spectrum was taken approximately 15 minutes after charging the tube with ethylene, and only free P^tBu_3 was visible by ^1H and $^{31}P\{^1H\}$ NMR spectroscopy.

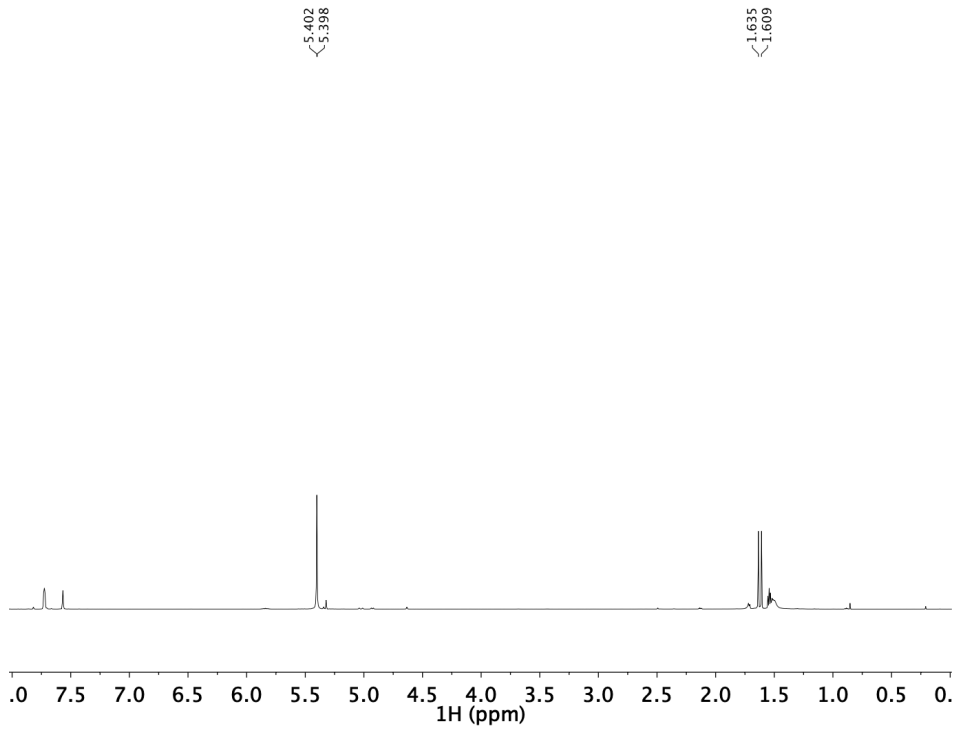

Figure 4.17. ^1H NMR spectrum of the addition of C_2H_4 to (P^tBu_3)PdMeCl and $NaBAr^F{}_4$ in CD_2Cl_2.

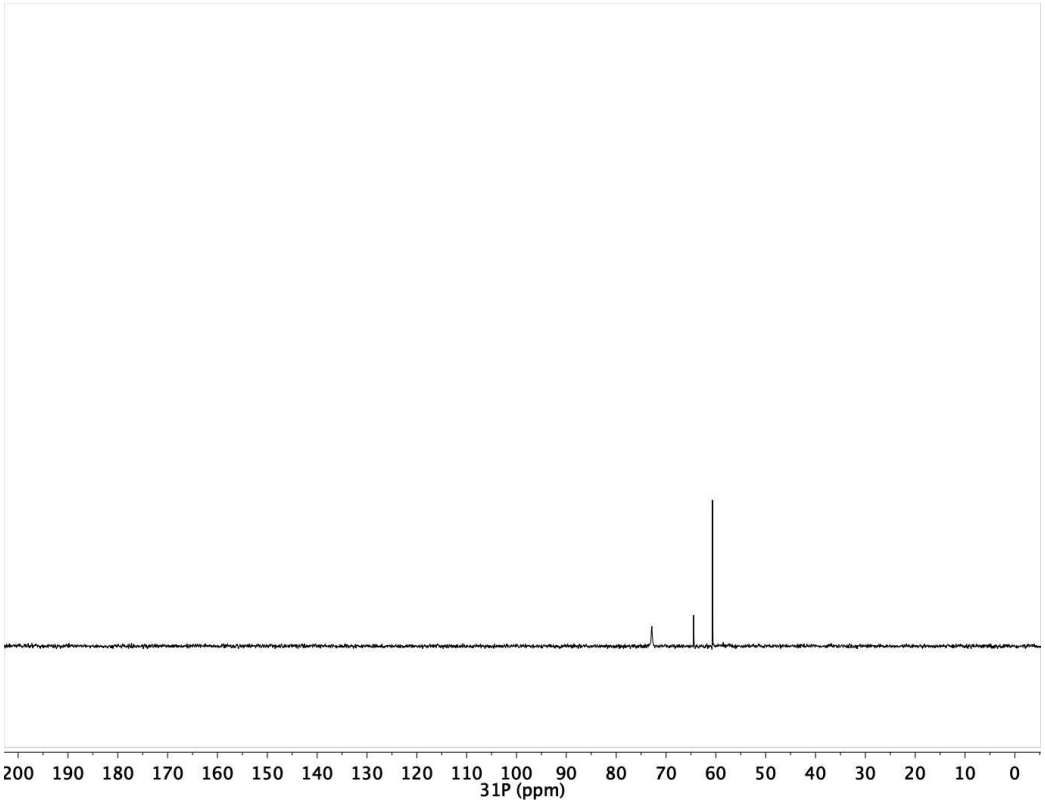

Figure 4.18. $^{31}P\{^{1}H\}$ NMR spectrum of the addition of C_2H_4 to (P^tBu_3)PdMeCl and $NaBAr^F{}_4$ in CD_2Cl_2.

General procedure for ENB homopolymerization catalyzed by [(mes)Ni(Me-Allyl)][BAr$^F{}_4$]

In a nitrogen glovebox, four septum-capped reaction tubes were charged with the desired amount of ENB and 4 mL dichloromethane. A separate vial was charged with [(mes)Ni(Me-allyl)][BAr$^F{}_4$] (20.9 mg, 0.019 mmol, in 1.6 mL DCM) was added. The vial was quickly swirled, and 400 uL of the corresponding solution was added to each septum-capped reaction tube such that they each contained 1 mM of the [(mes)Ni(Me-allyl)][BAr$^F{}_4$] catalyst solution and ENB concentrations ranging 250 mM and 1000 mM. The tubes were allowed to stir at room-temperature for two-hours outside of the glovebox, and were subsequently quenched with methanol. The monomer conversion was determined by ^{1}H NMR spectroscopy relative to a mesitylene internal standard.

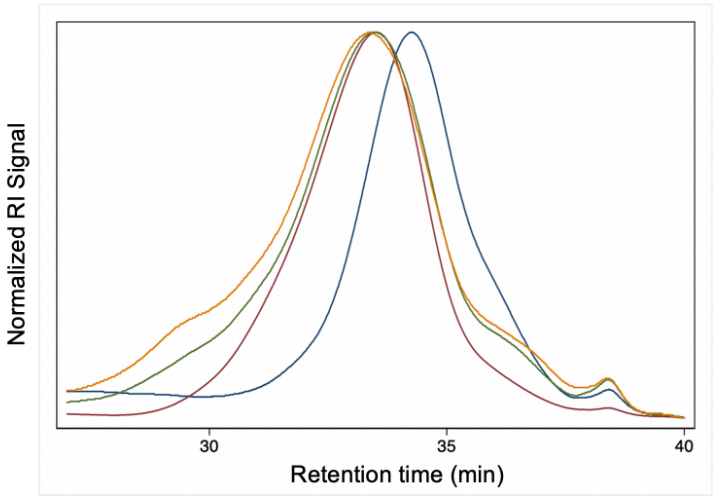

Figure 4.19. GPC overlay of ENB homopolymers obtained using $[(mes)Ni(Me\text{-}Allyl)]^+$.

Table 4.9. GPC characterization of ENB homopolymers obtained using $[(mes)Ni(Me\text{-}Allyl)]^+$.

[ENB]	Conversion	M_n (Da)	M_w (Da)	PDI
250 mM	10%	2,200	3,200	1.43
500 mM	15%	3,700	6,300	1.68
750 mM	19%	2,900	7,200	2.48
1000 mM	25%	3,900	8,300	2.13

Procedure for norbornene polymerization by [(mes)Ni(Me-allyl)][BAr$^F{}_4$]

In a nitrogen glovebox, a septum capped reaction tube was charged with norbornene (108 mg, 1.1 mmol) and 4 mL dichloromethane. To a separate vial was added [(mes)Ni(allyl)][BAr$^F{}_4$] (10.0 mg, 0.0099 mmol) and dichloromethane (800 μL) . To the reaction tube containing norbornene was then added 400 uL of the [(mes)Ni(allyl)][BAr$^F{}_4$] solution (0.0044 mmol). The tube was capped, and allowed to stir outside of the box at room-temperature for two hours. Precipitation of polymer was observed less than five minutes after addition of the [(mes)Ni(allyl)][BAr$^F{}_4$] solution. Conversion of monomer was determined by removing an aliquot from the reactions prior to quenching, and analyzing by ^{1}H NMR spectroscopy with respect to a mesitylene internal standard. By ^{1}H NMR analysis, the reaction went to full conversion. The tube was subsequently quenched with methanol and the reaction was dried *in vacuo.* The isolated white powder product (98 mg, 90% yield) was insoluble in toluene, pentane, THF, and chlorinated solvents, and precluded solution characterization.

General procedure for PR_3 Screening in the polymerization of ENB by [(mes)Ni(Me-allyl)][$BAr^F{}_4$]

In a nitrogen glovebox, six septum-capped reaction tubes were charged with ENB (151 μL, 1.1 mmol) and 4 mL dichloromethane. To the tubes was added a solution of phosphine in dichloromethane, P^{t}Bu$_3$, PPh$_3$, and PEt$_3$, respectively, such that the final concentration of phosphine in each tube would be either 1 mM or 2 mM, respectively. A separate vial was charged with [(mes)Ni(Me-allyl)][$BAr^F{}_4$] (28.8 mg, 0.026 mmol) and dichloromethane (2.4 mL). To each tube was added 400 μL of the Ni solution such that the concentration of Ni in each tube was 1 mM and the ENB concentration was 250 mM. The tubes were allowed to stir at room-temperature for two-hours outside of the glovebox. Aliquots of the tubes were taken to determine monomer conversion by ^{1}H NMR spectroscopy against a mesitylene internal standard. The reactions were quenched with methanol, dried *in vacuo*, and the product analyzed by GPC.

Table 4.10. GPC characterization of ENB homopolymers obtained using $[(mes)Ni(Me\text{-}allyl)]^+$ and PR_3.

Additive	Conversion	M_n (Da)	M_w (Da)	PDI
-	10%	2,200	3,200	1.4
1 eq P^tBu_3	61%	1,100	2,000	1.7
2 eq P^tBu_3	52%	1,200	2,100	1.9
1 eq PPh_3	55%	7,400	11,000	1.5
2 eq PPh_3	30%	330	360	1.1
1 eq PEt_3	56%	4,900	6,800	1.4
2 eq PEt_3	30%	1,500	1,500	1.02

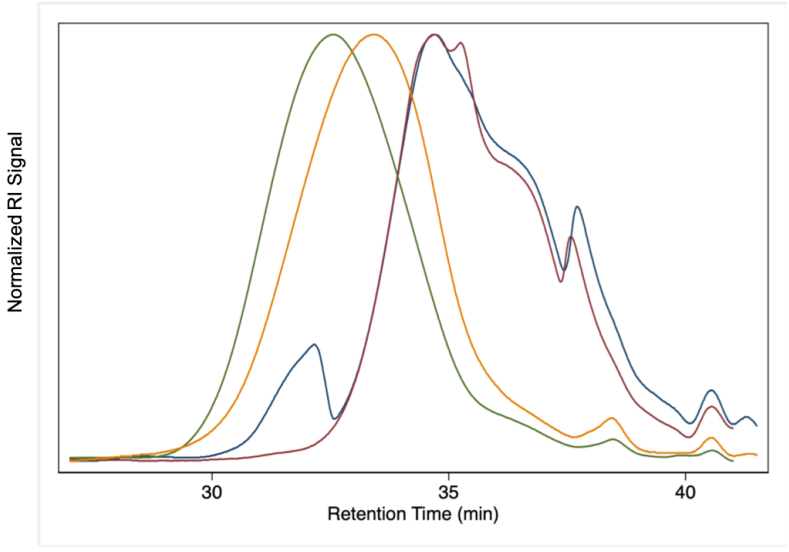

Figure 4.20. GPC overlay of ENB homopolymers obtained using $[(mes)Ni(Me\text{-}Allyl)]^+$ and PR_3: blue (1 equiv. P^tBu_3), red (2 equiv. P^tBu_3), green (1 equiv. PPh_3), yellow (1 equiv. PEt_3).

Procedure for the reaction of ENB with [(mes)Ni(Me-allyl)][BAr$^F_4$] in the presence of 1-hexene

In a nitrogen glovebox, four septum capped reaction tubes were charged with ENB (151 μL, 1.1 mmol) and 4 mL dichloromethane. To the tubes was added 1-hexene, such that the tubes were of increasing [1-hexene] (250 mM, 80 mM, 50 mM, and 30 mM, respectively). A separate vial was charged with [(mes)Ni(Me-allyl)][BAr$^F_4$] (20.8 mg, 0.019 mmol) and dichloromethane (2.4 mL). To each tube was added 400 uL of the Ni solution such that the concentration of Ni in each tube was 1 mM and the concentration of ENB was 250 mM. The tubes were allowed to stir at room-temperature for two-hours outside of the glovebox. Aliquots of the tubes were taken to determine monomer conversion by ^{1}H NMR spectroscopy against a mesitylene internal standard. The reactions were quenched with methanol, dried *in vacuo*, and analyzed by GPC.

Table 4.11. GPC Characterization of hexene-terminated ENB oligomers (M_n 870 – 2,300 Da).

[1-hexene] mM	Time	Conversion	M_n (Da)	M_w (Da)	PDI
250 mM	2 hrs	50%	870	1800	2.1
~80 mM	2 hrs	55%	1515	2300	1.5
50 mM	2 hrs	50%	1900	2600	1.3
~30 mM	2 hrs	41%	2300	3200	1.4

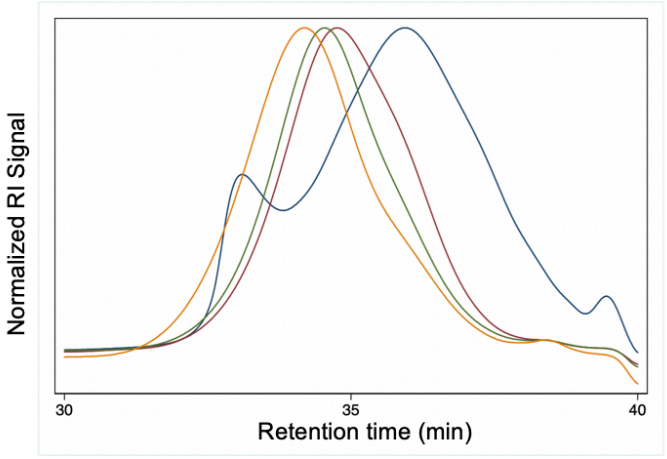

Figure 4.21. GPC overlay of ENB oligomers obtained via chain transfer with varying concentrations of 1-hexene using $[(mes)Ni(Me\text{-}Allyl)]^+$: blue (250 mM), red (80 mM), green (50 mM), yellow (30 mM).

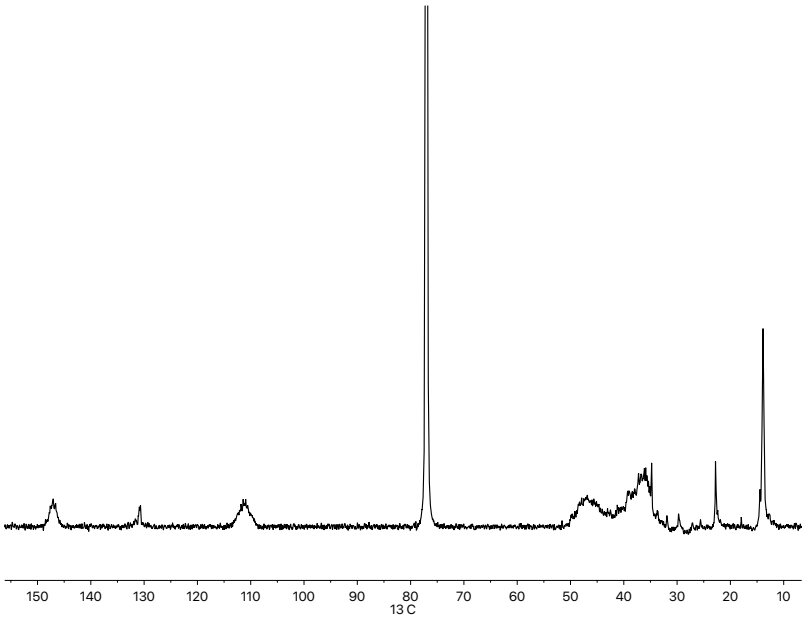

Figure 4.22. $^{13}C\{^{1}H\}$ NMR spectrum of polymer obtained via chain transfer with 1-hexene by cationic allyl Ni in $CDCl_3$.

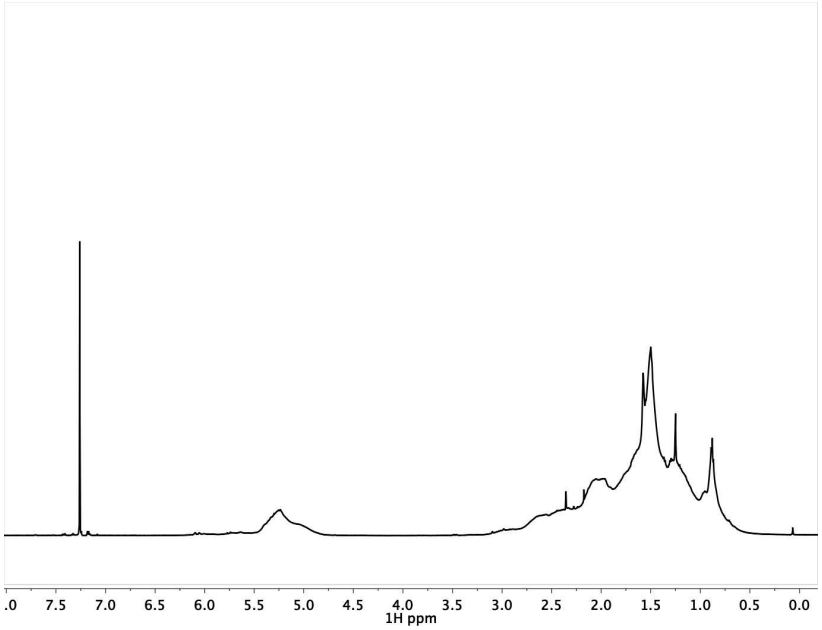

Figure 4.23. ^{1}H NMR spectrum of polymer obtained via chain transfer with 1-hexene by cationic allyl Ni in $CDCl_3$.

Procedure for the polymerization of ENB by [(mes)Ni(Me-allyl)][BAr^F_4] + PPh_3 in the presence of 1-hexene

In a nitrogen glovebox, four septum-capped reaction tubes were charged with ENB (151 uL, 1.1 mmol) and 4 mL dichloromethane. To the tubes was added 1-hexene, such that the tubes were of increasing [1-hexene] (250 mM, 80 mM, 50 mM, and 30 mM, respectively). A separate vial was charged with PPh_3 (13.0 mg, 0.050 mmol) in dichloromethane (2.6 mL). To each reaction tube was added 234 uL of the PPh_3 solution. A separate vial was charged with [(mes)Ni(Me-allyl)][BAr^F_4] (19.6 mg, 0.018 mmol) and dichloromethane (2.4 mL). To each tube was added 400 uL of the Ni solution such that the concentration of Ni and PPh_3 in each tube was 1 mM and the concentration of ENB was 250 mM. The tubes were allowed to stir at room-temperature for two-hours outside of the glovebox. Aliquots of the tubes were taken to determine monomer conversion by ^{1}H NMR spectroscopy against a mesitylene internal standard. The reactions were quenched with methanol, dried *in vacuo*, and analyzed by GPC.

Table 4.12. GPC characterization of hexane-terminated ENB oligomers (M_n 270 – 750 Da).

mM 1-hexene	additive	Time	Conversion	M_n	M_w	PDI
250 mM	1 eq PPh_3	2 hrs	73%	270	370	1.4
~80 mM	1 eq PPh_3	2 hrs	68%	460	670	1.5
50 mM	1 eq PPh_3	2 hrs	60%	660	990	1.5
~30 mM	1 eq PPh_3	2 hrs	78%	750	1200	1.6

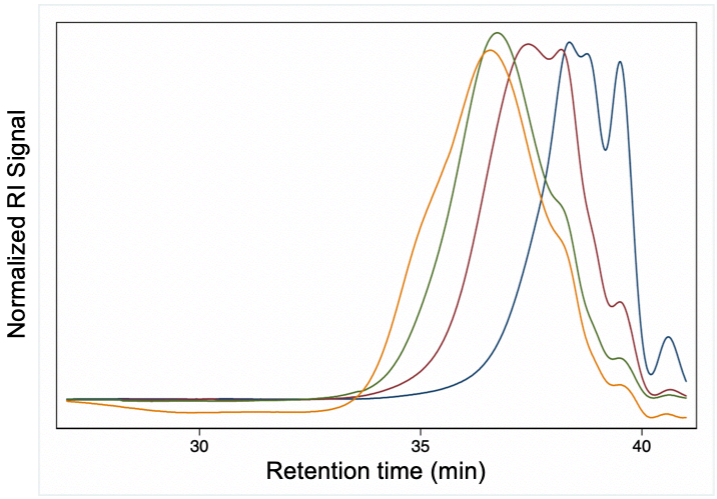

Figure 4.24. GPC overlay of ENB oligomers obtained via chain transfer with varying initial concentrations of 1-hexene using $[(mes)Ni(Me\text{-}allyl)]^+$ and PPh_3: blue (250 mM), red (80 mM), green (50 mM) yellow (30 mM).

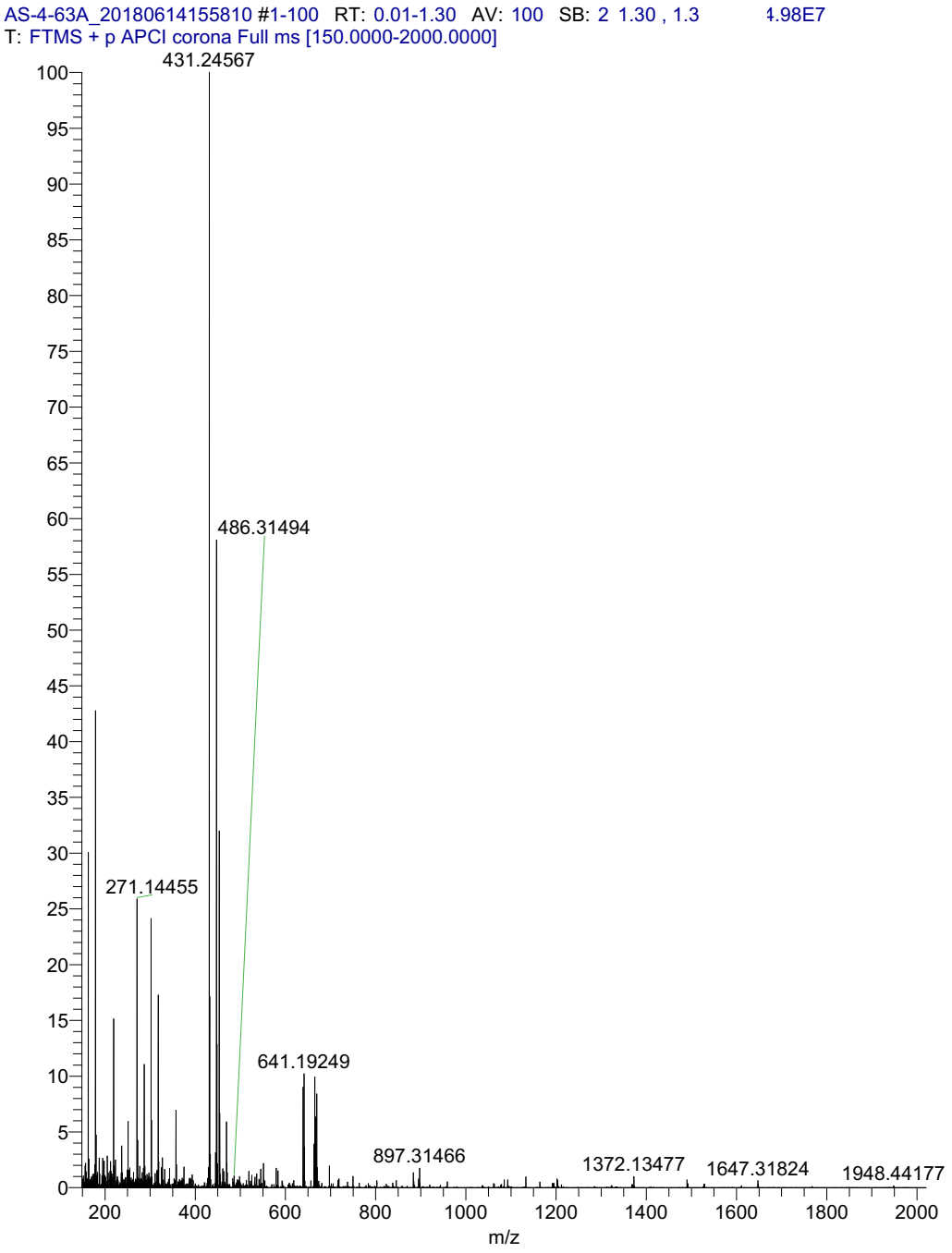

Figure 4.25. Mass spectrum of 1-hexene terminated ENB oligomer (M_n 270 Da by GPC)**.**

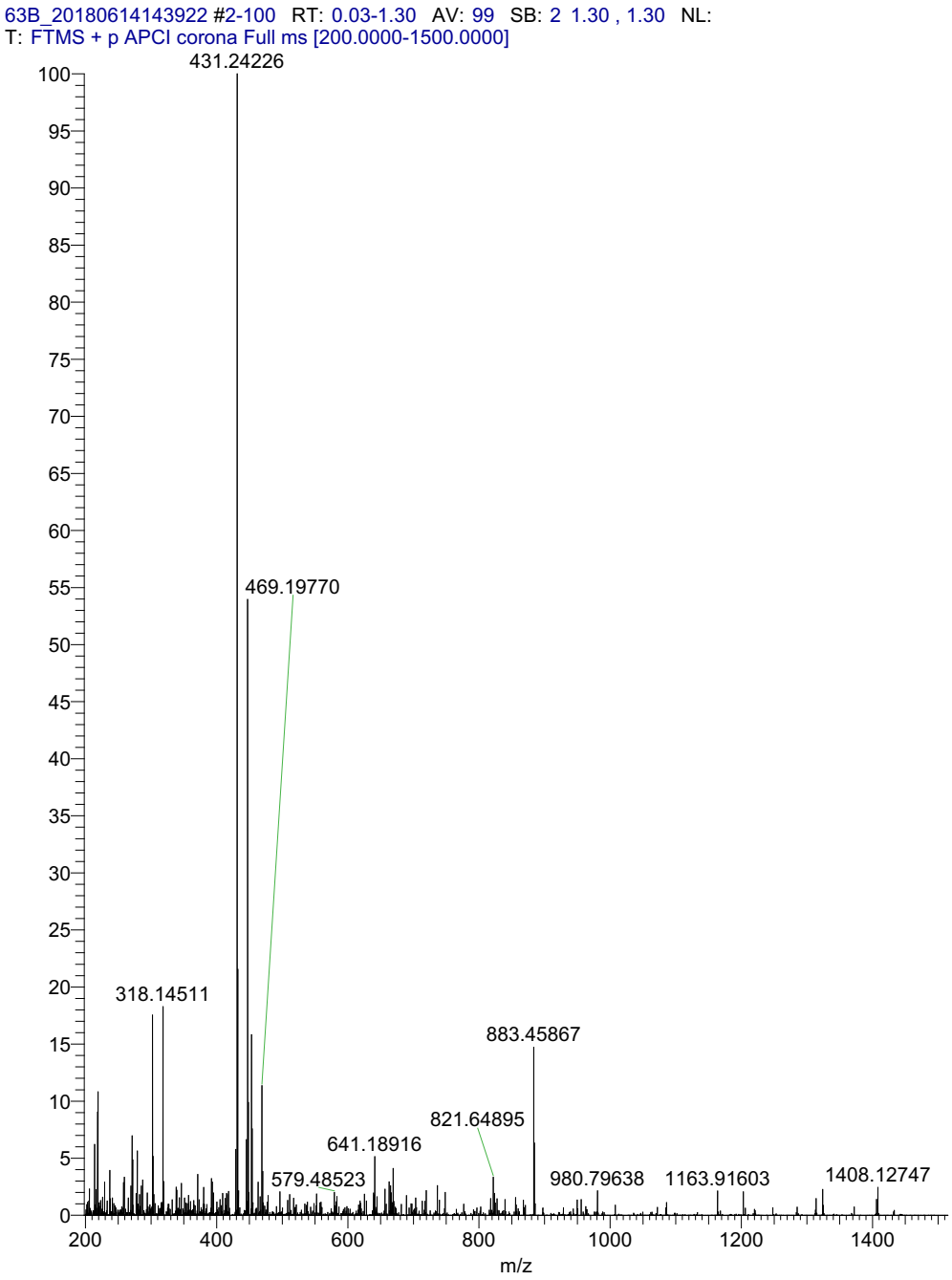

Figure 4.26. Mass spectrum of 1-hexene terminated ENB oligomer (M_n 460 Da by GPC).

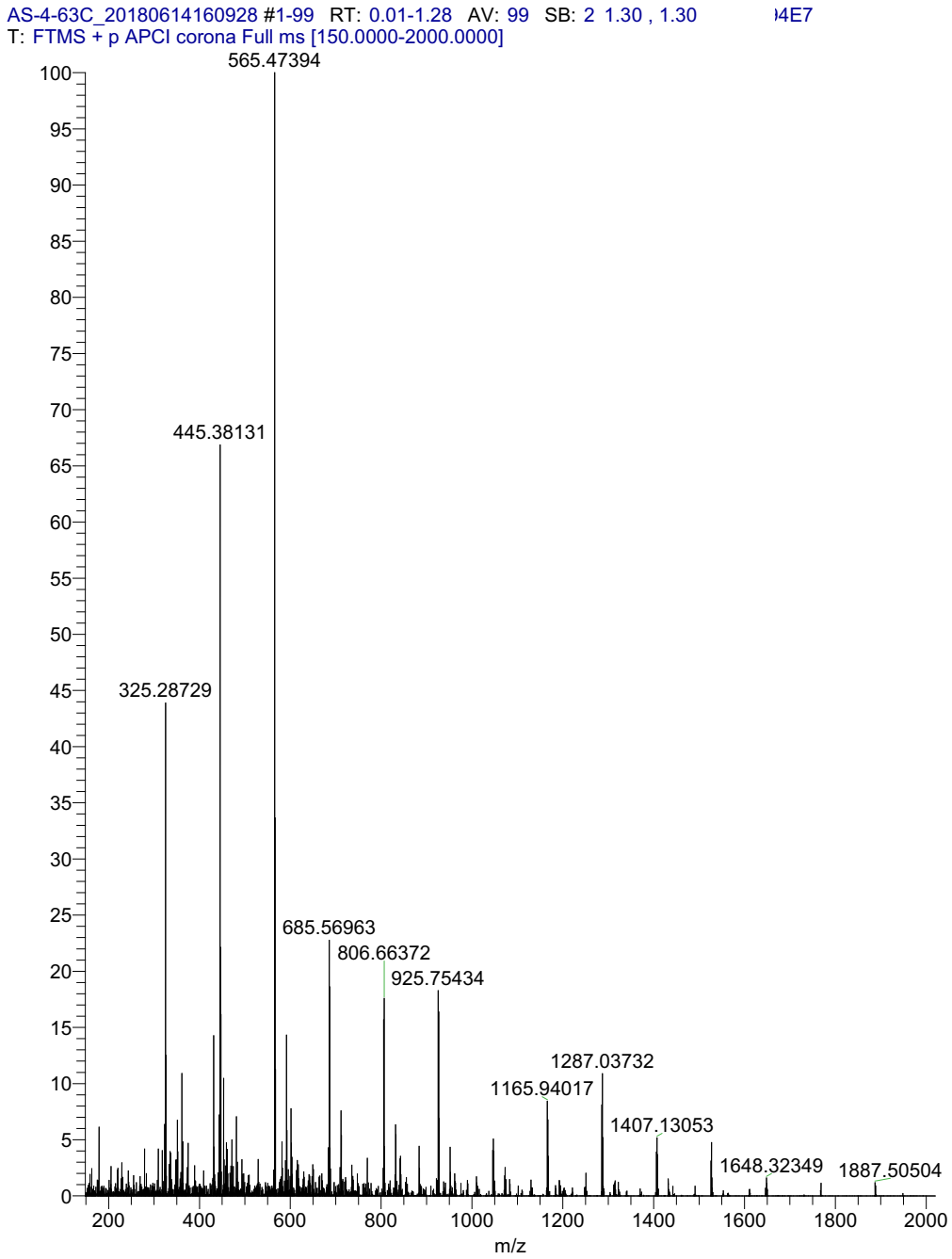

Figure 4.27. Mass spectrum of 1-hexene terminated ENB oligomer (M_n 660 Da by GPC).

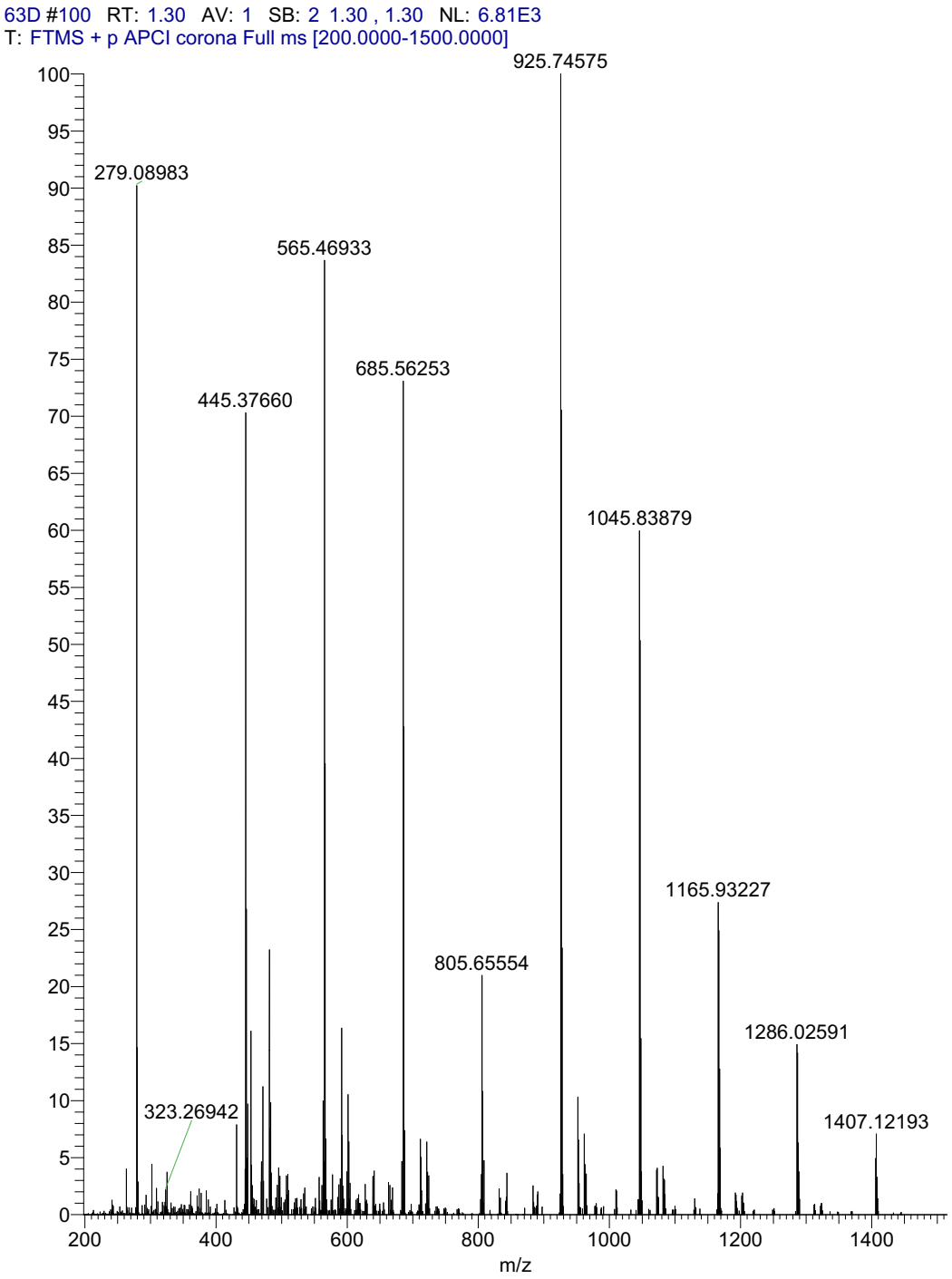

Figure 4.28. Mass spectrum of 1-hexene terminated ENB oligomer (M_n 750 Da by GPC).

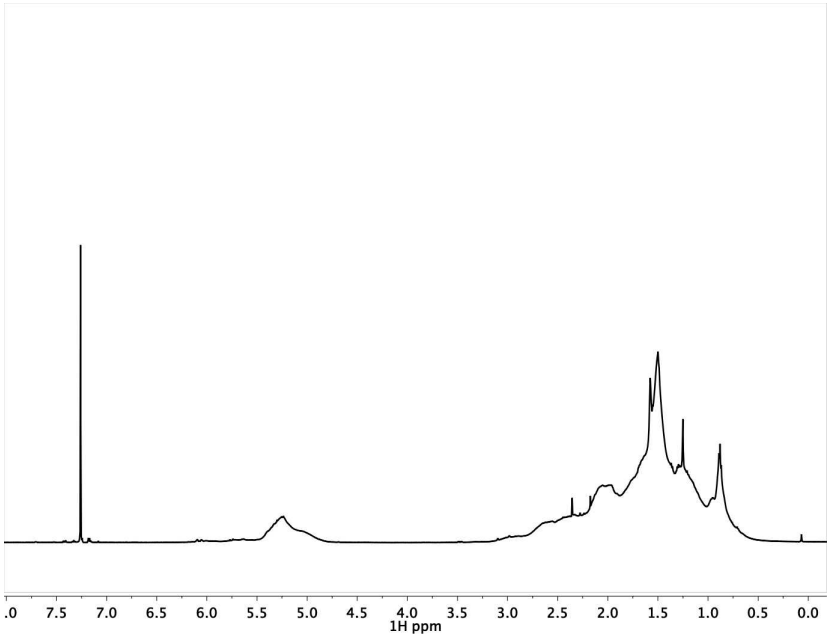

Figure 4.29. ^{1}H NMR spectrum of 1-hexene terminated ENB oligomer with an M_n of 660 Da in $CDCl_3$.

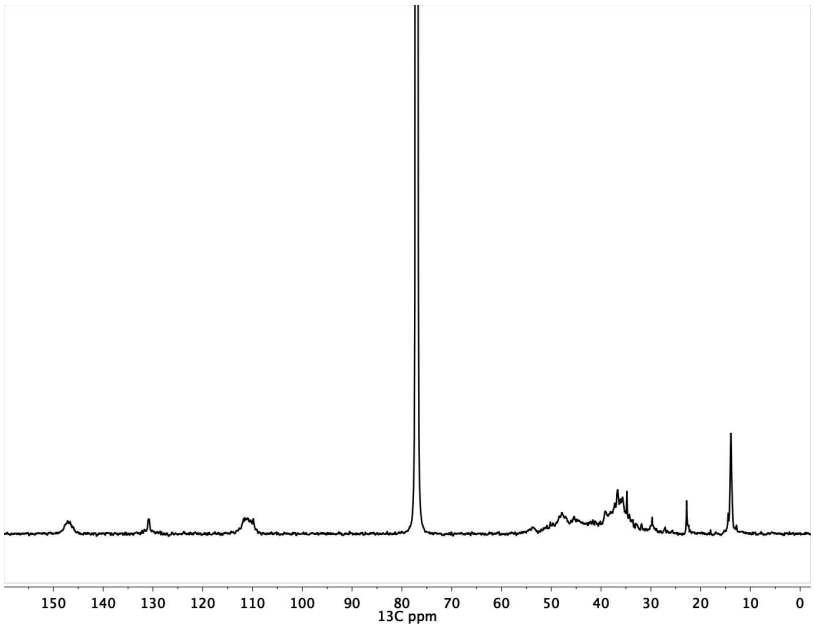

Figure 4.30. $^{13}C\{^{1}H\}$ NMR spectrum of 1-hexene terminated ENB oligomer with an M_n of 660 Da in $CDCl_3$.

General procedure for the reaction of ENB with [(mes)Ni(Me-allyl)][BAr$^F{}_4$] in the presence of 1 atm C_2H_4

In a glovebox, a Schlenk flask was charged with 5-ethylidene-2-norbornene in dichloromethane. In a separate septum-capped vial, a solution of [(mes)Ni(Me-allyl)][BAr$^F{}_4$] in dichloromethane was prepared. The Schlenk flask was purged with ethylene on a Schlenk line for approximately two minutes, and was allowed to stir under ethylene flow for approximately ten minutes at room temperature. The Schlenk flask was then charged with the Ni catalyst solution via syringe under a positive pressure of ethylene. The reaction was allowed to stir at room temperature under ethylene for two hours, at which point an aliquot from the reaction was removed to determine the monomer conversion via ^{1}H NMR spectroscopy against an internal mesitylene standard. The reaction was then quenched with methanol and pumped to dryness *in vacuo*. Product was analyzed by NMR spectroscopy, GPC, and atmospheric pressure chemical ionization mass-spectrometry.

Table 4.13. GPC characterization of ethylene-terminated ENB oligomers (M_n 740-930 Da).

additive	Catalyst loading	[monomer]	Conversion	M_n (Da)	M_w (Da)	PDI
-	1 mM	250 mM	10%	2200	3200	1.4
1 atm C_2H_4	1 mM	250 mM	100%	890	1600	1.8
1 atm C_2H_4	1 mM	250 mM	100%	930	1500	1.7
1 atm C_2H_4	1 mM	125 mM	100%	740	1200	1.6
1 atm C_2H_4	0.5 mM	125 mM	100%	750	1300	1.7

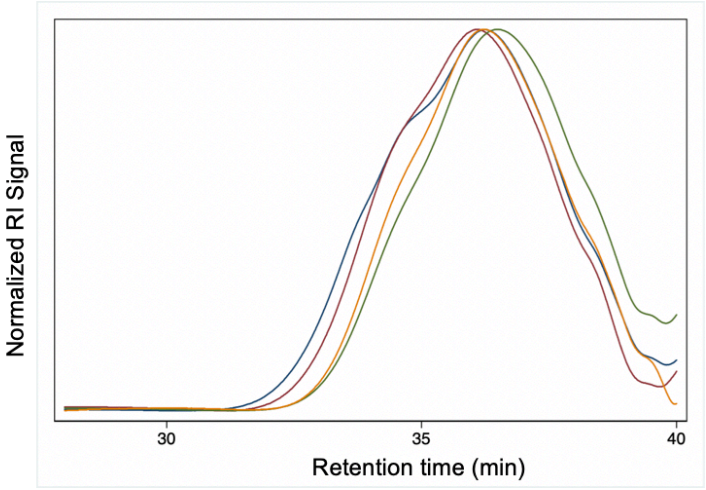

Figure 4.31. GPC trace overlay of ENB oligomer obtained via chain transfer by C_2H_4 using $[(mes)Ni(Me\text{-}allyl)]^+$.

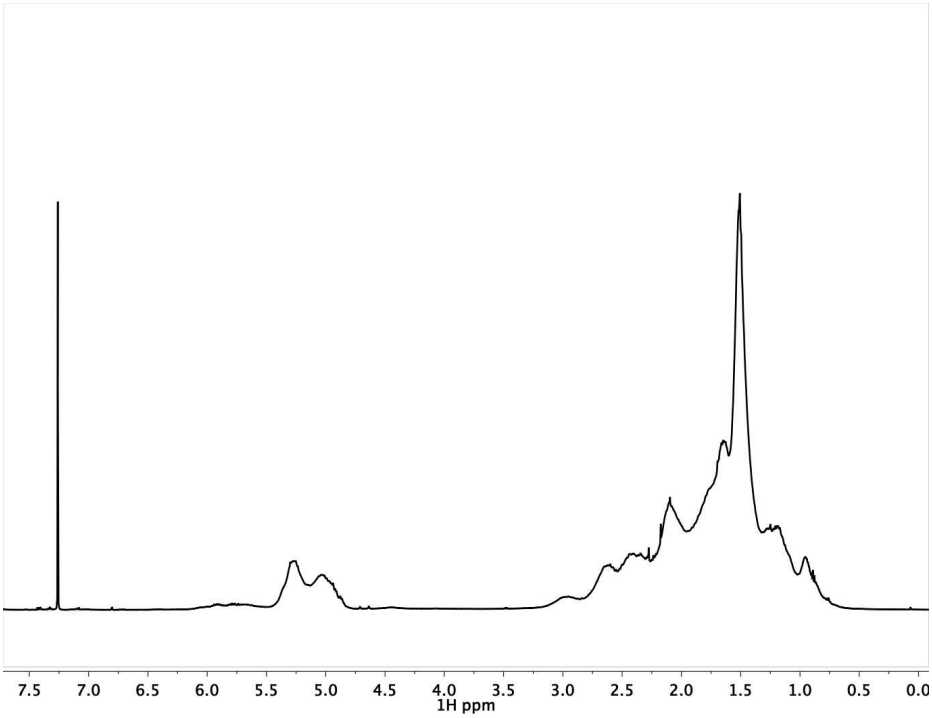

Figure 4.32. ^{1}H NMR of ethylene-terminated ENB oligomer (M_n 890 Da) in $CDCl_3$.

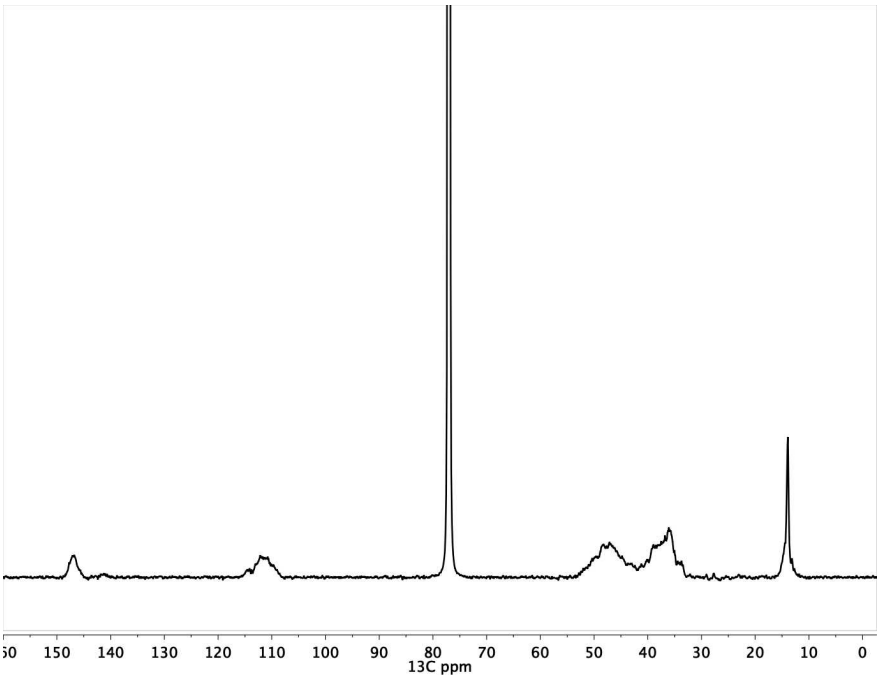

Figure 4.33. $^{13}C\{^{1}H\}$ NMR of ethylene-terminated ENB oligomer (M_n 890 Da) in $CDCl_3$.

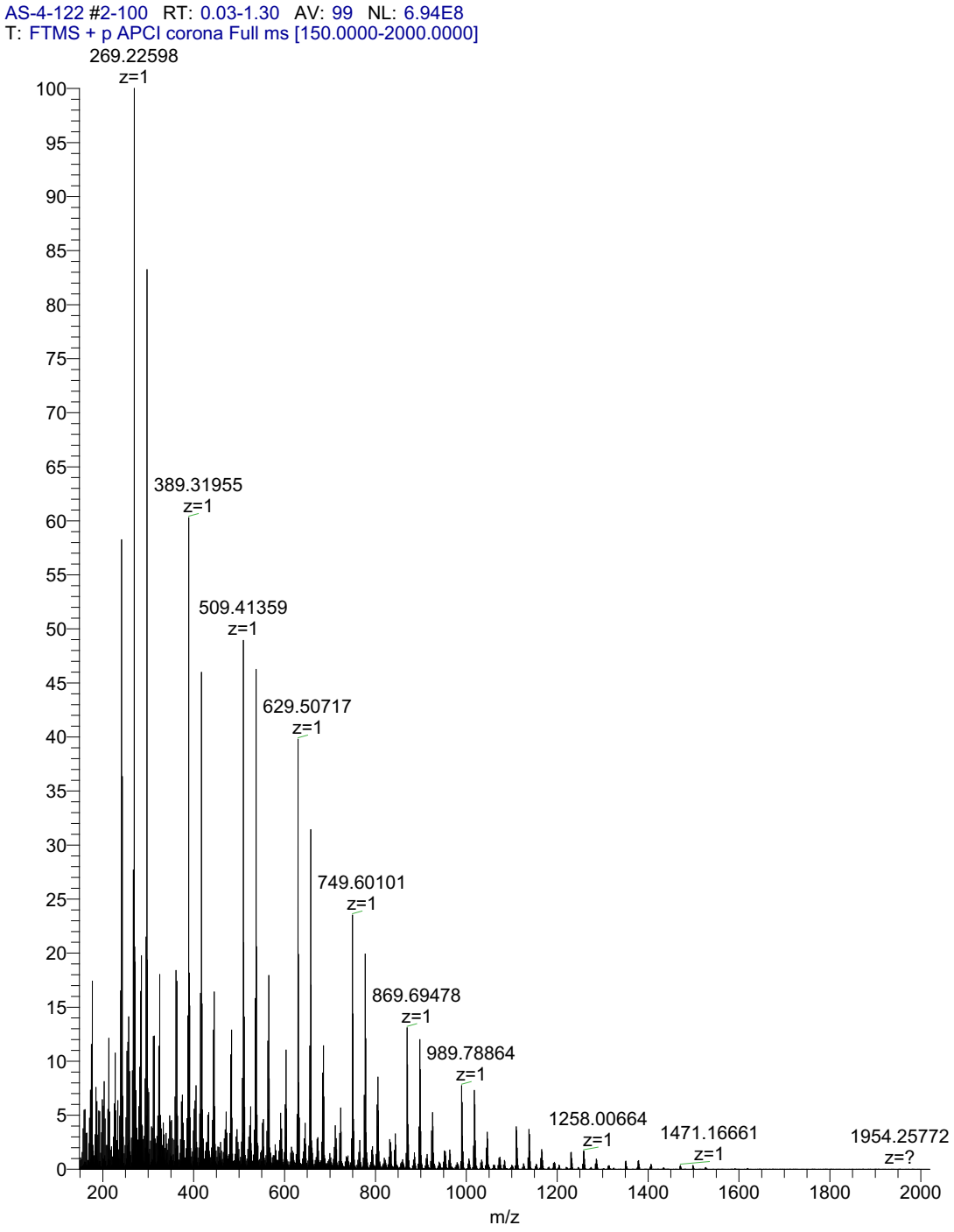

Figure 4.34. Mass spectrum of M_n 890 Da ethylene-terminated ENB oligomer.

Procedure for the polymerization of norbornene by [(mes)Ni(Me-allyl)][BAr^F_4] in the presence of 1 atm C_2H_4

In a glovebox, a Schlenk flask was charged with norbornene (105 mg, 1.1 mmol) in dichloromethane. In a separate septum-capped vial, a solution of [(mes)Ni(Me-allyl)][BAr^F_4] (10.0 mg, 0.0099 mmol) in dichloromethane (800 μL) was prepared. The Schlenk flask was purged with ethylene on a Schlenk line for approximately two minutes, and was allowed to stir under ethylene flow for approximately ten minutes at room temperature. The Schlenk flask was then charged with the Ni catalyst solution (400 μL) via syringe under a positive pressure of ethylene. The reaction was allowed to stir at room temperature under ethylene for two hours, at which point an aliquot from the reaction was removed to determine the monomer conversion via ^{1}H NMR spectroscopy against an internal mesitylene standard. The reaction was then quenched with methanol and pumped to dryness *in vacuo*. The monomer was determined to have been fully consumed in the reaction by ^{1}H NMR spectroscopy. The product was analyzed by GPC (M_n 2,040 Da, M_w 5,000 Da, PDI 2.4).

General procedure for the polymerization of ENB by [(mes)Ni(Me-allyl)][BAr^F_4] + PR_3 in the presence of 1 atm C_2H_4

In a glovebox, a Schlenk flask was charged with 5-ethylidene-2-norbornene in dichloromethane and PR_3, such that the total concentration of PR_3 in solution was 1 mM. In a separate septum-capped vial, a solution of [(mes)Ni(Me-allyl)][BAr^F_4] in dichloromethane was prepared. The Schlenk flask was purged with ethylene on a Schlenk line for approximately two minutes, and was allowed to stir under ethylene flow for approximately ten minutes at room temperature. The Schlenk flask was then charged with the Ni catalyst solution via syringe under a positive pressure of ethylene. The reaction was allowed to stir at room temperature under ethylene for two hours, at which point an aliquot from the reaction was removed to determine the monomer conversion via ^{1}H NMR spectroscopy against an internal mesitylene standard. The reaction was then quenched with methanol and pumped to dryness *in vacuo*. Product was analyzed by NMR spectroscopy, GPC, and MS-APCI (Table 4.2).

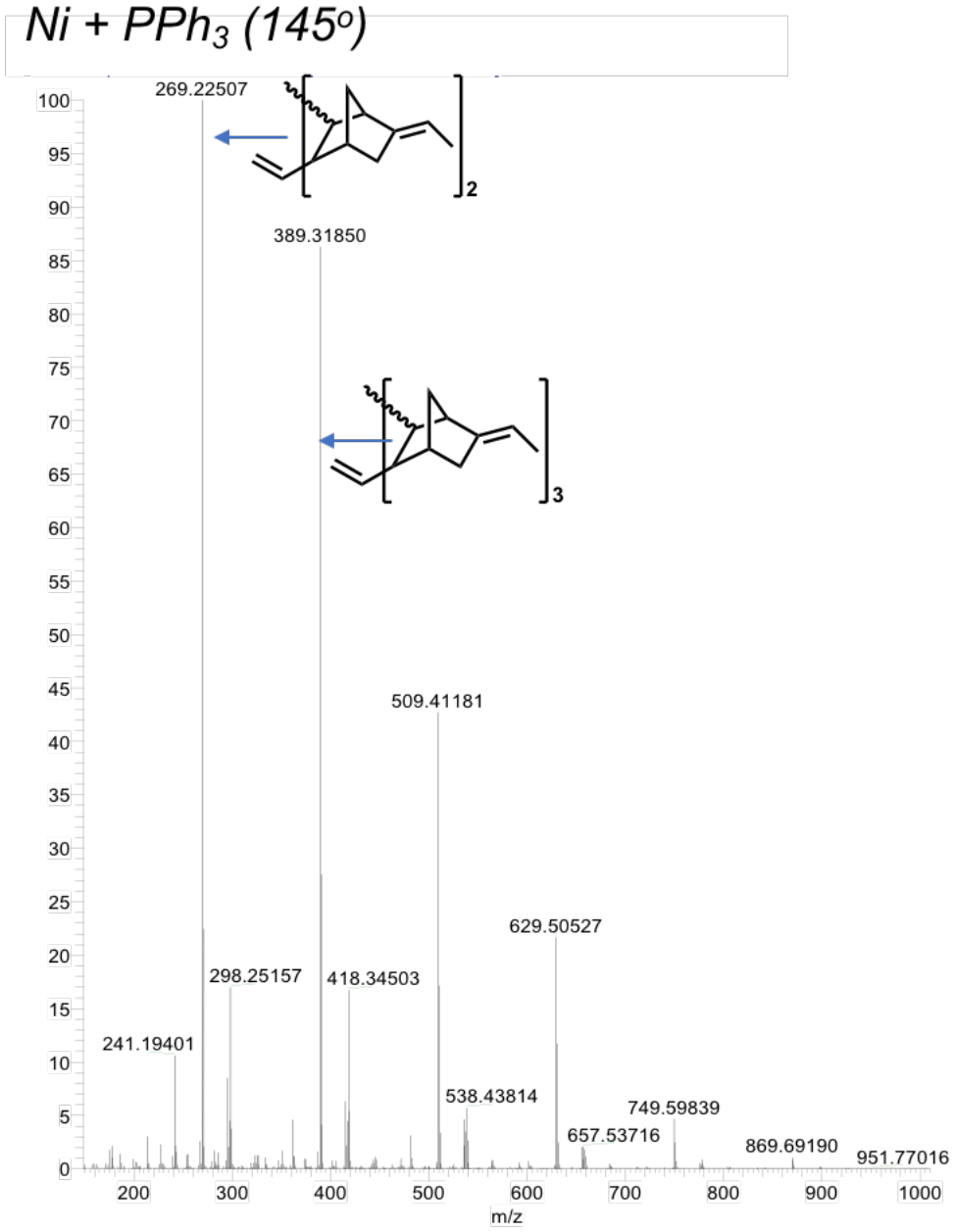

Figure 4.35. Mass spectrum of ethylene-terminated ENB oligomer using $[(mes)Ni(Me\text{-}allyl)]^+$ and PPh_3.

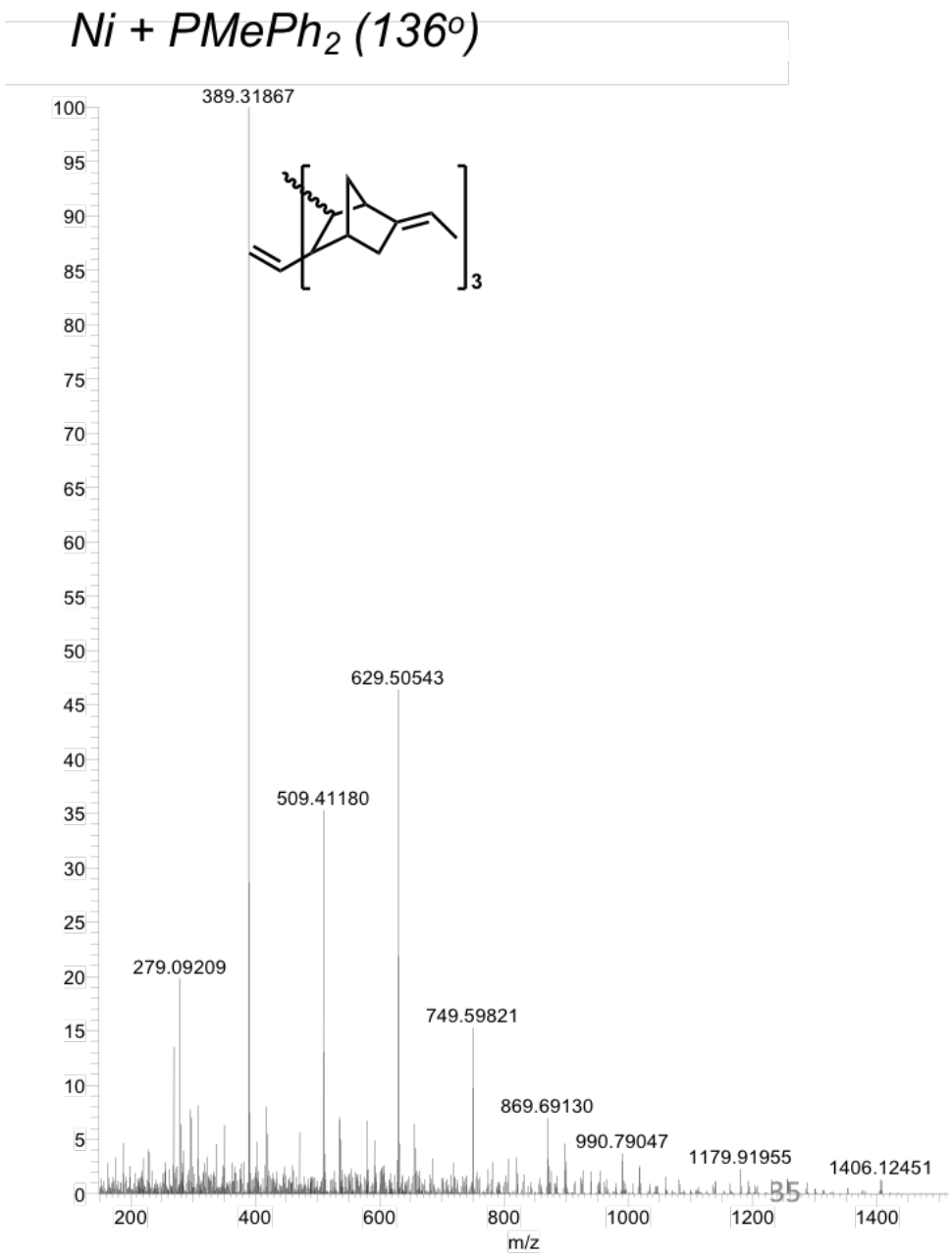

Figure 4.36. Mass spectrum of ethylene-terminated ENB oligomer using $[(mes)Ni(Me\text{-}allyl)]^+$ and $PMePh_2$.

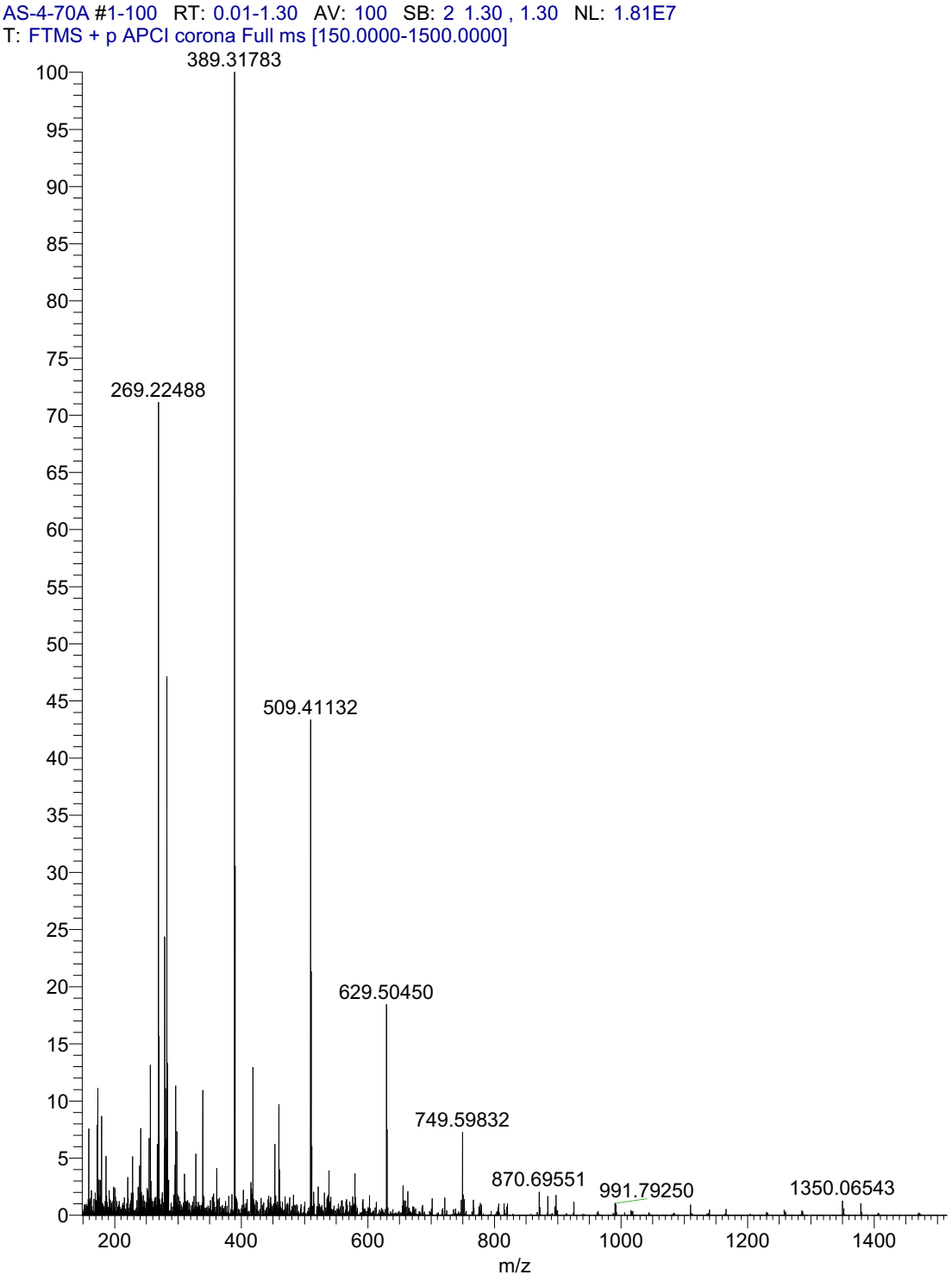

Figure 4.37. Mass spectrum of ethylene-terminated ENB oligomer using $[(mes)Ni(Me\text{-}allyl)]^+$ and PEt_3.

Polymerization of ENB at 200 psi C_2H_4 by [(mes)Ni(Me-allyl)][$BAr^F{}_4$]

In a glovebox, a 300 mL Parr reactor was charged with a solution of 5-ethylidene-2-norbornene in dichloromethane (250 mM, 28.5 mL). The reactor was removed from the glovebox, and charged with ethylene (200 psi) and vented twice. A solution of [(mes)Ni(Me-allyl)][$BAr^F{}_4$] in dichloromethane, (35.0 mg, 0.032 mmol) was quickly added to the Parr reactor at atmospheric pressure through an addition port, such that the total concentration of Ni would be 1 mM, and the port was quickly closed. The reactor was quickly charged with 200 psi ethylene, vented, and charged again with 200 psi ethylene (total time from addition of catalyst did not exceed five minutes). The reaction equilibrated to 100 psi, and was allowed to stir at room temperature for two hours. The reaction was vented, an aliquot was removed and analyzed by ^{1}H NMR spectroscopy to determine monomer conversion against and internal mesitylene standard, and the reaction was quenched with methanol and dried *in vacuo*.

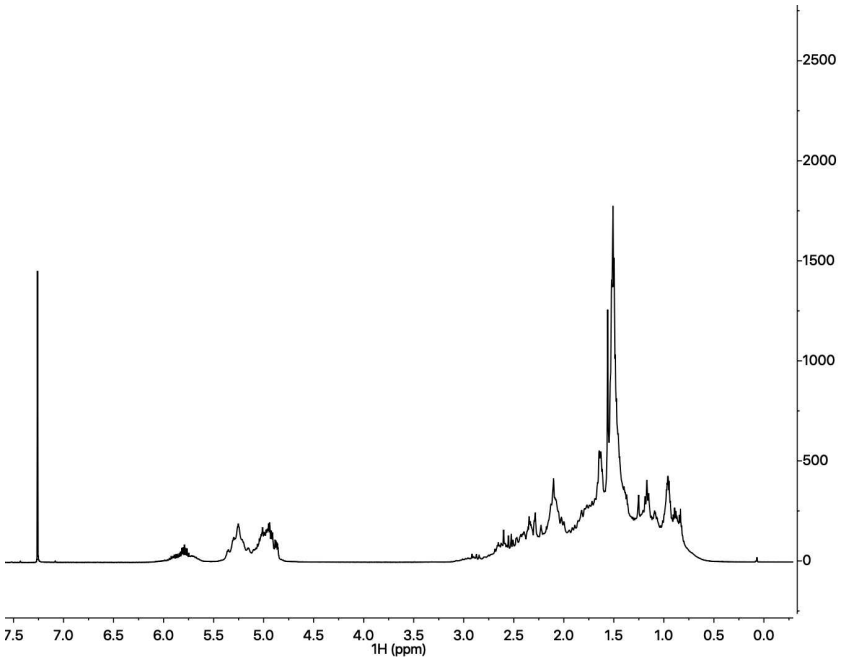

Figure 4.38. ^{1}H NMR spectrum of ENB oligomer obtained using $[(mes)Ni(Me\text{-}Allyl)]^{+}$ at 200 psi C_2H_4

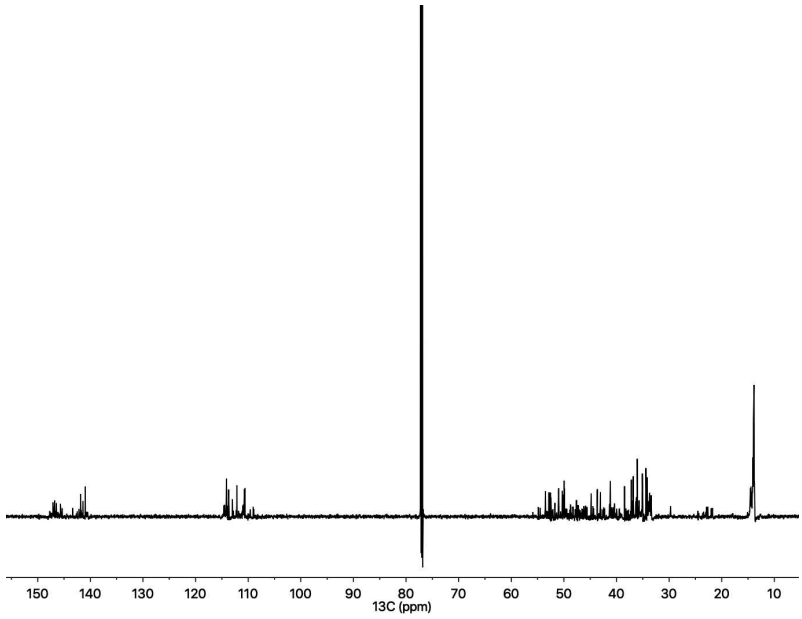

Figure 4.39. $^{13}C\{^{1}H\}$ NMR spectrum of ENB oligomer obtained using $[(mes)Ni(Me\text{-}Allyl)]^{+}$ at 200 psi C_2H_4

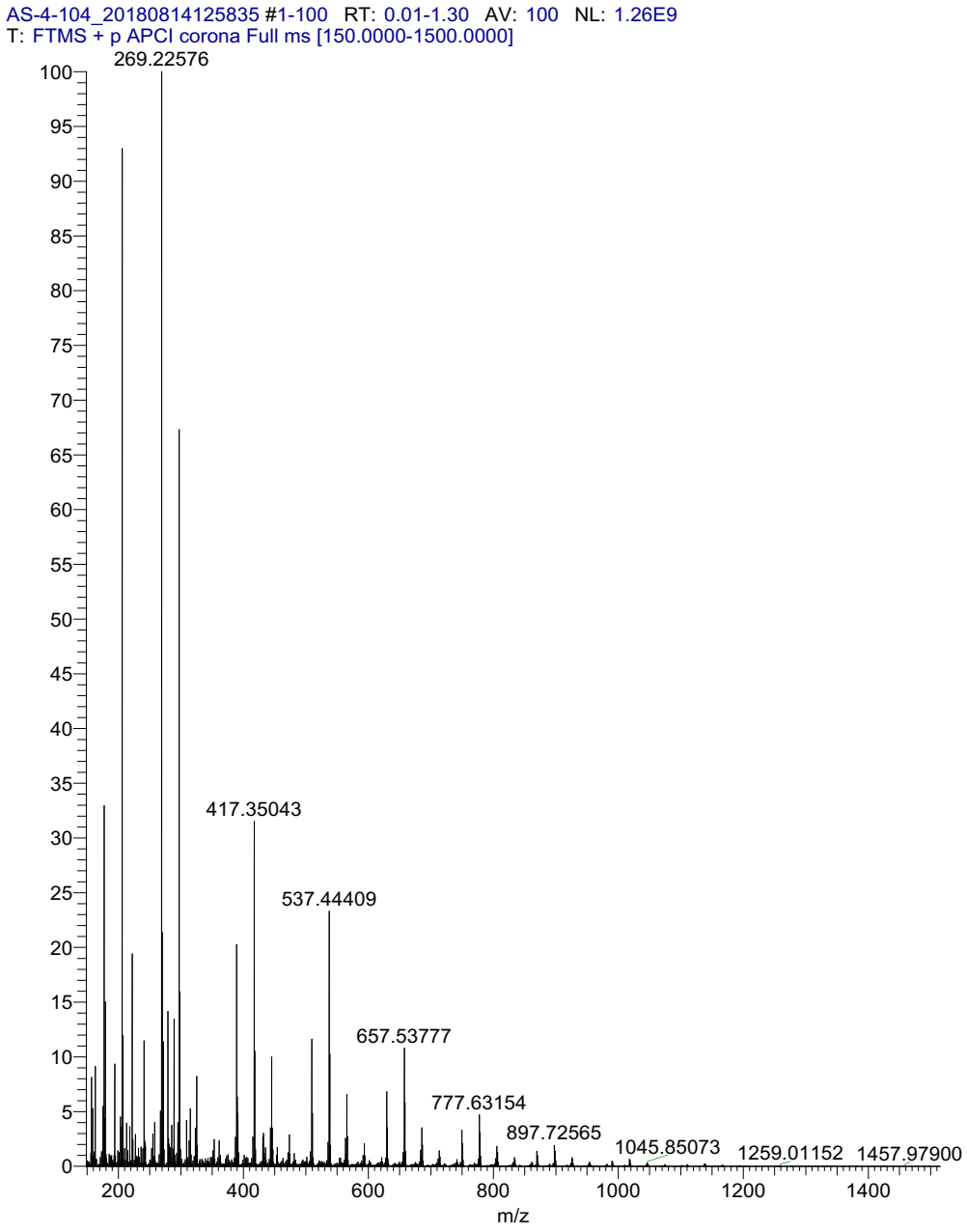

Figure 4.40. Mass spectrum of ENB oligomer obtained using $[(mes)Ni(Me\text{-}Allyl)]^+$ at 200 psi C_2H_4.

General procedure for the hydrogenation of ENB polymers and oligomers

The procedure was adapted from a protocol for the hydrogenation of bulky olefins.[153] In a nitrogen glovebox, a Schlenk flask was charged with ENB-derived material and anhydrous dichloromethane (resulting oligomer or polymer concentration of 500 mM) and the solution was bubbled with hydrogen at 0 °C for approximately two minutes. After allowing the mixture to stir under hydrogen for approximately ten minutes at 0 °C, a solution of $[(cod)Ir(PCy_3)(py)][PF_6]$ (1 mol% relative to polymer) was added in five equal portions over one hour at 0 °C, such that the final concentration of Ir in solution was 5 mM. After the final catalyst addition, the reaction was allowed to warm up slowly to room temperature over one hour, at which point the reaction was quenched with methanol (2 mL). The reaction was dried *in vacuo* and analyzed by ^1H NMR and $^{13}C\{^1H\}$ NMR spectroscopy, as well as GPC. It was determined that >90% hydrogenation of ENB polymers could be achieved.

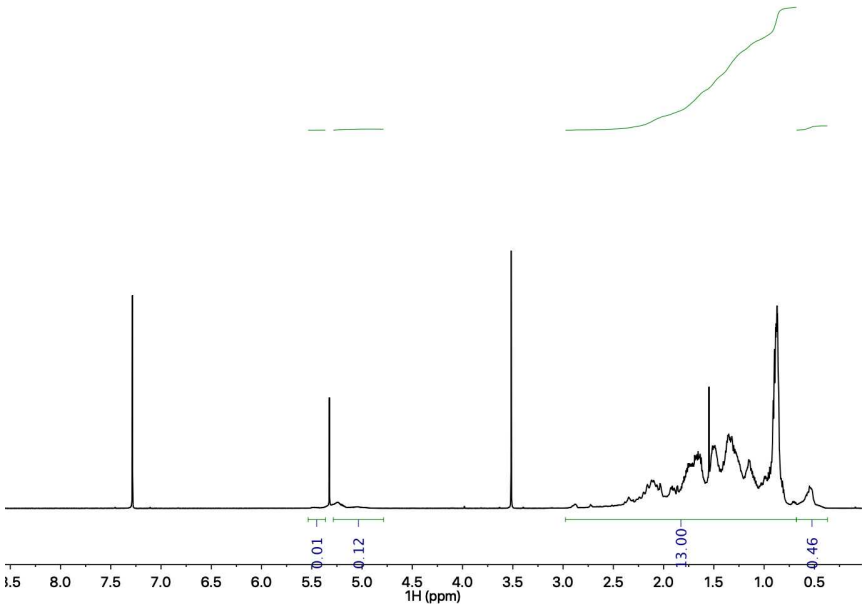

Figure 4.41. ^{1}H NMR spectrum of hydrogenated ENB oligomer (M_n 400 Da).

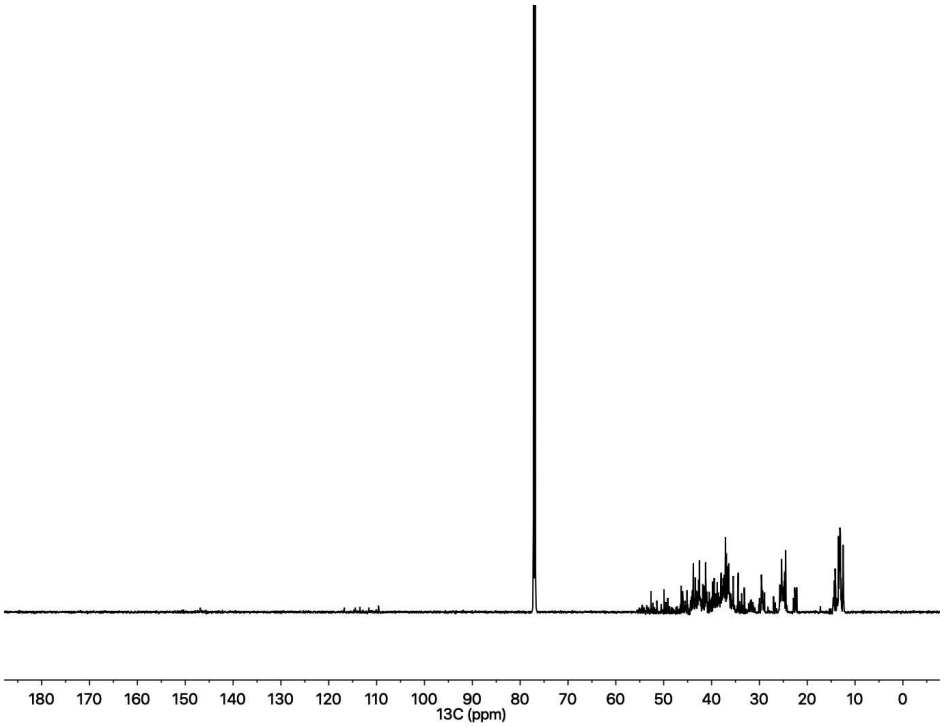

Figure 4.42. $^{13}C\{^{1}H\}$ NMR spectrum of hydrogenated ENB oligomer (M_n 400 Da).

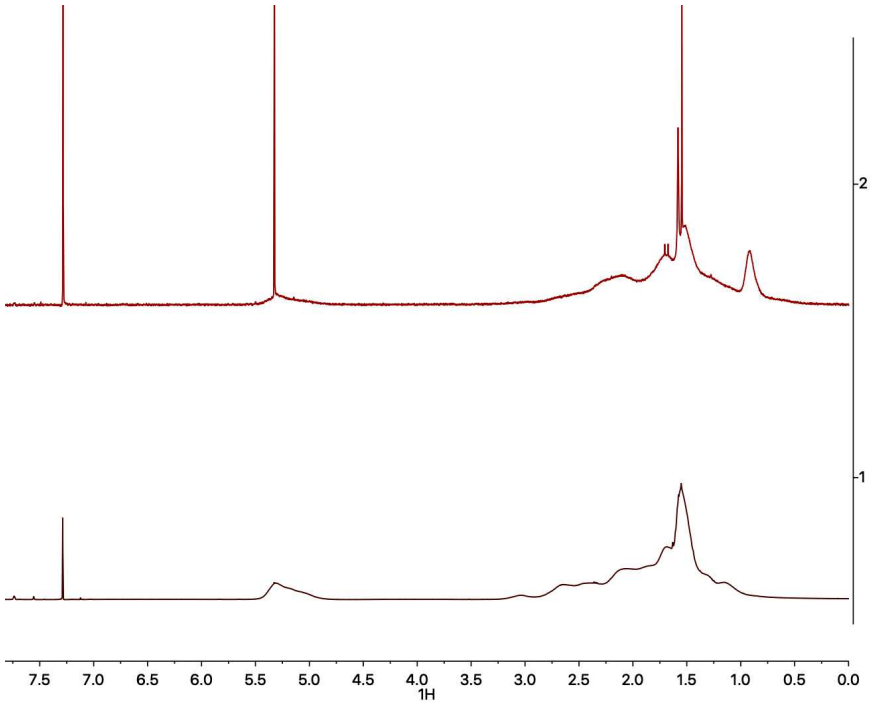

Figure 4.43. ENB homopolymer (M_n 25,000 Da) before (bottom) and after (top) hydrogenation.

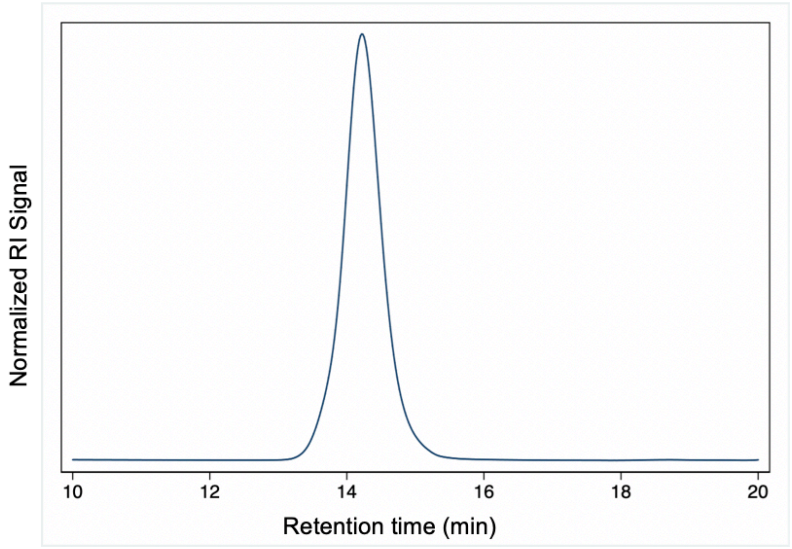

Figure 4.44. GPC trace of ENB homopolymer (M_n 25,000 Da) after hydrogenation.

DSC Characterization

Modified work-up for DSC measurements

Once the reaction was quenched with methanol, it was immediately filtered through a silica plug and dried *in vacuo*. The product was then dissolved in pentane, filtered through a short silica plug to remove any residual catalyst, and dried *in vacuo.* All DSC measurements were taken after determining T_D by TGA. First heat traces are reported in blue, second heat traces in red, and the cooling cycle in green.

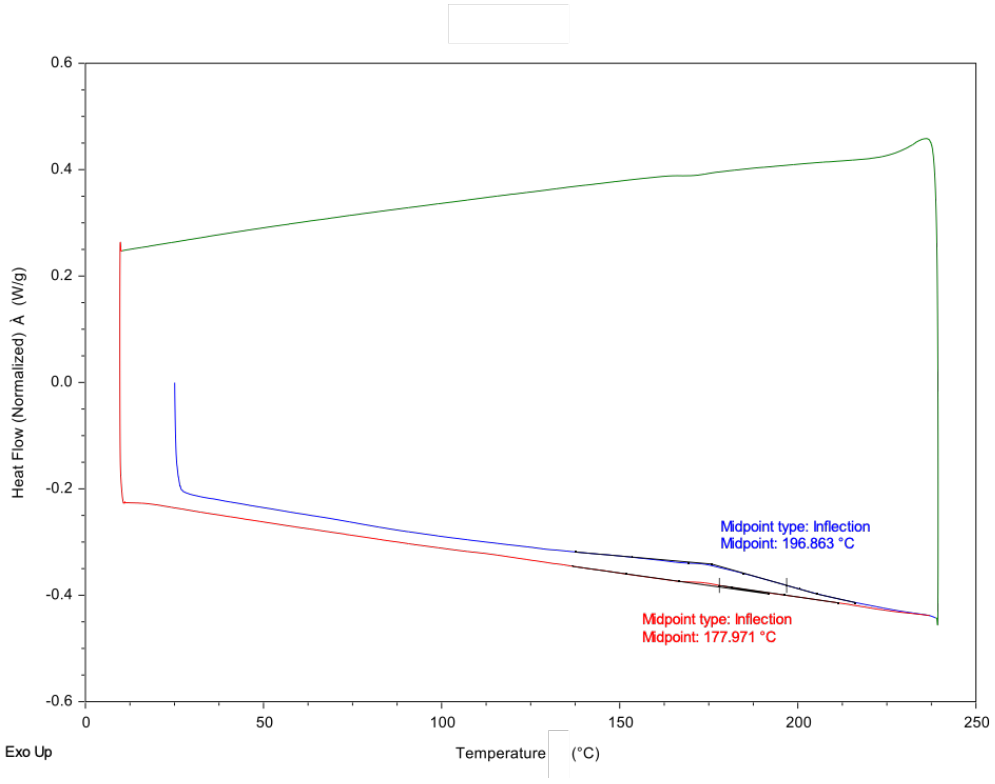

Figure 4.45. DSC trace to determine T_g of ENB homopolymer (M_n 25,000 Da).

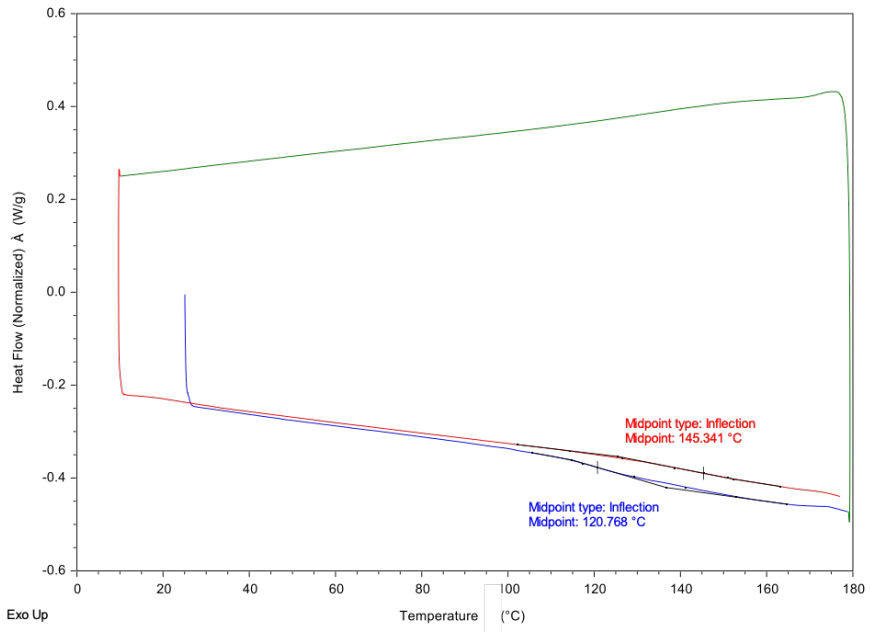

Figure 4.46. DSC trace to determine T_g of ethylene-terminated ENB oligomer (M_n 1,700 Da).

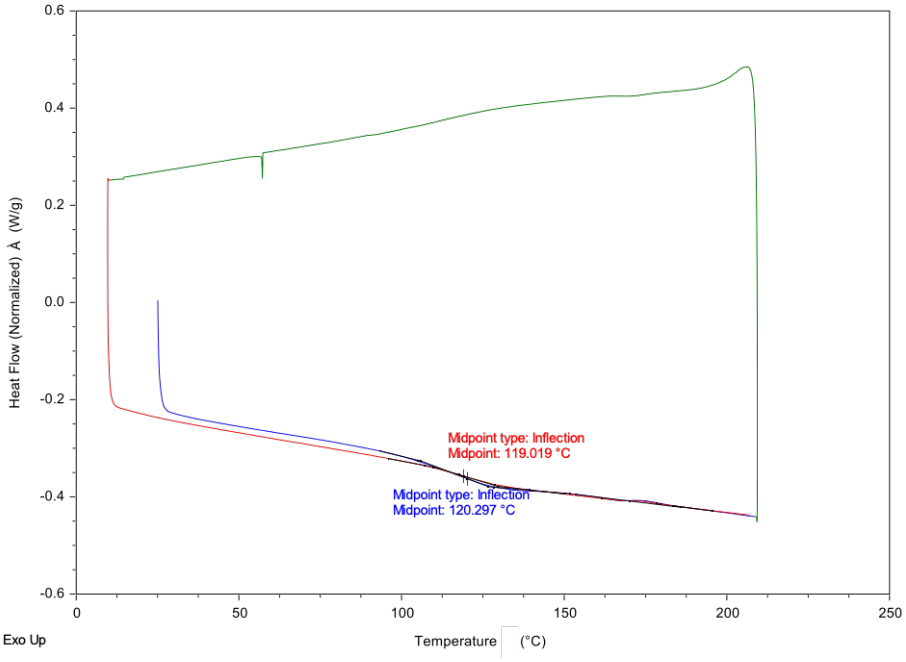

Figure 4.47. DSC trace to determine T_g of ethylene-terminated ENB oligomer (M_n 1,000 Da).

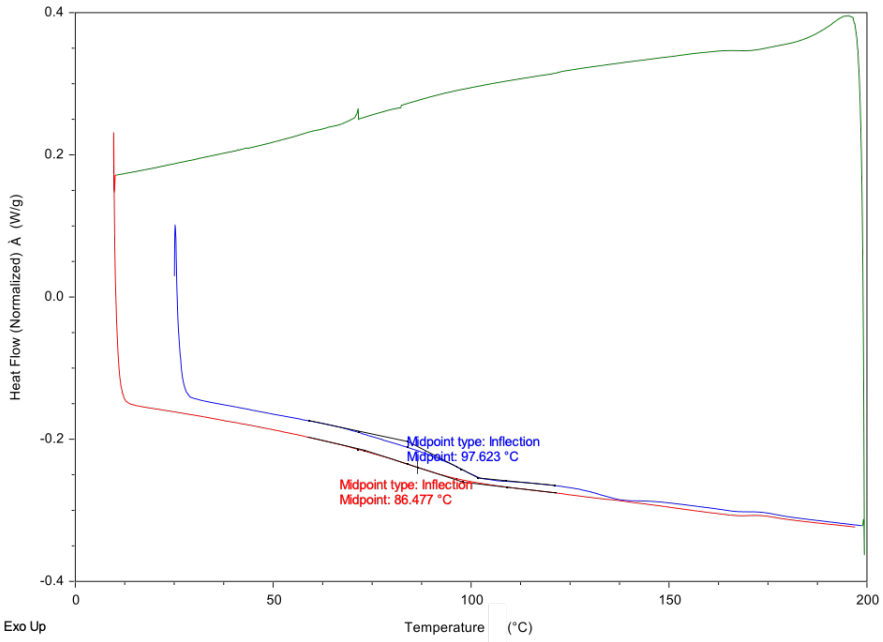

Figure 4.48. DSC trace to determine T_g of ethylene-terminated ENB oligomer (M_n 800 Da).

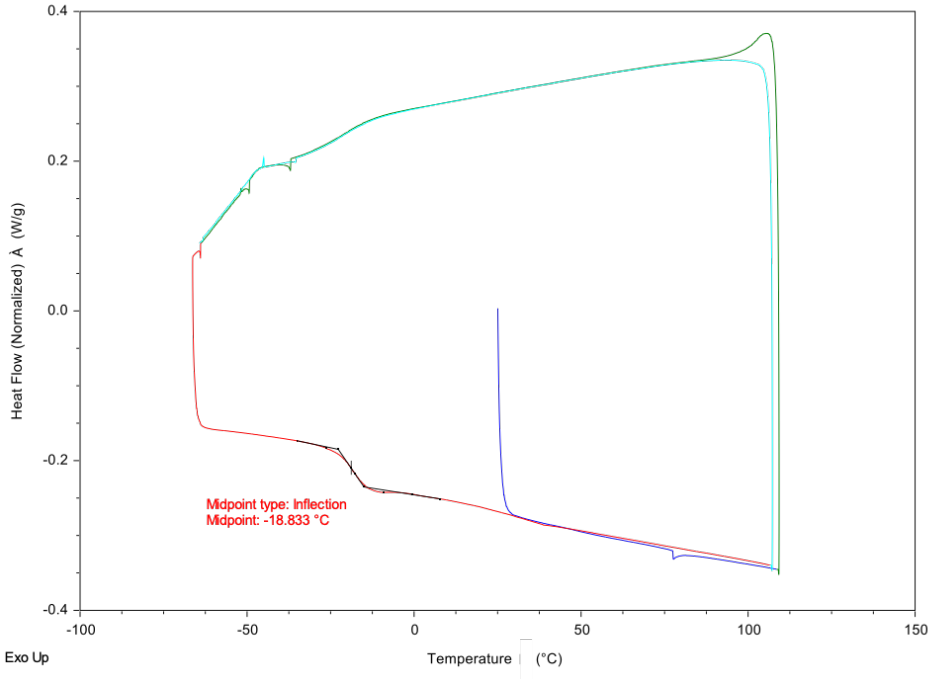

Figure 4.49. DSC trace to determine T_g of ethylene-terminated ENB oligomer (M_n 400 Da).

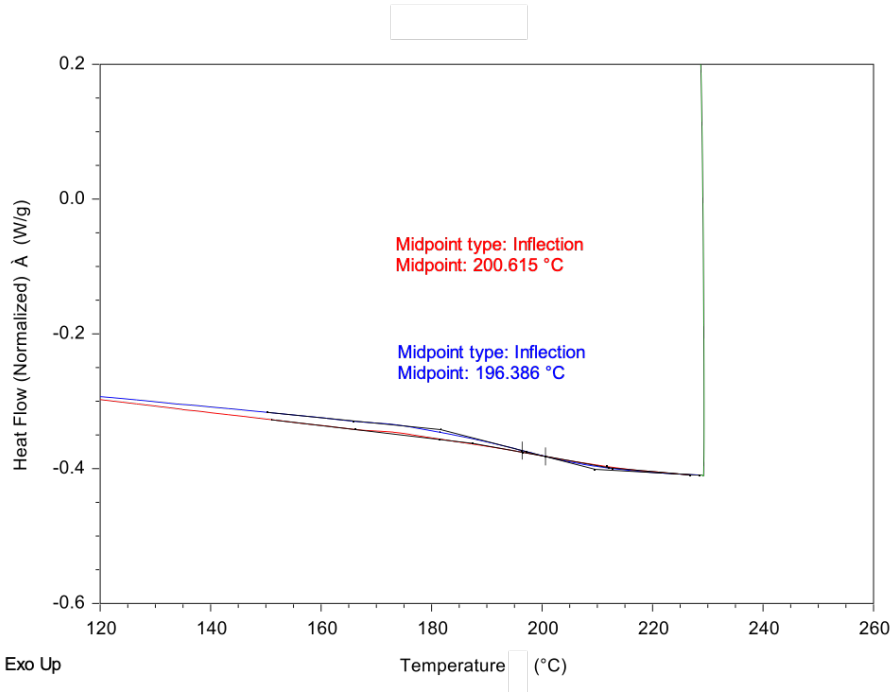

Figure 4.50. DSC trace to determine T_g of hexene-terminated ENB oligomer (M_n 2,500 Da).

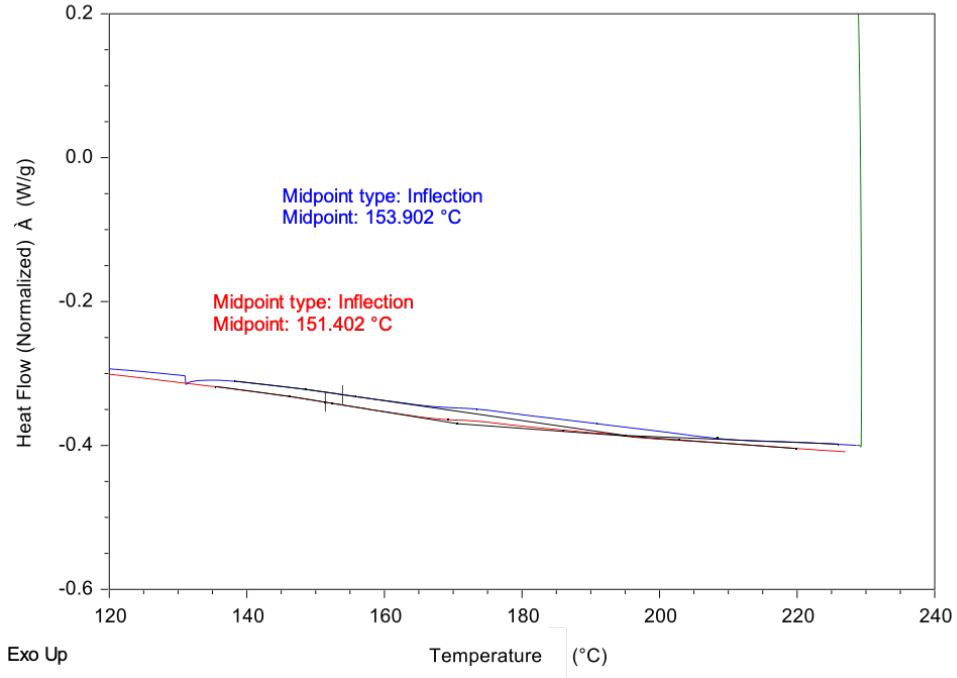

Figure 4.51. DSC trace to determine T_g of hexene-terminated ENB oligomer (M_n 1,900 Da).

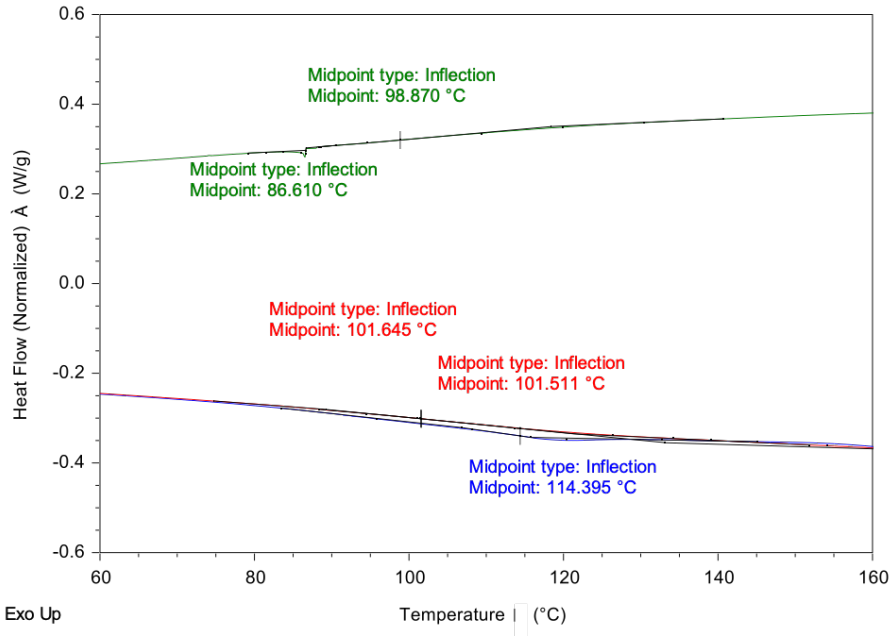

Figure 4.52. DSC trace to determine T_g of hexene-terminated ENB oligomer (M_n 1,070 Da).

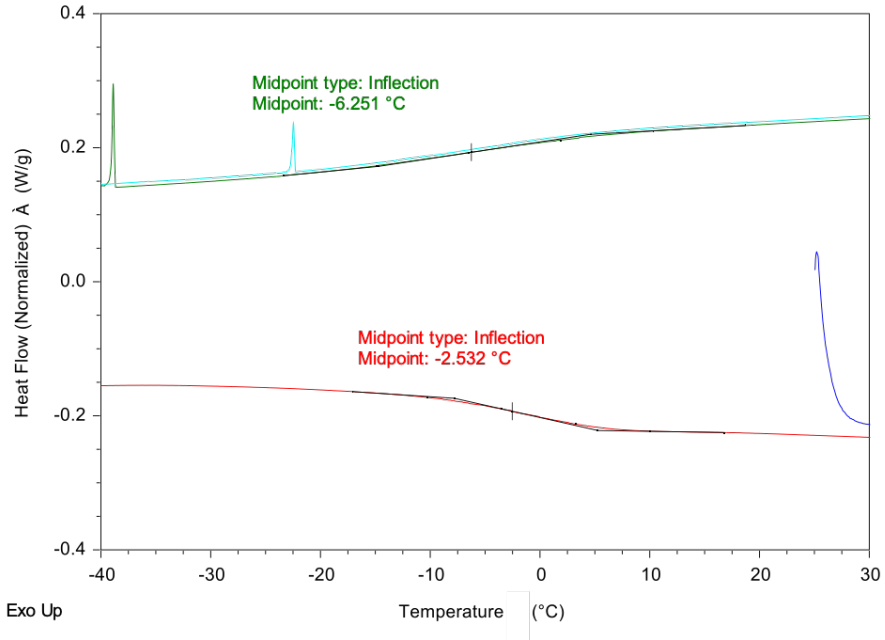

Figure 4.53. DSC trace to determine T_g of hexene-terminated ENB oligomer (M_n 600 Da).

REFERENCES

(1) Slone, Caroline S. Weinberger, Dana A. Mirkin, C. A. In *Progress in Inorganic Chemistry*; John Wiley & Sons, Inc., 1999; pp 233–351.

(2) Braunstein, P.; Naud, F. *Angew. Chemie - Int. Ed.* **2001**, *40*, 680.

(3) Vlugt, J. I. Van Der. *Eur. J. Inorg. Chem.* **2012**, 363.

(4) Miller, A. J. M. *Dalt. Trans.* **2017**, *46*, 11987.

(5) Jeffrey, J. C.; Rauchfuss, T. B. *Inorg. Chem.* **1979**, *18* (10), 2658.

(6) Darensbourg, Donald J. Kump, R. L. *Inorg. Chem.* **1978**, *17* (9), 2680.

(7) Chakraborty, S.; Bhattacharya, P.; Dai, H.; Guan, H. *Acc. Chem. Res.* **2015**, *48*, 1995.

(8) Bader, A.; Lindner, E. *Coord. Chem. Rev.* **1991**, *108*, 27.

(9) Barrett, B. J.; Iluc, V. M. *Inorganica Chim. Acta* **2017**, *460*, 35.

(10) Barrett, B. J.; Iluc, V. M. *Inorg. Chem.* **2014**, *53*, 7248.

(11) Braunstein, P.; Dedieu, A.; Rohmer, M.-M.; DeCian, A.; Rettig, S. J. *Organometallics* **2001**, *20*, 2966.

(12) Adams, G. M.; Weller, A. S. *Coord. Chem. Rev.* **2018**, *355*, 150.

(13) Kwong, F. Y.; Chan, A. S. C. *Synlett* **2008**, *10*, 1440.

(14) Larsen, C. R.; Erdogan, G.; Grotjahn, D. B. *J. Am. Chem. Soc.* **2014**, *136*, 1226.

(15) Kingsbury, J. S.; Hoveyda, A. H.; Hill, C. **2005**, *1* (8), 4510.

(16) Huang, J.; Stevens, E. D.; Nolan, S. P.; Petersen, J. L.; Orleans, N.; Virginia, W. *J. Am. Chem. Soc.* **1999**, *121*, 2674.

(17) Annibale, V. T.; Song, D. *RSC Adv.* **2013**, *3*, 11432.

(18) Weng, Zhiqiang. Teo, Shihui. Hor, T. S. A. *Acc. Chem. Res.* **2007**, *40*, 676.

(19) Deckers, P. J. W.; Hessen, B.; Teuben, J. H. *Angew. Chemie - Int. Ed.* **2001**, *40* (13), 2516.

(20) Agapie, T.; Day, M. W.; Henling, L. M.; Labinger, J. A.; Bercaw, J. E. *Organometallics*

2006, *25* (11), 2733.

(21) Empsall, H. D.; Hyde, E. M.; Jones, C. E.; Shaw, B. L. *J. Chem. Soc. Dalt. Trans.* **1974**, 1980.

(22) Chu, J.; Munz, D.; Jazzar, R.; Melaimi, M.; Bertrand, G. *J. Am. Chem. Soc.* **2016**, *138*, 7884.

(23) Zeineddine, A.; Estevez, L.; Mallet-Ladeira, S.; Miqueu, K.; Amgoune, A.; Bourissou, D. *Nat. Commun.* **2017**, 1.

(24) Chen, H.; Pan, W.; Huang, K.; Zhang, X.; Gong, D. *Polym. Chem.* **2017**, 1805.

(25) Crawford, L.; Cole-Hamilton, D. J.; Drent, E.; Bühl, M. *Chem. - A Eur. J.* **2014**, *20*, 13923.

(26) Drent, E.; Arnoldy, P.; Budzelaar, P. H. M. *J. Organomet. Chem.* **1993**, *455*, 247.

(27) Dong, Kaiwu. Sang, Rui. Zhihong, Wei. Liu, Jie. Duhren, Ricarda. Spannenberg, Anke. Jiao, Haijun. Neumann, Helfried. Jackstell, Ralf. Roberf, Franke, Beller, M. *Chem. Sci.* **2018**, *9*, 2510.

(28) Dong, K.; Sang, R.; Fang, X.; Franke, R.; Spannenberg, A.; Neumann, H.; Jackstell, R.; Beller, M. *Angew. Chemie - Int. Ed.* **2017**, *56*, 5267.

(29) Crawford, L.; Cole-hamilton, D. J.; Buhl, M. *Organometallics* **2015**, *34*, 438.

(30) Grotjahn, D. B.; Larsen, C. R.; Gustafson, J. L.; Nair, R.; Sharma, A. *J. Am. Chem. Soc.* **2007**, *129*, 9592.

(31) Frank, N.; Hanau, K.; Langer, R. *Inorg. Chem.* **2014**, *53*, 11335.

(32) Miller, Eileen M. Shaw, B. L. *J. Chem. Soc., Dalt. Trans.* **1974**, 480.

(33) MacDonald, M. G.; Kostelansky, C. N.; White, P. S.; Templeton, J. L. *Organometallics* **2006**, *25*, 4560.

(34) Kostelansky, C. N.; MacDonald, M. G.; White, P. S.; Templeton, J. L. *Organometallics* **2006**, *25*, 2993.

(35) Frauhiger, B. E.; Templeton, J. L. *Organometallics* **2012**, *31*, 2770.

(36) Bennett, M. A.; Allan, J.; Felixberger, J. K.; Sunderland, C.; Willis, A. C. *Inorg. Chem.* **1993**, *32*, 1951.

(37) Dong, K.; Fang, X.; Gu, S.; Jackstell, R.; Beller, M. *Nat. Commun.* **2017**, 1.

(38) Kita, M. R.; Miller, A. J. M. *J. Am. Chem. Soc.* **2014**, *136*, 14519.

(39) Smith, J. B.; Kerr, S. H.; White, P. S.; Miller, A. J. M. *Organometallics* **2017**, *36*, 3094.

(40) Grajeda, J.; Kita, M. R.; Gregor, L. C.; White, P. S.; Miller, A. J. M. *Organometallics* **2016**, *35*, 306.

(41) Kita, M. R.; Miller, A. J. M. *Angew. Chemie - Int. Ed.* **2017**, *56* (20), 5498.

(42) Gregor, L. C.; Grajeda, J.; White, P. S.; Vetter, A. J.; Miller, A. J. M. *Catal. Sci. Technol.* **2018**, *8*, 3133.

(43) Fairlamb, I. A. N. J. S.; Lee, A. F. In *RSC Catalysis Series*; 2013; pp 72–107.

(44) Vries, J. G. De. *Can. J. Chem.* **2001**, *79*, 1086.

(45) Miyaura, N.; Suzuki, A. *Chem. Rev.* **1995**, *95* (1), 2457.

(46) Bercaw, John E. Canty, Allan J. Goldberg, Karen I. Grice, Kyle A. Labinger, Jay A. Malinakova, Helena C. Moret, Marc-Etienne. Powers, David C. Racowski, Joy M. Ritter, Tobias. Sanford, Melanie, S. Scheuermann, Margaret L. Sharma, M. *Higher Oxidation State Organopalladium and Platinum Chemistry*; 2011.

(47) Vedernikov, A. N. *RSC Catal. Ser.* **2013**, No. 11, 108.

(48) Canty, A. J. *Acc. Chem. Res.* **1992**, *25* (3), 83.

(49) Bailey, W. D.; Luconi, L.; Rossin, A.; Yakhvarov, D.; Flowers, S. E.; Kaminsky, W.; Kemp, R. A.; Giambastiani, G.; Goldberg, K. I. *Organometallics* **2015**, *34*, 3998.

(50) Guari, Y.; Kamer, P. C. J.; Leeuwen, P. W. N. M. Van; Donnadieu, B.; Sabo-etienne, S.; Chaudret, B.; Lutz, M.; Spek, A. L. *Dalt. Trans.* **2013**, *42*, 6495.

(51) Cheng, G.; Yang, Y.; Liu, P.; Chen, P.; Sun, T.; Li, G.; Zhang, X.; Houk, K. N.; Yu, J.; Wu, Y. *J. Am. Chem. Soc.* **2014**, *136*, 894.

(52) Dang, Y.; Deng, X.; Guo, J.; Song, C.; Hu, W.; Wang, Z. *J. Am. Chem. Soc.* **2016**, *138*, 2712.

(53) Yang, Y.; Hong, X.; Yu, J.; Houk, K. N. *Acc. Chem. Res.* **2017**, *50*, 2853.

(54) Connor, A. R. O.; Urbin, S. A.; Moorhouse, R. A.; White, P. S.; Brookhart, M. *Organometallics* **2009**, *28*, 2372.

(55) O'Connor, A. R.; Brookhart, M. *J. Polym. Sci. Part A Polym. Chem.* **2010**, *48*, 1901.

(56) Gildner, P. G.; Colacot, T. J. *Organometallics* **2015**, *34*, 5497.

(57) Seechurn, C. C. C. J.; Kitching, M. O.; Colacot, T. J.; Snieckus, V. *Angew. Chemie - Int. Ed.* **2012**, *51*, 5062.

(58) Catellani, M.; Chiusoli, G. P. *Journal of Organometallic Chemistry*. 1988, pp C27–C30.

(59) Catellani, M.; Frignani, F. *Angew. Chemie Int. Ed. English* **1997**, *36* (1), 119.

(60) Brown, D. G.; Byers, P. K.; Canty, A. J. *Organometallics* **1990**, *0*, 1231.

(61) Smith, J. B.; Miller, A. J. M. *Organometallics* **2015**, *34*, 4669.

(62) Motoyama, Y.; Shimozono, K.; Nishiyama, H. *Inorganica Chim. Acta* **2006**, *359*, 1725.

(63) Niu, J. L.; Chen, Q. T.; Hao, X. Q.; Zhao, Q. X.; Gong, J. F.; Song, M. P. *Organometallics* **2010**, *29*, 2148.

(64) Herbert, D. E.; Ozerov, O. V. *Organometallics* **2011**, *30*, 6641.

(65) Ine, B.; SanMartin, R.; Domı, E.; Urtiaga, M. K.; Arriortua, I. *Organometallics* **2008**, *27*, 2833.

(66) Li, J.; Siegler, M.; Lutz, M.; Spek, A. L.; Gebbink, R. J. M. K.; Koten, G. Van. *Adv. Synth. Catal.* **2010**, *352*, 2474.

(67) Gong, J.; Zhang, Y.; Song, M.; Xu, C. *Organometallics* **2007**, *26*, 6487.

(68) Zhang, B.; Wang, W.; Shao, D.; Hao, X.; Gong, J.; Song, M. *Organometallics* **2010**, *29*, 2579.

(69) Yang, M.; Liu, Y.; Gong, J.; Song, M. *Organometallics* **2011**, *30*, 3793.

(70) Khake, S. M.; Soni, V.; Gonnade, R. G.; Punji, B. *Dalt. Trans.* **2014**, *43*, 16084.

(71) Pandey, D. K.; Khake, S. M.; Gonnade, R. G.; Punji, B. *RSC Adv.* **2015**, *5* (99), 81502.

(72) Hou, A.; Liu, Y.; Hao, X.; Gong, J.; Song, M. *J. Organomet. Chem.* **2011**, *696*, 2857.

(73) Garrou, P. E. *Chem. Rev.* **1981**, *81*, 229.

(74) Allred, A. L.; Rochow, E. G. *J. Inorg. Nucl. Chem.* **1958**, *5* (1), 1954.

(75) Gustowski, D. A.; Gatto, V. J.; Mallen, J.; Echegoyen, L.; Gokel, G. W. *J. Org. Chem.* **1987**, *52*, 5172.

(76) Raamat, E.; Kaupmees, K.; Ovsjannikov, G.; Trummal, A.; Kütt, A.; Saame, J.; Koppel, I.; Kaljurand, I.; Lipping, L. *J. Phys. Org. Chem.* **2013**, *26*, 162.

(77) Bercaw, J. E.; Durrell, A. C.; Gray, H. B.; Green, J. C.; Hazari, N.; Labinger, J. A.; Winkler, J. R. *Inorg. Chem.* **2010**, *49*, 1801.

(78) Churchill, M. R.; Wasserman, H. J.; Young, G. J. **1980**, No. Ii, 762.

(79) Lee, G. M.; Korobkov, I.; Baker, R. T. *J. Organomet. Chem.* **2017**, *847*, 270.

(80) Miller, A. J. M.; Labinger, J. A.; Bercaw, J. E. *Organometallics* **2010**, *29*, 4499.

(81) Kira, M.; Hino, T.; Sakurai, H. *J. Am. Chem. Soc.* **1992**, *114*, 6697.

(82) Walsh, R. *Acc. Chem. Res.* **1981**, *1537* (4), 246.

(83) Byers, P. K.; Canty, A. J.; Skelton, B. W.; Whiteb, A. H. *J. Chem. Soc., Dalt. Trans.* **1986**, 1722.

(84) Camasso, N. M.; Canty, A. J.; Ariafard, A.; Sanford, M. S. **2017**, 4382.

(85) Maleckis, A.; Kampf, J. W.; Sanford, M. S. *J. Am. Chem. Soc.* **2013**, *135*, 6618.

(86) Bayler, A.; Canty, A. J.; Edwards, P. G.; Skelton, B. W.; White, A. H. *J. Chem. Soc. Dalt. Trans.* **2000**, 3325.

(87) Powers, D. C.; Lee, E.; Ariafard, A.; Sanford, M. S.; Yates, B. F.; Canty, A. J.; Ritter, T. *J. Am. Chem. Soc.* **2012**, *134*, 12002.

(88) Canty, A. J. *Dalt. Trans.* **2009**, 10409.

(89) Canty, A. J.; Jin, H.; Skelton, B. W.; White, A. H. *Inorg. Chem.* **1998**, *2*, 3975.

(90) Kruis, D.; Markies, B. A.; Canty, A. J.; Boersma, J.; van Koten, G. *J. Organomet. Chem.* **1997**, *532*, 235.

(91) Nappi, M.; Gaunt, M. J. *Organometallics* **2018**, *38*, 143.

(92) Chen, C.; Luo, Y.; Fu, L.; Chen, P.; Lan, Y.; Liu, G. *J. Am. Chem. Soc.* **2018**, *140*, 1207.

(93) Wu, H.; Yang, B.; Zhu, L.; Lu, R.; Li, G.; Lu, H. *Org. Lett.* **2016**, *18*, 5804.

(94) Le, C. M.; Sperger, T.; Fu, R.; Hou, X.; Lim, Y. H.; Schoenebeck, F.; Lautens, M. *J. Am. Ceram. Soc.* **2016**, *138*, 1441.

(95) Alsters, P. L.; Engel, P. F.; Hogerheide, M. P.; Copijn, M.; Spek, A. L.; van Koten, G. *Organometallics* **1993**, *12* (5), 1831.

(96) Gossage, R. A.; Spek, A. L.; Koten, G. Van. *Organometallics* **1998**, *17*, 731.

(97) Bour, J. R.; Camasso, N. M.; Sanford, M. S. *J. Am. Chem. Soc.* **2015**, *137*, 8034.

(98) Ye, Y.; Sanford, M. S. *Synlett* **2012**, *23*, 2005.

(99) Yakelis, N. A.; Bergman, R. G. *Org. Lett.* **2005**, *24*, 3579.

(100) Gregor, L. C.; Grajeda, J.; Kita, M. R.; White, P. S.; Vetter, A. J.; Miller, A. J. M. *Organometallics* **2016**, *35*, 3074.

(101) Smith, Jacob B; Camp, Andrew; Farquhar, Alexandra; Kerr, Stewart H.; Chun-Hsing, Chen; Miller, A. J. M. *Submitted.* **2019**.

(102) Liu, X.; Bin, L.; Liu, Q. *Synth.* **2019**, *51*, 1293.

(103) Lin, L.; Romano, C. *J. Am. Chem. Soc.* **2016**, *138*, 10344.

(104) Larionov, E.; Lin, L. *J. Am. Chem. Soc.* **2014**, *136*, 16882.

(105) Mamone, P.; Gr, M. F.; Fromm, A.; Khan, B. A.; Gooßen, L. J. *Org. Lett.* **2012**, *14* (14), 3716.

(106) Gauthier, D.; Lindhardt, A. T.; Olsen, E. P. K.; Overgaard, J.; Skrydstrup, T. *J. Am. Chem. Soc.* **2010**, *132*, 7998.

(107) Lim, H. J.; Smith, C. R.; Rajanbabu, T. V. *J. Org. Chem.* **2009**, *74*, 4565.

(108) Li, G.; Kuo, J. L.; Han, A.; Abuyuan, J. M.; Young, L. C.; Norton, J. R.; Palmer, J. H. **2016**, 7698.

(109) Crossley, S. W. M.; Barabe, F.; Shenvi, R. A. *J. Am. Chem. Soc.* **2014**, *136*, 16788.

(110) Specht, Z. G.; Cortes-llamas, S. A.; Tran, H. N.; Niekerk, C. J. Van; Rancudo, K. T.; Golen, J. A.; Moore, C. E.; Rheingold, A. L.; Dwyer, T. J.; Grotjahn, D. B. *Chem. - A Eur. J.* **2011**, *17*, 6606.

(111) Grotjahn, D. B. *Pure Appl. Chem.* **2010**, *82* (3), 635.

(112) Hassam, M.; Taher, A.; Arnott, G. E.; Green, I. R.; Van Otterlo, W. A. L. *Chem. Rev.* **2015**, *115* (11), 5462.

(113) Jiang, Z.; Sen, A. *Organometallics* **1993**, *12* (4), 1406.

(114) Taylor, Arnold R. Keen, Gary. Eisenbraun, E. *J. Org. Chem.* **1977**, *42* (22), 3477.

(115) Sen, Ayusman; Lai, T.; Thomas, R. R. **1988**, *358*, 567.

(116) Jiang, Zhaozhong. Sen, A. *J. Am. Chem. Soc.* **1990**, *112* (26), 9655.

(117) Baxter, R. D.; Sale, D.; Engle, K. M.; Yu, J.; Blackmond, D. G. *J. Am. Chem. Soc.* **2012**, *134*, 4600.

(118) Bures, J. *Angew. Chemie - Int. Ed.* **2016**, *55*, 16084.

(119) Nielsen, C. D.; Bures, J. *Chem. Sci.* **2019**, *10*, 348.

(120) Lim, D.; Do, H.; Kim, H. *J. Appl. Polym. Sci.* **2006**, *102*, 2839.

(121) Park, J.; Kong, W.; Lee, S.; Wook, J.; Gyu, H.; Yeoul, B. *Int. J. Adhes. Adhes.* **2016**, *68*, 326.

(122) Fox, T. G.; Flory, P. J. *J. Appl. Phys.* **1950**, *21*, 581.

(123) Bermeshev, M. V.; Chapala, P. P. *Prog. Polym. Sci.* **2018**, *84*, 1.

(124) Flid, V. R.; Gringolts, M. L.; Shamsiev, R. S.; Finkelshtein, S. *Russ. Chem. Rev.* **2018**, *12*, 1169.

(125) Mu, H.; Pan, L.; Song, D.; Li, Y. *Chem. Rev.* **2015**, *115*, 12091.

(126) Blank, F.; Janiak, C. *Coord. Chem. Rev.* **2009**, *253* (7–8), 827.

(127) Ma, R.; Hou, Y.; Gao, J.; Bao, F. *J. Macromol. Sci. Part C Polym. Rev.* **2009**, *49*, 249.

(128) Makovetskii, K. L. *Polym. Sci.* **2008**, *50* (1), 22.

(129) Janiak, C.; Lassahn, P. G. *J. Mol. Catal. A Chem.* **2001**, *166* (2), 193.

(130) Zanchin, G.; Leone, G.; Pierro, I.; Rapallo, A.; Porzio, W.; Bertini, F.; Ricci, G. *Macromol. Chem. Phys.* **2017**, *218* (11), 1.

(131) Zanchin, G.; Leone, G.; Pierro, I.; Rapallo, A.; Porzio, W.; Bertini, F.; Ricci, G. *Macromol. Chem. Phys.* **2017**, *218* (11).

(132) Blank, F.; Scherer, H.; Janiak, C. *J. Mol. Catal. A Chem.* **2010**, *330* (1–2), 1.

(133) Osokin, Y. G. *Pet. Chem.* **2007**, *47* (1), 1.

(134) van Doremaele, G.; van Duin, M.; Valla, M.; Berthoud, A. *J. Polym. Sci. Part A Polym. Chem.* **2017**, *55* (18), 2877.

(135) Marathe, S.; Sivaram, S. **1994**, 1083.

(136) Sudo, A.; Morishita, H.; Endo, T. *J. Polym. Sci. Part A Polym. Chem.* **2010**, *48* (17), 3896.

(137) Bermeshev, M. V; Bulgakov, B. A.; Genaev, A. M.; Kostina, J. V; Bondarenko, G. N.; Finkelshtein, E. S. *Macromolecules* **2014**, *47*, 5470.

(138) Hennis, A. D.; Polley, J. D.; Long, G. S.; Sen, A.; Yandulov, D.; Lipian, J.; Benedikt, G. M.; Rhodes, L. F.; Huffman, J. *Organometallics* **2001**, *11*, 2802.

(139) Morishita, Hidetada; Sudo, Atsushi; Endo, T. *J. Polym. Sci. Part A Polym. Chem.* **2009**, *47*, 3982.

(140) Blank, F.; Vieth, J. K.; Ruiz, J.; Rodríguez, V.; Janiak, C. *J. Organomet. Chem.* **2011**, *696* (2), 473.

(141) Bermeshev, M. V.; Bulgakov, B. A.; Genaev, A. M.; Kostina, J. V.; Bondarenko, G. N.; Finkelshtein, E. S. *Macromolecules* **2014**, *47* (16), 5470.

(142) Goodall, B. L.; Benedikt, G. M.; McIntosh III, L. H.; Barnes, D. A. *US Pat. 5468819* **1995**, *08* (20130101), 1.

(143) Goodall, B. L.; Benedikt, G. M.; Mcintosh, I. L. H.; Barnes, D. A.; Rhodes, L. F. **1997**, *08* (20060101), 1.

(144) Goodall, B. *Late Transit. Met. Polym. Catal.* **2003**, *1*, 101.

(145) Bermeshev, M. V; Chapala, P. P. *Prog. Polym. Sci.* **2018**, *84*, 1.

(146) Wang, L.; Wang, X.; Yang, M.; Wang, Y.; Li, L.; Liu, B.; Kim, I. *Macromol. Res.* **2011**, *19* (10), 1071.

(147) Li, H.; Li, J.; Zhang, Y.; Mu, Y. *Polymer (Guildf).* **2008**, *49* (12), 2839.

(148) Karpov, G. O.; Bermesheva, E. V.; Zudina, A. V.; Asachenko, A. F.; Minaeva, L. I.; Topchiy, M. A.; Gribanov, P. S.; Nechaev, M. S.; Bermeshev, M. V. *Dokl. Chem.* **2018**, *479* (2), 523.

(149) Barnes, D. A.; Benedikt, G. M.; Goodall, B. L.; Huang, S. S.; Kalamarides, H. A.; Lenhard, S.; McIntosh, L. H.; Selvy, K. T.; Shick, R. A.; Rhodes, L. F. *Macromolecules* **2003**, *36* (8), 2623.

(150) Lipian, John; Mimna, Richard A.; Fondran, John C.; Yandulov, Dmitry; Shick, Robert A.; Goodall, Brian L.; Rhodes, L. F. *Macromolecules* **2002**, *35*, 8969.

(151) Yamashita, M.; Takamiya, I.; Jin, K.; Nozaki, K. *Organometallics* **2006**, *25* (19), 4588.

(152) Alberti, D.; Goddard, R.; Porschke, K.-R. *Organometallics* **2005**, *24*, 3907.

(153) Crabtree, H.; Morris, E. *J. Organomet. Chem.* **1977**, *141*, 205.